



City Research Online

City, University of London Institutional Repository

Citation: Hafiz bin Haji Khozali, Muhammed (1981). Computer aided mathematical modelling of turbulent flow for orifice metering. (Unpublished Doctoral thesis, The City University)

This is the accepted version of the paper.

This version of the publication may differ from the final published version.

Permanent repository link: <https://openaccess.city.ac.uk/id/eprint/17894/>

Link to published version:

Copyright: City Research Online aims to make research outputs of City, University of London available to a wider audience. Copyright and Moral Rights remain with the author(s) and/or copyright holders. URLs from City Research Online may be freely distributed and linked to.

Reuse: Copies of full items can be used for personal research or study, educational, or not-for-profit purposes without prior permission or charge. Provided that the authors, title and full bibliographic details are credited, a hyperlink and/or URL is given for the original metadata page and the content is not changed in any way.

City Research Online:

<http://openaccess.city.ac.uk/>

publications@city.ac.uk

بِسْمِ اللّٰهِ الرَّحْمٰنِ الرَّحِیْمِ

COMPUTER AIDED MATHEMATICAL MODELLING

OF

TURBULENT FLOW FOR ORIFICE METERING

A Thesis

Submitted to the Department

of

Systems Science, The City University

by

Muhammed Hafiz bin Haji Khozali

In Partial Fulfilment of the

Requirements for the Degree

of

Doctor of Philosophy.

May 1981.

IMAGING SERVICES NORTH

Boston Spa, Wetherby
West Yorkshire, LS23 7BQ
www.bl.uk

BEST COPY AVAILABLE.

VARIABLE PRINT QUALITY

untuk...

isteri dan anak-anakku...

to...

my wife and children...

ABSTRACT.

The time-averaged Navier-Stokes' partial differential equations have been used in the mathematical modelling of fluid flow for steady, incompressible non-cavitating, high Reynolds number turbulence through an orifice plate. The model developed for orifice plates was based on a particular closed form turbulent model: the $k-\epsilon$ two equation model developed at Imperial College, London and embodied in the TEACH-T finite difference computer code. A basic model for axisymmetric flow through an orifice meter was developed by appropriate modification of the TEACH-T program to incorporate orifice plate geometry, upstream/downstream distances, Reynolds number, inlet velocity profile and the calculation of output quantities of interest such as discharge and pressure loss coefficients. The model was tested for convergence and general adequacy on an orifice of diameter ratio $\beta = .7$ in a 4 inch pipe line and at a Reynolds number of 10^5 . Quantitative tests were then conducted on thin orifice plates in the range $.3 < \beta < .7$. Results were compared with those from BSI 1042 for discharge coefficients (flange, D-D/2 and corner tappings) and published results for pressure loss coefficients.

The results show that the discharge coefficients predictions are within $\pm 3\%$ of experiment with very close agreement in the mid-range ($\beta \approx .45$). The pressure loss coefficients predictions are within 15% of experiment.

Sensitivity tests were then conducted to see how these coefficients varied with such quantities as inlet velocity

profile, turbulence levels and orifice plate thickness. These results indicated that the orifice is relatively insensitive to velocity profiles (1/12 power law and uniform) and turbulence levels. Also below a certain orifice plate thickness ratio the discharge coefficient is almost constant.

It is concluded that such modelling can be a most valuable aid in understanding the behaviour of the orifice meter and similar devices. In particular this would aid in the design of novel flow meters based on the differential pressure principle.

Extensive mathematical and computational details including the derivation of the $k-\epsilon$ model equations from first principles are relegated to appendices. A source listing of the developed model is also provided in appendix G.

ACKNOWLEDGEMENTS.

The author would like to express his appreciations to all those who have given help during his course of study at The City University, London.

First of all I would like to express my gratitude to my supervisor Professor L.Finklestein and co-supervisor Dr.F.Abdullah from whom I indebted so much, especially in initiating the work.They have always given me valuable guidance constantly throughout my study in the department.I am particularly grateful to Dr.F.Abdullah for the day to day guidance including matters concerning programming and computing.Without such regular help and encouragement I feel I may not have been able to complete this work.It is a privilege to have been worked under the direction of both of my supervisors.

The interests shown, and a deep concern towards this work given by Dr.A.D. Gosman from Imperial College, London in a warm discussions together with Dr. F.Abdullah at the beginning of the course is very much appreciated.These discussions and later important suggestions on the turbulence model have given me much initial help in understanding the very thorough and challenging subject of fluid mechanics and associated numerical modelling procedures.

The main financial support for this work was provided by the National University of Malaysia(UKM) under tutorship grants.This generous financial support is also greatly acknowledged.

PREFACE

A large number of flowmeters are available on the market employing a variety of principles. In the past theoretical techniques have been of limited use in the design of the geometry of such meters because of the complexity of the (usually turbulent) flow. The modern processing power of the digital computer is likely to change this state of affairs. This work is concerned with exploring the feasibility of developing such computer models for an important flowmeter, namely the orifice meter.

The thin circular orifice plate is the most widely used flow rate measuring element with applications in industry and elsewhere. In operation it is characterised by two parameters: the discharge coefficient and the pressure loss introduced by its insertion. In the past a vast amount of experimentation has been undertaken to determine these parameters (particularly the discharge coefficient).

The objectives of this theoretical study were: (i) To develop a valid computer model to incorporate the orifice geometry, the inlet flow conditions and the output quantities of interest such as the various orifice discharge coefficients and the pressure loss coefficient. (ii) To apply this model to a range of orifice geometries and compare the results with those published in BSI1042 and elsewhere. (iii) To investigate the sensitivity of the discharge and pressure loss coefficients to some changes in orifice geometry and inlet flow conditions.

CONTENTS

ABSTRACT	i
ACKNOWLEDGEMENTS	iii
CONTENTS	v
NOMENCLATURE	x
<u>CHAPTER 1 : INTRODUCTION</u>	1
<u>CHAPTER 2 : MATHEMATICAL FORMULATIONS AND SOLUTION PROCEDURES</u>	5
2.1 INTRODUCTION	5
2.2 TIME-DEPENDENT NAVIER-STOKES' EQUATIONS	6
2.21 The Equations	6
2.3 THE TIME-AVERAGED NAVIER-STOKES' EQUATIONS.....	7
2.4 THE $k-\epsilon$ MODEL	9
2.41 Introduction	9
2.42 General Conservation Equations	9
2.5 PROBLEMS OF SOLVING EQUATIONS	14
2.51 Assessment of Difficulties	14
2.52 Main Features of Numerical Solution	16
2.53 Brief Method of Deriving Algebraic Equations	16
2.6 SOLUTION PROCEDURE OF FINITE-DIFFERENCE EQUATIONS	21
2.61 Brief Outline of Procedure	21
2.7 CONCLUDING REMARKS.....	23
<u>CHAPTER 3 : DEVELOPMENT OF A MODEL FOR THIN ORIFICE PLATES</u>	24
3.1 INTRODUCTION	24
3.2 MODIFICATIONS TO TEACH-T PROGRAM	25
3.21 Geometry	25
3.22 Grid Distributions	23

3.23 Boundaries	34
3.24 Boundary Conditions	34
3.25 Calculations of Output Quantities	45
3.3 OTHER PROGRAMMING DETAILS	51
3.4 TESTS ON A $\beta = .7$ THIN ORIFICE PLATE	53
3.41 Introduction	53
3.42 Choice of Upstream/Downstream Distances	54
3.43 Grid Distribution Selection	58
3.44 Sensitivity of Convergence Criteria	60
3.45 Results for $\beta = .7$ Orifice Tests	63
3.5 CONCLUDING REMARKS.	69
<u>CHAPTER 4 : APPLICATIONS OF MODEL AND QUANTITATIVE VALIDATIONS ..</u>	<u>72</u>
4.1 INTRODUCTION	72
4.2 DISCHARGE AND PRESSURE LOSS COEFFICIENTS FOR DIFFERENT β	72
4.3 VELOCITY PROFILE DEPENDENCE	76
4.31 Power-law Profile	73
4.32 Flat Profile	79
4.4 TURBULENCE INTENSITIES AND LENGTH SCALE FACTOR DEPENDENCE	81
4.5 ORIFICE PLATE THICKNESS DEPENDENCE	87
4.6 REYNOLDS NUMBER DEPENDENCE	93
4.7 CONCLUDING REMARKS	96
<u>CHAPTER 5 : CONCLUSIONS</u>	<u>99</u>
BIBLIOGRAPHY	102
APPENDICES	111
<u>APPENDIX A</u>	111
A.1 DERIVATION OF NAVIER-STOKES DIFFERENTIAL EQUATIONS	111
A.2 VORTICITY FORM OF THE NAVIER-STOKES EQUATIONS OF MOTION	116

<u>APPENDIX B</u>	119
B.1 REDUCTION OF NAVIER-STOKES EQUATIONS TO BERNOULLI'S EQUATION ..	119
B.2 APPLICATION OF BERNOULLI'S EQUATION TO ORIFICE PLATES'.....	122
<u>APPENDIX C: MATHEMATICAL FORMULATIONS OF TURBULENCE</u>	127
C.1 INTRODUCTION	127
C.2 THE TIME-DEPENDENT NAVIER-STOKES' EQUATIONS	128
C.21 The Equations	128
C.22 Laminar and Turbulent Flows	129
C.23 Difficulty of Solutions	129
C.3 STATISTICAL THEORY OF TURBULENCE ,.....	130
C.31 Introduction	130
C.32 Derivation of Reynolds Equations	133
C.33 Kinetic Energy of Mean and Turbulent Flows	135
C.34 Statistical Description of Turbulent Flows	138
C.4 THE CLOSURE PROBLEM	141
C.5 THE (k- ϵ) EFFECTIVE VISCOCITY MODEL	143
C.51 Basic Concept	143
C.52 An Algebraic Formula for μ_t	144
C.53 Scalar Turbulent Diffusivity $\Gamma_{\phi,t}$ for ϕ	149
<u>APPENDIX D: DERIVATION OF THE (k-ϵ) TURBULENT MATHEMATICAL MODEL.</u>	151
D.1 ASSUMPTIONS IN THE TURBULENCE MODEL	151
D.2 THE k-EQUATION.....	151
D.3 THE ϵ -EQUATION	155
<u>APPENDIX E: DERIVATION AND SOLUTION PROCEDURES OF FINITE DIFFERENCE EQUATIONS</u>	172
E.1 INTRODUCTION	172
E.2 TRANSPORT FINITE DIFFERENCE EQUATIONS FOR SCALAR VARIABLES ...	172

E.21 Convective and Diffusive Flux Expression	174
E.22 The Source Term S^{ϕ}	178
E.23 The Complete Difference Equations	179
E.3 FINITE DIFFERENCE MOMENTUM EQUATIONS	181
E.4 HANDLING OF PRESSURE LINKAGE	182
E.41 Pressure Solution	183
E.42 Derivation of Pressure-Correction Equation	186
E.5 MISCELLANEOUS MATTERS	189
E.51 Numerical Stability and Convergence of Solution	189
E.52 Accuracy of Solution	192
E.53 Allowance of Mass-flow Imbalance	193
E.6 SOLUTION PROCEDURE OF FINITE DIFFERENCE EQUATIONS	195
E.61 Introduction	195
E.62 The Line By Line Procedure	195
E.7 CONCLUDING REMARKS	199
<u>APPENDIX F: NEAR WALL REMEDIES</u>	201
F.1 INTRODUCTION	201
F.2 WALL FUNCTIONS	202
F.21 Equation of mean Motion	204
F.22 Turbulence Energy k	206
F.23 Rate of Energy Dissipation ϵ	209
F.3 INCORPORATION OF WALL BOUNDARY CONDITIONS	212
F.31 Introduction	212
F.32 Momentum Equation	213
(i) Tangential Velocity	213
(ii) Corner Treatments	217

F.33 Turbulence Quantities	220
(i) Turbulence Energy k	220
(ii) Energy Dissipation ϵ	225
<u>APPENDIX G: PROGRAM FLOWCHART, SUBROUTINES AND PROGRAM LISTING</u>	227

NOMENCLATURE

<u>Symbol</u>	<u>Meaning</u>
A	Cross-Sectional Area
A_j	Coefficients in Finite Difference Equations
B	Body Force per Unit Mass
B_j	Coefficient in Finite Difference Equations
b_f	Constant of Linearised Source Term
C_1, C_2	Constants in ϵ -Equation
C_c, C_v	The Contraction and Velocity Coefficients
C_D, C_d	Constant in k-Equation (for dissipation term) or Discharge Coefficient
C_f	{ Flow Coefficient (ie Discharge Coefficient with Velocity of Approach Factor, $\frac{1}{\sqrt{(1-\beta^4)}}$ Included) or Constant of Linearised Source Term
C_μ	Turbulence Constant
C_j', C_j''	Coefficients in Finite Difference Equations
\hat{d}	Dilation ($=s_{ll} = \frac{\partial \hat{u}_l}{\partial x_l}$)
D_1	Pipe Diameter
D_2	Orifice Plate Diameter
DXU	Upstream Distance
DXD	Downstream Distance
E	Integration Constant
EPSX	Compression/Expansion Factor
f	Relaxation Factor
G	{ Generation or Production of Turbulence Energy or Density x Velocity

g	Acceleration Due to Gravity
i	Turbulence Intensity
k	Turbulence (kinetic) Energy
l	Length Scale
l_m	Mixing Length
M	Residual Mass Source
m	Orifice Area Ratio (A_2/A_1)
\dot{m}'''	Mass Source/Unit Volume
P, p	Pressure (Mean and Fluctuating)
Pe	Peclet Number ($= \rho UL/\Gamma$), L: Linearised Dimension
ρ	($= -\overline{u_i u_j} S$)
\dot{q}	Combined Convection and Diffusion Rate Across a Surface
Re	Reynolds Number ($= UL/\nu$)
r	Radial Distance From Axis of Symmetry
\dot{S}'''	Generation per Unit Volume
S^ϕ	Source Term for Variable ϕ
S_P^ϕ, S_U^ϕ	Constants of Linearised Source Term
S_{ij}	Mean Strain Rate ($= \frac{1}{2} (\frac{\partial U_i}{\partial x_j} + \frac{\partial U_j}{\partial x_i})$)
t	Time or Thin Orifice Plate Thickness
T_{ij}	$\left\{ \begin{array}{l} (-\sum_{ij} - \rho \overline{u_i u_j}), \text{Stresses due to Mean Strain Rate } S_{ij}, \\ \text{Mean Pressure } P \text{ and Turbulent Fluctuations } -\rho \overline{u_i u_j}. \end{array} \right.$
U^+	Non-Dimensional Velocity in wall Region ($= U/U_\tau$)
u	Velocity Scale
U_i	Mean Velocity Component in Direction- i
U_τ	Friction Velocity ($= \sqrt{\tau_w/\rho}$)
$-\rho \overline{u_i u_j}$	Reynolds Stresses
$-\rho \overline{u_j \phi'}$	Turbulent Scalar Fluxes

u	Velocity Fluctuations in Direction-x
U	Mean Velocity in Direction-X
v	Radial Direction Velocity Fluctuations
V	Mean Radial Velocity
X	Distance Measured in Direction of Flow
X	General Cartesian Coordinates
y	Normal Distance From The Wall
y^+	Local Reynolds Number ($= U_{\tau} y/\nu$)

Greek Symbols

β	Orifice Plate to Pipe Diameter Ratio ($= D_2/D_1$)
δ	Convergence Criteria
δ_{ij}	Kronecker Delta ($=1$ if $i=j$, zero otherwise)
ϵ_{ijk}	Alternating Tensor ($=+1$ if i,j,k forms a cyclic permutation of 1,2,3, $=-1$ if i,j,k forms an anticyclic permutation of 1,2,3, and has value zero if any two of i,j,k are equal).
δV	
∇	Gradient Operator ($= i \frac{\partial}{\partial x} + j \frac{\partial}{\partial y} + k \frac{\partial}{\partial z}$)
ϵ	Dissipation Rate
γ	($= \rho g$)
ρ	Fluid Density
ν	Kinematic Viscosity ($= \mu \rho^{-1}$)
λ	Taylor Microscale ($< \ell$) or Length Scale Factor
τ	Shear Stress
τ_{ij}	Reynolds Stress ($= -\rho \overline{u_i u_j}$)
\mathcal{K}	Von Karman Constant
ϕ	Dependent Variable

μ	Laminar Viscosity
μ_t	Turbulent Viscosity
σ_k	Prandtl/Schmidt Number for k-equation
σ_ϵ	Prandtl/Schmidt Number for ϵ =equation
$\Gamma_{\phi, eff}$	Effective Exchange coefficient for variable ϕ
ω	{ Vorticity Vorticity Fluctuation
Ω	Mean Vorticity

Subscripts

1,2,3	{ Direction of Cartesian Coordinate System, Region Upstream of Orifice Plate, at Orifice Plate and Vena Contracta
eff	'Effective' (or Turbulent Value)
f	'False Value'
Max	Maximum Value
in	'inlet'
av	average
t	turbulent value
w	Value at Particular Boundary, w
wall	Value at wall
N,S,E,W,P,	Node Points
n,s,e,w,	Mid-node Points
ew,ns,	Subscripts for Cross-sectional Area for Scalar Cells

Superscripts

*	Guessed Value or Value of Previous Iteration
old	Previous Iteration.
ϕ	Value Relating to Variable ϕ
'	Corrected Value (eg. $U = U^* + U'$)

A

Instantaneous Values

Average with respect to time.

CHAPTER 1.

INTRODUCTION.

Orifice meters are extensively used in engineering applications in industry. The orifice plate is one of the oldest known devices for measuring fluid flow (NEL, 1960). Records show it was used by the Romans for regulating water flow to householders.

About sixty to seventy years ago, the importance of the orifice plate was realised. This was largely based on the extensive and pioneering work of Judd (who presented the original discharge coefficients for concentric, eccentric and segmental type orifices in 1916, NEL(1960)). The simplicity of manufacture of the orifice plate gradually led to its very widespread use. So much so it is now the most common flow rate measuring device being used for measuring large volumes of gases and liquids for sale and for the control of flow rates in continuous processes.

As the use of orifice meters became widespread a huge amount of experimental work was carried out to investigate the properties of orifice meters. This eventually led to the establishment of various national (BSI, ANSI, DIN) and international (ISO) standards for flow metering using thin orifice plates.

The working equations for orifice metering are derived from Bernoulli's equation which describes inviscid high Reynolds number turbulent flow (see Appendix B for their derivation). For real fluids

Bernoulli's equation is only approximate and this is reflected in the fact that the discharge coefficient in the working equation needs to be determined experimentally. The more fundamental equations are the Navier-Stokes' (Appendix A) from which Bernoulli's equation can be formulated (see Appendix B).

Up to recent times the possibility of solving the general Navier-Stokes' equations for turbulent flows was considered impracticable because of the vast range of length and time scales encountered in such flows. Recently however, advances in the processing power of digital computers coupled with the development ^{of} approximate 'closed' models of turbulence based on the time average Navier-Stokes' equations enable one to solve the Navier-Stokes equations for a class of flows of engineering interest. Among these are those where recirculation occurs such as that encountered downstream of an orifice. A highly successful turbulent model that has been tested extensively is the so-called 'k-ε' 'two' equation turbulent model developed at Imperial College, London (Gosman, 1979). Such a model has been successfully tested against recirculating flows similar to those encountered downstream of an orifice plate. In fact the model has been applied successfully to a sudden expansion flow (Gosman, 1979) including the prediction of reattachment lengths. This flow forms the example flow in the program TEACH-T (for Teaching Elliptic Axisymmetrical Characteristics Heuristically for Turbulent flow) available from Imperial College.

The flow in an orifice meter is more complex because in addition to a downstream expansion region there is an upstream region

where the flow is forced to contract by the presence of the orifice plate. The importance of the orifice in flowmetering led to author to investigate the possibility of modifying the TEACH-T program to model the thin orifice plate. This then formed the basis for the present study. The main objectives were to develop a model for orifice metering, to test this model with available data for discharge and pressure loss coefficients and to perform some sensitivity tests using the model for both geometric and flow parameters.

The layout of the thesis is such that in chapter 2 the mathematical formulations and numerical procedures for the computer solution adopted in TEACH-T program are outlined. Details are provided in Appendix E. Although this is not original work it has been presented here for the sake of completeness. The basic derivation of the $k-\epsilon$ models are also mentioned. The derivation is from first principles including that of the Navier-Stokes equations.

In chapter 3 the development of orifice plate model is described. This includes the modifications necessary to the TEACH-T computer program to incorporate geometry, boundary conditions, upstream/downstream modelling regions, choice of number of grids and their distributions etc based on a $\beta = 0.7$ orifice plate.

The bulk of the results are presented and discussed in more detail in chapter 4 for such quantities as discharge and pressure loss coefficients and sensitivity of the orifice plate to variations of parameters such as velocity profile, turbulence levels, orifice thickness and Reynolds number. Chapter 5 concludes the results and gives summary

and recommendations for future studies.

The thesis contains a large number of Appendices (A-G) where much of the mathematical detail is described. Appendix A shows the derivation of the Navier-Stokes' equation for general flows. The vorticity form of the equation is also presented since this forms the basis for deriving the ϵ -equation (discussed in Appendix D).

The reduction of the Navier-Stokes' equation to Bernoulli equation which in turn applies to orifice plate is given in Appendix B.

The time-dependent and time-averaged Navier-Stokes' equations were given in Appendix C under Mathematical Formulations of Turbulence. The basic concept of the $k-\epsilon$ effective viscosity model is also mentioned. Appendix D gives the derivations of the $k-\epsilon$ turbulent mathematical model from first principles.

The incorporation of wall boundary conditions and wall functions under the title 'Near Wall Remedies' is discussed in Appendix F. The formulations of finite difference equations for the variables of interest and the SIMPLE (for Semi-Implicit Method for Pressure Linked Equation) and LBL (for Line By Line) solution procedures were presented in Appendix E. Finally Appendix G gives the program flowchart, subroutines and FORTRAN program listing for the model developed in this study.

CHAPTER 2.MATHEMATICAL FORMULATIONS AND SOLUTION PROCEDURES.2.1: INTRODUCTION.

In attempting to model fluid flow processes, it is necessary to derive some mathematical formulations which adequately describe the flow.

For Newtonian fluids (ie those fluids where shear stresses are directly proportional to velocity gradients) such equations have been formulated. These are the well known Navier-Stokes' differential equations which are derived on the assumption that the fluid may be treated as continuum (for derivation of the equations see Appendix A).

In this chapter, the various differential equations describing turbulent flow are stated beginning with the Navier-Stokes' equations, leading to the time-averaged Reynolds equations and finally the derived (k- ϵ) turbulent model for axi-symmetric pipe flow. Details of the derivation of these equations are provided in the Appendices.

Section 2.4 deals with the problems of solving the transport equations of the (k- ϵ) model and includes the assessment of difficulties and main features of numerical solutions. Brief outline of the solution procedure will be given in section 2.5 (for details see Appendix E).

2.2: TIME-DEPENDENT NAVIER-STOKES' EQUATIONS.

2.21: The Equations.

The basic conservation equations governing fluid flows are those of mass and momentum which expresses the Navier-Stokes' equations. For steady and compressible flow, they may be expressed in Cartesian tensor as,

Mass Conservation.

$$\frac{\partial \rho}{\partial t} + \frac{\partial}{\partial x_j} (\rho \hat{u}_j) = 0 \quad (2.1)$$

Momentum Conservation.

$$\frac{\partial}{\partial t} (\rho \hat{u}_i) + \hat{u}_j \frac{\partial}{\partial x_j} (\rho \hat{u}_i) = \frac{\partial}{\partial x_j} \hat{\sigma}_{ij} + \rho B_i \quad (2.2)$$

$$\text{where } \hat{\sigma}_{ij} = -\hat{p} \delta_{ij} + 2\mu \hat{s}_{ij} - \frac{2}{3}\mu \hat{d} \delta_{ij} \quad (2.3)$$

\hat{u}_i = instantaneous velocity in direction-i (i=1,2,3),

\hat{p} = instantaneous local pressure,

B_i = body force per unit mass in direction-i

$$\hat{s}_{ij} \equiv \frac{1}{2} \left(\frac{\partial \hat{u}_i}{\partial x_j} + \frac{\partial \hat{u}_j}{\partial x_i} \right) \quad (2.4)$$

= instantaneous rate of strain tensor,

δ_{ij} = kronecker delta (=1 if i=j; =0 if i≠j)

ρ = fluid density,

μ = fluid viscosity, and

\hat{d} ($\equiv \hat{s}_{ll} = \frac{\partial \hat{u}_l}{\partial x_l}$) = dilation.

Equations (2.2)(which is actually three equations for $i=1,2,3$) is derived from Newton's Second law of motion and is commonly called the Navier-Stokes' equations. Equation (2.1) is the continuity equation which expresses the conservation of mass in a given control volume.

2.3: THE TIME-AVERAGED NAVIER-STOKES' EQUATIONS.

These equations are formed basically by decomposing instantaneous quantities (which depend on space and time) into their means, denoted by capital letters (which depend only on space) and fluctuating quantities, denoted by small letters. The time-mean of the latter quantities are zero (see Appendix C).

By introducing these mean and fluctuating components into equations (2.1) and (2.2), the following equations are obtained for steady incompressible ^{flow} (with body forces neglected),

Continuity.

$$\frac{\partial}{\partial x_j} U_j = 0 \quad (2.5)$$

Momentum.

$$U_j \frac{\partial}{\partial x_j} U_i = \frac{1}{\rho} \frac{\partial}{\partial x_j} \left\{ \Sigma_{ij} - \rho \overline{u_i u_j} \right\} \quad (2.6)$$

where
$$\Sigma_{ij} = -P \delta_{ij} + 2\mu S_{ij} \quad (2.7)$$

and
$$\sigma_{ij} = -p\delta_{ij} + 2\mu s_{ij} \quad (2.8)$$

are mean and fluctuating stress tensor, due to pressure and viscous forces,

$$S_{ij} = \frac{1}{2} \left(\frac{\partial U_i}{\partial x_j} + \frac{\partial U_j}{\partial x_i} \right) \quad (2.9)$$

is mean strain rate tensor,

δ_{ij} = kronecker delta,

ρ = fluid density,

μ = fluid viscosity,

$$\hat{\sigma}_{ij} = \Sigma_{ij} + \sigma_{ij} ; \bar{\sigma}_{ij} = 0,$$

$$\hat{u}_i = U_i + u_i ; \bar{u}_i = 0,$$

$$\hat{p} = P + p ; \bar{p} = 0,$$

and $\hat{s}_{ij} = S_{ij} + s_{ij} , \bar{s}_{ij} = 0.$

Equations (2.6) are called the Reynolds equations. It is interesting to note that this equation has the same form as equation (2.2) (for a steady incompressible flow and body forces neglected) if \hat{u}_k 's are replaced by U_k 's and stresses $\hat{\sigma}_{ij}$ are replaced by $(\Sigma_{ij} - \rho \overline{u_i u_j})$.

Thus the equations of mean flow are the same as the ordinary equations of motion except that there are additional virtual stresses, called the Reynolds stresses given by,

$$\tau_{ij} = -\rho \overline{u_i u_j} \quad (2.10)$$

which represent the mean rate of transfer of mean momentum across a surface due to velocity fluctuations (Lin(ed), 1959). The turbulence model prescribes how these correlations and other correlations, $-\overline{\rho \phi' u_j}$ arise from scalar convective non-linear terms, are to be found. This problem is called the closure problem which is discussed in Appendix C.

2.4: The k- ϵ Model.

2.41 Introduction.

In Appendix D the (k- ϵ) model has been derived. Here the transport equations for the mean velocities and for the turbulent quantities k and ϵ are stated together with the continuity equation. As we are interested in axi-symmetric pipe flow, these equations are represented in cylindrical polar coordinates (X,r) where X and r are the axial and radial directions respectively.

2.42: General Conservation Equations.

For steady turbulent flows, the governing equations of motion with body forces neglected may be written as follows, (see Appendices A and D for derivations).

(i) Hydrodynamic Equations.

Continuity.

$$\frac{\partial}{\partial x}(\rho U r) + \frac{\partial}{\partial r}(\rho V r) = 0 \quad (2.11)$$

U-Momentum(direction-X).

$$\frac{1}{r} \left\{ \frac{\partial}{\partial x} (\rho U r U) + \frac{\partial}{\partial r} (\rho V r U) \right\} = \frac{1}{r} \left\{ \frac{\partial}{\partial x} (r \mu_{eff} \frac{\partial U}{\partial x}) + \frac{\partial}{\partial r} (r \mu_{eff} \frac{\partial U}{\partial r}) \right\} - \frac{\partial P}{\partial x} + S^U \quad (2.12)$$

V-Momentum(direction-r or -y).

$$\frac{1}{r} \left\{ \frac{\partial}{\partial x} (\rho U r V) + \frac{\partial}{\partial r} (\rho V r V) \right\} = \frac{1}{r} \left\{ \frac{\partial}{\partial x} (r \mu_{eff} \frac{\partial V}{\partial x}) + \frac{\partial}{\partial r} (r \mu_{eff} \frac{\partial V}{\partial r}) \right\} - \frac{\partial P}{\partial r} - \mu_{eff} \frac{V}{r^2} + S^V \quad (2.13)$$

(ii) Non-hydrodynamic Equations.

Turbulence Energy, k.

$$\frac{1}{r} \left\{ \frac{\partial}{\partial x} (\rho U r k) + \frac{\partial}{\partial r} (\rho V r k) \right\} = \frac{1}{r} \left\{ \frac{\partial}{\partial x} (r \frac{\mu_{eff}}{\sigma_k} \frac{\partial k}{\partial x}) + \frac{\partial}{\partial r} (r \frac{\mu_{eff}}{\sigma_k} \frac{\partial k}{\partial r}) \right\} + G - \rho C_D \epsilon \quad (2.14)$$

Turbulence Dissipation Rate, ϵ .

$$\frac{1}{r} \left\{ \frac{\partial}{\partial x} (\rho U r \epsilon) + \frac{\partial}{\partial r} (\rho V r \epsilon) \right\} = \frac{1}{r} \left\{ \frac{\partial}{\partial x} (r \frac{\mu_{eff}}{\sigma_\epsilon} \frac{\partial \epsilon}{\partial x}) + \frac{\partial}{\partial r} (r \frac{\mu_{eff}}{\sigma_\epsilon} \frac{\partial \epsilon}{\partial r}) \right\} + C_1 G \frac{\epsilon}{k} - C_2 \rho \frac{\epsilon^2}{k} \quad (2.15)$$

where S^U and S^V are source terms for U and V respectively and,

$$G = \mu_t \left\{ 2 \left[\left(\frac{\partial U}{\partial x} \right)^2 + \left(\frac{\partial V}{\partial r} \right)^2 + \left(\frac{V}{r} \right)^2 \right] + \left(\frac{\partial U}{\partial r} + \frac{\partial V}{\partial x} \right)^2 \right\} \quad (2.16)$$

σ_k and σ_ϵ appearing in equations (2.14) and (2.15) are the effective Prandtl/Schmidt numbers for turbulence energy and dissipation rate respectively.

Auxiliary.

S^U and S^V are given by (Gosman, 1976),

$$S^U \equiv \frac{\partial}{\partial x} (\mu_{\text{eff}} \frac{\partial U}{\partial x}) + \frac{1}{r} \frac{\partial}{\partial r} (r \mu_{\text{eff}} \frac{\partial V}{\partial x}) \quad (2.17)$$

$$S^V \equiv \frac{\partial}{\partial x} (\mu_{\text{eff}} \frac{\partial U}{\partial r}) + \frac{1}{r} \frac{\partial}{\partial r} (r \mu_{\text{eff}} \frac{\partial V}{\partial r}) - \mu_{\text{eff}} \frac{V}{r^2} \quad (2.18)$$

where $\mu_{\text{eff}} = \mu + \mu_t \quad (2.19)$

and $\mu_t = C_{\mu} \rho \frac{k^2}{\epsilon} \quad (2.20)$

Equations (2.11) through (2.15) have been written for the cylindrical polar coordinates system(x,r).

It may be of interest to note that for cartesian coordinates the transport equations are the same if r is taken to be identical with y and r is set to 1 except the $\mu_{\text{eff}} V/r^2$ term in the V-momentum equation. This term is set to zero. Such equations would then apply to plane two dimensional flows but they are not of interest to us in this study.

μ_{eff} given in the auxiliary ^{equation (2.19)} is the effective viscosity which represents the summation of both laminar and turbulent transport effects. At high Reynolds number ie for a fully turbulent flow (to which the (k- ϵ) model is restricted) the molecular transport effects μ , is comparatively small, hence (2.19) gives,

$$\mu_{eff} = \mu_t \quad (2.21)$$

The source terms S^U and S^V cover additional terms associated with non-uniform viscosity μ_t in the flow domain. Their influence is generally small except where changes in fluid property have considerable effects, particularly near to a wall. These effects will be discussed in Appendix F under wall treatment.

G represents the generation or production of turbulence energy, k from the mean flow by the action of turbulent shear stress and ϵ is the rate of viscous dissipation of k to heat by the smallest turbulent eddies.

The σ 's and C 's are generally empirical functions, but for high Reynolds number flows, they are assumed to be constants having values given by the following table 2.1

C_μ	C_D	C_1	C_2	σ_k	σ_ϵ	\mathcal{K}	E
.09	1.0	1.44	1.92	1.0	1.22	.4187	9.793

Table 2.1: Constants of Computation.

where the value of σ_ϵ was obtained from equation (D.75) (see Appendix D) with $\mathcal{K} = .4187$.

It may be noted that equations (2.14) and (2.15) for turbulent transport, have similar pattern as those of the mean flow equations (see equations (2.12) and (2.13)) if the following substitutions have been made,

$$S^k = G - C_D \rho E \quad (2.22)$$

$$S^E = C_1 G \frac{E}{k} - C_2 \rho \frac{E^2}{k} \quad (2.23)$$

Here, S^k and S^E are respectively called the source terms for turbulence energy, k and its dissipation rate, E .

It is therefore, in general the set of equations (2.11) through (2.15) may be written into a single elliptic equation of the form,

$$\frac{1}{r} \left\{ \frac{\partial}{\partial x} (\rho U r \phi) + \frac{\partial}{\partial r} (\rho V r \phi) \right\} = \frac{1}{r} \left\{ \frac{\partial}{\partial x} (r \Gamma_{xy} \frac{\partial \phi}{\partial x}) + \frac{\partial}{\partial r} (r \Gamma_{xy} \frac{\partial \phi}{\partial r}) \right\} + S^\phi \quad (2.24)$$

where $r=1$ converts the equation from the cylindrical to rectangular cartesian form.

The description of turbulent flows as indicated by equation (2.24) presumes that the mean values of the dependent variables may be represented by this form of equation together with the appropriate boundary conditions.

Equation (2.24) represents a 2-D time-averaged form of the Navier-Stokes' equations. This implies that the flow must be 2-D and the

time-dependence of the flow may be characterised by a turbulence model and the model assures isotropic diffusion with the effective exchange coefficient, $\Gamma_{\phi, \text{eff}}$ is given by,

$$\Gamma_{\phi, \text{eff}} = \Gamma_{\phi, l} + \Gamma_{\phi, t} \quad (2.25)$$

which represents the summation of both the laminar $\Gamma_{\phi, l}$ and the turbulent $\Gamma_{\phi, t}$ exchange coefficient effects.

The term S^{ϕ} in equation(2.24) is the source term of the respective flow variables. The expressions of $\Gamma_{\phi, \text{eff}}$ and S^{ϕ} depend on physical meaning given to ϕ and on the contents of its governing equations. The definitions of ϕ , $\Gamma_{\phi, \text{eff}}$ and S^{ϕ} are given in the following table 2.2(Gosman, 1979).

G , μ_{eff} and μ_t are given in equations (2.16), (2.19) and (2.20) respectively. From table 2.2 it can be seen that the units of $\Gamma_{\phi, \text{eff}}$ are those of viscosity; in fact $\Gamma_{\phi, \text{eff}}$ is often obtained by dividing the effective viscosity μ_{eff} by the appropriate Prandtl/Schmidt number.

2.5: PROBLEMS OF SOLVING EQUATIONS.

2.51 Assessment of Difficulties.

The set of equations given by (2.24) seem to be complex in the sense that they are interlinked, furthermore,

Conserved Property.	ϕ	$\Gamma_{\phi, \text{eff}}$	S^{ϕ}
Mass	1	0	0
Direction-X Momentum	U	μ_{eff}	$-\frac{\partial P}{\partial x} - \frac{1}{\tau} \left\{ \frac{\partial}{\partial x} (\tau \mu_{\text{eff}} \frac{\partial U}{\partial x}) + \frac{\partial}{\partial r} (\tau \mu_{\text{eff}} \frac{\partial V}{\partial x}) \right\}$
Direction-r-or-y Momentum	V	μ_{eff}	$-\frac{\partial P}{\partial r} - \mu_{\text{eff}} \frac{V}{\tau^2} + \frac{1}{\tau} \left\{ \frac{\partial}{\partial x} (\tau \mu_{\text{eff}} \frac{\partial U}{\partial r}) + \frac{\partial}{\partial r} (\tau \mu_{\text{eff}} \frac{\partial V}{\partial r}) \right\}$
Turbulence Energy	k	$\frac{\mu_{\text{eff}}}{\sigma k}$	$G - c_D \rho \varepsilon$
Dissipation Rate	ε	$\frac{\mu_{\text{eff}}}{\sigma \varepsilon}$	$c_{1G} \frac{\varepsilon}{k} - c_2 \rho \frac{\varepsilon^2}{k}$

Table 2.2: Definitions of ϕ , $\Gamma_{\phi, \text{eff}}$ and S^{ϕ} of Equation (2.24).

(i) they are non-linear, this may arise from convection and source terms.

(ii) for each variable (U, V, k and ϵ) to be solved, its transport equation contains velocity components which appear simultaneously.

(iii) complexity-second-order partial differential equations.

All these features render the equations not suitable for direct analytical calculations. It is therefore necessary to use numerical methods of solutions.

2.52: Main Features of Numerical Solution.

The equations already stated use the 'primitive' variables namely the velocities and pressures. These are formulated as finite difference equations and solved iteratively using the SIMPLE (for Semi-Implicit Method for Pressure Linked Equations) algorithm's procedure to obtain the pressure. All other transport equations are solved by LBL (for Line By Line) method of TDMA (for Tri-Diagonal Matrix Algorithms).

2.53: Brief Method of Deriving Algebraic Equations.

The main features of numerical method is to reduce the governing partial differential equations into an equivalent set of algebraic equations which involve approximation.

There are methods of transforming the partial differential equations into the finite difference form-this includes Taylor series expansion and the micro-integration of Gosman(1976).In this study,the latter method is used (for more detail see Appendix E).

(a):Finite Difference Equations for Scalar Variables.

When the partial differential equations of (2.24) is integrated over the control volume (see fig.2.1) and by using Gauss theorem to replace the volume integrals into surface ones,the following expressions will be obtained(see Appendix E for details),

$$\dot{q}_e - \dot{q}_w + \dot{q}_n - \dot{q}_s = \int_V S^\phi dV \quad (2.27)$$

where \dot{q} 's are combined convection and diffusion terms, S^ϕ being the source term for scalar variables, ϕ and V is the control volume over which the integration was performed.e,w,n and s are points on the boundaries of the control volume (cell) situated mid-way between nodes E,W,N and S from point P as shown in fig.2.1.

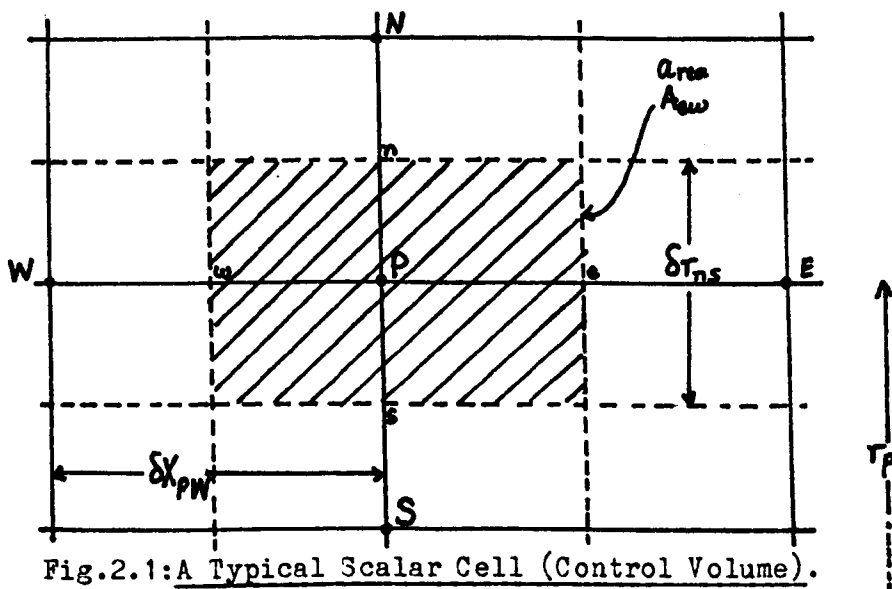


Fig.2.1: A Typical Scalar Cell (Control Volume).

Each of the \dot{q} 's are then related to the values of ϕ at node points in the calculation domain, which has the form, for example, for the west boundary, (see also fig. E.2, Appendix E)

$$\dot{q}_w = \rho_w U_w \frac{1}{2} (\phi_P + \phi_W) A_w - \Gamma_{\phi, w} A_w \frac{(\phi_P - \phi_W)}{\Delta X_{PW}} \quad (2.28)$$

for small local Peclet number, ($-2 < Pe_w < +2$) where,

$$Pe_w = \frac{\rho_w U_w \Delta X_{PW}}{\Gamma_{\phi, w}} \quad (2.29)$$

For large $|Pe|$ i.e. for $Pe \gg +2$ or $Pe \ll -2$, \dot{q}_w has the following forms,

$$\left. \begin{aligned} \dot{q}_w &= \rho_w U_w A_w \phi_W \quad \text{if } Pe_w \gg 2 \\ \dot{q}_w &= \rho_w U_w A_w \phi_P \quad \text{if } Pe_w \leq -2 \end{aligned} \right\} \quad (2.30)$$

In equations (2.28) and (2.30), subscripts P and W refer to the central and west nodes respectively and w denotes the intermediary cell boundary mid-way between nodes P and W.

By employing the 'hybrid scheme' (i.e. the combination of central and upwind differencing), equations (2.28) and (2.30) may be rewritten as,

$$\frac{\dot{q}_w}{\rho_w U_w A_w} = \begin{cases} \frac{1}{2} [(1 + 2Pe_w^{-1})\phi_W + (1 - 2Pe_w^{-1})\phi_P], & -2 < Pe_w < 2 \\ \phi_W & Pe_w \gg 2 \\ \phi_P & Pe_w \leq -2 \end{cases} \quad (2.31)$$

Similar treatments apply for other boundaries of the control volume to obtain the fluxes \dot{q}_e, \dot{q}_n and \dot{q}_s . By assembling these flux expressions and by linearising the source terms, S^{ϕ} , the complete finite difference equations for scalar variables has the form (see Appendix E for its derivation),

$$(a_p - S_p^{\phi})\phi_p = \sum_n a_n \phi_n + S_U^{\phi} \quad (2.32)$$

$$\text{where } a_p = \sum_n a_n \quad (2.33)$$

\sum_n = summation over neighbours (N, S, E, W),

$$a_W = \rho_w U_w A_w f_w \quad \text{etc.} \quad (2.34)$$

and f_w etc. are given by equation (E.18) (see Appendix E). S_p^{ϕ} and S_U^{ϕ} may be deduced from S^{ϕ} for each scalar variables (k and ϵ ; and see table 2.2).

(b): Finite Difference Equations for Momentum Equations.

The finite difference momentum equations have similar form as equation (2.32) for scalar variables, except with additional terms due

to pressure gradients. The control volumes of velocity components are displaced since their locations themselves are displaced as can be seen in fig.2.2.

The finite difference equations for momentum have the form,

$$(a_p - S_p^U) U_p = \sum_n a_n U_n + A_{ew} (P_w - P_p) + S_u^U \quad (2.35)$$

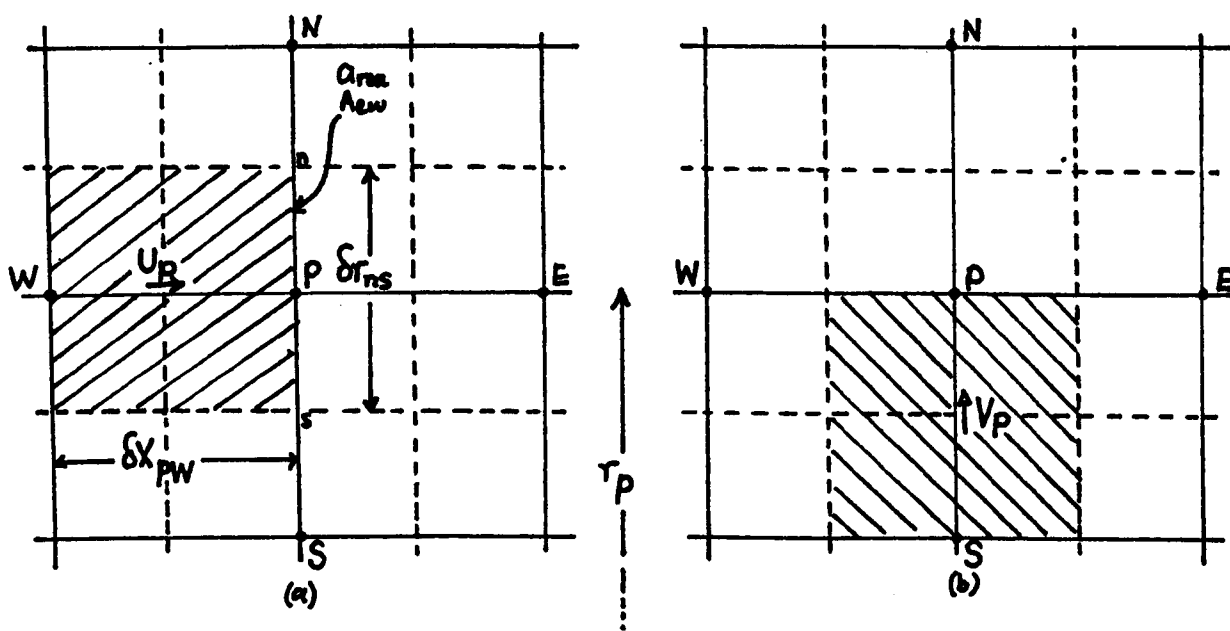


Fig.2.2: A Typical U- and V- cells (control volumes).

where a_p, a_w etc. are similar to equations (2.33) and (2.34) but f_w now is a hybrid difference function of local Reynolds number, Re_w where,

$$Re_w = \frac{\rho_w U_w \Delta x_{pw}}{\mu_w} \quad (2.36)$$

$$A_{ew} = r_p \Delta \tau_{ns} \quad (2.37)$$

The remaining unknown pressures are obtained from pressure

correction(p')- equation which is obtained by combining continuity and momentum equations(see Appendix E for p' -equation derivation). This equation has the form,

$$a_p p'_p = \sum_n a_n p'_n + M_p \quad (2.38)$$

where $a_p = \sum_n a_n$

$$\sum_n \equiv \text{summation over neighbours}$$

$$a_w = \rho_w D_w A_{ew} \quad \text{etc.} \quad (2.39)$$

$$D_w = A_{ew}/a_p \quad (2.40)$$

$$A_{ew} = r_p \delta r_{ns} \quad (2.41)$$

Here S_u^ϕ is now represents the local continuity imbalance in the prevailing velocity fields and denoted by M_p , and $S_p^\phi = 0$.

2.6: SOLUTION PROCEDURE OF FINITE DIFFERENCE EQUATIONS.

2.61: Brief Outline of Procedure.

Having constructed algebraic equations for all nodes in the calculation domain, next job will be to solve those set of equations

simultaneously with appropriate boundary conditions.

Since the equations are non-linear and inter-linked, to solve the finite difference equations is by iterative method, which employs inner and outer iteration sequences. The inner iteration sequence is employed to solve the finite difference equations for the individual variables, while the outer iteration sequence involves the cyclic application of the following steps,

Assemble coefficients of momentum equations and estimated values of axial and radial velocities (denoted by U^* and V^*) are obtained from the momentum equations using the prevailing pressures, p^* .

The coefficients of the p' -equation (for the pressure correction) are next assembled and this equation is solved by the LBL method (see Appendix E).

The velocities and pressures are then adjusted (corrected) from the relations like,

$$U'_w = D_w (P'_W - P'_P) \quad (2.42)$$

$$U = U^* + U' \quad (2.43)$$

$$P = P^* + P' \quad (2.44)$$

The equations for the remaining variables (k and ϵ) are then solved in turn, first by assembling the coefficients of the transport

finite difference equations to obtain k and ϵ .

Regard the new values of the variables as improved estimates and the whole process is repeated until satisfactory solution is obtained-this will be discussed later in Appendix E, under 'convergence'.

2.7: CONCLUDING REMARKS.

Mathematical formulations and solution procedure of solving the governing finite difference equations have been discussed briefly (details will be obtained in Appendix E). The main points of the chapter may be summarised as follows:

The basic conservation differential equations which govern the transport of mass and momentum have been presented for time-dependent and time-averaged form.

The general form of the closed k - ϵ model equations for mean flow variables and turbulence quantities (k and ϵ) have been stated and their manner of solution using a finite difference formulation has been discussed (details are discussed in Appendices D and E).

Much of the work presented in this chapter has been derived by researchers at Imperial College, London. This work has been presented here for the sake of completeness.

CHAPTER 3.DEVELOPMENT OF A MODEL FOR THIN ORIFICE PLATES.3.1: INTRODUCTION.

This chapter shows how a mathematical model is developed for thin orifice plates. The model is tested on an orifice plate with orifice to pipe diameter ratio of 0.7. The model is based on the solution of the set of coupled differential equations described in the previous chapter. The variables to be solved for are velocities: U (axial), V (radial) and turbulent quantities: k (kinetic energy), ϵ (dissipation rate). The pressure, p , being a derived quantity may be obtained from pressure correction equation (described in Appendix E).

The development of a model for orifice metering requires:

(i) The modification of the TEACH-T program, developed at Imperial College, London to incorporate the geometry of the orifice meter and output quantities of interest.

(ii) Choice of upstream/downstream distances.

(iii) Selection of number of finite difference grid points in region of interest.

(iv) Determination of an adequate convergence criteria to the

iterative solution procedure for solving the equations.

Steps (ii),(iii) and (iv) are approached iteratively to obtain the final model described in section 3.4.

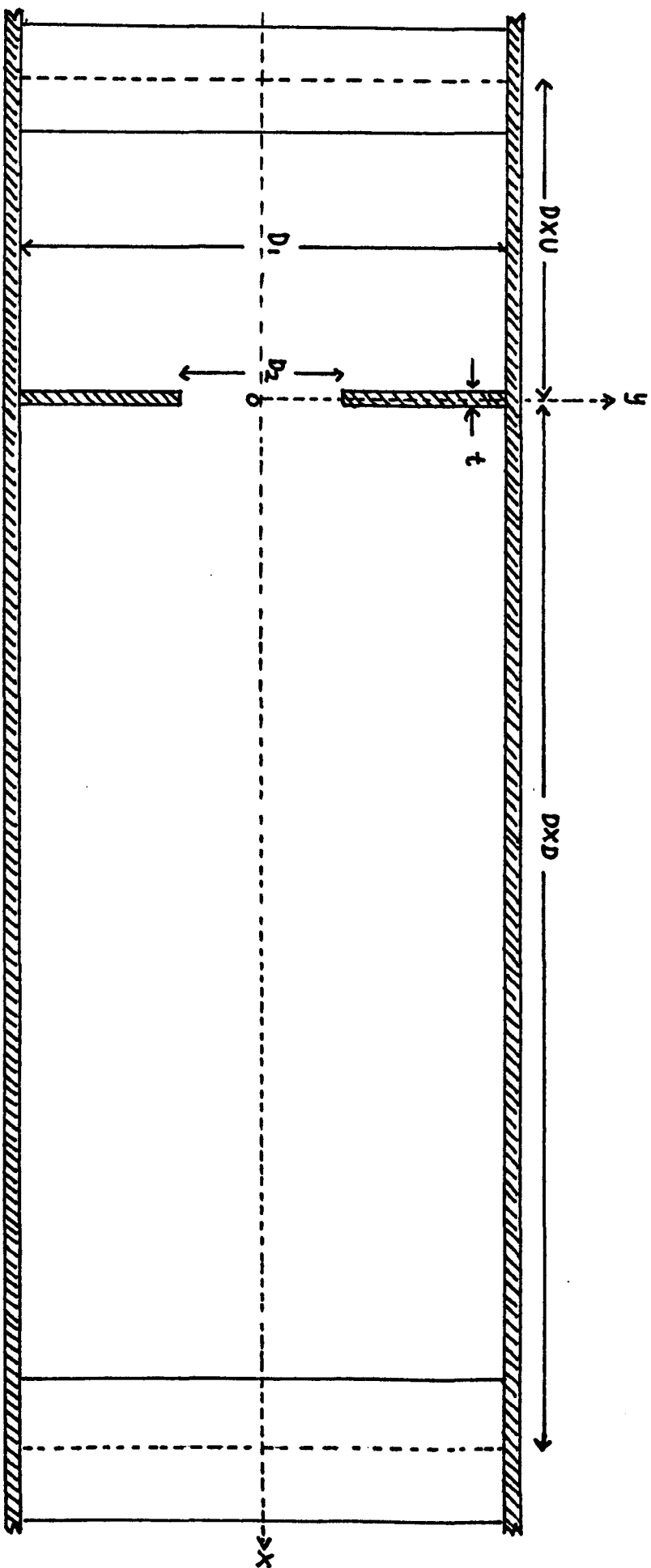
3.2:MODIFICATIONS TO TEACH-T PROGRAM.

3.21 Geometry.

Figure 3.1 shows a cross-sectional diagram of location of a thin orifice plate which is co-axial with the pipe axis denoted by OX. The diameter of the pipe is 4 inches. The y-axis passes through the orifice plate and perpendicular to OX. The orifice plate is assumed to be very thin similar to the one shown in figure 3.2(b) which is an idealised form of the plate shown in fig.3.2(a). The practical reason why orifice plates are always thin will become clear when plate thickness dependence on discharge coefficients is discussed later in section 3.45(iii).

There are three basic dimensions for orifice meter to be considered namely the plate thickness t , the orifice diameter D_2 and the pipe diameter D_1 .

Non-dimensional geometrical parameters which are so important in orifice metering are the orifice to pipe diameter ratio, β and the thickness to plate diameter ratio, t/D_2 . These two parameters may be formed from the basic parameters quite easily. The square of the former parameter $m = \beta^2$ being the ratio of the total cross-sectional area, is a



D_1 : Pipe Diameter

DXU : Upstream Distance

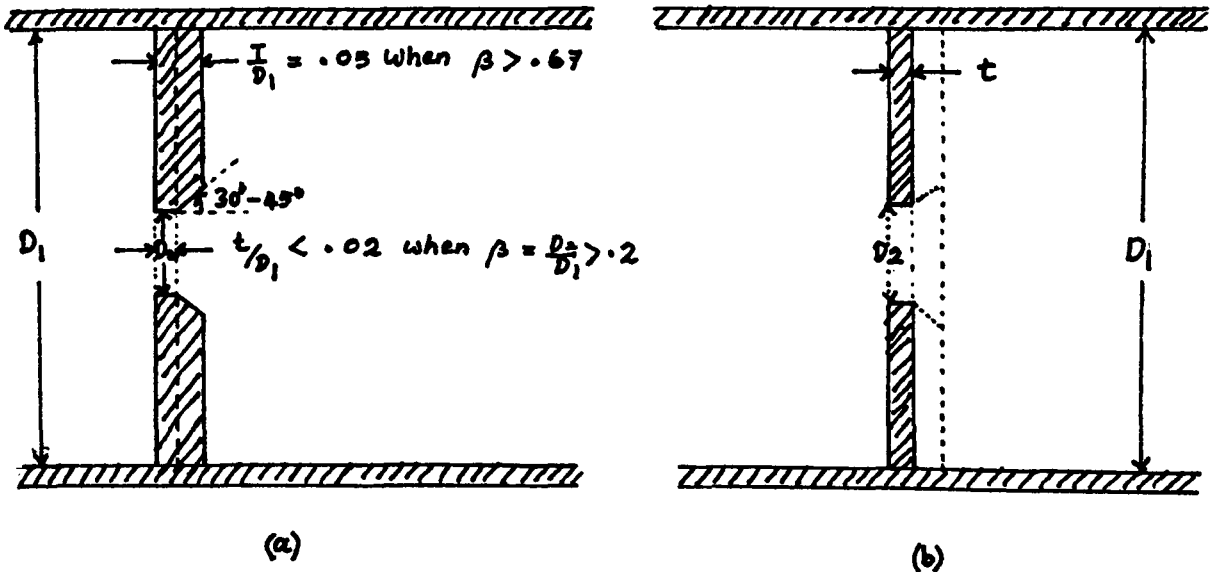
D_2 : Orifice Diameter

DXD : Downstream Distance

t : Orifice Plate Thickness

Fig.3.1 : A sketch of Orifice Plate location in a Pipeline.

measure of the extent to which the constriction obstructs the flow. The latter parameter is a convenient specification of the orifice geometry.



D_1 = pipe diameter,
 D_2 = orifice diameter,
 t = plate thickness,
and T = overall plate thickness.

Fig.3.2:(a) A Standard Orifice Plate, BSI1042 (1964).

(b) An Idealised Form of Orifice Plate, Ward Smith (1971).

The variable quantities that must be chosen in a model are the distances of inlet and outlet boundaries from the y-axis denoted by DXU and DXD respectively, the number of grids upstream and downstream regions and orifice area ratio, m . The selection of the number of grids in both regions and the distances of upstream and downstream boundaries will be discussed in section 3.4.

3.22 Grid Distributions.

For the purpose of solution, the flow domain is overlaid with a rectangular meshes (grids) when viewed in the y- or r-X plane. This divides the domain of interest completely into a set of non-overlapping subdomains as shown in fig.3.3.

The grid lines are shown in solid lines. The intersections of these grid lines where spacing are in general arbitrary, are called the node points. Control volumes are shown in dotted lines which are drawn mid-way between those grid lines. The arrangement of the grid lines are such that the bounding surfaces coincide with those control volumes. In this figure also one can define the thickness of the orifice plate t by the bounding faces of the orifice plate (which consists of front or upstream face, rear or downstream face and bottom face of the orifice plate) coincident with the control volumes.

In this particular study, the author has chosen a uniform spacing in the radial direction, while in the axial direction, the grids are contracting and expanding following a geometrical progression (with a constant factor $EPSX$ which is defined as the expansion/compression factor) between successive intervals. The grid lines are intended to be crowded just upstream of the orifice plate as expected, because the flow streamlines become crowded as the flow advances from left to right (see figure 3.4). After leaving the orifice, the grids are expanded.

A typical cluster of U-, V- and scalar-cells is shown in

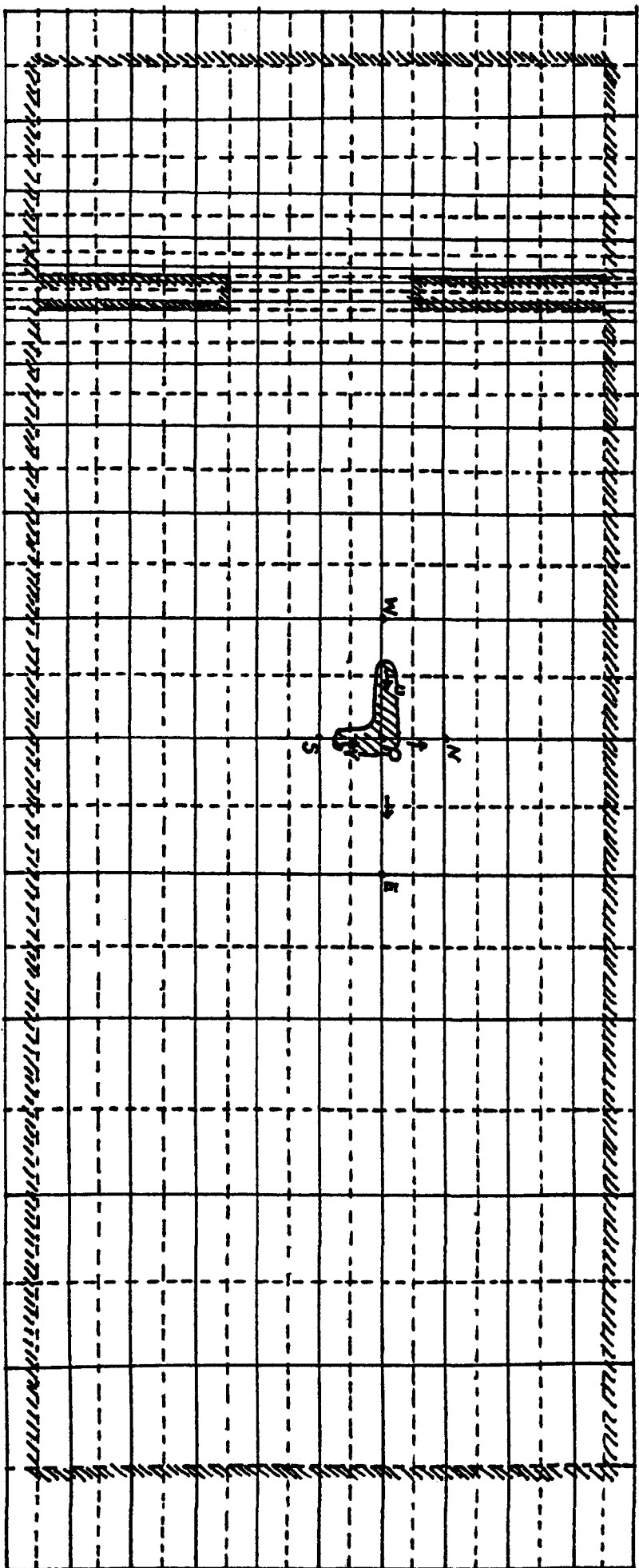


Fig. 3.3: Guide line Distributions.

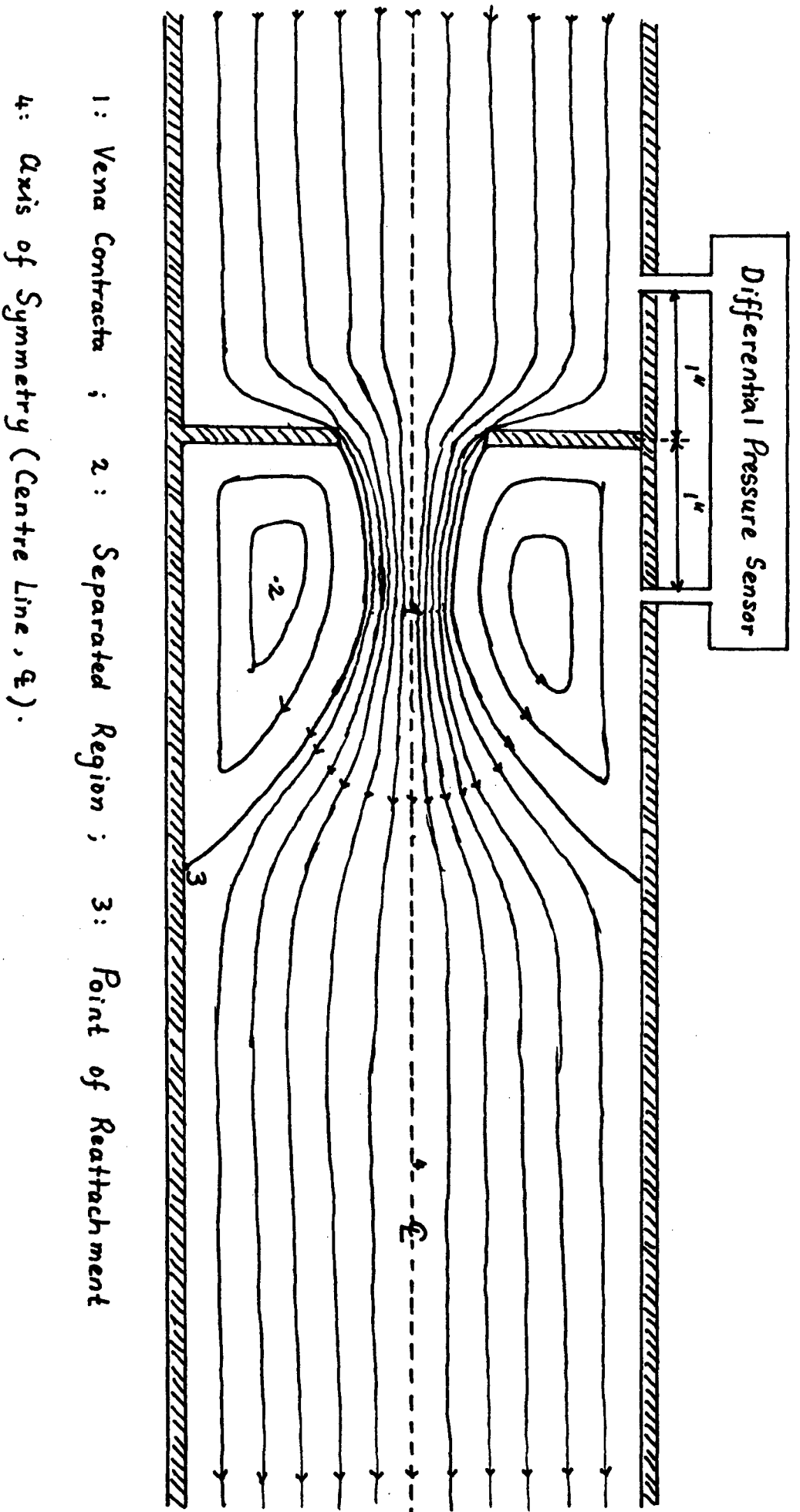


Fig. 3.4 : Orifice Flow sketch.

fig.3.3 whereas fig. 3.5 shows the individual control volumes of the velocity components and scalar quantities (eg.k,the turbulence energy and ϵ the dissipation rate). Each cells surround the point of location of the relevant variables.The variables are stored in different locations of the grids.The values of the flow variables are represented by averages over the respective control volumes.Refering to fig.3.5(c),all the scalar variables p,k,ϵ are stored at grid nodes.The velocities are stored at locations mid-way between the nodes where pressure which drives them are stored.The nodes of a typical grid cluster are labelled as P,N,S,E and W (as shown in fig.3.5).

The location of the variables in the manner described above forms a staggered grid system which has the advantage that the variables U,V and p are stored in such a way that pressure gradients are easy to evaluate.Furthermore,the velocities are located where they are needed for the calculation of convective fluxes.

Figure 3.6 shows the computational domain of calculation which is actually the upper half of fig.3.3 (this is taken because of the consequence of the symmetry situation).Again the grid lines are arranged in such a way that the bounding surfaces(wall boundaries,which include top walls of pipe, front face, bottom face and rear face of the orifice plate,symmetry axis and inlet/outlet boundaries),coincide with the boundaries of the control volumes(shown as dotted lines). This is advantageous for ensuring conservation and for flux calculations.In the finally chosen model the number of grid lines in axial direction, N_I is taken to be 32 with (16/16) grid distributions upstream/downstream

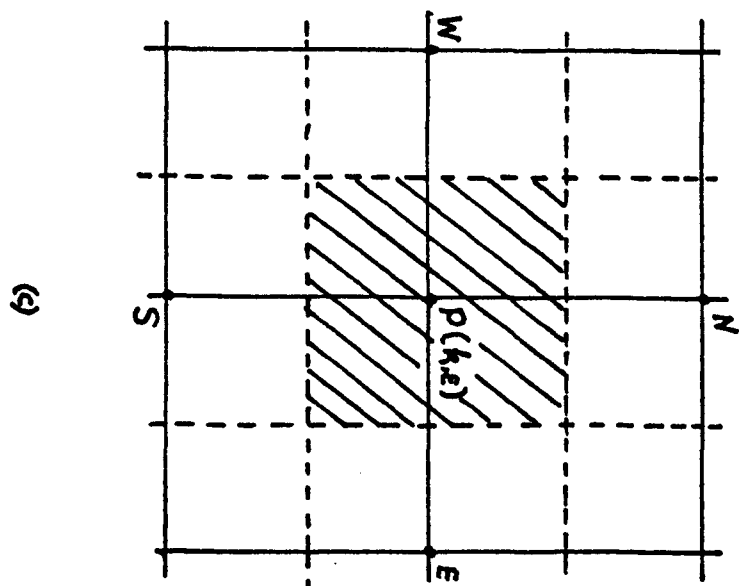
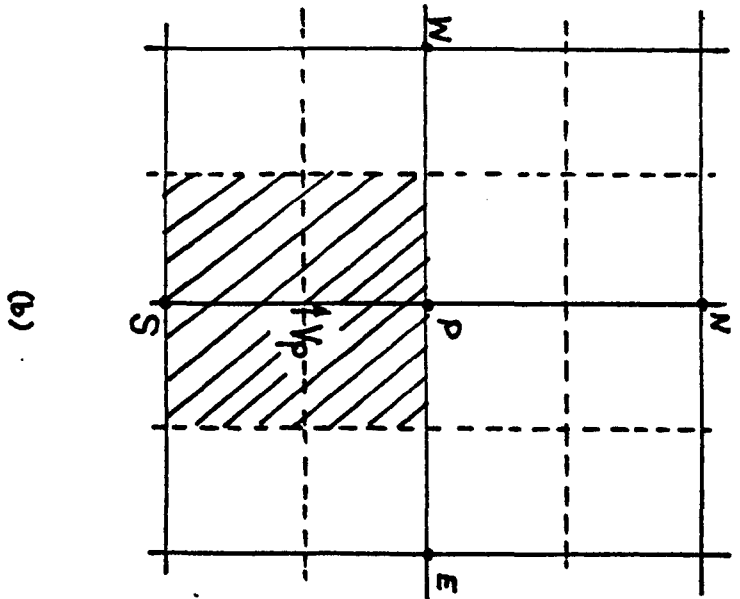
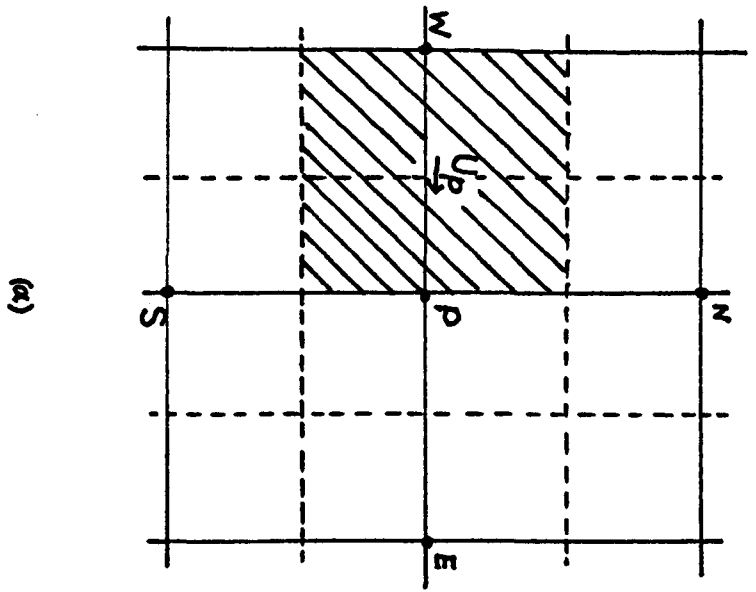


Fig. 3.5: A Typical U-, V- and Scalar- Cells (Control Volumes).

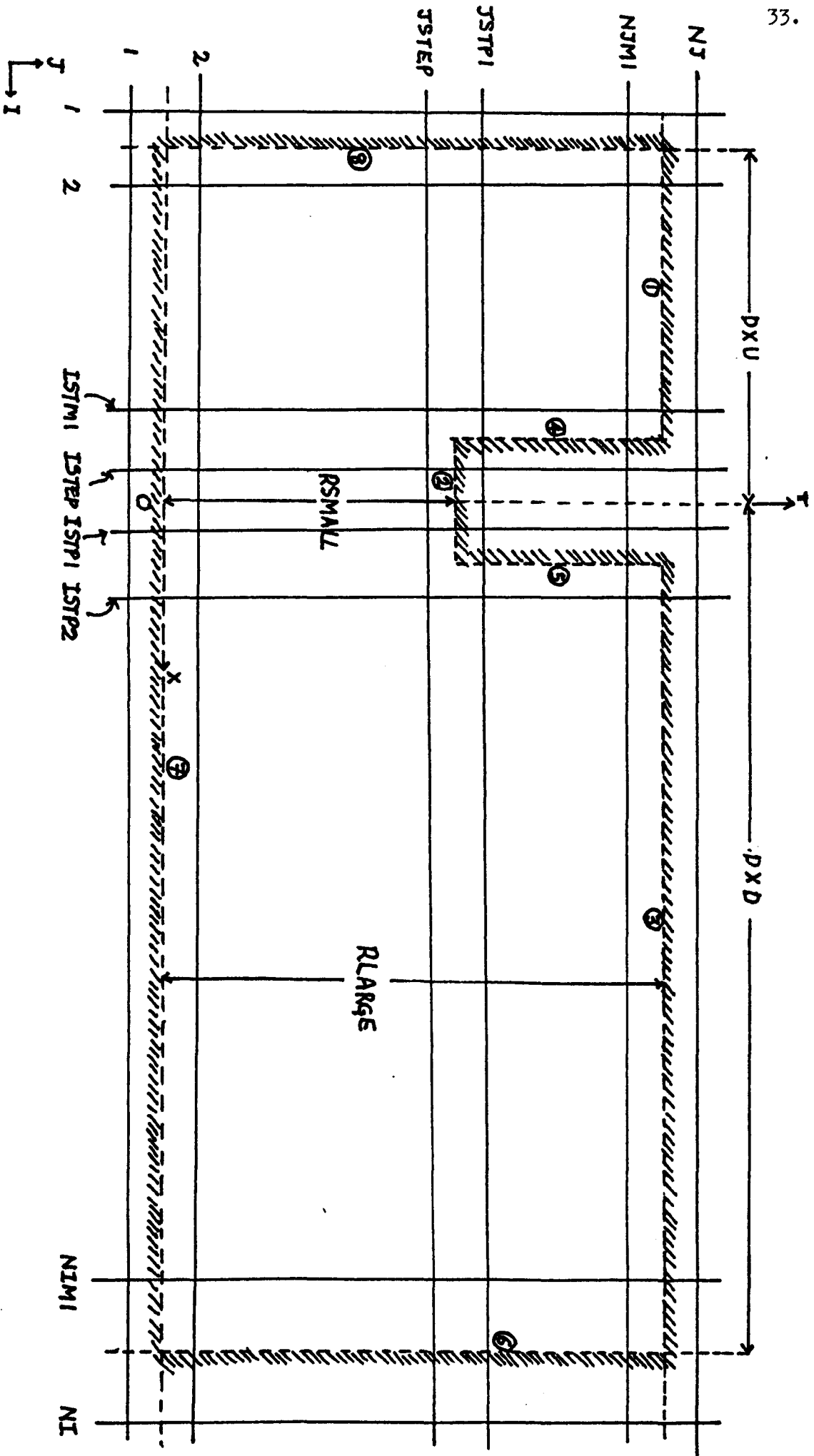


Fig. 3.6 : Computational Domain of Calculation.

regions. In radial-direction, the number of grids, N_J is taken to be 22. The reason for the choice of these parameters will be discussed in section 3.4. Other computational details will be found in section 3.3.

3.23: Boundaries.

The boundaries of the computational domain are shown in fig. 3.6. They consist of eight boundaries altogether; inlet, outlet, symmetry axis and wall boundaries. The wall boundaries themselves are made up of five solid boundaries (two of which are top wall boundaries in regions 1 and 3, two boundaries being front face and rear face of the orifice plate denoted by numbers 4 and 5 and the last boundary is the bottom wall of the orifice plate in region 2). As has been mentioned earlier, these boundaries as well as inlet and outlet boundaries coincide with the control volumes. The inlet and outlet boundaries are specified by distances DXU and DXD respectively from OY -axis. Top pipe walls and bottom face of the orifice plate are at distances $R (=RLARGE)$ and $r (=RSMALL)$ respectively from the axis of symmetry (R and r stand for pipe and orifice radius respectively).

3.24: Boundary Conditions.

Since the working equations of motion in this study is of an elliptic type, it is necessary to supply conditions for each variables at the boundaries of the flow domain. In this particular study, the variables for which boundary conditions to be supplied are those for velocity components in axial and radial directions, U and V and turbulent quantities k and ϵ . The pressures may not be modified on boundary, since they are inter-dependent with velocity components

through momentum transport equations-where velocities are prescribed, pressures need not be.

(i) At Inlet.

At the inlet all velocity components and turbulent quantities must be prescribed. The radial velocity V is set to zero. For the axial velocity, U two velocity profiles were used, one is of uniform (or flat) profile and the other is of power law which has the form,

$$U(r) = U_{max} \left(1 - \frac{r}{R}\right)^{\frac{1}{p}} \quad (3.1)$$

where R and r are respectively the pipe and orifice radius, p is a function of pipe Reynolds number Re given by (Blake (et al), 1976)

$$p = 7.48 + 5.83 \times 10^{-5} (Re_1) - 4.16 \times 10^{-2} (Re_1)^2 \quad (3.2)$$

and U_{max} is given by,

$$U_{max} = \frac{1}{2} \left(1 + \frac{1}{p}\right) \left(2 + \frac{1}{p}\right) U_{in} \quad (3.3)$$

where U_{in} is the averaged inlet axial velocity. Equation (3.3) was obtained by integrating equation (3.1) to obtain the average flow velocity U_{in} .

For uniform profile, the mean axial velocity U is set to,

$$U = U_{in} \quad (3.4)$$

where the average inlet axial velocity U_{in} is given by,

$$U_{in} = \frac{\mu Re_1}{\rho D_1} \quad (3.5)$$

which is a known value if fluid viscosity μ , pipe Reynolds number Re_1 , fluid density ρ and pipe diameter D_1 are given values.

While the mean axial velocity U has known inlet value, the radial velocity V is assumed to be of zero value on the axis of symmetry throughout the domain of calculation.

The inlet profiles of turbulence energy k and its dissipation rate ϵ are given by specifying turbulence intensity i and length scale factor λ through the following relationship,

$$k = k_{in} = i U_{in}^2 \quad (3.6)$$

$$\epsilon = \epsilon_{in} = \frac{k_{in}^{\frac{3}{2}}}{\lambda} \quad (3.7)$$

$$l = \lambda R \quad (3.8)$$

where l = length scale,
 λ = length scale factor,
 R = pipe radius,
 i = intensity of turbulence,
 k = turbulence (kinetic) energy,
 ϵ = dissipation rate

and the subscript 'in' stands for 'inlet'.

The dissipation rate has been assumed to follow a mixing length hypothesis.

Initially the values of i, λ, U_{in} and R are given from where the inlet values of k_{in} and ϵ_{in} are obtained from relations (3.6) through (3.8).

(ii) At Outlet.

The flow at ^{the} outlet is assumed to be outwardly directed and independent of x , (the axial direction). This would be the case far downstream of the orifice. This implies a zero gradient at the flow outlet, i.e.

$$\frac{\partial u}{\partial x} = 0 \quad (3.9)$$

Since overall mass balance is applied to the entire domain of flow this automatically ensures mass balance (continuity) at the outlet. The application of upwind difference (see Appendix E) demands that ϕ_{out} is immaterial for all variables except for velocities which are needed for mass conservation in the pressure-correction (p')-equation (see Appendix E, also for the derivation of p' -equation).

(iii) At the Symmetry Axis.

At the axis of symmetry $r=0$, the total normal flux is set to

zero,ie

$$\frac{\partial \phi}{\partial r} = 0 \quad (3.10)$$

for all variables except radial velocity V since it has zero value at the axis of symmetry. This may be achieved by setting to zero the appropriate coefficients in the finite difference equations.

(iv) At Walls.

The division of wall boundaries into five regions in modelling the orifice plate has been mentioned earlier (see section 3.23). Here the insertion of wall boundary conditions are briefly presented (more detail will be discussed in Appendix F).

Basically the wall boundary conditions are introduced by modifying the source term S^ϕ of the individual variables ϕ . By expressing the source term as a linear relation,

$$\int_V S^\phi dV = S_P^\phi \phi_P + S_U^\phi \quad (3.11)$$

the terms S_P^ϕ and S_U^ϕ may be deduced from integrated and linearised form of the source.

(a) For Mean Tangential Velocities.

A tangential velocity, say U_P for a node P nearest to a wall boundary (see fig.F.2, Appendix F) is obtained from usual momentum

balance. A boundary condition on U_p can be introduced by modifying the source term S_p^U for axial velocity U .

The modification is made in such a way that the values λ of S_p^U are decreased to bring the velocity zero on the walls. The modification on S_p^U is to decrease its value to

$$S_p^U = (S_p^U)_{old} - t_m \cdot \delta X_{pW} \quad (3.12)$$

$$\text{and } S_U^U = 0 \quad (3.13)$$

where δX_{pW} is the distance of point W from P and $(S_p^U)_{old}$ is the value of S_p^U at previous iteration.

If the point P falls in the inertial sublayer (ie. when $y^+ > 11.63$), t_m (see Appendix F) takes value given by,

$$t_m = \frac{\rho C_\mu^{\frac{1}{4}} k_{pW}^{\frac{1}{2}} \mathcal{K}}{\ln(E y_p^+)} \quad (3.14)$$

whereas when P is within viscous sublayer ($y^+ \leq 11.63$),

$$t_m = \frac{\mu}{y_p} \quad (3.15)$$

where ρ = fluid density,

μ = fluid viscosity,

y_p = normal distance of point P from the wall,

$$k_{pW} = \frac{1}{2} (k_p + k_W),$$

(3.16)

and C_μ , K and E are empirical constants with

$$K = \text{Von Karman constant} = .4137$$

$$E = \text{Integration constant} = 9.793$$

$$C_\mu = \text{Constant of turbulence} = .09.$$

Wall shear stress τ_w is given by,

$$\tau_w = t_m \cdot U_p \quad (3.17)$$

where t_m has the value as in equation (3.14) ^{or eqn. (3.15) depending on position of P} and U_p is the tangential axial velocity at the node point P (see also pg. 216).

Similar treatments may be carried out for radial velocity V having east/west walls of the control volume coincident with front face or rear face of orifice plate (see Appendix F, fig F.2(b) or (c)).

(b) Turbulence Energy.

The source term for turbulence kinetic energy S^k consists of two terms; the generation term G and the dissipation term $C_D \rho E$ according to,

$$S^k = G - C_D \rho E \quad (3.18)$$

$$\text{where } G = \mu_t \left\{ 2 \left[\left(\frac{\partial U}{\partial x} \right)^2 + \left(\frac{\partial V}{\partial r} \right)^2 + \left(\frac{V}{r} \right)^2 \right] + \left(\frac{\partial U}{\partial r} + \frac{\partial V}{\partial x} \right)^2 \right\} \quad (3.19)$$

$$\mu_t = C_\mu \rho \frac{k^2}{\epsilon} \quad (3.20)$$

k = turbulence energy,

ϵ = dissipation rate,

ρ = fluid density,

C_D, C_μ are constants at high Reynolds number given by table 2.

1.

By linearising the source term in the manner like equation (3.11) with $\phi \equiv k$, the following expressions for S_p^k and S_u^k may be deduced as,

$$S_p^k = -d_t \cdot \delta V \quad (3.21)$$

$$S_u^k = G \cdot \delta V \quad (3.22)$$

where δV is the control volume which encloses the point P where turbulence energy is stored. d_t (see Appendix F) can take either from,

$$d_t = \frac{C_D \rho C_\mu^{3/4} k_p^{*1/2} \ln(E y_p^+)}{\mathcal{K} y_p} \quad (3.23)$$

or from

$$d_t = \frac{C_D \rho C_\mu^{3/4} k_p^{*1/2} y_p^+}{y_p} \quad (3.24)$$

depending on whether $y^+ >$ or ≤ 11.63 , where

$$y_p^+ = \frac{\rho y_p}{\mu} \cdot k_p^{*1/2} C_\mu^{1/4} \quad (3.25)$$

k_p is the value of the turbulence energy at the node point P and k_p^* is

the value of k_p of previous iteration.

The modification of the generation term G appearing in equation (3.22) may be obtained as described in appendix F.

(c) Energy Dissipation Rate, ϵ .

The source term S^ϵ as usual is incorporated through the source treatment, from where the expression S_P^ϵ and S_U^ϵ are obtained.

Since in the wall flows, unlike k which falls to zero at the wall, ϵ reaches its maximum value there. This makes ϵ -balance for a cell extending to the wall difficult. This difficulty is overcome by adopting a fixed value for ϵ_p (irrespective of y^+) based on 'equilibrium' relation (see Appendix F for more detail). The value of ϵ at node point P is taken to be,

$$\epsilon_p = \frac{c_\mu^{3/4} k_p^{3/2}}{K y_p} \quad (3.26)$$

In the program this fixed value of ϵ is achieved by setting the linearisation constant $S_P^\epsilon, S_U^\epsilon$ to be

$$S_P^\epsilon = -\gamma \quad (3.27)$$

$$S_U^\epsilon = \epsilon_p \gamma \quad (3.28)$$

where γ is a large number of the order 10^{30} .

(d) Corner Treatments.

The treatments at the corners of the orifice plate will be discussed in Appendix F. Here the essential points of the treatments are given. The velocity cells (axial, U or radial, V cells) at the two corners of the orifice plate are shown in figure 3.7 (see also fig. F.3 of Appendix F). Consider the V-cell at the corner A, it can be seen that half of the east wall of the cell (control volume) coincides with front face of the orifice plate and half of its face is 'exposed' to the flow domain.

The contribution of flux from the east wall of the V-cell, \dot{q}_e is then given by,

$$\dot{q}_e = \rho_c \cdot U_p \cdot \frac{1}{2} A_{ewr} \quad (3.29)$$

where

$$\rho_c = \frac{1}{2} (\rho_w + \rho_p) \quad (3.30)$$

$$A_{ewr} = r_v \cdot \delta y_{ps} \quad (3.31)$$

and c is a point mid-way between W and P enclosed by the U-cell (see fig. 3.7).

By replacing equations (3.30) and (3.31) into equation (3.29), and linearising the result in the same way as in equation (F.36) (see Appendix F), then the 'linearisation constants' S_p^U and S_U^U are given as,

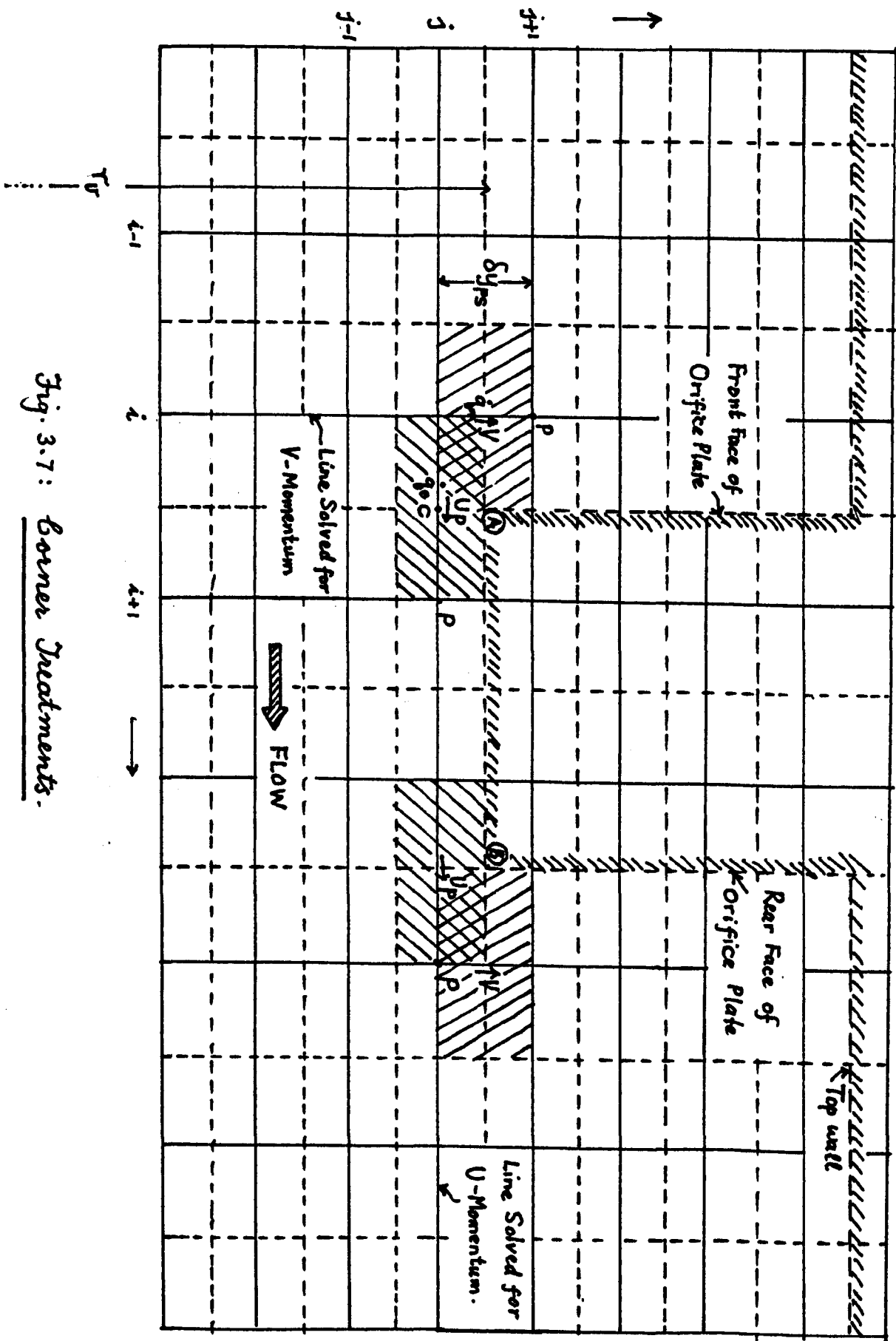


Fig. 3.7: Corner Treatments.

$$S_P^U = -\frac{1}{4}(\rho_p + \rho_w) \cdot A_{ewr} \quad (3.32)$$

$$S_U^U = 0 \quad (3.33)$$

where the negative sign has been introduced to promote stability.

The treatments at the corner B are similar to those at the corner A.

3.25 Calculation of Output Quantities.

(A): Pressure Variations.

Figure 3.8 shows the variations of pressure along pipe wall which may be illustrated as follows.

As fluid flows from upstream side of the orifice plate towards the device, (from left to right), the pressure on the pipe wall decreases very slowly. This is because of the dissipation of energy as heat due to frictions at the wall. In the absence of the orifice plate device, the pressure would continue to fall down slowly as can be seen in figure 3.8 indicated by a straight line ABC.

Immediately in front of the orifice plate, there is a small increase in pressure on the pipe wall. This is because part of the impact pressure on the front face of the plate is conveyed to the wall. In the immediate neighbourhood of the constriction, there is a rapid

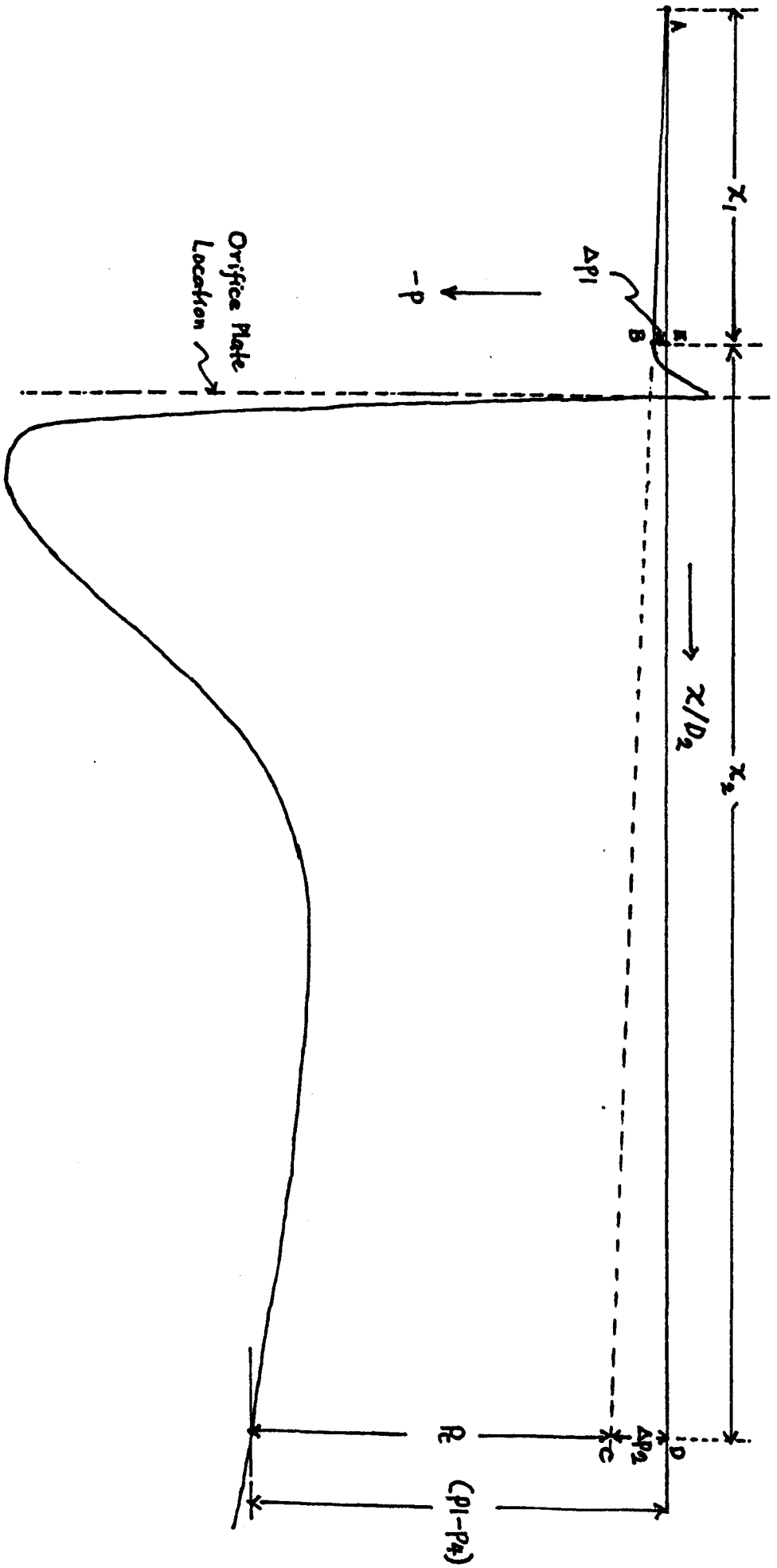


Fig. 3.8: A sketch of wall Pressure Distribution.

variation of pressure because of the presence of the orifice constriction in the metering. This pressure decreases to a minimum at the vena contracta, where the corresponding velocity is a maximum.

Downstream of the vena contracta, the pressure increases. This is because the flowing stream area increases and the fluid velocity falls to its initial value. At this zone, the pressure distribution recovers although the level of pressure is lower than that at the upstream. The pressure does not reach quite the value that it would have had in the absence of the orifice plate.

The total pressure drop (due to wall frictional forces and constriction), $(p_1 - p_4)$ is known as the net pressure loss and is due to the dissipation of energy as heat in the damping of turbulent eddies by internal friction (both wall friction and friction induced by the orifice plate).

Pressure drops across an orifice plate Δp are usually expressed in non-dimensional form, leading to the discharge and pressure loss coefficients which will be discussed now.

(a) The Discharge Coefficient, C_D .

The discharge coefficient, C_D is related to β -ratio, inlet velocity U_{in} and pressure difference Δp across the orifice plate by the following relationship,

$$C_D = U_{in} \sqrt{\frac{\rho(\frac{1}{\beta^4} - 1)}{2\Delta p}} \quad (3.34)$$

For each values of β , which is obtained from

$$\beta = \frac{j-1}{N-2} \quad (3.35)$$

where j = the index of horizontal plane next to bottom wall of the orifice plate (or JSTEP, see figure 3.6),

and N = maximum value of j -index (or NJ , see fig. 3.6),

the corresponding value of U_{in} is obtained from

$$U_{in} = \frac{\mu Re_2}{\rho D_1} \beta \quad (3.36)$$

where μ = fluid viscosity,

ρ = fluid density,

Re_2 = orifice Reynolds number,

D_1 = pipe diameter, and

β = orifice to pipe diameter ratio

are supposed to be given values.

Now, for each values of $t/0_2$ (which is obtained from program calculation) there are corresponding values of Δp . Therefore with a given value of ρ and known quantities of β and U_{in} (from equations (3.35) and (3.36)), the discharge coefficient C_D can be computed from equation (3.34).

In this particular study, the discharge coefficients for

flange, $(D-D/2)$ and corner tappings will be considered. As defined in the orifice metering literature flange pressure tappings are located at one inch upstream and one inch downstream of the orifice plate, corner tappings are located at the orifice plate and $(D-D/2)$ tappings are located one diameter upstream and half a diameter downstream of the plate. Invariably the grid locations do not coincide exactly with these positions. In the program code was added to locate the position of a particular tapping and the pressure at this particular tapping was obtained by linear interpolation between the pressures at the neighbouring grid nodes.

(b) Pressure Loss Coefficient, K .

The theoretical pressure loss coefficient, K_{theo} is defined as (Ward Smith, 1971),

$$K_{theo} = \frac{(p_1 - p_4)}{\frac{1}{2} \rho U_{in}^2} \quad (3.37)$$

where p_1 = static pressure upstream of orifice plate (where U_{in} is prescribed),

p_4 = pressure downstream of of orifice plate (where pressure is recovered),

ρ = fluid density, and

U_{in} = inlet velocity.

The corrected pressure drop, p_c (see fig.3.8) due to constriction is less than the overall total pressure drop (due to both

the constriction and wall frictional forces), $(p_1 - p_4)$. The corrections of pressure loss coefficient may be obtained as follows.

(c) Corrected Pressure Loss coefficient, "corrected K_{theo} ".

As remarked earlier, the static pressure increases downstream of vena contracta region, but does not however quite reach the value that it would have had in the absence of the orifice—the difference being the pressure loss denoted by p_c . This pressure loss is thus the extra resistance due to the orifice plate in the pipe line.

From figure 3.8 it can be seen that,

$$p_c = (p_1 - p_4) - \Delta p_2 \quad (3.38)$$

From two similar triangles ABE and ACD, Δp_2 is related to known values of x_1 , x_2 and Δp_1 by,

$$\Delta p_2 = \Delta p_1 \frac{|x_1 + x_2|}{|x_1|} \quad (3.39)$$

where x_1 = the distance of the point of smallest pressure just upstream of orifice plate to a point on the wall on the second grid line of the computational domain (see figure 3.3),

x_2 = the distance from the point on the pipe wall of minimum pressure just upstream of the orifice plate to the point on the pipe wall at the last grid of the computational domain (in the downstream region, see figure 3.8),

Δp_1 = the pressure drop just upstream of the orifice plate.

By combining equations (3.38) and (3.39) will result,

$$p_c = (p_1 - p_4) - \Delta p_1 \frac{|\alpha_1 + \alpha_2|}{|\alpha_1|} \quad (3.40)$$

from where the corrected pressure loss coefficient is given by,

$$\text{"corrected } K_{\text{theo}} \text{"} = \frac{p_c}{\frac{1}{2} \rho U_{in}^2} \quad (3.41)$$

where ρ and U_{in} are respectively fluid density and inlet velocity.

3.3 OTHER PROGRAMMING DETAILS.

The SIMPLE algorithm (discussed in Appendix E) is incorporated into the modified TEACH-T (for Teaching Elliptic Axi-symmetrical Characteristics Heuristically for Turbulent flow) computer program. For the algorithms, the stability is secured by the choice of appropriate relaxation factors defined by equation (E.51) (see Appendix E) with values of .5 for velocity components, U and V, 1.0 for pressure correction, p' and .7 for turbulent quantities k and ϵ as well as for turbulent viscosity μ_t .

In applying the LBL procedure without updating the coefficients for any particular variable ϕ , the number of sweeps is employed—as many 'sweeps' as necessary may be employed until the desired solution is obtained. A number of sweeps of 3 is adequate for

velocity components and turbulent quantities. The value of 5 is needed for p' in such a way that continuity will be satisfied.

In the computations, a converged solution is achieved when the source (denoted by SORCE) which is the largest value of residual sources for U, V and p' is less than a specified preset value δ called the maximum source (denoted by SORMAX)-the sensitivity of convergence criteria is discussed later.

The p' -equation can be satisfied by several pressure fields, so the pressure needs to be specified and it is specified at location $IPREF=2, JPREF=2$ (where $IPREF$ and $JPREF$ are the I- and J-indices of location where pressure is fixed) and the value is kept fixed at that position. All other pressures are measured relative to it.

For iteration monitoring, the cumulative number of iterations performed is calculated and stored as NITER. The absolute sum of the residual sources is stored as $RESOR\phi$ ($\phi = U, V, k$ and ϵ), for p' -equation the absolute mass sources are stored as RESORM. The field values at each iteration sequence is specified at location $IMON=12, JMON=8$. The variable arrays are printed out before and after the iteration sequence values during the sequence are printed out at intervals of $INDPRI=250$. The constants of turbulence necessary for the programming are given in table 2.1 (see Chapter 2). For more complete picture of the program, see program listing provided at the end of Appendix G.

3.4 TEST ON A $\beta = .7$ THIN ORIFICE PLATE.

3.41 Introduction.

The following subsections discuss the actual model development of the orifice plate. As a starting point the author used upstream distance from orifice plate, DXU to be $2D_1$ (where D_1 is the pipe diameter) and downstream distance, DXD is varied from 5 to 35 pipe diameters. Power law velocity profile, (see equation 3.1) has been used to run the program. Also as a starting point a convergence criteria $\delta = .01$ (1%) was chosen.

As has been noted earlier that the distances DXU and DXD were measured from inlet/outlet boundaries to the OY-axis and not to the faces of the orifice plate at upstream/downstream region (see fig.3.1). However, since the orifice plate used has been assumed to be very thin, $t/D_2 \rightarrow 0$ (where t is the plate thickness and D_2 being the orifice diameter), this gives negligible error.

Basically a correct model can be said to have been obtained when: (i) sufficiently high upstream and downstream distances have been chosen, (ii) the grid distribution is sufficiently fine and (iii) the convergence criteria δ is sufficiently small. The criteria of sufficiency being that quantities of interest such as discharge and pressure loss coefficients become asymptotically constant with respect to changes in these variables. This will become clearer as model results are presented later.

3.42 Choice of Upstream/Downstream Distances.

(i) Upstream Choice.

Computer tests have been made for different grid distributions upstream and downstream of orifice plate for a given value of β ($= .7$). The author has been using equal number of grid distributions ^{in the} upstream and downstream regions. Initially (11/11) grid distributions (meaning that 11 grid lines are used in upstream/downstream regions, in such a way that the total number of these grid lines give the total number, NI) have been used. The discharge coefficients (for flange, $(D-D/2)$ and the corner tapings) and pressure loss coefficients are then noted on a table. Similar tests were carried out for (12/12), (13/13), (14/14), (15/15) and (16/16) grid distributions. Graphs of discharge and pressure loss coefficients are then plotted against downstream distance DXD (measured in pipe diameters) as shown in figures 3.9 and 3.10. In these results an initial choice for the upstream distance was taken as $DXU=2$ diameters.

From figure 3.9 it can be seen that (11/11), (12/12), (13/13) and (14/14) grid distributions are all too coarse as the discharge coefficient does not become asymptotically constant as the downstream distance is increased. The other distributions (15/15 and 16/16) are reasonably constant at large DXD with the (16/16) distribution being the best. In this latter distribution the value of discharge coefficient appears to level off at $DXD=5$ diameters and then rise very slowly and slightly.

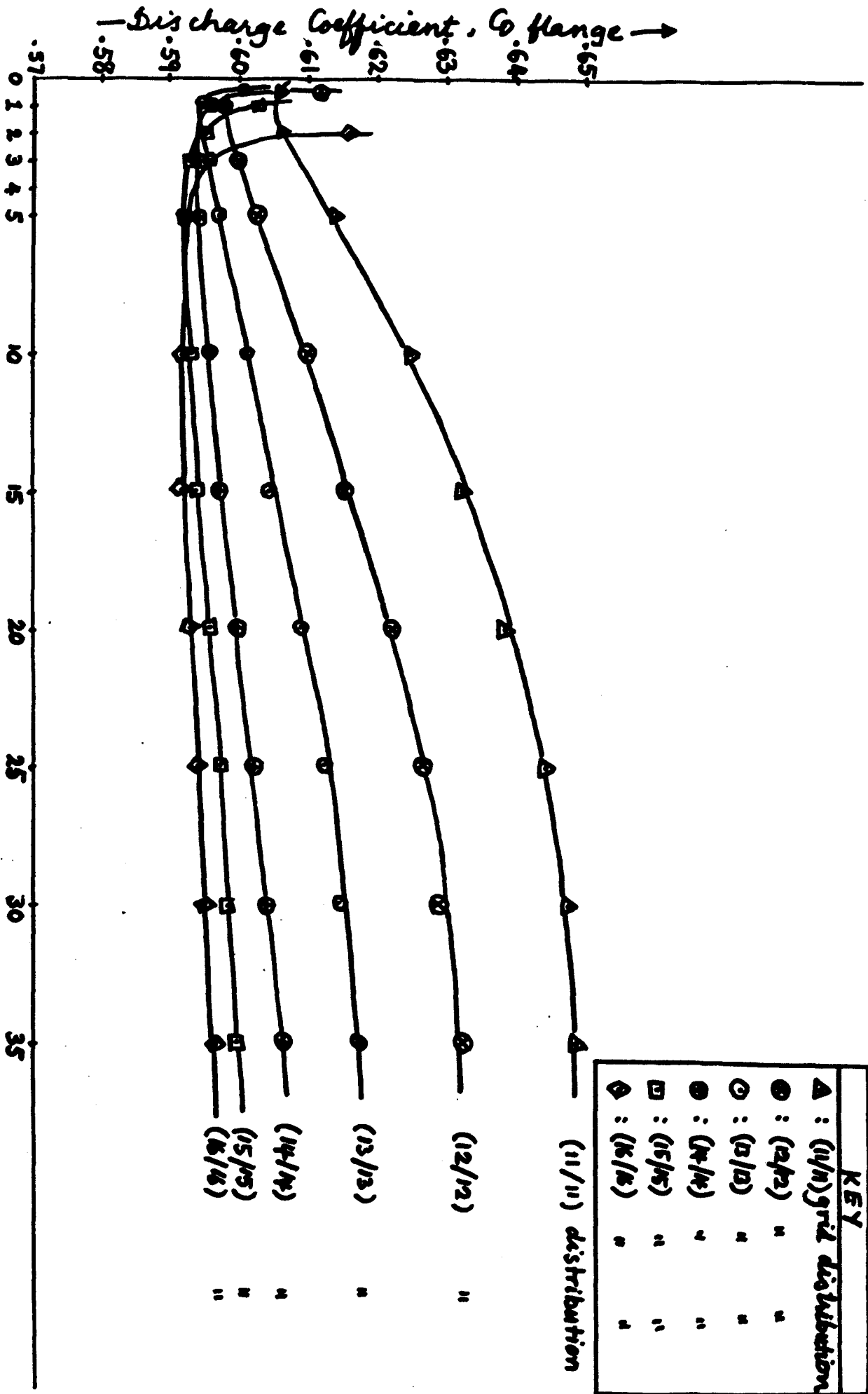


Fig. 3.9: Variations of Theoretical Discharge Coefficient (Flange) with Downstream Distances for Different Grid Distributions.

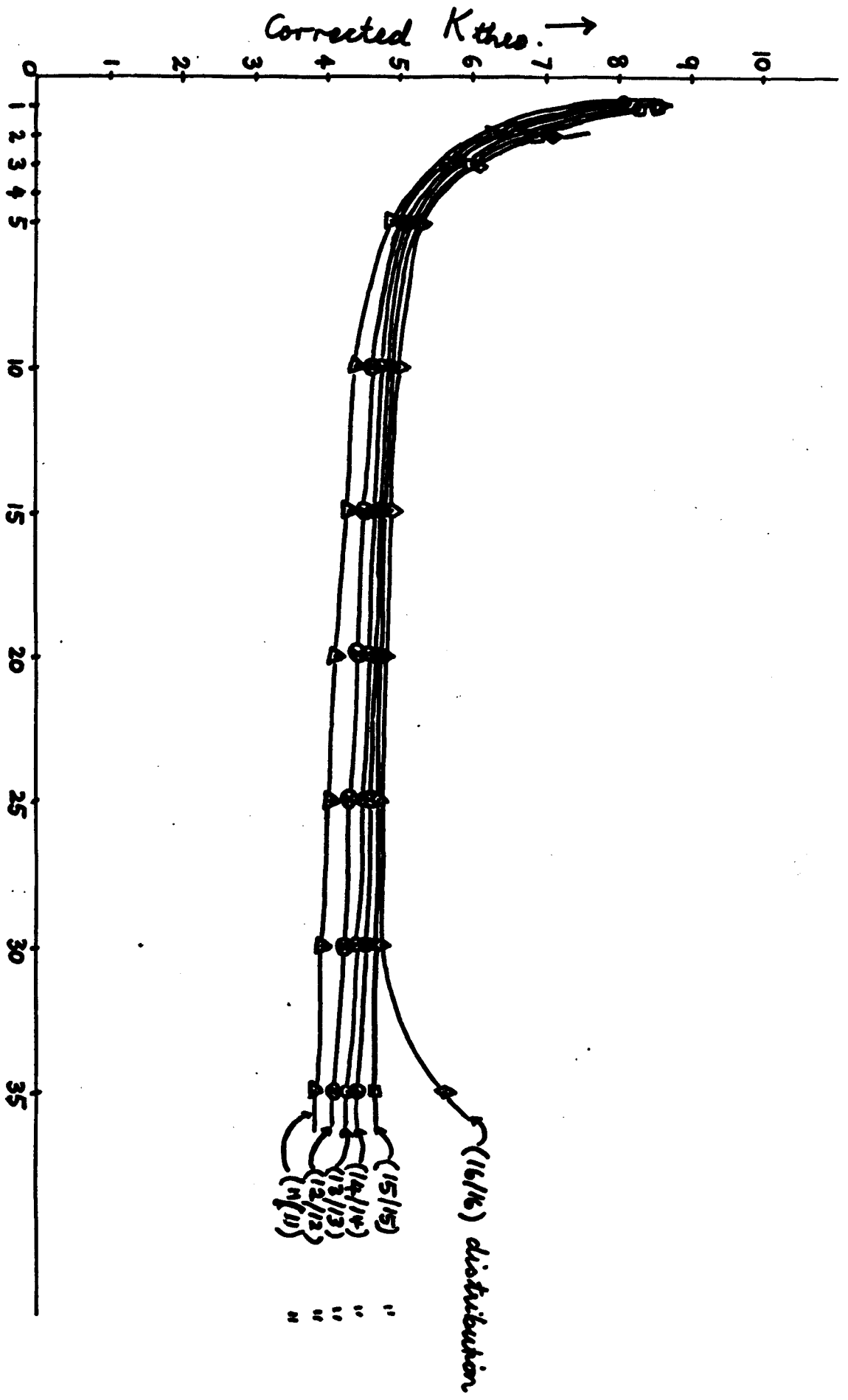


Fig. 3.10: Variations of Corrected Fresnel Loss Coefficient with Downstream Distances for Different Guide Distributions.

Results for the pressure loss coefficients (figure 3.10) give a similar though not so pronounced trend. Again the (16/16) distribution is the best but here the approximately asymptotically constant region begins from $DXD=10$. The asymptotic results for both discharge and pressure loss coefficients are encouragingly reasonably close to experiment with discharge coefficient (flange) in the range .59-.60 (BSI 1042 result being .6122) and the pressure loss coefficient in the range 4.6-5.0 (experimental result being 4.198-Ward Smith, 1971).

To determine the upstream distance DXU , the downstream distance DXD was fixed at 25 diameters and DXU was varied for a (16/16) distribution. Results for discharge and pressure loss coefficients are presented graphically in figure 3.11. These indicate an asymptotic region for $DXU > 4$. It was therefore decided to fix $DXU=5$ diameters.

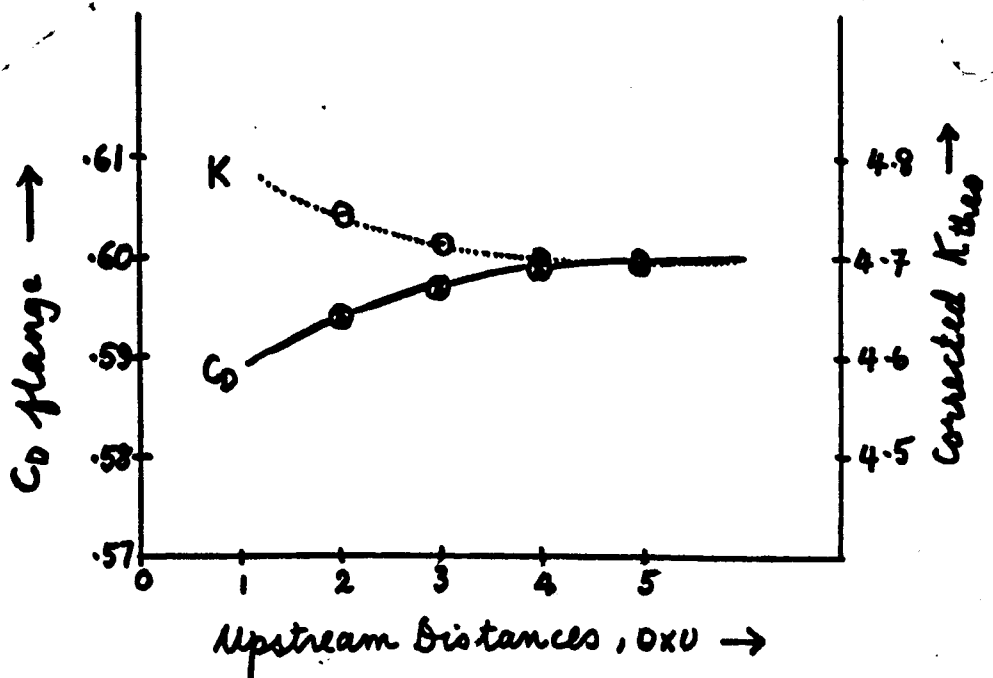


Fig. 3.11: To Find Upstream Distance, DXU for the Model.

(ii) Downstream Choice.

Having obtained the upstream distance DXU to be 5 diameters, trials have been made to vary downstream distances in order to obtain a suitable distance for the model. Computer tests have been carried out as before with a (16/16) grid distribution but with varying DXD and keeping $DXU=5$ diameters fixed. Curves of discharge coefficients (for flange tap) and pressure loss coefficients are then plotted versus DXD (figure 3.12). It can be noted that when downstream distance DXD is greater than 10 diameters, the curves of discharge coefficients and pressure loss coefficient are both approximately asymptotically constant.

A reasonable choice for DXD was then taken to be 15 leading to a final choice of $DXU=5$ and $DXD=15$. Interestingly, F. Durst and A.K. Rastogi in analysing a plane turbulent flow problem with separation used distances of 5.5 and 12.5 channel widths upstream and downstream of an obstructing device (see Durst et al, 1979). These choices are similar to the ones arrived at in this study.

3.43 Grid Distribution Selection.

Having selected that 5 diameters upstream and 15 diameters downstream are the best distances for the model, the next stage is to confirm that (16/16) grid distributions would be the best choice for the model. For this, computer tests for (11/11), (12/12), (13/13), (14/14), (15/15) and (16/16) grid distributions have been carried out using same conditions as previous tests but now

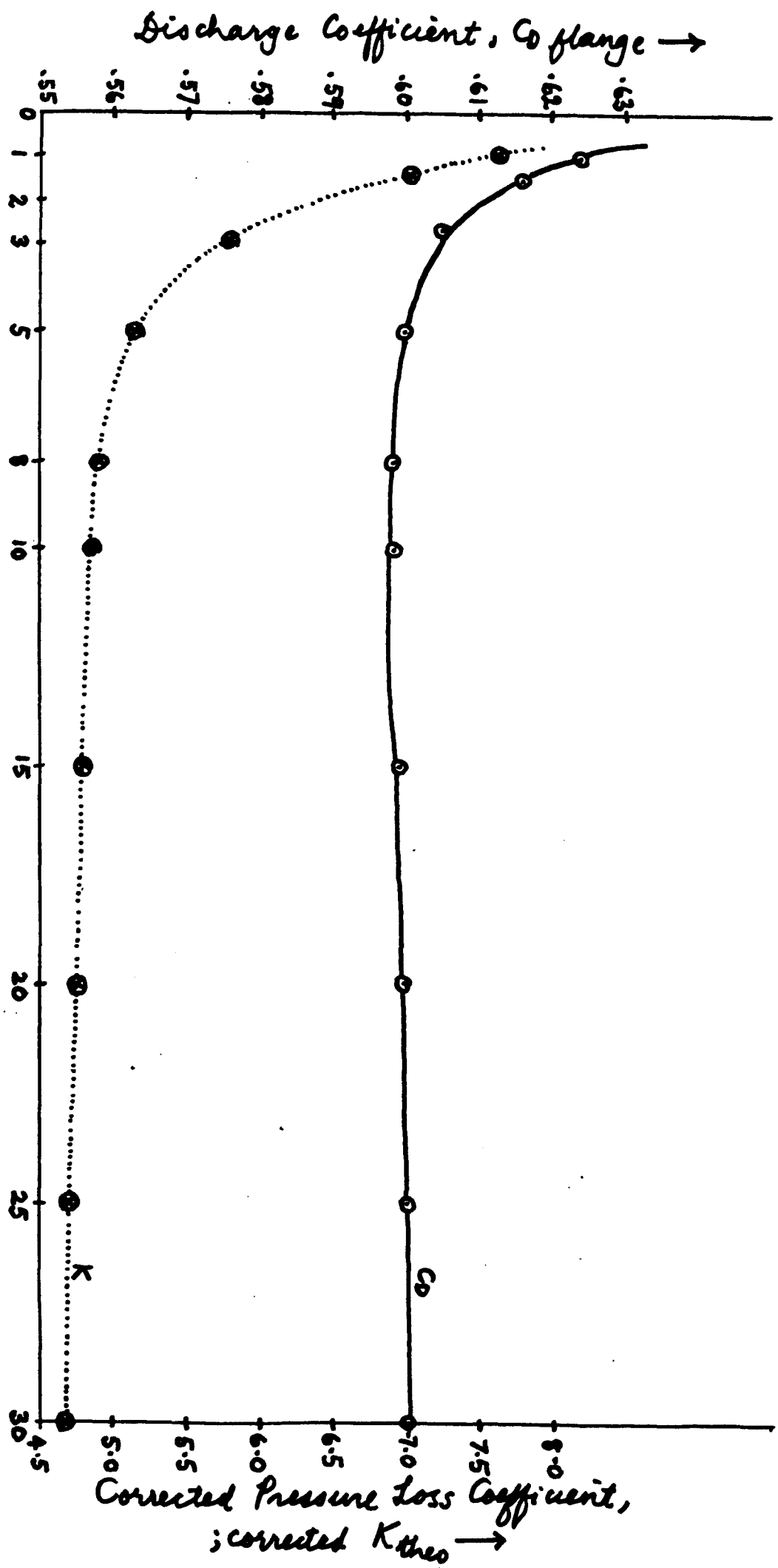


Fig. 3.12: To Find Downstream Distance for the model.

using 5 and 15 diameters for the upstream and downstream distances from the orifice plate. Curves of discharge coefficient (for flange tap) and pressure loss coefficient were plotted versus those grid distributions as shown in fig.3.13. Both curves begin to level up when grid distributions are increased until after the (15/15) grid distribution, the results are essentially constant. Interestingly the curve for discharge coefficient tends to have a value approximately .596 (compared with experimental data .6122), whereas the corresponding pressure loss coefficient curve has a value about 4.76 (compared with experimental data 4.198).

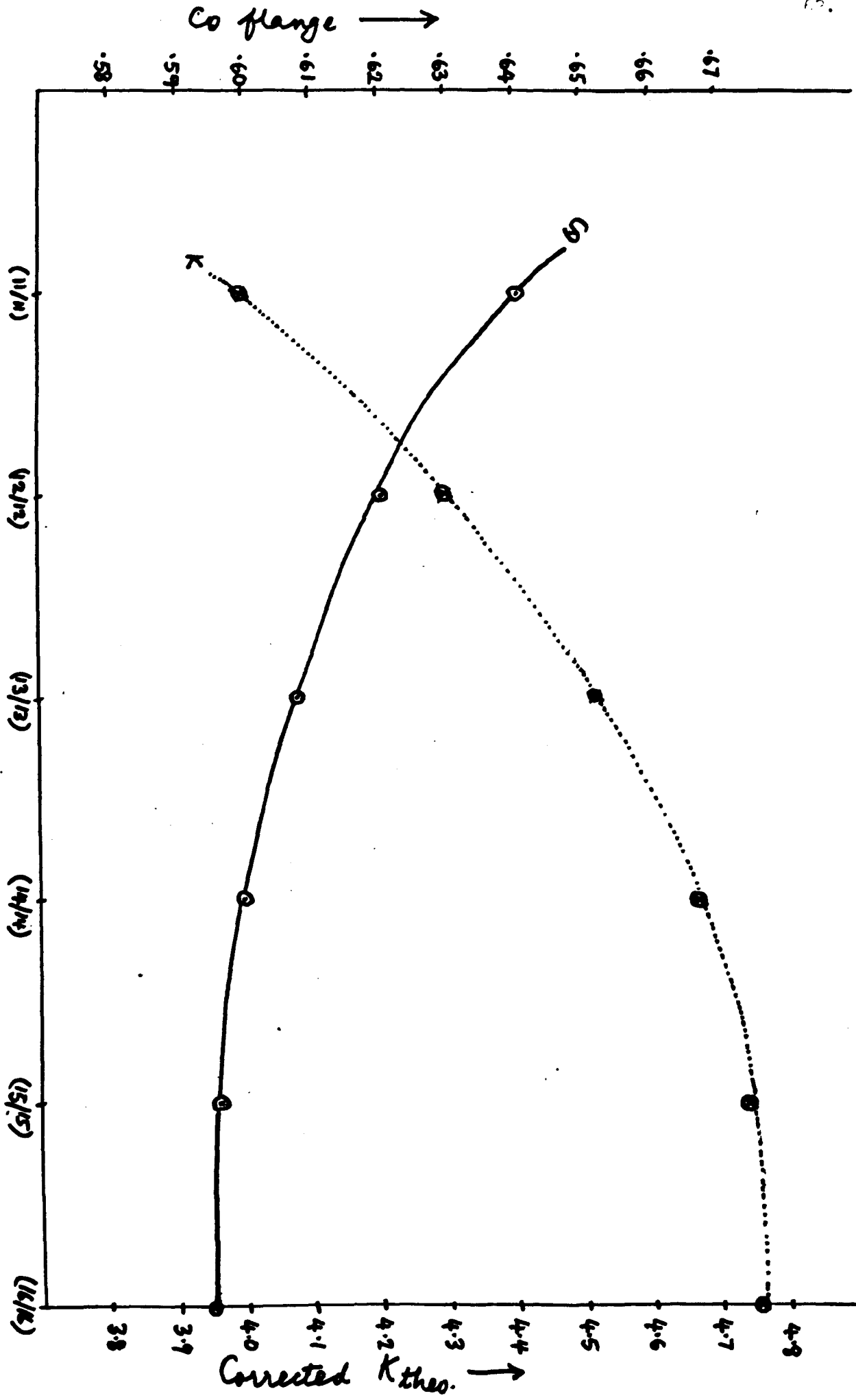
From above arguments it can be concluded that the best model for orifice metering is chosen to be 5 diameters upstream and 15 diameters downstream for the distances from the OY-axis and with (16/16) grid distribution. The total number of grids $NI = 32$ in the axial direction and $NJ = 22$ grids in the radial direction have been used. From now onwards, this model will be used as basis for computer tests of other parameter dependences that will be discussed later.

3.44 Sensitivity of Convergence Criteria.

The number of iterations to obtain a solution depend strongly on the convergence criteria δ chosen. The convergence criteria should therefore not too stringent. The value chosen in the previous runs was $\delta = .01$ (1%). The value of δ was varied and the results are presented in table 3.1 for a $\beta = .7$ orifice meter with fixed levels of turbulence intensity, i and length scale factor λ . In obtaining those values of pressure loss coefficient and discharge coefficient, a power

Theoretical Discharge Coefficients							
δ	C_D flange	$C_D (D-D/2)$	C_D corner	$K_{theo.}$	Corrected $K_{theo.}$	$K_{exp.}$	NITER
5	.6297	.6140	.6262	3.062	2.655	4.198	31
4	.6286	.6188	.6308	2.916	2.916	4.198	32
3	.6181	.6084	.6335	3.310	3.550	4.198	33
2	.6040	.5811	.6359	4.832	4.591	4.198	35
1	.5984	.6102	.5937	4.476	4.069	4.198	128
.1	.5983	.6104	.5936	5.148	4.740	4.198	193
.01	.5983	.6104	.5936	5.182	4.774	4.198	310
.005	.5983	.6104	.5936	5.180	4.722	4.198	327
.001	.5983	.6104	.5936	5.182	4.775	4.198	390

Table 3.1 : Convergence Criteria, δ .



(Upstream/downstream) grid distribution →
 Fig. 3.13: To confirm (16/16) Grid Distribution is the Best Choice.

law velocity profile has been used. The table also includes the number of iterations (NITER) required to obtain a solution.

From the table 3.1, it can be seen that the values of discharge and pressure loss coefficients are constant when δ changes from .001 to .1 (see also figure 3.14).

It can be concluded therefore that the value of 1% for δ is to be the right choice, since this value is in the range $.001 < \delta < .1$.

3.45 Results for $\beta = .7$ Orifice Plate Tests.

In this section some results are presented for the $\beta = .7$ orifice plate with the developed model. These results are presented again together with results for other β ratio orifice plates in Chapter 4 where also some conclusions are drawn.

(i) Velocity Profile Dependence.

Table 3.2 presents the dependence of velocity profile on the discharge and pressure loss coefficients. Three commonly used pressure tapings; namely the flange, $(D-D/2)$ and corner tapings were considered. The velocity profiles used were of power law type (see equation 3.1) and flat (or uniform) type (see equation 3.4). The corresponding experimental values of discharge obtained from BSI 1042 are also presented and should be compared with the power law results.

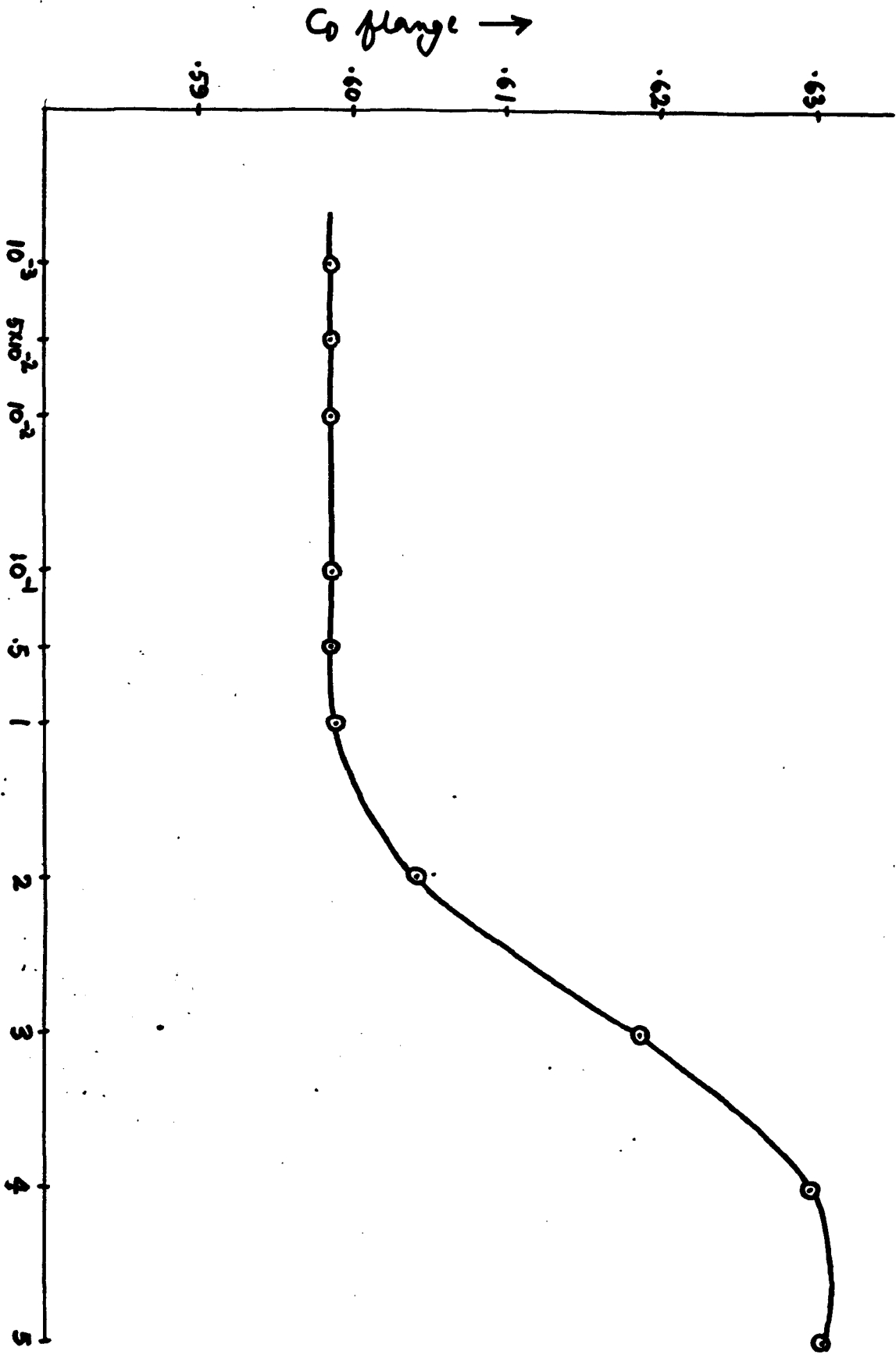


Fig. 3.14: The Choice of Convergence Criterion.

Theoretical Discharge Coefficients						Experimental Discharge Coefficients			Theoretical Pressure Loss Coefficients K_{theo} .		Corrected K_{theo} .		K_{exp} .
C_D flange		C_D ($D-D/2$)		C_D corner		C_D flange	C_D ($D-D/2$)	C_D corner	power	flat	power	flat	
power	flat	power	flat	power	flat								
.5983	.5902	.6104	.6028	.5936	.5838	.6122	.6182	.6133	5.182	4.367	4.774	4.929	4.198

Table 3.2 Velocity Profile Dependence for a $\beta = 0.7$ Orifice Plate.

Row	i	λ	Theoretical Discharge Coefficients			Experimental Discharge Coefficients			K_{theo} .	Corrected K_{theo} .	K_{exp} .
			C_D flange	C_D ($D-D/2$)	C_D corner	C_D flange ($D-D/2$)	C_D corner				
(a)	.03	.005	.5983	.6104	.5936	.6122	.6182	.6133	5.182	4.774	4.198
(b)	.09	.005	.5991	.6112	.5984	.6122	.6182	.6133	5.167	4.749	4.198
(c)	.03	.015	.5978	.6099	.5928	.6122	.6182	.6133	5.194	4.788	4.198
(d)	.09	.015	.5986	.6108	.5941	.6122	.6182	.6133	5.177	4.760	4.198
(e)	.02	.64	.5883	.6023	.5805	.6122	.6182	.6133	5.412	5.054	4.198

Table 3.3 Effects of Changing Turbulence Intensity i and length Scale Factor λ for a $\beta = 0.7$ Orifice Plate.

Theoretical and corrected theoretical pressure loss coefficients K_{theo} and "corrected K_{theo} ", the quantities of which were defined by equations (3.37) and (3.41) are given also on the table. The corresponding values of the experimental data, K_{exp} obtained from Ward Smith's formula for $\beta = .7$ were also given.

(ii) Turbulence Intensity, i and Length Scale Factor λ Dependence.

The variations of discharge coefficients C_D and pressure loss coefficients, K with turbulence intensity i and length scale factor λ may be found in table 3.3. Power law velocity profile has been used in obtaining those coefficients.

(iii) Orifice Plate Thickness Dependence.

Table 3.4 shows the dependence of discharge and pressure loss coefficients on the orifice plate thickness which is specified by t/d_2 . However the values of the reciprocal of t/d_2 are presented in the table. The variation in orifice plate thickness is achieved in the program by varying the grid expansion/contraction factor EPSX which is also tabulated. Again, a power law velocity profile has been used.

These results indicate why thin orifice plates are generally used in orifice metering. This is essentially because above some value of D_2/t the value of the discharge coefficient (flange) is practically constant (see figure 3.15).

A thick orifice plate would be undesirable in a practical situation because as it wore (became thinner) the value of the discharge coefficient would change.

EPSX	D ₂ /t	Theoretical Discharge Coefficients			Experimental Discharge Coefficients.			K _{theo}	Corrected K _{theo}	K _{exp.}
		C _D flange	C _D (D-D/2)	C _D corner	C _D flange	C _D (D-D/2)	C _D corner			
1.30	4.665	.6995	.7190	.6894	.6122	.6182	.6133	3.785	3.252	4.155
1.40	10.66	.6621	.6803	.6540	.6122	.6182	.6133	4.205	3.707	4.196
1.50	23.79	.6323	.6483	.6270	.6122	.6182	.6133	4.636	4.177	4.198
1.55	35.13	.6213	.6380	.6169	.6122	.6182	.6133	4.798	4.348	4.198
1.60	51.48	.6130	.6275	.6096	.6122	.6182	.6133	4.991	4.514	4.198
1.65	74.81	.6075	.6242	.6032	.6122	.6182	.6133	5.017	4.587	4.198
1.70	107.8	.6045	.6208	.5988	.6122	.6182	.6133	5.042	4.603	4.198
1.75	154.1	.6015	.6174	.5963	.6122	.6182	.6133	5.117	4.691	4.198
1.80	218.6	.6005	.6158	.5949	.6122	.6182	.6133	5.149	4.730	4.198
1.85	307.6	.5994	.6135	.5943	.6122	.6182	.6133	5.167	4.754	4.198
1.90	429.5	.5983	.6104	.5936	.6122	.6182	.6133	5.182	4.774	4.198

Table 3.4: Orifice Plate Thickness Dependence for $\beta = .7$

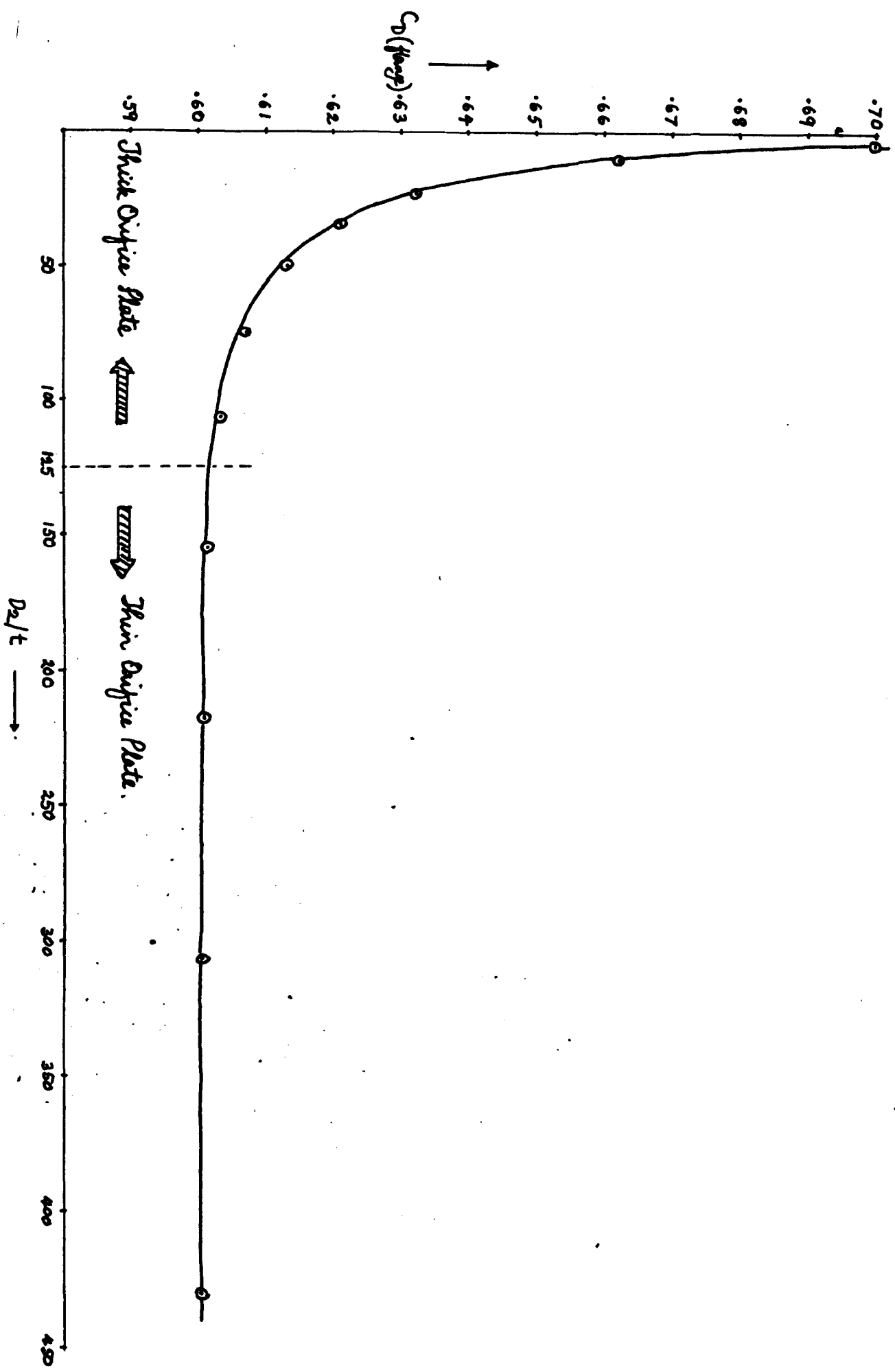


Fig. 3.15: Variation of Discharge Coefficients (Kings) with Plate Thickness.

(iv) Pressure Distributions along Pipe Wall.

Figure 3.16 presents a computer result of pressure variations along pipe wall for a $\beta = .7$ orifice meter. The velocity profile used to get the result was again a power law type defined earlier. The curve obtained is very similar to the one presented in BSI 1042 (pg.21).

3.5 CONCLUDING REMARKS.

The development of the model for orifice metering has been presented in this chapter. The essential features of the model development may be summarised as follows,

The geometry of the orifice metering has been shown with the locations of inlet and outlet boundaries from the orifice plate. Variable number of grid distributions upstream and downstream of the orifice plate were also noted.

In the interest of the computations and the modifications required to the TEACH-T program, the domain of calculations has been shown which includes the wall boundaries, inlet/outlet boundaries and also symmetry axis. Incorporation of boundary conditions and inlet velocity profiles were also presented.

The calculation of discharge coefficients and pressure loss coefficients have been presented briefly including the correction required for computing the pressure loss coefficient.

← Wall Pressure Distributions

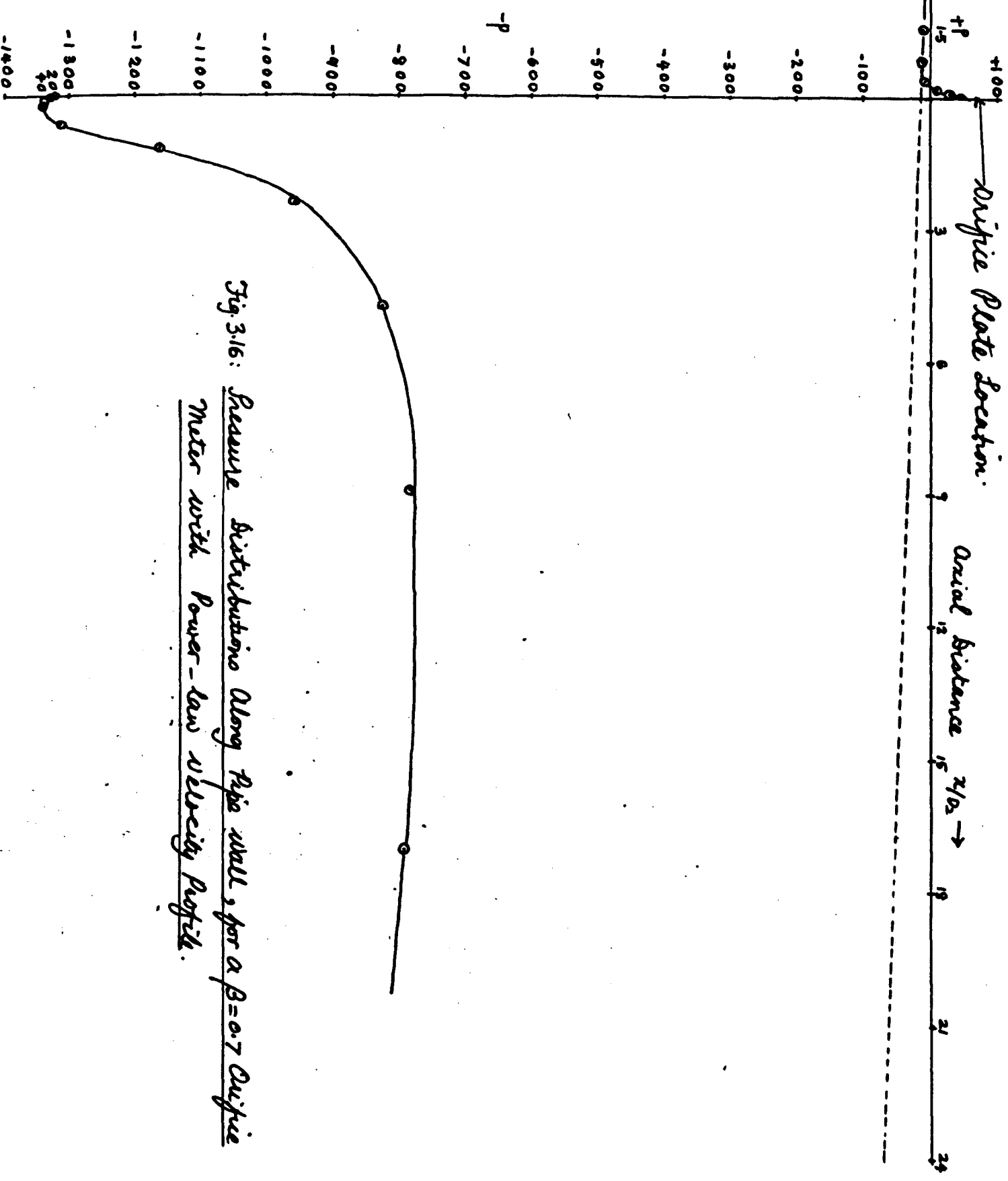


Fig. 3.16: Pressure Distributions Along Pipe Wall, for a $\beta = 0.7$ Orifice Meter with Power-law Velocity Profile.

The developed computer program was then run extensively with $\beta = .7$ orifice plate to investigate upstream/downstream distances, grid distributions and convergence criteria. This had to be done in the somewhat iterative fashion as explained. The finally chosen model was one with a (16/16) grid distribution upstream/downstream of the orifice plate and with upstream and downstream distances of 5 and 15 diameters respectively. The resulting model was one with a (32x22) grid distribution (22 in the radial direction) which gave a grid independent converged solution.

Lastly, some detailed results for a $\beta = .7$ orifice meter were presented for the discharge and pressure loss coefficients. These indicated encouraging agreement with experiments. These results are presented again and discussed more fully in the next chapter where additional results for other β ratio orifice plates are also presented.

It is of interest to state the run times and storage requirements for the developed model. The program was run on the ULCC CDC7600 machine and the departmental PRIME550 mini computer. For the CDC machine the typical run time is 40 seconds and for the PRIME it was 150 minutes. With regard to program size the program required 33 K Words of 60 *bit* memory on the CDC7600 machine. As may be realised the development of the basic model required many runs of the program (approximately 250).

CHAPTER 4.

APPLICATIONS OF MODEL AND QUANTITATIVE VALIDATIONS.

4.1: INTRODUCTION.

Having discussed the developments of a model based on a $\beta = .7$ diameter ratio thin orifice plate in the last chapter, it remains to present more detailed validations for a range of β values.

In this chapter, such results are presented for $.3 \leq \beta \leq .7$ for orifice discharge and pressure loss coefficients.

First we present the results for direct comparison with those from BSI1042 (1964) for discharge coefficients and Ward Smith (1971) for pressure loss coefficient. For these results, the following was assumed,

- (i) a power law inlet velocity profile,
- (ii) a low level of turbulence at the inlet,
- (iii) a thin orifice plate, and
- (iv) a Reynolds number of 1×10^5 .

We then proceed in section 4.3 onwards to present results for variations in the above quantities. These results are not compared with

experimental results as generally corresponding experimental data do not exist. The results however do indicate the sensitivity of the orifice meter coefficients to such changes.

4.2: DISCHARGE AND PRESSURE LOSS COEFFICIENTS FOR DIFFERENT β .

Table 4.1 presents the discharge and pressure loss coefficients for the different values of orifice to pipe diameter ratio β . It can be seen that the values of the computed discharge coefficients for flange and corner tapplings are decreasing very slowly as β ratio increases, while the corresponding experimental coefficients show the reverse behaviour (ie increases with increasing β). For D-D/2 tapping, the computed discharge coefficient decreases with increasing β in the range $.3 \leq \beta \leq .5$ and starts to rise again beyond $\beta = .55$. However the corresponding values of experimental discharge coefficient increases slowly with increasing values of β .

From the table also, it can be seen that the computed values of discharge coefficients at the extreme ranges of β are not as reliable as those values which lie between the extremities of β . This is in agreement with the proposal of Stearn et al (1951). The computed values at the 'central' region of the β range agree very well with the data. As an example the predicted discharge coefficient for flange tap for $\beta = .45$ was found to be .6059 compared with data .6050 from BSI1042. It is only about .1% in error. Similarly the predicted values of the coefficients with D-D/2 and corner tapplings are respectively within about .4% and .1% (see fig.4.1).

β	Theoretical Discharge Coefficients			Experimental Discharge Coefficients.			K theo.	Corrected K theo	K exp
	C_D flange	C_D (0-0/2)	C_D corner	C_D flange	C_D (0-0/2)	C_D corner			
.3	.6187	.6178	.6192	.5995	.5990	.6002	292.2	291.8	297.6
.35	.6109	.6100	.6115	.6008	.6014	.6021	155.3	154.8	153.5
.4	.6082	.6073	.6087	.6033	.6045	.6045	87.36	86.90	85.07
.45	.6059	.6053	.6063	.6050	.6079	.6067	51.68	51.24	49.57
.5	.6036	.6037	.6039	.6073	.6131	.6088	31.70	31.27	29.87
.55	.6024	.6037	.6023	.6096	.6148	.6110	19.87	19.44	18.36
.6	.6016	.6048	.6007	.6112	.6165	.6123	12.63	12.21	11.36
.65	.6004	.6070	.5981	.6125	.6163	.6130	8.086	7.672	6.985
.7	.5983	.6104	.5936	.6122	.6182	.6133	5.182	4.774	4.198

Table 4.1 : β -ratio Dependence.

Percentage Variations of Discharge Coefficients.

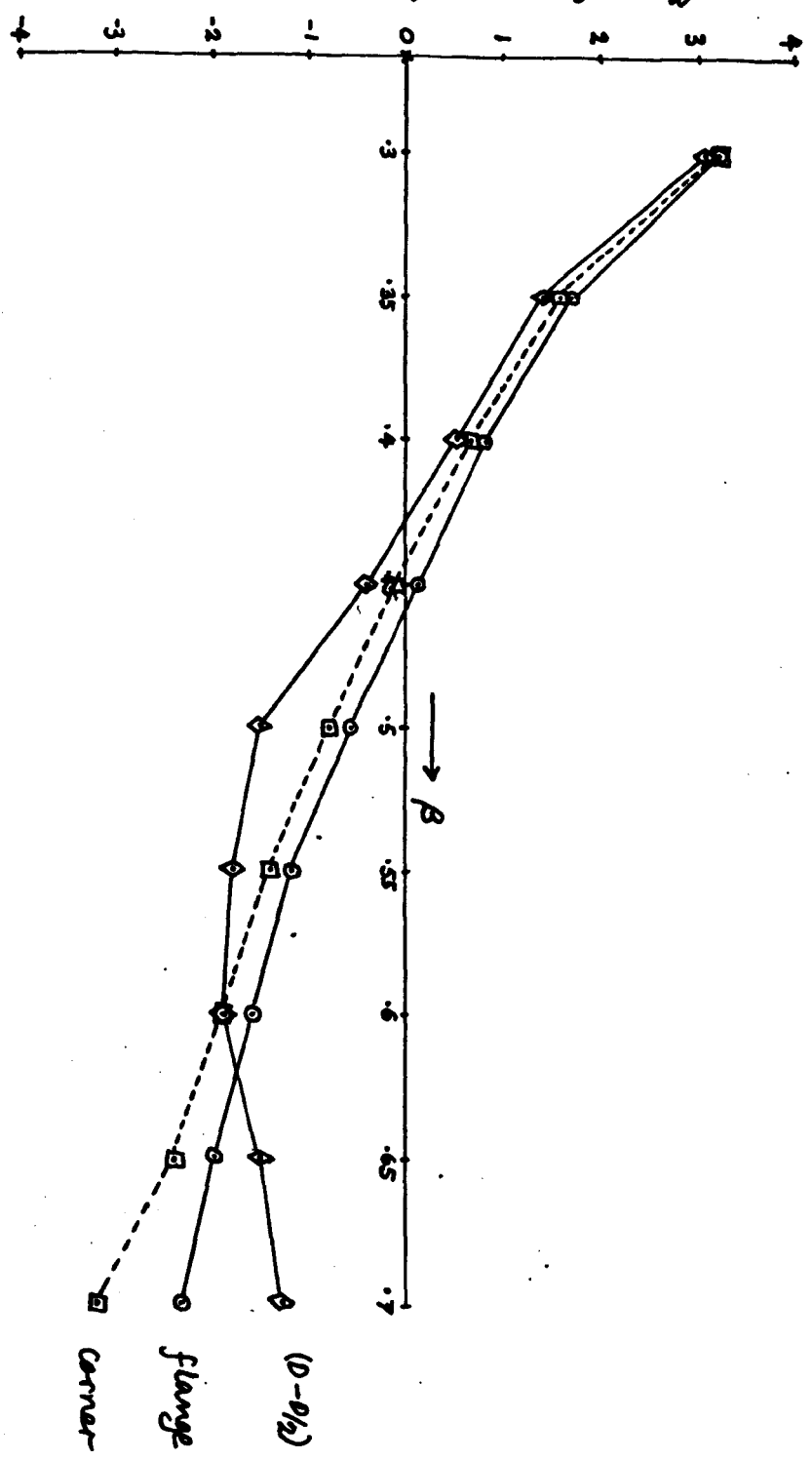


Fig. 4.1: Variations of Discharge Coefficients with β -ratio
(Comparison with BSI 1042, 1964).

Figure 4.1 shows the percentage variations of the computed discharge coefficients for the whole range, $.3 \leq \beta \leq .7$ for all three pressure tappings considered. It can be said that the variations of the coefficients for the tappings with the available data are within $\pm 3.2\%$

Table 4.1 also shows that the theoretical and corrected theoretical pressure loss coefficients decrease with increasing β ratio, this is in accordance with the experimental data. K_{theo} is the theoretical value of pressure loss coefficient when the effects of frictional resistances due to pipe wall and due to orifice plate are included, whereas 'corrected K_{theo} ' is the pressure loss coefficient corrected for the pipe wall loss and therefore represents the loss due only to the orifice plate. These latter values must be compared with the experimental data, K_{exp} .

Figure 4.2 presents the percentage variations of the corrected pressure loss coefficients with the available data for $.3 \leq \beta \leq .7$. It can be seen that the variations increase with increasing β . The error is minimal for $\beta = .35$ but increases with β to a maximum of 14% at $\beta = .7$.

4.3: VELOCITY PROFILE DEPENDENCE.

Two types of velocity profiles have been used in the present study, namely the power-law and flat velocity profiles. The latter profile has been used to show a typical profile sensitivity for the computed orifice coefficients.

Percentage errors in Corrected Pressure Loss Coefficients.

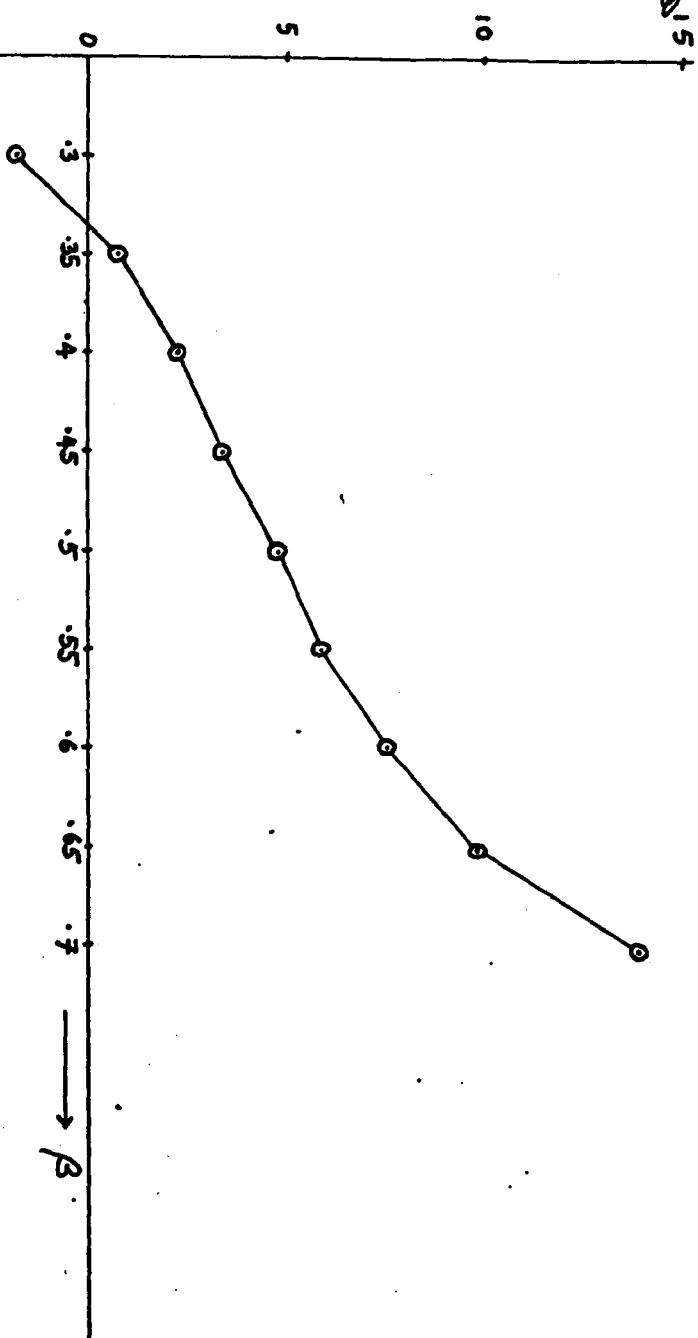


Fig. 4.2: Variations of Pressure Loss Coefficients (Corrected K_{th}),
with Experimental Data of Ward Smith, 1971,
for Different Values of β -ratio.

4.31: Power-law Profile.

The power-law velocity profile is defined by the curves which obey a simple-law curve (Blake, 1976) given by,

$$U(r) = U_{max} \left(1 - \frac{r}{R}\right)^{\frac{1}{p}} \quad (4.1)$$

where U_{max} is the maximum fluid velocity at the central region of the flow distributions, r is the radial distance from axis of symmetry where fluid velocity is the highest, R is the pipe radius. The power-law index p is given by

$$p = 7.48 + 5.83 \times 10^{-5} \times Re_1 - 4.16 \times 10^{-12} \times (Re_1)^2 \quad (4.2)$$

where Re_1 is the pipe Reynolds number which is related to orifice Reynolds number Re_2 by

$$Re_1 = \beta Re_2 \quad (4.3)$$

where β is the orifice to pipe diameter ratio. It is clear that from equations (4.2) and (4.3) the index p depends on both β and the orifice Reynolds number Re_2 .

It is this velocity profile that has been used in the developed model for orifice metering and the quantitative results presented in Table 4.1.

4.32: Flat Profile.

For a particular pipe cross-sectional area, if the fluid flow across the section is always uniform (ie the flow does not depend on radial distance, r from axis of symmetry), the flow profile is said to be flat (or uniform) and is given by

$$U_{in} = \frac{\mu Re_1}{\rho D_1} \quad (4.4)$$

where μ = fluid viscosity,

ρ = fluid density,

D_1 = pipe diameter

and Re_1 = pipe Reynolds number.

The variations of discharge and pressure loss coefficients with velocity profiles are obtained from table 4.2 for β in the range $.3 \leq \beta \leq .7$. All the values of discharge coefficients with flat profile are slightly lower than those values when power law profile has been used for the model.

Figure 4.3 shows the variations of discharge coefficients with all three pressure tappings. The curves were obtained by comparing the coefficients for flat profile with those computed for the power-law profile (the basic model results). It can be seen that the variations are quite small for $.3 \leq \beta \leq .5$ but then increase with β to a maximum error of -1.6% at $\beta = .7$.

Percentage Variations of Discharge Coefficients.

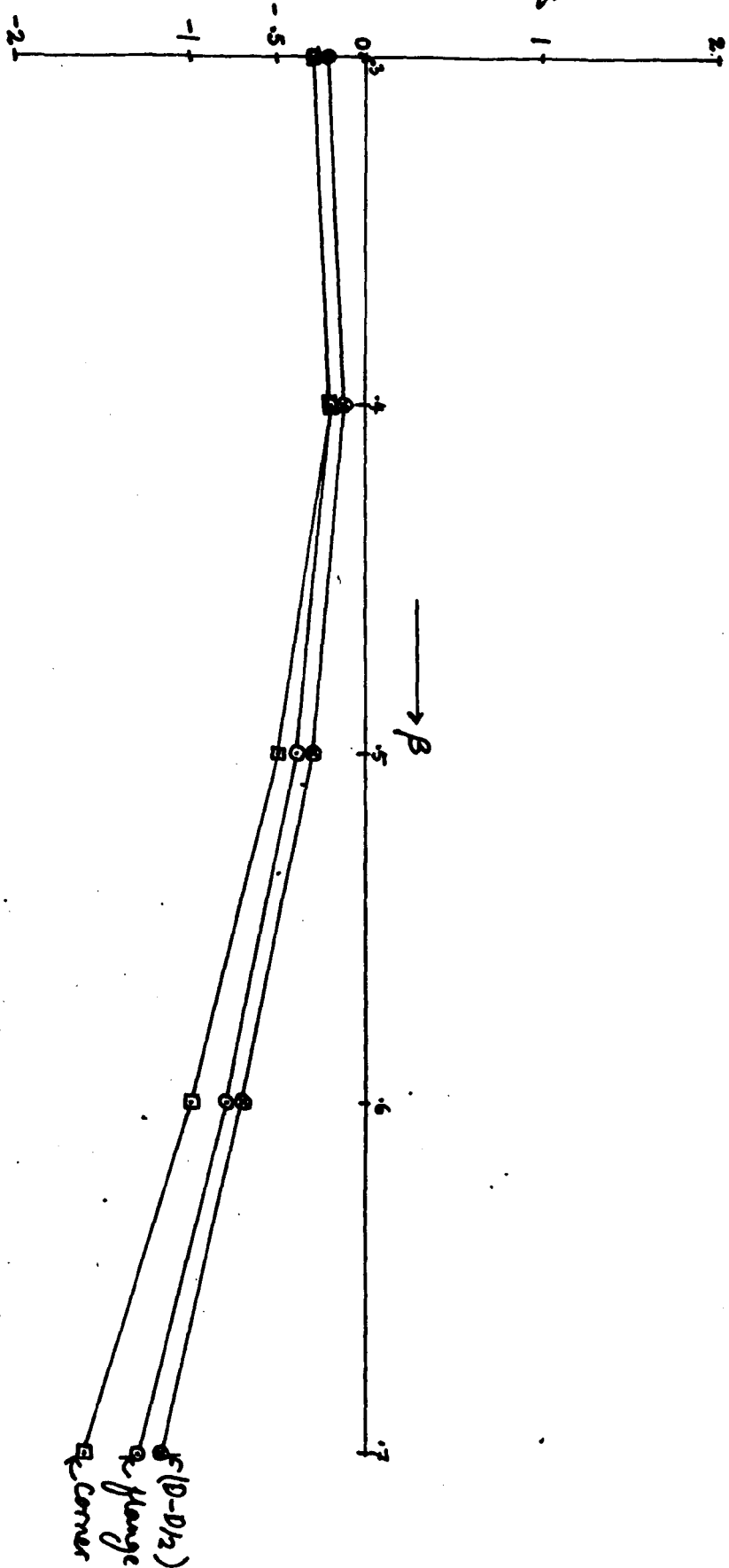


Fig. 4.3: Sensitivity of Velocity Profile Towards Discharge Coefficients for Different Values of Ratio to Pipe Diameter Ratio β (Comparison with Model).

Table 4.2 also presents the variations of the theoretical pressure loss coefficients (corrected and uncorrected) with β ratio. These predicted variations increased with increasing β beyond $\beta > .4$.

The percentage variations of the corrected pressure loss coefficients from the model values are found in figure 4.4. It has been noted that as β ratio is increased, the variations of the predicted pressure loss correction coefficients increase to a maximum deviation of 3.2% at $\beta = .7$.

4.4: TURBULENCE INTENSITIES AND LENGTH SCALE FACTOR DEPENDENCE.

The level of turbulence intensity i used to obtain the model for orifice metering has been quite low (3%) whereas the length scale factor λ was even lower (0.5%). These values of i and λ are varied to assess their sensitivity on the discharge and pressure loss coefficients.

There are essentially two methods that author employed to show the dependence of the orifice coefficients on i and λ . Firstly, either i or λ are varied keeping the other fixed, or both of them are increased simultaneously by the same factor. Secondly, the values of i and λ were obtained from previous computations downstream of the orifice plate and these values are then used to simulate the program. The reason for doing this is because just downstream of the orifice plate the flow will be extremely turbulent and would

Theoretical Discharge Coefficients.											
$\beta = \frac{D_2}{D_1}$	C_D flange		$C_D (D - D/2)$		C_D corner		$K_{theo.}$		Corrected $K_{theo.}$		$K_{exp.}$
	power	flat	power	flat	power	flat	power	flat	power	flat	
.3	.6187	.6171	.6178	.6163	.6192	.6176	292.2	293.7	291.8	293.2	297.6
.4	.6082	.6070	.6073	.6064	.6087	.6074	87.36	87.70	86.90	87.20	85.07
.5	.6036	.6012	.6037	.6016	.6039	.6011	31.70	31.99	31.27	31.51	29.87
.6	.6106	.5967	.6048	.6005	.6007	.5949	12.63	12.88	12.21	12.42	11.36
.7	.5983	.5902	.6104	.6028	.5936	.5838	5.182	4.367	4.774	4.929	4.198

Table 4.2 : Sensitivity Towards Velocity Profile.

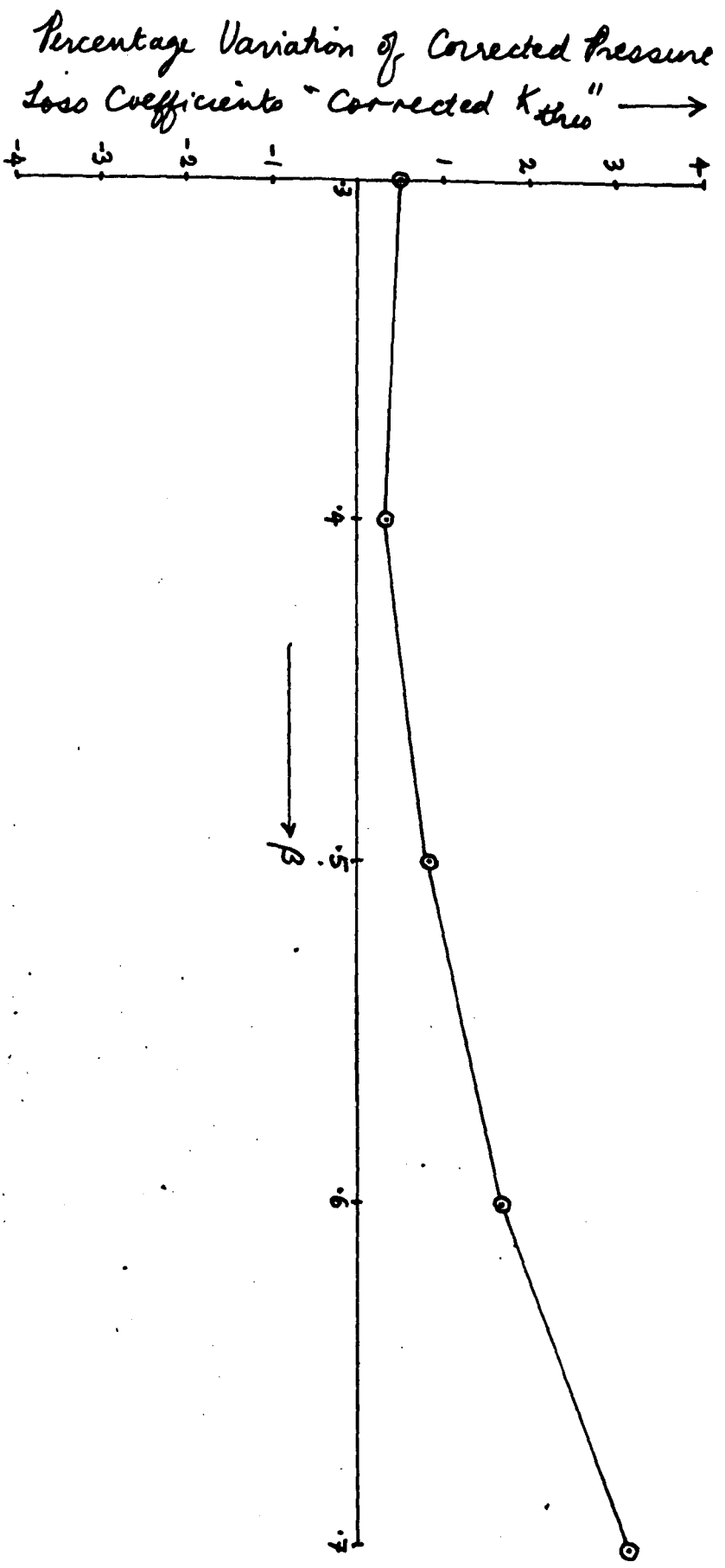


Fig. 44: Sensitivity of Velocity Profile Towards Pressure

Loss Coefficient for Different Values of β

(Comparison with Model)

realistically represent a highly turbulent field.

Table 4.3 shows the effects of changing the turbulence intensities i and length scale factor λ for $\beta = .7$ orifice plate. The power-law profile has been used to simulate flow fields. The model values of orifice coefficients appearing in row (a) are used for the comparison.

Row	i	λ	Theoretical Discharge Coefficients			$K_{theo.}$	Corrected $K_{theo.}$
			C_D flange	C_D ($D - D/2$)	C_D corner		
(a)	.03	.005	.5983	.6104	.5936	5.182	4.774
(b)	.09	.005	.5991	.6112	.5948	5.167	4.749
(c)	.03	.015	.5978	.6099	.5928	5.194	4.788
(d)	.09	.015	.5986	.6108	.5941	5.177	4.760
(e)	.02	.64	.5883	.6023	.5805	5.412	5.054

Table 4.3: Effects of Changing Turbulence Intensity i and Length Scale Factor λ for a $\beta = 0.7$ Orifice Plate.

In the second, third and fourth rows of the table the orifice coefficients have been obtained by the use of the first method described above. The values appearing in row (b) have been obtained by tripling the turbulence intensity i while keeping the length scale factor λ fixed (.5%). Although the results of discharge coefficients are slightly greater than those of model values, the variations are very small .13% (for flange), .13% (for $D - D/2$) and .20% (for corner) respectively. This shows that changing i has a small affect on the

discharge coefficient for all tappings.

The corresponding corrected pressure loss coefficient has slightly lower value than the model value. This variation is also small, within .5%.

The orifice coefficients appearing in row (c) of the table was obtained by tripling the length scale factor λ and the turbulence intensity i unchanged (3%). It can be seen that the computed discharge coefficients do not vary so much with the model values. They are within .08% (flange), .08% ($D-D/2$) and .3% (corner) respectively. Similarly the variation of corrected pressure loss coefficient is very small, within .3%. It therefore can be concluded that by tripling the length scale factor and keeping turbulence intensity unchanged do not affect the orifice coefficients since their variations with model values are negligibly small.

Similarly very small variations occur when both i and λ are increased by same factor of 3, (see row (d)).

It may be summarised therefore, by using the first method discussed earlier, that the orifice coefficients (ie discharge and pressure loss coefficients) are not sensitive to turbulence intensity i and length scale λ that may typically be encountered.

In obtaining values of discharge and pressure loss coefficients in table 4.3 in row (e), an entirely different approach has been adopted. The author found the average turbulence energy k across a

radius downstream of the orifice plate at the last grid line of the computational domain, where the variations of the energy across the pipe are small. From there the turbulence intensity i may be computed according to relation

$$i = k_{av} / U_{in}^2 \quad (4.5)$$

where k_{av} is the average inlet turbulence kinetic energy and U_{in} being the inlet velocity.

The averaged inlet dissipation rate ϵ_{av} has been obtained from previous computational results in similar manner to that described above. Since k_{av} and ϵ_{av} are related by

$$\epsilon_{av} = k_{av}^{3/2} / l \quad (4.6)$$

where

$$l = \lambda R \quad (4.7)$$

(R being the pipe radius) then the length scale factor λ may be computed from above relations as ϵ_{av} , k_{av} and R are known values.

It was unfortunate however to adopt this type of approach since the computed i is always less than 3% (the model value) whereas for length scale factor λ always very much greater than .5% (the model value for λ). For a particular values of $i=0.02$ and $\lambda = .64$ which was obtained by this method (see table 4.3 in row (e)), the computed results for discharge and pressure loss coefficients were tabulated. It can be seen that this type of approach has produced a significant variation on

the orifice coefficients.

The variations of orifice coefficients with the model values are within 1.7% (flange), 1.3% (D-D/2) and 2.2% (corner) respectively, whereas for corrected pressure loss coefficient is about 5.9%.

All the results for the variations in i and λ are summarised in table 4.4.

Predicted / Theoretical Discharge and Pressure Loss Coefficients				
Row	C_D flange	C_D (D-D/2)	C_D Corner	Corrected K_{theo} .
(b)	+ .13	+ .13	+ .20	- .5
(c)	- .08	- .08	- .13	+ .3
(d)	+ .05	+ .06	+ .08	- .3
(e)	- 1.7	- 1.3	- 2.2	+ 5.9

Table 4.4: Percentage Variations of Orifice Coefficients With Changes of i and λ .

4.5: ORIFICE PLATE THICKNESS DEPENDENCE.

The model developed in this study was for a thin orifice plate based on a $\beta = .7$ and power-law velocity profile. In this section, the above model will also be used to demonstrate how a thick orifice plate would affect the orifice coefficients (ie the discharge

and pressure loss coefficients). For this, a series of computer programs were run by using the model with different values of compression/expansion factor $EPSX$ from where the orifice plate thickness has been defined. All results of the coefficients were tabulated as can be seen in table 3.4. It can be noted the discharge coefficients for all three commonly used pressure tapings decrease with increasing $EPSX$ until a certain value where the discharge coefficients are essentially constant. This is the thin orifice plate region.

For a more clear visualisation, the variations of discharge coefficients (for each tapings) were plotted versus D_2/t (the reciprocal of t/D_2 - the convenient specification for plate thickness). This can be seen in fig. 4.5. The curves show they tend to level off at asymptotic values of ~ 0.6 (flange), ~ 0.61 (D-D/2) and ~ 0.59 (corner) respectively. For the sake of comparison, the experimental data for discharge coefficients for both tapings are however shown tabulated on the same figure 4.5. From these results thin orifice plate region can be defined as that where the discharge coefficients are asymptotically constant. For flange and corner tapings this would be for a value of $D_2/t \gg 125$ or $t/D_2 \ll .008$. It is interesting to note that for the D-D/2 tapings the asymptotic region occurs when $D_2/t \gg 350$ or $t/D \ll .003$.

It is of interest to note that BSI1042 recommend that the orifice plate thickness should be such that ,

$$t/D_1 < .02 \quad \text{when } \beta > .2$$

(see figure 3.2 in chapter 3). In terms of t/D_2 this inequality

Discharge Coefficients, $C_D \rightarrow$

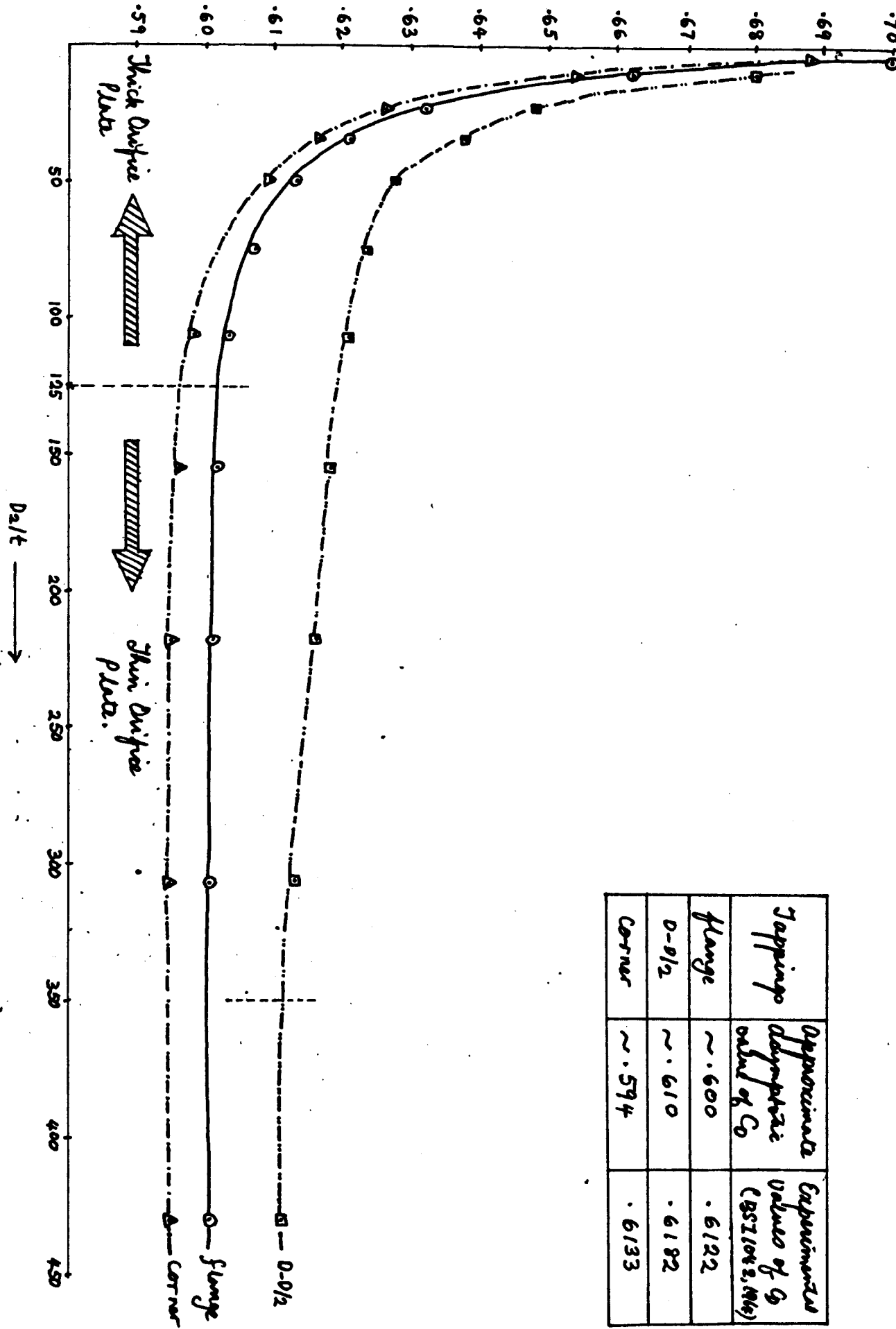


Fig. 4.5:

Variation of Discharge Coefficients with Plate Thickness.

Tapping	Approximate asymptotic value of C_D	Experimental Value of C_D (BSI 1982, 196)
Flange	~.600	.6122
D- $D/2$	~.610	.6182
Corners	~.594	.6133

becomes,

$$t/D_2 < .02 / \beta \quad \text{for } \beta > .2$$

So for $\beta = .7$

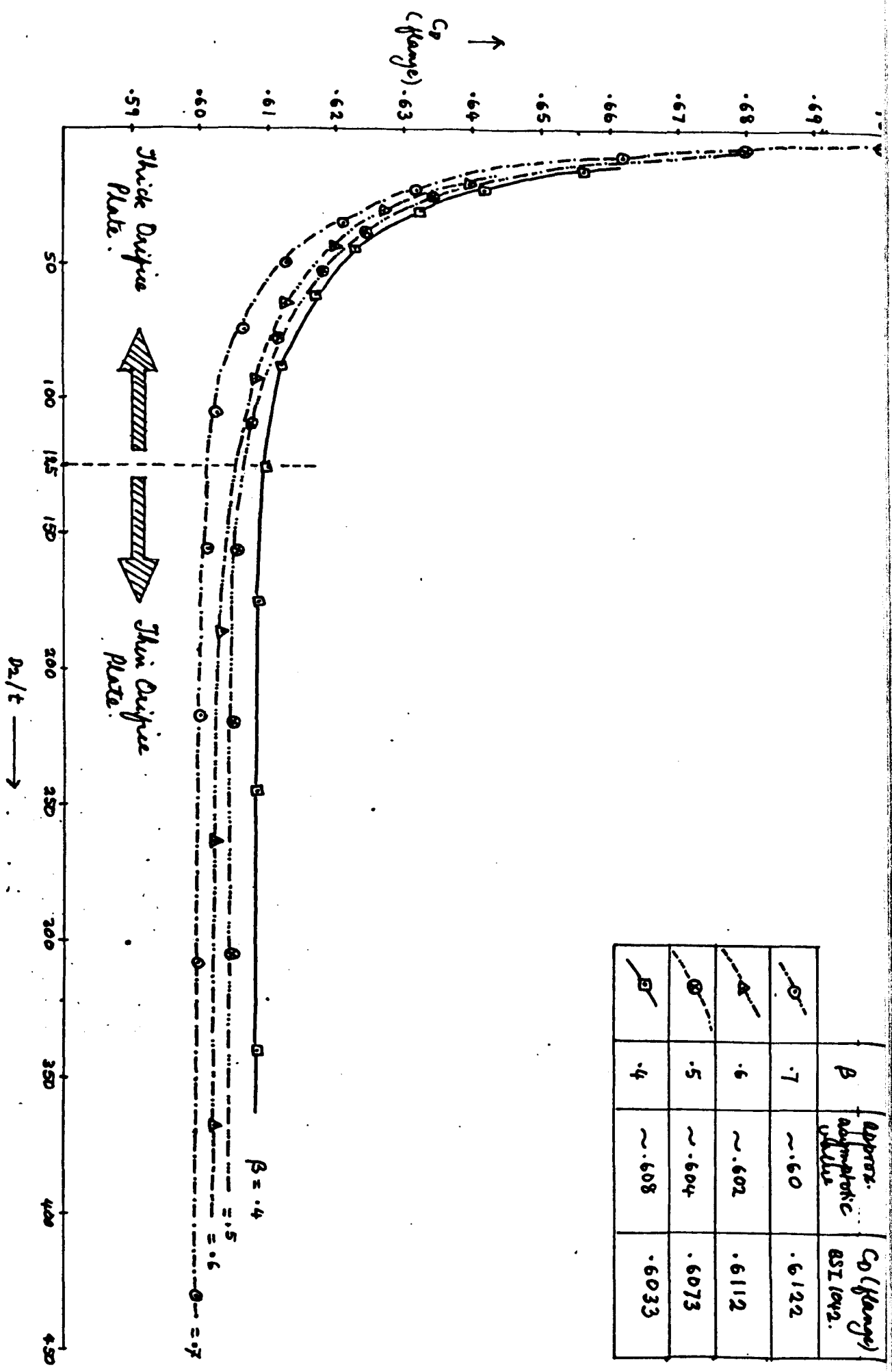
$$t/D_2 < .03 \text{ or } D_2/t > 33$$

The results of this study indicate that the orifice plate should be thinner to ensure that the discharge coefficients (and pressure loss coefficients) are in an asymptotically constant region (see figure 4.5).

The curves therefore have indicated that the discharge coefficients does depend on the plate thickness markedly. The thicker the orifice plate, the greater is the discharge coefficients. Thick orifice plates are therefore not practically used for orifice metering as discharge coefficient would vary as the orifice plate became thinner (due perhaps to wear).

Figure 4.6 shows the variations of discharge coefficients with plate thickness for different values of β in the range $.4 \leq \beta \leq .7$. Each curve however shown only for flange tap. It can be seen that the curves are constant.

The variations of the corrected pressure loss coefficient with orifice plate thickness (for $\beta = .7$ orifice) is shown in figure 4.7 (results taken from table 3.4). This also shows an asymptotically constant region for thin orifice plates ($D_2/t > 150$).



β	Approx. asymptotic values	C_D (Range) ISI 1042.
.7	~.60	.6122
.6	~.602	.6112
.5	~.604	.6073
.4	~.608	.6033

Fig. 4.6: Variation of Discharge Coefficients (Range top) with Plate Thickness, for different β values.

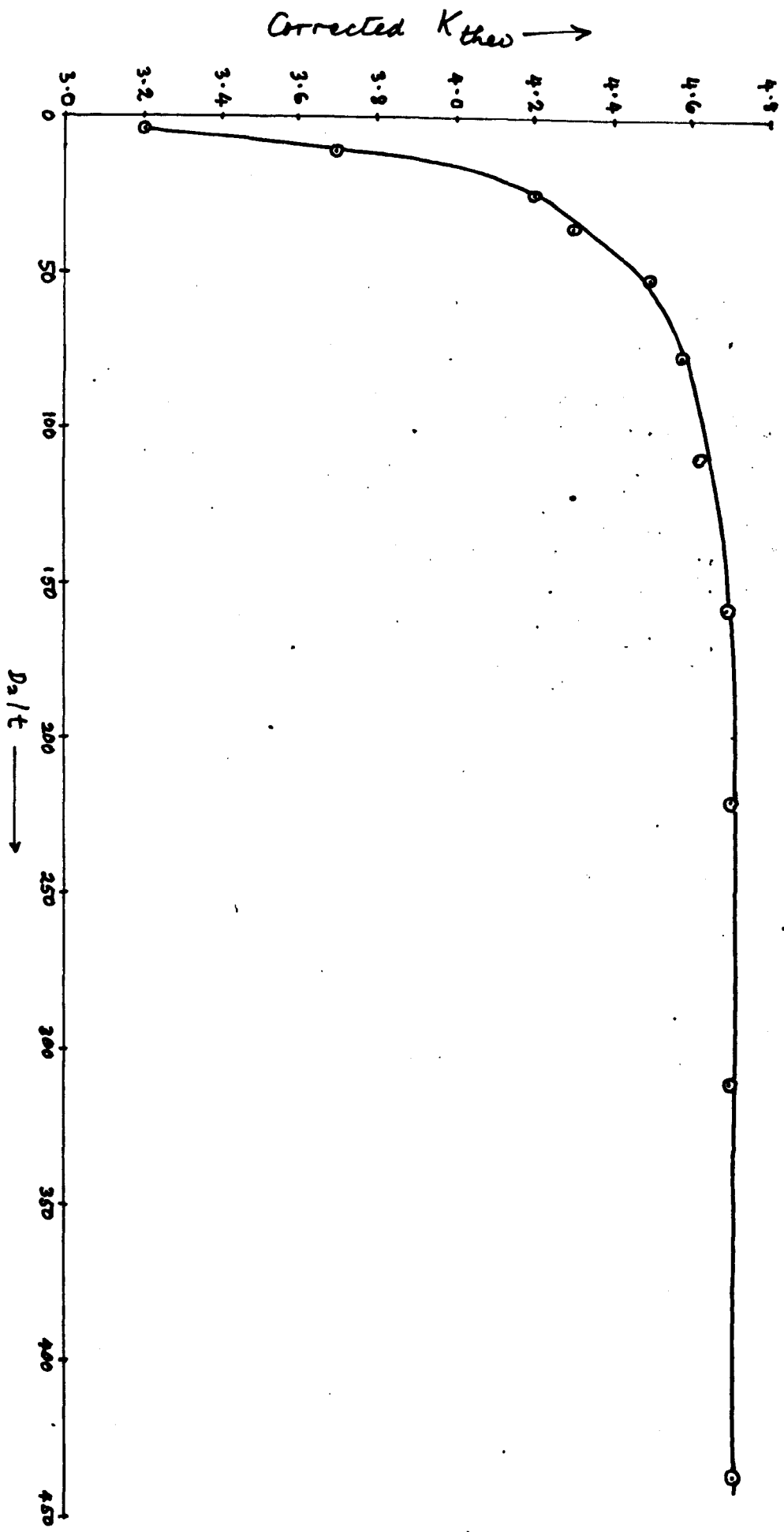


Fig 4.7: Variation of Coefficient of Contraction with Plate Thickness.

4.6: REYNOLDS NUMBER DEPENDENCE.

The Reynolds number of 1×10^5 has been used for modelling a $\beta = .7$ orifice plate. The following will demonstrate how the change of orifice Reynolds number affects the discharge and pressure loss coefficients. As already mentioned previously the power-law velocity profile has been used for the model.

Table 4.5 shows the variations of discharge and pressure loss coefficients with orifice Reynolds number. From the table it can be seen that the predicted discharge coefficients increase with the Reynolds number. The corresponding experimental data show the opposite behaviour (ie decreasing values with increasing orifice Reynolds number). The percentage variations of the coefficients with the data are also shown in the table.

Orifice Reynolds Number	Theoretical Discharge Coefficients			Experimental Discharge Coefficients			Percentage Variations		
	C_D flange	C_D (D-D/2)	C_D Corner	C_D flange	C_D (D-D/2)	C_D Corner	C_D flange	C_D (D-D/2)	C_D Corner
1×10^5	.5983	.6104	.5936	.6122	.6182	.6133	-2.3%	-1.3%	-3.2%
2.5×10^5	.6235	.6368	.6164	.6082	—	—	+2.5%	—	—
1×10^6	.6356	.6509	.6253	.6037	—	.6085	+5.3%	—	+2.8%

Table 4.5: Variations of Discharge Coefficients with Orifice Reynolds Number.

The variations of the corrected pressure loss coefficient may be obtained from table 4.6. The table shows the coefficients decrease with increasing Reynolds number. The percentage variations from the experimental data are also shown in the table.

Orifice Reynolds Number, Re_s	$K_{theo.}$	Corrected $K_{theo.}$	K_{exp}	Percentage Variations
1×10^5	5.182	4.774	4.198	+13.7%
2.5×10^5	4.623	4.281	4.198	+2.0%
1×10^6	4.318	4.058	4.198	-3.3%

Table 4.6: Variations of Corrected Pressure Loss Coefficients with Orifice Reynolds Number.

It is interesting to note that although the variations with Reynolds number show marked changes in the computed results compared with small changes in the experimental results. The computed results have errors which fall either side of the experimental results as the Reynolds number is increased. In fact for the corrected pressure loss coefficients a much better comparison with experiment is achieved at high Reynolds number.

Before concluding this chapter, it should be pointed out that after the author had completed his study on orifice metering, a paper entitled 'Numerical Modelling of Turbulent Flow Through Thin Orifice Plates' by R.W. Davis and G.E. Mattingly was discovered. This was presented at a symposium, 'Proceedings of the Symposium on Flow in Open

Channels and Closed Conduits' held at NBS, Gaithersburg, M.D (issued October, 1977). Their model was also based on the k- ϵ turbulent TEACH-T computer model and therefore the following will show how the discharge coefficients in their study compare with the results obtained in the present study. The comparison are however for D-D/2 and corner tappings and with β ratio in the range $0.4 \leq \beta \leq .7$. There is no data on discharge coefficient with flange tap and pressure loss coefficients to compare with.

Table 4.7 shows the comparison of the computed discharge coefficients (for D-D/2 and corner tappings) with data of Davis and Mattingly (1977). They have used a power-law velocity profile with 1/9-th. power index p, whereas in the present study the power index of $\sim 1/12$ has been used. The results indicate quite similar values except for the $\beta = .7$ (D-D/2) tapping result. Typically the variations for the other results are $\leq 1 \sim 2\%$. Bearing in mind that the results were obtained completely independently the agreement is quite encouraging.

$\beta = D_2/D_1$	$C_D (D - D/2)$		$C_D (corner)$		Percentage Variations	
	Present Study	Davis and Mattingly	Present Study	Davis and Mattingly	$C_D (D - D/2)$	$C_D (corner)$
.4	.6073	.615	.6087	.616	-1.3	-1.2
.5	.6037	.609	.6039	.607	-.9	-.5
.6	.6048	.616	.6007	.602	-1.8	-.2
.7	.6104	.637	.5936	.591	-4.2	+ .4

Table 4.7: β -ratio Dependence -Comparison With Data of Davis and Mattingly (1977).

4.7: CONCLUDING REMARKS.

The quantitative results presented in this chapter for $0.3 \leq \beta \leq 0.7$ orifice plate computer simulations lead to the following conclusions.

(a) The discharge coefficients (flange $D-D/2$ and corner tappings) can be predicted to within approximately $\pm 3\%$ of those reported in BSI 1042. In the mid-range $\beta = 0.45$ the agreement is excellent whereas the maximum deviation occurs at the extremities $\beta = 0.3, \beta = 0.7$.

(b) The pressure loss introduced by the orifice plate can be calculated to within 15% of that obtained experimentally. For $0.3 \leq \beta \leq 0.5$ the error is less than 5% whereas after $\beta = 0.5$ the error increases rapidly to maximum (15%) at $\beta = 0.7$. A plausible explanation for this is that at high β the pressure drop across the orifice is small so any errors in the calculation procedure will be magnified and also errors arising from calculating the correction required to account for the pipe wall loss will be significant. At small β the pressure loss due to the orifice is large compared to the wall loss and therefore such errors will not arise.

(c) Various sensitivity tests were done with the following results.

(i) The velocity profile affects the orifice coefficients, the difference between a power-law profile (approximately $1/12$ index) and a

flat or uniform profile being about $1/4 - 1.5\%$ for discharge coefficients and $1/2 - 3\%$ for pressure loss coefficients.

(ii) In general typical variations in turbulence intensities and length scales have a very small effect on the orifice coefficients (both pressure loss and discharge coefficients). However high turbulence levels such as those encountered 10-15 diameters downstream of an orifice plate lead to significant changes ($1 - 2\%$ for discharge coefficients and 6% for pressure loss coefficients).

(iii) The orifice plate thickness has a marked affect on both coefficients when the thickness is above some particular value. This was found to be $D_2/t < 125$ for flange and corner tapings and $D_2/t < 350$ for D-D/2 tapings, where D_2 is the orifice diameter, t the thickness. This inequalities define what is meant by a thin orifice plate. They seem to violate that from BSI 1042 implying that the orifice plate should be thinner.

(iv) The results presented were for $Re_2 = 1 \times 10^5$. Increasing the Reynolds number led to changes in the coefficients contrary to experiment (BSI 1042) where they are essentially constant. The reason for this is unknown and need to be explored further. It was interesting to note that although the theoretical results varied with Reynolds number they straddled the experimental result.

(d) Independent results presented by Davis and Mattingly at an NBS symposium were discovered after completion of this study. Comparison of their results with those presented here showed an

encouragingly close agreement.

In conclusion it would appear that the basic model can be used to calculate quantities of interest to the designer and user of orifice plates. Although the maximum errors of $\pm 3\%$ in calculation of discharge coefficients are too large for accurate metering the basic trends found are correct. In contrast the pressure loss errors of 15% are sufficiently useful for practical design purposes.

CHAPTER 5CONCLUSIONS

The study presented in this thesis set out to apply the $k-\epsilon$ turbulent mathematical model developed at Imperial College London, to orifice metering. Before embarking on this the author explored the underlying theory behind the $k-\epsilon$ model and this has been presented in this thesis together with programming details. Most of this work has been relegated to the various mathematical appendices.

The careful development of the orifice meter model presented in Chapter 3 followed by detailed application results to thin orifice plates presented in Chapter 4 (summarised in section 4.7) has clearly shown the value of this type of modelling. The prediction of discharge coefficients for a range of diameter ratio values (β) to within a few percent ($\pm 3\%$) and pressure loss coefficients to within 15% indicates that such models will find increasing applications in future studies of the orifice meter and other related differential pressure flow metering devices such as venturi meters and various forms of nozzles.

It would appear that a combined experimental/theoretical approach to the understanding and design of flow meters in this class would be useful and timely. Timely in the sense that the processing power of digital computers has reached the stage, as indicated in this thesis, where extremely useful results for the previously intractable problems of turbulent recirculating flows can be solved.

To give some idea of the power of this approach it should be realised that if the results presented in Chapter 4 were reproduced experimentally, they would require (according to the author's estimate) at least 120 separate experimental runs. Each of these would be costly and time consuming.

Although the present model developed applies to two dimensional axisymmetric flow through a concentric orifice plate, in theory turbulent models such as the $k-\epsilon$ model presented here, can be applied to three dimensional flows, for example those encountered at bends upstream of an orifice meter. The limitations on such modelling are still the large store and computing time requirements for a solution.

More easily solved problems at present would be the incorporation of swirl into a two dimensional axisymmetric flow. This would require the addition of another component of velocity W in the azimuthal or out-of-the plane θ -direction. The $k-\epsilon$ model would have to be modified and then solved for this additional variable.

Regarding the best form of man-machine (computer) dialogue it would appear that future work should concentrate on the development of interactive programs with extensive use of graphic facilities (such as those available in our departmental PRIME 550 computers). With the addition of extensive pre and post-processing facilities to basic analysis programs (such as the one developed here for orifice meters), very effective interaction will be achieved. For example the preprocessor could prompt the user regarding the orifice geometry and

flow conditions required by the user, whereas a post processor could be used to interrogate the resulting solution to investigate pressure, velocity and turbulence fields anywhere in the flow calculation domain as well as displaying the entire field graphically if required. For example flow streamlines could be displayed as could pressure contours and velocity vectors. This area is an important area for further investigations. General and extensive work on pre and post processors is being done by various interested groups within the Interactive Computing Facility (ICF) of the Science Research Council.

Looking further into the future it would appear likely that finite element based equivalents of the TEACH-T finite difference code will be developed. These may have the advantage of greater flexibility in describing complex boundaries and boundary conditions. In addition much of the finite element software such as mesh generation preprocessors and post processing 'viewers' will then be appropriate.

BIBLIOGRAPHY.

1. Allen D.N.(1954).
Relaxation Methods.
Mc.Graw-Hill,N.Y.
2. Alvi et al(1978)
Loss Characteristics of Orifices and Nozzles
ASME J.Fluid Eng.100,pg.299
3. Ananyan A.K.(1957),(Translated from Russian).
Fluid Flow in Bends of Conduits.
Published by The Israel Program for Scientific Translations.
4. Batchelor G.K.(1970)
The Theory of Homogeneous Turbulence
Cambridge University Press.
5. Blake K.A.et al (1976)
IMEKO VII Congress
Practical Measurement for Improving Efficiency,Vol.4.
London.
6. Bradshaw P.(1971)
An Introduction to Turbulence and Its Measurement.
Pergamon Press Oxford,N.Y.,Toronto,Sydney.
7. Bradshaw(Editor),(1976)
Topics in Applied Physics,Vol.12.
Springer-Verlag,Berlin,Heidelberg,N.Y.

8. British Standard 1042 Part 1 (1964).
Methods For the Measurement of Fluid Flow in Pipes.
British Standard Institution, London.
9. Buckingham, E. (1956).
Notes On Some Recently Published Experiments on Orifice Meters.
Trans. Amer. Soc. Mech. Engrs., 73, pg. 379-387.
10. Carl E.P. (1965).
A Computational Methods for Viscous Flow Problem.
J. Fluid Mech. 21, pg. 611.
11. Concoran et al (1956).
Momentum Transfer in Fluids.
Academic Press Inc. Publishers, New York.
12. Cotton K.C. (Editor), (1966).
Flow Measurement Symposium,
The American Society of Mechanical Engineers, N.Y.
13. Daly B.J. and Harlow F.H. (1970).
Transport Equations in Turbulence.
Phys. Fluids 13, pg. 2634.
14. David W.C. and Frank T.B. (1974).
Implicit Solutions of the Unsteady Navier-Stokes' Equation for
Laminar Flow Through An Orifice Within a Pipe.
Computers and Fluids, 2, pg. 295.
15. Deardroff J.W. (1970).
A Numerical Study of 3-D Turbulent Channel Flow at High Reynolds
Numbers.
J. Fluid Mechanics, 41, pg. 453-480.

16. Donkin C.T.B.(1959).
Elementary Practical Hydraulics of Flow in Pipes.
Oxford University Press,N.Y.,Toronto.
17. Durst F.et al (Editors),(1979).
Turbulent Shear flows 1.
Springer-Verlag,Berlin Heidelsburg,New York.
18. Enzo O.et al (1967).
Computational and Experimental study of a Captive Annular Eddy.
J.Fluid Mech.,28,pg.43-64.
19. Fluid Meters-Their Theory and Application.
Fifth Edition-ASME N.Y.(1959)
20. Gibson M.M.(et al),(1977).
Fundamentals of Turbulence and Their Application in Calculation
Methods.
Department of Mechanical Engineering,Imperial College,London.
Notes for a Lecture Course FS/77/6
21. Gosman A.D. et al (1969)
Heat and Mass Transfer in Recirculating Flows.
Academic Press,London and New York.
22. Gosman A.D.et al (1973).
Calculation of Recirculating Flows.
Mechanical Engineering Department Report,HTS/74/2,Imperial
College,London.
23. Gosman A.D. and Ideriah F.J.K.(1976)
TEACH-T:A General Computer Program for Two-Dimensional Turbulent,
Recirculating Flows.
Department of Mechanical Engineering,Imperial College,London.

24. Greenspan D.(1969).
Numerical Studies of Steady,Viscous,Incompressible Flow in a Channel With a Step.
J.Eng.Math.,3,pg.21-28.
25. Greenspan D.(1973).
Numerical Studies of Viscous,Incompressible Flow Through an Orifice For Arbitrary Reynolds Number.
Int.J.for Num.Methods in Eng.,6,pg.489-496.
26. Hafiz M. and Abdullah F.(1978).
Derivation of Mathematical Equations for Describing Turbulent Flows in Relation to Flow Metering.
Departmental Report DSS/MH-FA/166
27. Hall G.W.(1963).
Analytical Determination of the Discharge Characteristics of Cylindrical Tube Orifices.
J.Mech.Eng.Science,180,pg.331-345.
28. Halmi D.(1973).
Practical Guide to the Evaluation of the Metering Performance of Differential Producers.
ASME J.Fluid Eng.,95,pg.127-141.
29. Hanjalic K. and Launder B.E.(1972).
A Reynolds Stress Model of Turbulent and Its Application to Thin Shear Flows.
J.Fluid Mech.,52,pg.609.
30. Hinze J.O.(1959).
Turbulence:An Introduction to Its Mechanism and Theory.
Mc.Graw-Hill Book Company,Inc.N.Y.,Toronto,London.

31. Hodgson J.L.(1917).
The Commercial Metering of Air, Gas and Steam.
Proc.Instn.Civil Engrs.,204,pg.103.
32. Ideriah F.J.K.(1977).
Turbulent Natural and Forced Convection in Plumes and Cavities.
Ph.D.Thesis,University of London.
33. Jones W.P. and Launder B.E.(1972).
Prediction of Laminarization with a 2-Equation Model of
Turbulence.
Int.J.Heat Mass Transfer,15,pg.301.
34. Kays W.M.(1966).
Convective Heat and Mass Transfer
Mc.Graw-Hill,N.Y.
35. Kubo I.and Gouldin F.C.(1975).
Numerical Calculations of Turbulent Swirling Flow.
ASME J.Fluids Eng.,97,pg.310.
36. Launder B.E.and Spalding D.B.(1972).
Mathematical Models of Turbulence
Academic Press,London and New York.
37. Launder B.E.(Editor),(1975).
Studies in Convection,Theory,Measurement and Application,Vol.1
Academic Press,London,New York,San Fransisco.
38. Launder B.E.(1975).
Progress in the Development of a Reynolds Stress Turbulence
Closure.
J.Fluid Mech.,68,pg.537-566.

39. Leslie D.C.(1973).
Development in the Theory of Turbulence.
Clarendon Press,Oxford.
40. Lin C.C.(Editor),(1959).
Turbulent Flows and Heat Transfer.
London Oxford University Press.
41. Lin C.C.(1961).
Statistical Theories of Turbulence.
Priceton University-Press Princeton,N.Y.
42. Lichtarowicz et al (1965).
Discharge Coefficients for Incompressible non-cavitating Flow
Through Long Orifices.
J.Mech.Eng.Sc.,7,no.2,pg.210.
43. Longwell H.L.(1966).
Mechanics of Fluid Flow.
The Mc.Graw-Hill Book Company,N.Y.
St.Louis,San Fransisco,Toronto,London,Sydney.
44. Lumley J.L. and Khajeh Nouri,B.(1974).
Computational Modelling of Turbulent Transport.
Proc.2nd.IUGG-IUTAM Symposium on Atmospheric Diffusion in
Environmental Pollution.
Academic Press.
45. Mills R.D.(1963).
Numerical Solutions of Viscous Flow Through A Pipe Orifice
at Low Reynolds Number.
J.Mech.Eng.Sc.,10,pg.133-140.

46. Moon L.F. and Rudinger G. (1977).
Velocity Distribution in an Abruptly Expanding Circular Duct.
ASME J. Fluid Eng., 99, pg. 226.
47. N.E.L. (1962).
Flow Measurement in Closed Conduits.
Proceedings of a Symposium held at a National Engineering
Laboratory, 27th.-30th. September 1960, Vols. 1 and 2.
Her Majesty's Stationary Office.
48. Odus R.B. (1966).
Analytical and Numerical Studies of the Structure of Steady
Separated Flows.
J. Fluid Mech., 24, pg. 113-151.
49. Ower E. and Pankhurst R.C. (1966).
The Measurement of Air Flow (4th. Edition)
Pergamon Press.
50. Patankar S.V. and Spalding D.B. (1967).
Heat and Mass Transfer in Boundary Layers.
Morgan-Grampian, London.
51. Patankar S.V. and Spalding D.B. (2nd. Edition, 1970).
Heat and Mass Transfer in Boundary Layers.
Intertext Books, London.
52. Patrick J.R. (1972).
Computational Fluid Dynamics.
Hermosa Publishers.
53. Reynolds R.J. (1974).
Turbulent Flows in Engineering.
John Willey and Sons.

54. Runchal A.K. and Wolfshtein (1969).
Numerical Integration Procedure for the steady State Navier
Stokes' Equations.
J.Mech.Eng.Sc., 11, pg.445-453.
55. Salimanu D.O.(1975).
Mathematical and Programming Details af the TEACH-T and -L
Recirculating Flow Code.
Argonne National Laboratory Technical Memorendum ANL-CT-76-22.
56. Schubauer G.B.and Klebanoff (1950).
Investigation of Separation of the Turbulent Boundary Layer.
NACA TN 2133 (1950),also NACA Report 1030 (1951).
57. Shames I.H.(1962).
Mechanics of Fluids.
International Student Edition.
Mc.Graw-Hill Kogakusha Ltd.Tokyo,Dusseldorf,Johannesburg.
58. Southwell R.V.(1946).
Relaxation Methods in Theoretical Physics.
Oxford University Press,N.Y.
59. Sovran G.(Editor),(1967).
Fluid Mechanics of Internal flow.
Elsevier Publishing Company,
Amsterdam-London-New York.
60. Spalding D.B.(1972).
A Novel Finite Difference Formulation for Differential Expressions
Involving Both First and Second Derivatives.
Int.J.for Num.Methods in Eng.,4,pg.551-559.

61. Stearn R.F. et al (1951).
Flow Measurement With Orifice Meters.
D. Van Nostrand company. Inc. Toronto, New York, London.
(see page 16 for comments on measurement difficulties for extreme values of β).
62. Taylor C.M. (Editor), (1980).
Recent Advances in Numerical Methods in Fluids, Vol. 1.
Pineridge Press, Swansea.
63. Tennekes H. and Lumley J.L. (1972).
A First Course in Turbulence.
The MIT Press, Cambridge, Massachusetts and London.
64. Ward Smith A.J. (1963).
The Flow and Pressure Losses in Smooth Pipe Bends of Constant Cross-Section.
J. Royal Aeronautical Society, 67, pg. 437.
65. Ward Smith A.J. (1971).
Pressure Losses in Ducted Flows.
Butterworths, London. (see equation 4.45 page 188 for pressure loss results.)

APPENDIX AA.1: DERIVATION OF NAVIER-STOKES' DIFFERENTIAL EQUATIONS

An infinitesimal volume of fluid element which at time t has the shape given by fig:A.1 will be considered. Its velocity in space $x_i \equiv (x, y, z)$ $i=1, 2, 3$ will be denoted by $\hat{u}_i(x_i, t)$ and moves following the fluid so that its acceleration will be given by the substantial derivative of the velocity. We also assume the body force per unit mass will be denoted by,

$$\underline{B} = B_x \underline{i} + B_y \underline{j} + B_z \underline{k} \quad (\text{A.1})$$

and is not shown in the figure.

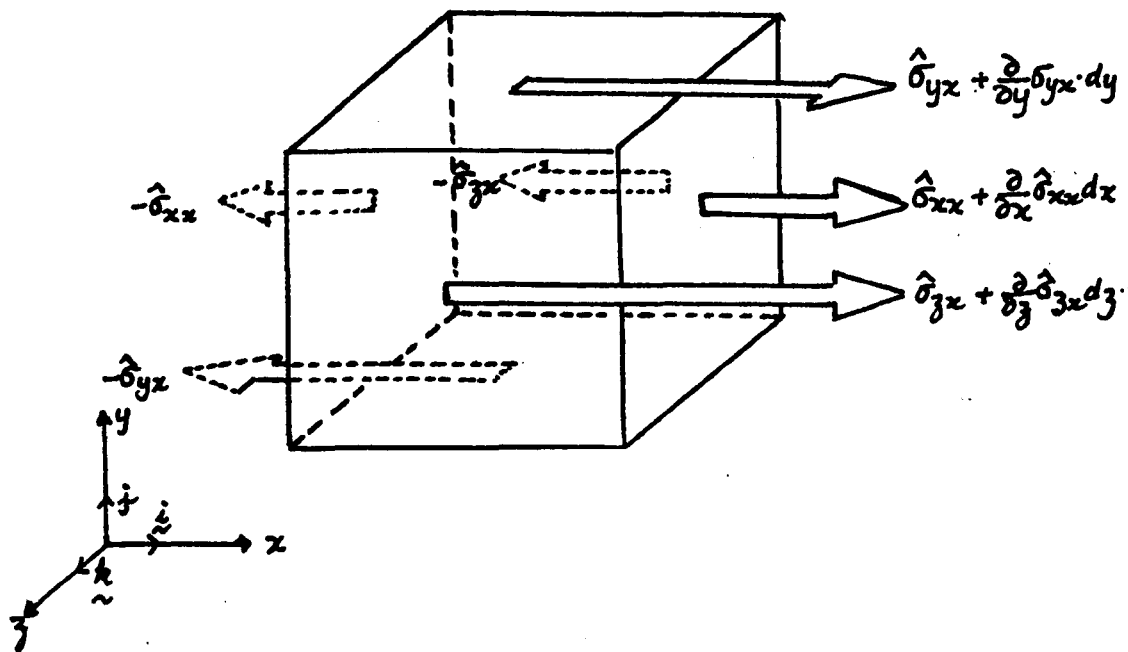


Fig:A.1 Shear and normal stresses in the x-direction

If the fundamental statement of Newton's second law in terms of momentum for an inertial reference is applied to the volume element, the following expression,

$$d\underline{F} = \frac{D}{Dt} (dm \underline{\hat{u}}) \quad (\text{A.2})$$

will be obtained where $d\underline{F}$ is an infinitesimal force, $\frac{D}{Dt} (\equiv \underline{\hat{u}} \cdot \nabla + \frac{\partial}{\partial t})$ is the substantial or total derivative (see Shames, 1962), dm is the mass of the infinitesimal fluid and $\underline{\hat{u}} = \hat{u}_i(x_i, t)$.

The force $d\underline{F}$ may be resolved into its components, namely the surface force $d\underline{f}$ and the body force $\underline{B}dm$ to yield,

$$d\underline{f} + \underline{B}dm = dm \frac{D}{Dt} \underline{\hat{u}} \quad (\text{A.3})$$

where dm is assumed to be constant. In the x-direction, equation (A.3) becomes,

$$df_x + B_x dm = dm \left(\hat{u}_x \frac{\partial}{\partial x} \hat{u}_x + \hat{u}_y \frac{\partial}{\partial y} \hat{u}_x + \hat{u}_z \frac{\partial}{\partial z} \hat{u}_x + \frac{\partial}{\partial t} \hat{u}_x \right) \quad (\text{A.4})$$

From the figure also, the following expression for the surface force in x-direction, may be obtained,

$$df_x = \frac{\partial}{\partial x} \hat{\sigma}_{xx} dx \cdot dy dz + \frac{\partial}{\partial y} \hat{\sigma}_{yx} dy \cdot dx dz + \frac{\partial}{\partial z} \hat{\sigma}_{zx} dz \cdot dx dy \quad (\text{A.5})$$

which relates it with stresses $\hat{\sigma}_{ij}$.

By replacement of equation (A.5) into (A.4), the following

relations for the x-, -y and z-directions will be obtained,

$$\left. \begin{aligned} & \left(\frac{\partial}{\partial x} \hat{\sigma}_{xx} + \frac{\partial}{\partial y} \hat{\sigma}_{yx} + \frac{\partial}{\partial z} \hat{\sigma}_{zx} \right) dv + B_x \rho dv \\ & \qquad \qquad \qquad = \rho dv \left(\hat{u}_x \frac{\partial}{\partial x} \hat{u}_x + \hat{u}_y \frac{\partial}{\partial y} \hat{u}_x + \hat{u}_z \frac{\partial}{\partial z} \hat{u}_x + \frac{\partial}{\partial t} \hat{u}_x \right) \\ & \left(\frac{\partial}{\partial y} \hat{\sigma}_{yy} + \frac{\partial}{\partial z} \hat{\sigma}_{zy} + \frac{\partial}{\partial x} \hat{\sigma}_{xy} \right) dv + B_y \rho dv \\ & \qquad \qquad \qquad = \rho dv \left(\hat{u}_y \frac{\partial}{\partial y} \hat{u}_y + \hat{u}_z \frac{\partial}{\partial z} \hat{u}_y + \hat{u}_x \frac{\partial}{\partial x} \hat{u}_y + \frac{\partial}{\partial t} \hat{u}_y \right) \\ & \left(\frac{\partial}{\partial z} \hat{\sigma}_{zz} + \frac{\partial}{\partial x} \hat{\sigma}_{xz} + \frac{\partial}{\partial y} \hat{\sigma}_{yz} \right) dv + B_z \rho dv \\ & \qquad \qquad \qquad = \rho dv \left(\hat{u}_z \frac{\partial}{\partial z} \hat{u}_z + \hat{u}_x \frac{\partial}{\partial x} \hat{u}_z + \hat{u}_y \frac{\partial}{\partial y} \hat{u}_z + \frac{\partial}{\partial t} \hat{u}_z \right) \end{aligned} \right\} \text{(A.6)}$$

where dv has replaced $dx dy dz$ (the volume element) and dm equals ρdv ;

ρ is the fluid density. Above set of equations (A.6) may be represented by a tensor notation,

$$\frac{\partial}{\partial x_j} \hat{\sigma}_{ji} + \rho B_i = \frac{D}{Dt} \rho \hat{u}_i \quad \forall i, j = 1, 2, 3 \quad \text{(A.7)}$$

where $\hat{\sigma}_{ji} = \hat{\sigma}_{ij}$ is a 'diagonally symmetric' tensor and repeated indices implies summation—i.e. Einstein notation. Equation (A.7) represents a general fluid flow when coupled with continuity equation,

$$\frac{\partial}{\partial t} \rho + \frac{\partial}{\partial x_i} (\rho \hat{u}_i) = 0, \quad i = 1, 2, 3 \quad \text{(A.8)}$$

which would be obtained from the consideration of mass conservation.

The sresses $\hat{\sigma}_{ij}$ cause deformations of fluid elements and since these deformations are determined by deformation rates (or spatial variations $\frac{\partial}{\partial x_j} \hat{u}_i$ of the instantaneous velocities \hat{u}_i) it is possible to relate those sresses with these deformation rates. The average normal sresses is related to the instantaneous pressure \hat{p} by,

$$\frac{1}{3} \hat{\sigma}_{ij} = -\hat{p} \quad \text{(A.9)}$$

The rates of deformation is split up into two parts— the symmetric \hat{s}_{ij} and antisymmetric parts \hat{r}_{ij} where,

$$\frac{\partial \hat{u}_i}{\partial x_j} = \hat{s}_{ij} + \hat{r}_{ij} \quad (\text{A.10})$$

with
$$\hat{s}_{ij} = \frac{1}{2} \left(\frac{\partial \hat{u}_i}{\partial x_j} + \frac{\partial \hat{u}_j}{\partial x_i} \right) \quad (\text{A.11})$$

and
$$\hat{r}_{ij} = \frac{1}{2} \left(\frac{\partial \hat{u}_i}{\partial x_j} - \frac{\partial \hat{u}_j}{\partial x_i} \right) \quad (\text{A.12})$$

The symmetrical part determines the deformation of fluid elements and is called rate of strain(or deformation) tensor, while the antisymmetric part determines a rotation of the fluid elements without deformation.

If the fluid is considered Newtonian, there must be a relation between stresses $\hat{\sigma}_{ij}$ and the strain rate tensor \hat{s}_{ij} , so,

$$\hat{\sigma}_{ij} = 2\mu \hat{s}_{ij} \quad \text{for } i \neq j \quad (\text{A.13})$$

where μ is the fluid viscosity.

For $i = j$, there is an additional contribution from pressure \hat{p} which causes either a compression or an expansion of the fluid elements thus,

$$\hat{\sigma}_{ij} = 2\mu \hat{s}_{ij} - \hat{p} \delta_{ij} + \lambda \hat{d} \delta_{ij} \quad \forall i, j \quad (\text{A.14})$$

where δ_{ij} : the kronecker delta (or unit second order tensor),

$$\hat{d} (= s_{ii} = \frac{\partial \hat{u}_i}{\partial x_i}) : \text{ the dilation} \quad (\text{A.15})$$

and λ is a constant to be determined. This constant may be obtained by the following contraction (summation) process:

$$\hat{\sigma}_{ii} = 2\mu \hat{s}_{ii} - \hat{p} \delta_{ii} + \lambda \hat{d} \delta_{ii} \quad (\text{A.16})$$

from where $\lambda = -\frac{2}{3}\mu$ for if $\hat{d} (= \hat{s}_{ii}) \neq 0$ (A.17)

after relations (A.9) and (A.15) have been used and the fact that,

$$\delta_{ii} = 3 \quad (\text{A.18})$$

By replacing equation (A.17) into (A.14) we obtain,

$$\hat{\sigma}_{ij} = 2\mu \hat{s}_{ij} - \hat{p} \delta_{ij} - \frac{2}{3}\mu \hat{d} \delta_{ij} \quad (\text{A.19})$$

Equations (A.7) and (A.8) now become, after slight arrangement,

$$\frac{\partial}{\partial t}(\rho \hat{u}_i) = \frac{\partial}{\partial x_j} \left\{ -\hat{p} \delta_{ij} + 2\mu \hat{s}_{ij} \right\} - \frac{2}{3} \frac{\partial}{\partial x_i} \left(\mu \frac{\partial u_i}{\partial x_i} \right) + \rho \theta_i \quad (\text{A.20})$$

$$\frac{\partial}{\partial t} \rho + \frac{\partial}{\partial x_i} (\rho \hat{u}_i) = 0 \quad (\text{A.8})$$

which forms a general expression for the Navier-Stokes' differential equations for compressible flow. However for a steady incompressible flow with body forces neglected equations (A.20) and (A.3) now reduce to,

$$\hat{u}_j \frac{\partial}{\partial x_j} \hat{u}_i = \frac{1}{\rho} \frac{\partial}{\partial x_j} \hat{\sigma}_{ij} \quad (\text{A.21})$$

and
$$\frac{\partial \hat{u}_i}{\partial x_i} = 0 \quad (\text{A.22})$$

where
$$\hat{\sigma}_{ij} = -\hat{p}\delta_{ij} + 2\mu\hat{s}_{ij} \quad (\text{A.23})$$

and
$$\hat{s}_{ij} = \frac{1}{2}\left(\frac{\partial \hat{u}_i}{\partial x_j} + \frac{\partial \hat{u}_j}{\partial x_i}\right) \quad (\text{A.24})$$

as the instantaneous rate of strain.

A.2: VORTICITY FORM OF THE NAVIER-STOKES' EQUATIONS OF MOTION

Referring back to equation (A.21) now with body forces included, we have,

$$\hat{u}_j \frac{\partial}{\partial x_j} \hat{u}_i = \frac{1}{\rho} \frac{\partial}{\partial x_j} \hat{\sigma}_{ij} + B_i \quad (\text{A.25})$$

If relations (A.23) and (A.24) are used, then equation (A.25) is equivalent to

$$\hat{u}_j \frac{\partial}{\partial x_j} \hat{u}_i = -\frac{1}{\rho} \frac{\partial}{\partial x_i} \hat{p} + \nu \frac{\partial^2}{\partial x_j \partial x_j} \hat{u}_i + B_i \quad (\text{A.26})$$

where $\nu = \mu\rho^{-1}$ is the kinematic fluid viscosity.

Now expression $\hat{u}_j \frac{\partial}{\partial x_j} \hat{u}_i$ on the left hand side of (A.26) can be represented into other forms through,

$$\begin{aligned} \hat{u}_j \frac{\partial}{\partial x_j} \hat{u}_i &= \hat{u}_j \left(\frac{\partial \hat{u}_i}{\partial x_j} - \frac{\partial \hat{u}_j}{\partial x_i} \right) + \hat{u}_j \frac{\partial}{\partial x_i} \hat{u}_j \\ &= 2\hat{u}_j \hat{\tau}_{ij} + \frac{\partial}{\partial x_i} \left(\frac{1}{2} \hat{u}_j \hat{u}_j \right) \\ &= 2\hat{u}_j \left(-\frac{1}{2} \varepsilon_{ijk} \hat{\omega}_k \right) + \frac{\partial}{\partial x_i} \left(\frac{1}{2} \hat{u}_j \hat{u}_j \right) \end{aligned}$$

$$= -\varepsilon_{ijk} \hat{u}_j \hat{\omega}_k + \frac{\partial}{\partial x_i} \left(\frac{1}{2} \hat{u}_j \hat{u}_j \right) \quad (\text{A.27})$$

where $\hat{\omega}_k$ is the instantaneous vorticity associated with the rotation tensor, \hat{r}_{ij} and is defined by,

$$\hat{\omega}_k = \varepsilon_{ijk} \frac{\partial}{\partial x_i} \hat{u}_j \quad (\text{A.28})$$

where ε_{ijk} is the alternating tensor having values zero if any two of i, j, k are equal; $+1$ if i, j, k forms a cyclic permutation of $1, 2, 3$ and -1 if i, j, k forms an anticyclic permutation of $1, 2, 3$.

The second term on the right hand side of (A.26) may also be written as,

$$\nu \frac{\partial^2}{\partial x_j \partial x_j} \hat{u}_i = \nu \frac{\partial}{\partial x_j} \left(\frac{\partial \hat{u}_i}{\partial x_j} - \frac{\partial \hat{u}_j}{\partial x_i} \right) + \nu \frac{\partial}{\partial x_i} \left(\frac{\partial \hat{u}_j}{\partial x_j} \right) \quad (\text{A.29})$$

which in turn reduces to,

$$\nu \frac{\partial^2}{\partial x_j \partial x_j} \hat{u}_i = -\nu \varepsilon_{ijk} \frac{\partial}{\partial x_j} \hat{\omega}_k \quad (\text{A.30})$$

after continuity is applied to the second term of equation (A.29) and

$$\hat{r}_{ij} = -\frac{1}{2} \varepsilon_{ijk} \hat{\omega}_k \quad (\text{A.31})$$

has been used. Now by replacing equations (A.27) and (A.30) into (A.26) we obtain

$$-\varepsilon_{ijk} \hat{u}_j \hat{\omega}_k + \frac{1}{2} \frac{\partial}{\partial x_i} (\hat{u}_j \hat{u}_j) = -p \frac{\partial \hat{p}}{\partial x_i} - \nu \varepsilon_{ijk} \frac{\partial}{\partial x_j} \hat{\omega}_k + \theta_i \quad (\text{A.32})$$

which is the vorticity form of the Navier-Stokes' equations.

APPENDIX B

B.1 REDUCTION OF NAVIER-STOKES' EQUATIONS TO BERNOULLI EQUATION

If we assume that the viscous effects of the fluid are neglected and the fluid itself is irrotational (i.e when $\hat{\omega}_k = 0$) then equation (A.32) reduces to a simpler form,

$$\frac{\partial}{\partial x_i} (\frac{1}{2} \hat{u}_i \hat{u}_j) = -\frac{1}{\rho} \frac{\partial \hat{p}}{\partial x_i} + B_i \quad \forall i, j = 1, 2, 3 \quad (B.1)$$

For all $i = 1, 2, 3$ the following expression will be obtained,

$$\frac{\partial}{\partial x_i} (\frac{1}{2} \hat{u}_1^2) + \frac{\partial}{\partial x_i} (\frac{1}{2} \hat{u}_2^2) + \frac{\partial}{\partial x_i} (\frac{1}{2} \hat{u}_3^2) = -\frac{1}{\rho} \frac{\partial \hat{p}}{\partial x_i} + B_i \quad (B.2)$$

or in unit vector forms, (as can be seen in figure B.1), equation (B.2) becomes,

$$\underline{i} \frac{\partial}{\partial x_1} (\frac{1}{2} \hat{u}_1^2) + \underline{i} \frac{\partial}{\partial x_1} (\frac{1}{2} \hat{u}_2^2) + \underline{i} \frac{\partial}{\partial x_1} (\frac{1}{2} \hat{u}_3^2) = -\underline{i} \frac{1}{\rho} \frac{\partial \hat{p}}{\partial x_1} \quad (B.3)$$

$$\underline{j} \frac{\partial}{\partial x_2} (\frac{1}{2} \hat{u}_1^2) + \underline{j} \frac{\partial}{\partial x_2} (\frac{1}{2} \hat{u}_2^2) + \underline{j} \frac{\partial}{\partial x_2} (\frac{1}{2} \hat{u}_3^2) = -\underline{j} \frac{1}{\rho} \frac{\partial \hat{p}}{\partial x_2} - g \underline{j} \quad (B.4)$$

$$\underline{k} \frac{\partial}{\partial x_3} (\frac{1}{2} \hat{u}_1^2) + \underline{k} \frac{\partial}{\partial x_3} (\frac{1}{2} \hat{u}_2^2) + \underline{k} \frac{\partial}{\partial x_3} (\frac{1}{2} \hat{u}_3^2) = -\underline{k} \frac{1}{\rho} \frac{\partial \hat{p}}{\partial x_3} \quad (B.5)$$

where \underline{i} , \underline{j} and \underline{k} are unit vectors along x, y and z respectively.

By adding equations (B.3), (B.4) and (B.5) and noting that (see fig: B.1),

$$\hat{j} = \nabla x_2 \quad (\text{B.6})$$

we obtain,

$$\nabla(\frac{1}{2}\hat{V}^2) = -\frac{1}{\rho}\nabla\hat{p} - g\nabla x_2 \quad (\text{B.7})$$

where

$$\nabla \equiv \hat{i}\frac{\partial}{\partial x_1} + \hat{j}\frac{\partial}{\partial x_2} + \hat{k}\frac{\partial}{\partial x_3} \quad (\text{B.8})$$

and

$$\hat{V}^2 = \hat{u}_1^2 + \hat{u}_2^2 + \hat{u}_3^2 \quad (\text{B.9})$$

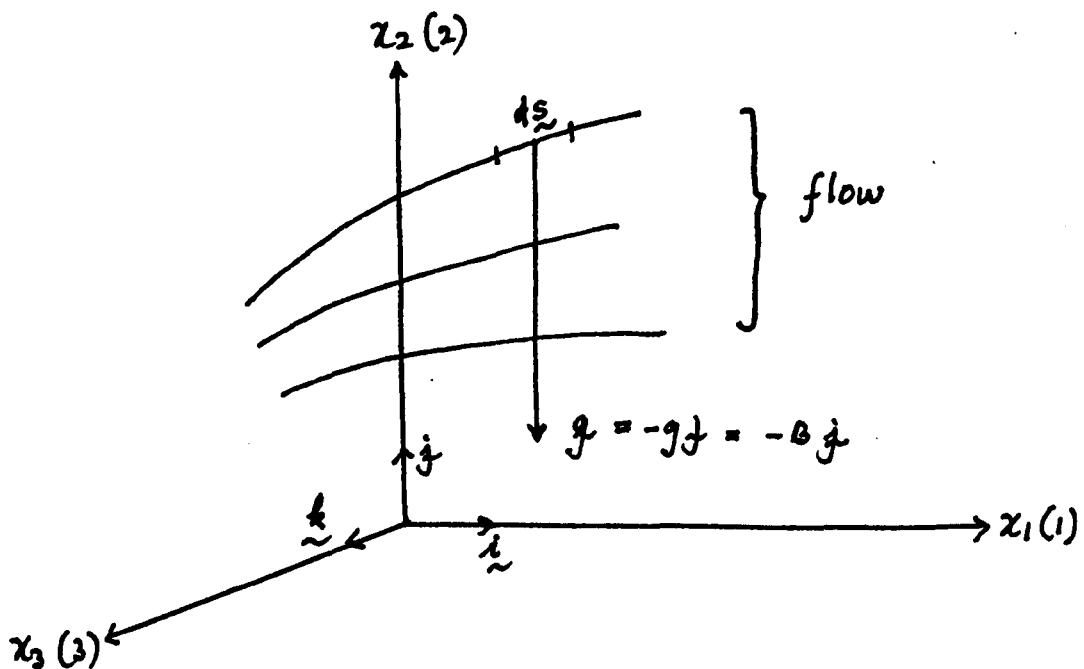


Fig.B.1: A Body Force(Gravitational) Acting on An Elemental Displacement

Vector, $d\mathbf{s}$.

On taking a scalar product of (B.7) with any displacement vector denoted by,

$$d\mathbf{s} = \hat{i}dx_1 + \hat{j}dx_2 + \hat{k}dx_3 \quad (\text{B.10})$$

and assuming that,

$$x_2 = z \quad (\text{B.11})$$

a perpendicular distance from (x_1-x_3) plane, the following total differentials will be obtained,

$$d\left(\frac{1}{2}V^2\right) = -\frac{1}{\rho}d\hat{p} - g dz \quad (\text{B.12})$$

and on integration, the Bernoulli's equation will result,

$$\text{i.e.} \quad \frac{1}{2}V^2 + \frac{1}{\rho}P + gz = C_3 \quad (\text{B.13})$$

where C_3 is a constant. Equation (B.13) sometimes is written in the following form,

$$\frac{V^2}{2g} + \frac{P}{\gamma} + z = C_4 \quad (\text{B.14})$$

where

$$\gamma = \rho g \quad (\text{B.15})$$

and C_4 is another constant. The terms on the left hand side of equation (B.14) are respectively called velocity head, pressure head and potential (or elevation) head.

The Bernoulli's equation which has been derived in equations (B.13) or (B.14) used the assumptions that the fluid flow is steady, incompressible, irrotational, no energy loss due to viscous effects, adiabatic (i.e. no heat is added to, or removed from the fluid)

and the change in the internal energy is negligible.

B.2 APPLICATION OF BERNOULLI'S EQUATION TO ORIFICE PLATE

By applying the Bernoulli's equation (B.14) for sections 1 and 3 of fig. B.2 we have, for horizontal pipe,

$$\frac{p_1}{\gamma} + \frac{v_1^2}{2g} = \frac{p_3}{\gamma} + \frac{v_3^2}{2g} \quad (\text{B.16})$$

where $\gamma = \rho g$ (B.15)

and from continuity, we have,

$$Q = A_1 v_1 = A_2 v_2 = A_3 v_3 \quad (\text{B.17})$$

Assuming that there is no energy loss due to frictional effects, equation (B.16) becomes, by using continuity equation (B.17),

$$p_1 - p_3 = \frac{\gamma}{2g} v_3^2 \left\{ 1 - \left(\frac{A_3}{A_1} \right)^2 \right\} \quad (\text{B.18})$$

The flow rate through section 3 is given by,

$$Q = A_3 v_3 \quad (\text{B.19})$$

$$= \frac{A_3}{\sqrt{1 - \left(\frac{A_3}{A_1} \right)^2}} \sqrt{\frac{2}{\rho} (p_1 - p_3)} \quad (\text{B.20})$$

where v_3 in equation (B.18) has been replaced into equation (B.19) to obtain equation (B.20). The flow rate given by (B.20) has been obtained

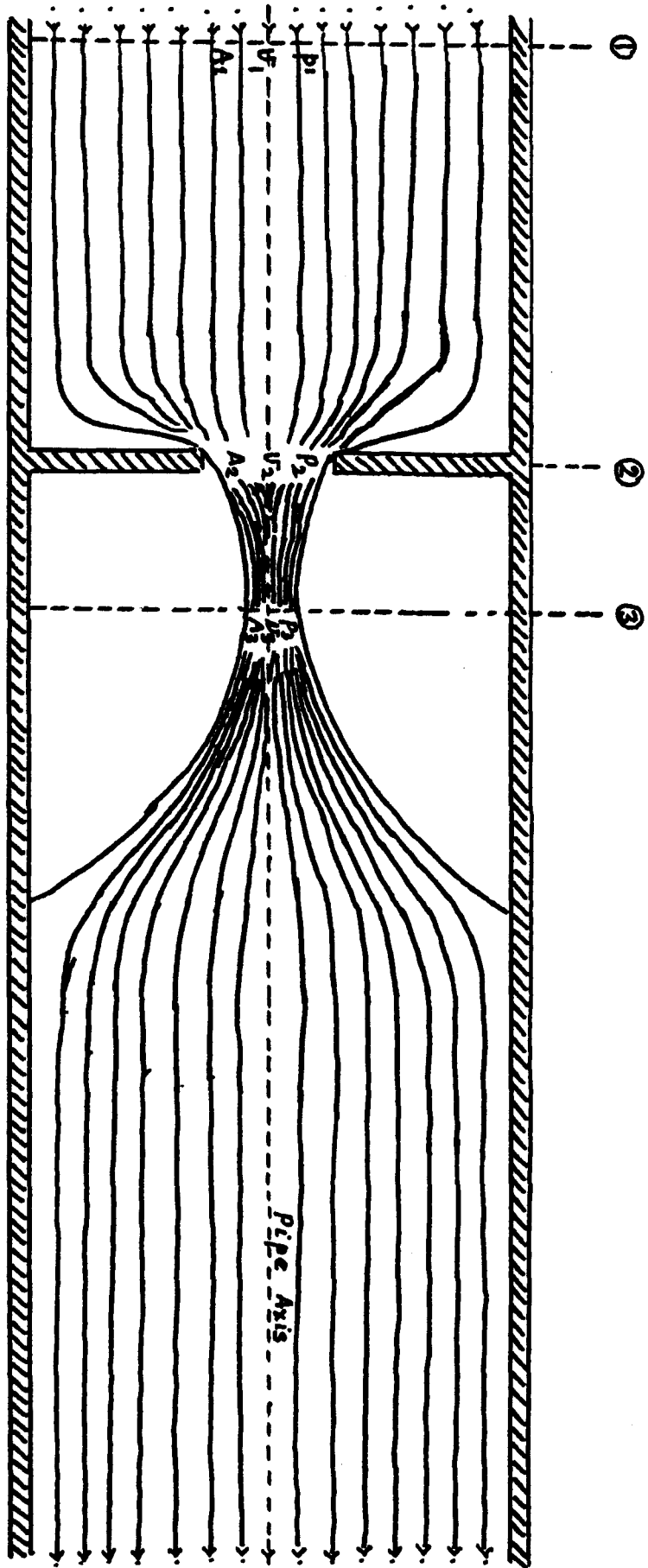


Fig. 8.2: Application of Bernoulli's Equation to Pipe Plate.

by assuming that there is no energy loss due to friction, so equation (B.20) represent the flow rate of a perfect fluid in terms of pressure difference in the meter. This equation may be rewritten as,

$$Q_{theo} = \frac{A_3}{\sqrt{1 - \left(\frac{A_3}{A_1}\right)^2}} \sqrt{\frac{2}{\rho}(p_1 - p_3)} \quad (B.21)$$

where Q_{theo} stands for theoretical flow rate. In practice however, because of the frictional resistances, the actual rate, Q_{act} is less than the theoretical ones, i.e. Q_{theo} . These two quantities are related by,

$$Q_{act} = C_v Q_{theo}. \quad (B.22)$$

where a coefficient, C_v , known as the coefficient of velocity, defined by

$$C_v = \frac{\text{actual velocity at vena contracta}}{\text{Theoretical velocity at vena contracta}} \quad (B.23)$$

has been introduced. The actual rate of flow is now written as (by replacing B.21 into B.22),

$$Q_{act} = \frac{C_v A_3}{\sqrt{1 - \left(\frac{A_3}{A_1}\right)^2}} \sqrt{\frac{2}{\rho}(p_1 - p_3)} \quad (B.24)$$

The cross-sectional area A_3 which is the smallest cross section of the flow (called the vena contracta) is unknown and less than A_2 the geometrical throat formed by the orifice. Define another coefficient, C_c as follows,

$$C_c = \frac{A_3}{A_2} < 1 \quad (\text{B.25})$$

in such a way that equation (B.25) is related to this latest coefficient by,

$$Q_{act} = \frac{C_v C_c A_2}{\sqrt{1 - C_c^2 \left(\frac{A_3}{A_1}\right)^2}} \sqrt{\frac{2}{\rho} \Delta p} \quad (\text{B.26})$$

when relation (B.25) has been used and Δp is a pressure drop across the orifice, replacing $(p_1 - p_3)$. Since C_c as well as C_v are functions of $\beta^2 = m = \frac{A_2}{A_1}$ (where A_2 and A_1 are respectively the orifice and pipe cross-sectional areas), C_c in the denominator of (B.26) is absorbed into $\frac{A_2}{A_1}$ and C_c and C_v in the numerator of (B.26) are combined to form a single coefficient C_d , then the equation (B.26) may be written as,

$$Q_{act} = C_f A_2 \sqrt{\frac{2}{\rho} \Delta p} \quad (\text{B.27})$$

where

$$C_f = \frac{C_d}{\sqrt{1 - \left(\frac{A_2}{A_1}\right)^2}} \quad (\text{B.28})$$

is called the flow coefficient (which is the coefficient of discharge with velocity-of-approach defined by the dimensionless term $\frac{1}{\sqrt{1 - (A_2/A_1)^2}}$ included); C_f is also called discharge coefficient of orifice with velocity of approach factor included or called 'higher' coefficient of discharge (Buckingham, 1956).

In our present study, the quantity Q_{act} from equation (B.27) may be obtained from the program, by

$$Q_{act} = U_{in} A_1 \quad (\text{B.29})$$

where U_{in} and A_1 are the inlet velocity through the cross-sectional area A_1 of the pipe. By combining equations (B.27), (B.28) and (B.29), the following equation for the discharge coefficient C_d ,

$$C_d = U_{in} \sqrt{\frac{\rho \left(\frac{1}{\beta^4} - 1\right)}{2 \Delta p}} \quad (\text{B.30})$$

is obtained.

It should be noticed that equation (B.30) is the same as equation (3.34) (see Chapter 3), where β is the orifice to pipe diameter ratio ($= \frac{D_2}{D_1}$, where D_2 is the orifice diameter and D_1 is the pipe diameter), ρ is the fluid density, U_{in} is the inlet velocity and Δp is the pressure drop across the orifice plate.

APPENDIX C.MATHEMATICAL FORMULATIONS OF TURBULENCE.C.1: INTRODUCTION.

In modelling flow processes it is necessary to formulate some mathematical equations which describe the flow. For Newtonian fluids such equations have been formulated. These are the well-known Navier-Stokes' differential equations (for the derivation of the equations see appendix A). These equations apply to almost all flows of engineering interest including those encountered in flow metering.

To solve the Navier-Stokes' differential equations numerically, would require an excessively fine finite difference meshes in both space and time. Even with present day computers this is not feasible. The approach adopted is to treat turbulent flow on a statistical approach based on means and fluctuating correlations. In this Appendix the statistical description of turbulence is introduced, Reynolds equation is derived by time averaging the Navier-Stokes' equations, as well as turbulent kinetic energy equation. The problem of closure in the Reynolds equation is discussed in section C.4, and the particular closure leading to the (k- ϵ) effective viscosity model is introduced. Derivation of the (k- ϵ) model is discussed in Appendix D.

C.2 THE TIME-DEPENDENT NAVIER-STOKES' EQUATIONS.

C.21 The Equations:

For unsteady, compressible flow, the conservation transport equations are:

Mass Conservation.

$$\frac{\partial}{\partial t} \rho + \frac{\partial}{\partial x_j} (\rho \hat{u}_j) = 0 \quad (\text{C.1})$$

Momentum Conservation.

$$\frac{\partial}{\partial t} (\rho \hat{u}_i) + \hat{u}_j \frac{\partial}{\partial x_j} (\rho \hat{u}_i) = \frac{\partial}{\partial x_j} \hat{\sigma}_{ij} + \rho B_i \quad (\text{C.2})$$

where $\hat{\sigma}_{ij} = -\hat{p} \delta_{ij} + 2\mu \hat{s}_{ij} - \frac{2}{3} \mu \hat{d} \delta_{ij}$ (C.3)

$$\hat{s}_{ij} = \frac{1}{2} \left(\frac{\partial \hat{u}_i}{\partial x_j} + \frac{\partial \hat{u}_j}{\partial x_i} \right) \quad (\text{strain tensor}) \quad (\text{C.4})$$

$$\hat{d} = s_{11} = \frac{\partial \hat{u}_1}{\partial x_1} \quad (\text{dilation}) \quad (\text{C.5})$$

u_i = velocity in direction- i ($i = 1, 2, 3$),

p = pressure,

B_i = body force/unit mass in direction- i ,

δ_{ij} = kronecker delta,

ρ = fluid density,

μ = fluid viscosity,

and $\hat{\Lambda}$ -sign indicates instantaneous quantities.

Equation (C.2) has been derived from Newton's second law of motion (see Appendix A). It is called the Navier-Stokes' equations. Equation (C.1) is a continuity equation which expresses the conservation of mass in a given control volume.

C.22 Laminar and Turbulent Flows.

The Navier-Stokes' equations apply both for laminar and turbulent flows. They consist of four equations with six unknowns, namely \hat{u}_i ($i=1,2,3$), \hat{p} , ρ and μ . In addition to above equations two other auxiliary relations are required to completely describes the flow;

(i) an equation of state which may be expressed generally by,

$$\rho = \rho(\hat{p}, T) \quad (C.6)$$

where T is a local temperature and \hat{p} is an instantaneous pressure. If fluid is incompressible ρ is a constant.

(ii) an equation expressing the conservation of energy which is not stated here as it is not central to our later discussions on turbulent models.

C.23 Difficulty of Solutions.

The Navier-Stokes' equations are non-linear and this one fact that makes their solutions difficult. Although the set of Navier-Stokes'

do not have a general solution, they may be solved under various restrictive assumptions (eg. for a low Reynolds number laminar flow in pipes or for plane boundary-layer turbulent flows). With the aid of digital computers more complicated laminar flows can be considered.

On the other hand, for turbulent flows, especially those with recirculation (eg. the flow just downstream of an orifice) this presents considerable difficulties, since such flows are essentially 3-D and unsteady. In addition, the time and length scales of the turbulent motion vary over many orders of magnitude—that is from those characteristic of pipe size and flow velocity down to microscales approaching molecular dimensions. Thus although the Navier-Stokes' equations are deterministic, to solve them for turbulent flows by computer would require an excessively fine finite difference meshes in space.

Almost all in engineering applications, the flow properties are time-averaged in order to reduce the excessive fine meshes for their predictions. In this study the approach employed for turbulent flows is based on the time-averaged equations.

C.3 STATISTICAL THEORY OF TURBULENCE.

C.31 Introduction:

The notion of fluctuations of velocity fields in study of turbulence is fundamental. The fluctuations vary with time and space. In

a steady laminar flow, the velocity does not depend on time, while in turbulence it fluctuates in a fairly unpredictable way. The process of these fluctuations are perfectly compatible with the notion of randomness. Consequently, turbulence may be described best by a statistical approach characterised by means and correlations.

If a fluid flow is treated randomly, we may introduce a concept of mean quantities. For example, the velocities $\hat{u}_i(x_i, t)$, $i=1, 2, 3$ at any position x_i , may be measured as a function of time and then averaged these measurements, as

$$\overline{\hat{u}_i(x_i, t)} = U_i(x_i) = \frac{1}{2T} \int_{t-T}^{t+T} \hat{u}_i(x_i, t) dt \quad (C.7)$$

This integral represents the limit of averaging measurements taken at successive moments of time and will itself fluctuate depending on the starting position and duration of the averaging processes. The time T represents the interval over which the averaging is to be carried out and it will have to be large compared to any of the frequencies of the fluctuations. Since \hat{u}_i is a time dependence quantity, U_i will then vary slightly with time T , but as T is made very large, the variation will be negligible and U_i is consequently independent of time.

Mathematically this time-average is defined as,

$$\overline{\hat{u}_i(x_i, t)} = U_i(x_i) = \lim_{T \rightarrow \infty} \frac{1}{2T} \int_{t-T}^{t+T} u_i(x_i, t) dt \quad (C.8)$$

while experimentally, the averaging process is continued until the fluctuations in $\overline{\hat{u}_i}$ are acceptably very small.

If above definition depends on the starting time of integration, statisticians define the averaging process in a different way. For example, if one decides to find the fluid velocity in pipe, one would imagine making experiments on a large number of pipes at the same time. If there are N pipes with corresponding velocities $\hat{u}_i^{(j)}(x_i, t)$, t being the time at which the imaginary measurements are made, then define an ensemble average by,

$$\langle \hat{u}_i(x_i, t) \rangle = \lim_{N \rightarrow \infty} \frac{1}{N} \sum_{j=1}^N \hat{u}_i^{(j)}(x_i, t) \quad (C.9)$$

Here, $\langle \rangle$ means a realisation average while $\overline{\quad}$ is an average with respect to time. If $\langle \hat{u}_i(x_i, t) \rangle$ defined by (C.9) is independent of time, $\overline{\hat{u}_i(x_i, t)}$ is also independent of time, then the time average equals ensemble average, i.e.

$$\overline{\hat{u}_i(x_i, t)} = \langle \hat{u}_i(x_i, t) \rangle \quad (C.10)$$

Condition given by (C.10) is known as the ergodic hypothesis.

Since the fluid flow is fluctuating rapidly and randomly, it is convenient to assume that the instantaneous velocities $\hat{u}_i(x_i, t)$ may be split up into their components—the mean velocities $U_i(x_i)$ and the fluctuating parts $u_i(x_i, t)$ in such a way that,

$$\hat{u}_i(x_i, t) = U_i(x_i) + u_i(x_i, t), \quad i = 1, 2, 3 \quad (C.11)$$

where the mean quantities $U_i(x_i)$ given by,

$$U_i(x_i) = \overline{\hat{u}_i(x_i, t)} \quad (C.12)$$

do not fluctuate, while $u_i(x_i, t)$ are fluctuating quantities with zero mean, ie

$$\overline{u_i(x_i, t)} = 0 \quad (C.13)$$

which would be obtained by time-averaging (C.11) and then using (C.12).

The instantaneous pressure \hat{p} is also decomposed into its mean and fluctuating parts ie,

$$\hat{p} = P + p \quad (C.14)$$

C.32 Derivation of Reynolds Equation.

Recalling equations (A.21) and (A.22) (see Appendix A) and by assuming that the instantaneous quantities may be resolved into their mean and fluctuating components, represented respectively by the capital and small letters, in such way that,

$$\hat{u}_i = U_i + u_i \quad ; \quad \overline{u_i} \equiv 0 \quad (C.15)$$

$$\hat{p} = P + p \quad ; \quad \overline{p} \equiv 0 \quad (C.16)$$

$$\hat{\sigma}_{ij} = \Sigma_{ij} + \sigma_{ij} \quad ; \quad \overline{\sigma_{ij}} \equiv 0 \quad (C.17)$$

$$\hat{S}_{ij} = S_{ij} + s_{ij} ; \overline{s_{ij}} \equiv 0 \quad (\text{C.18})$$

with
$$\Sigma_{ij} = -P\delta_{ij} + 2\mu S_{ij} \quad (\text{C.19})$$

$$\sigma_{ij} = -p\delta_{ij} + 2\mu s_{ij} \quad (\text{C.20})$$

where
$$S_{ij} = \frac{1}{2} \left(\frac{\partial U_i}{\partial x_j} + \frac{\partial U_j}{\partial x_i} \right) \quad (\text{C.21})$$

and
$$s_{ij} = \frac{1}{2} \left(\frac{\partial u_i}{\partial x_j} + \frac{\partial u_j}{\partial x_i} \right) , \quad (\text{C.22})$$

then we have the following expressions,

$$(U_j + u_j) \frac{\partial}{\partial x_j} (U_i + u_i) = \frac{1}{\rho} \frac{\partial}{\partial x_j} (\Sigma_{ij} + \sigma_{ij}) \quad (\text{C.23})$$

$$\frac{\partial}{\partial x_i} (U_i + u_i) = 0 \quad (\text{C.24})$$

On averaging with respect to time, the following equations will be obtained,

$$U_j \frac{\partial}{\partial x_j} U_i = \frac{1}{\rho} \frac{\partial}{\partial x_j} (\Sigma_{ij} - \rho \overline{u_i u_j}) \quad (\text{C.25})$$

and
$$\frac{\partial U_i}{\partial x_i} = 0 \quad (\text{C.26})$$

Equation (C.26) is the continuity equation and equation (C.25) is called the Reynolds equation which may be rewritten into a more simpler form by,

$$U_j \frac{\partial}{\partial x_j} U_i = \frac{1}{\rho} \frac{\partial}{\partial x_j} T_{ij} \quad (\text{C.27})$$

where

$$\tau_{ij} = \Sigma_{ij} - \rho \overline{u_i u_j} \quad (C.28)$$

and Σ_{ij} is given by equation (C.19).

It can be seen that equation (C.27) has the same form as equation (A.21) (see Appendix A) if the U_k 's are replaced by \hat{u}_k 's and τ_{ij} by $\hat{\sigma}_{ij}$.

Thus the equations of mean flow are the same as the ordinary equations of motion, except that there are additional virtual stresses denoted by,

$$\tau_{ij} = -\rho \overline{u_i u_j} \quad (C.29)$$

appear in the mean equations (C.27). These stresses are called the Reynolds stresses, which represent the mean rate of momentum transfer across a fluid layer due to velocity fluctuations. The turbulence model then ascribes how this correlation (relation C.29) and other correlation, $-\rho \overline{\phi' u_j}$ (where ϕ' and u_j are scalar and velocity fluctuations) arising from scalar convective non-linear terms, are to be found. This involves the problem of closure which will be discussed in section (C.4).

C.33 Kinetic Energy of Mean and Turbulent Flows.

By multiplying the Reynolds equation (C.27) by U_i , we should

get the following equation,

$$\begin{aligned} U_j \frac{\partial}{\partial x_j} \left(\frac{1}{2} U_i U_i \right) &= \frac{1}{\rho} \frac{\partial}{\partial x_j} (U_i T_{ij}) - \frac{1}{\rho} T_{ij} \frac{\partial}{\partial x_j} U_i \\ &= \frac{1}{\rho} \frac{\partial}{\partial x_j} (U_i T_{ij}) - \frac{1}{\rho} T_{ij} S_{ij} \end{aligned} \quad (C.30)$$

In obtaining equation (C.30) the following facts have been used, that since both T_{ij} and S_{ij} are symmetric tensors, they are 'survive' in the expression $T_{ij} \frac{\partial U_i}{\partial x_j}$ as $\frac{\partial U_i}{\partial x_j}$ contains the symmetric S_{ij} and antisymmetric tensors R_{ij} .

When equation (C.28) for T_{ij} is replaced into equation (C.30), the result so-obtained is called the equation for mean kinetic energy, ie

$$\begin{aligned} U_j \frac{\partial}{\partial x_j} \left(\frac{1}{2} U_i U_i \right) &= \frac{\partial}{\partial x_j} \left(-\frac{P}{\rho} U_j + 2\nu U_i S_{ij} - \overline{u_i u_j} U_i \right) \\ &\quad - 2\nu S_{ij} S_{ij} + \overline{u_i u_j} S_{ij} \end{aligned} \quad (C.31)$$

In arriving equation (C.31) the assumption that the fluid density ρ is constant has been used.

The equation for the turbulent kinetic energy (or just turbulent energy), $k = \frac{1}{2} \overline{u_i u_i}$ may be obtained as follows;

Multiplying equation (C.23) with $(U_i + u_i)$ and replacing \sum_{ij} and σ_{ij} by (C.19) and (C.20), the following expressions, with slight rearrangement, will be obtained,

$$\begin{aligned}
& (U_i U_j + U_i u_j + u_i U_j + u_i u_j) \frac{\partial}{\partial x_j} (U_i + u_i) \\
&= \frac{1}{\rho} (U_i + u_i) \frac{\partial}{\partial x_j} (-P \delta_{ij} + 2\mu S_{ij}) \\
&+ \frac{1}{\rho} (U_i + u_i) \frac{\partial}{\partial x_j} (-p \delta_{ij} + 2\mu s_{ij}) \quad (C.32)
\end{aligned}$$

By time-averaging of equation (C.32), the following will be obtained, after some slight manipulations,

$$\begin{aligned}
& U_j \frac{\partial}{\partial x_j} \left(\frac{1}{2} U_i U_i \right) + \frac{\partial}{\partial x_j} (\overline{u_i u_j} U_i) - \overline{u_i u_j} \frac{\partial U_i}{\partial x_j} + U_j \frac{\partial}{\partial x_j} \left(\frac{1}{2} \overline{u_i u_i} \right) \\
&+ \overline{u_i u_j} \frac{\partial U_i}{\partial x_j} + \frac{\partial}{\partial x_j} \left(\frac{1}{2} \overline{u_i u_i u_j} \right) = \frac{\partial}{\partial x_j} \left(-\frac{P U_i}{\rho} + 2\nu U_i S_{ij} \right) - 2\nu \overline{S_{ij} S_{ij}} \\
&+ \frac{\partial}{\partial x_j} \left(-\frac{\overline{p u_j}}{\rho} + 2\nu \overline{u_i s_{ij}} \right) - 2\nu \overline{s_{ij} s_{ij}} \quad (C.33)
\end{aligned}$$

On subtraction of equation (C.31) from equation (C.33) the equation for the turbulence energy, k will be obtained as follows

$$\begin{aligned}
& U_j \frac{\partial}{\partial x_j} \left(\frac{1}{2} \overline{u_i u_i} \right) = \frac{\partial}{\partial x_j} \left(-\frac{\overline{p u_j}}{\rho} + 2\nu \overline{u_i s_{ij}} - \frac{1}{2} \overline{u_i u_i u_j} \right) \\
& \text{(Convection)} \qquad \qquad \qquad \text{(Diffusive Transport)} \\
& - \overline{u_i u_j} S_{ij} - 2\nu \overline{s_{ij} s_{ij}} \quad (C.34) \\
& \text{(Production)} \qquad \qquad \text{(Dissipation)}
\end{aligned}$$

C.34 Statistical Description of Turbulent Flows.

In a steady, homogeneous pure shear flow, in which all averaged quantities except U_j are independent of position and in which S_{ij} is constant, the production of turbulence energy and its dissipation rate balance each other (Tennekes, 1972) so,

$$-\overline{u_i u_j} S_{ij} = 2\nu \overline{S_{ij} S_{ij}} \quad (C.35)$$

or symbolically is denoted by,

$$\rho = \epsilon \quad (C.36)$$

where

$$\rho = -\overline{u_i u_j} S_{ij} \quad (C.37)$$

is the energy production of turbulence and

$$\epsilon = 2\nu \overline{S_{ij} S_{ij}} \quad (C.38)$$

its dissipation rate.

By employing the scale relation,

$$S_{ij} \sim \frac{u}{l} \quad (C.39)$$

and the Reynolds stresses estimate,

$$-\overline{u_i u_j} \sim u^2 \quad (C.40)$$

where u and l are respectively the velocity and length scales, then the production term ρ may be estimated by,

$$\begin{aligned} \rho &= -\overline{u_i u_j} S_{ij} \sim u^2 S_{ij} \\ &= A u l S_{ij} S_{ij} \end{aligned} \quad (C.41)$$

where A is an undetermined coefficient which is of order one for most simple flows (Tennekes, 1972). Equation (C.35) now becomes, by using equation (C.41) as production term,

$$A R_l S_{ij} S_{ij} = 2 \overline{s_{ij} s_{ij}} \quad (C.42)$$

where

$$R_l = \frac{u l}{\nu} \quad (C.43)$$

is the Reynolds number associated with length scale l .

It can be seen from equation (C.42) that when R_l is large, the term $S_{ij} S_{ij}$ must be very much smaller than $\overline{s_{ij} s_{ij}}$ for equality to be maintained, so

$$S_{ij} S_{ij} \ll \overline{s_{ij} s_{ij}} \quad (C.44)$$

stating that the mean strain rate S_{ij} is very much smaller than that of the fluctuating strain rate s_{ij} when Reynolds number is large.

Since strain rates have the dimension of frequency (sec^{-1}), inequality (C.44) also implies that the eddies which contribute most

to the energy dissipation have very small convective time scales compared to that of the mean flow, which in turn suggest that there should be very little interactions between s_{ij} and S_{ij} .

The energy exchange between mean flow and the turbulence is governed by the dynamics of the large eddies since these eddies contribute most to the turbulence production ρ which increases with increasing eddy size (see eqn. C.41). The energy extracted by the turbulence from the mean flow mainly at scales comparable to the length scale l .

The rate of energy transferred by the large eddies is of the order u^2 with time scale of the order $\frac{l}{u}$. The dissipation rate is thus estimated by the ratio of energy transferred to the time scale, hence

$$\begin{aligned} \epsilon &\sim \frac{u^2}{l/u} \\ &= B \frac{u^3}{l} \end{aligned} \quad (C.45)$$

for some coefficient B of order one.

Since at high Reynolds number s_{ij} and S_{ij} are not strongly interacted, then small-scale structure of turbulence tends to be independent of any orientation effects introduced by the mean shear so all averages relating to small eddies do not change under rotations or reflections of the coordinate system. This small-scale structure is called isotropic and so any length scale for the estimate of s_{ij} must be very much smaller than the length scale l , for $\rho = \epsilon$ is always to be maintained. Here the small scale λ is introduced, called the Taylor

microscale.

C.4 THE CLOSURE PROBLEM.

In the Reynolds equation (C.27), there are six additional variables have been introduced, $(-\overline{\rho u_i u_j})$. These are due to the contribution of the turbulent motion to the mean stress tensor. This tensor is called the Reynolds stress tensor and is composed of one point correlation and is designated by relation (C.29).

This Reynolds stress is a diagonally symmetric $\tau_{ij} = \tau_{ji}$ with the diagonal components of τ_{ij} are normal stresses (pressures) - their values are τ_{nn} by putting $i=j$. In many flows these normal stresses contribute little to the transport of mean momentum (Tennekes, 1972). The off-diagonal components of τ_{ij} ($i \neq j$) are shear (or tangential) stresses - they play a dominant rôle in the theory of mean momentum transfer by turbulent motion this also play a decisive rôle in determining the flow behaviour as the fine-scale effects are primarily expressed through them.

The system of transport equations cannot be solved unless τ_{ij} is specified in terms of other mean variables - the system of equations must be closed. In principle it is possible to derive additional transport for those unknown correlations by multiplying the Navier-Stokes' equation by \hat{u}_k and averaging with respect to time, the resulting new equation however contains further unknown higher order correlations of the form $\overline{u_i u_j u_k}$ generated by the convective non-linear

inertia terms $u_j \frac{\partial u_i}{\partial x_j}$. Indeed the differential equations for the n-th order velocity correlations can be derived similarly from the basic Navier-Stokes' equations, but it will always comprise the unknown velocity correlations of the (n+1)-th order, as a consequence of the non-linear character of the turbulence. It happens that in the process, there are more unknowns than equations. Therefore at one stage, it will be necessary to make attempts to guess a relation between the unknown correlation τ_{ij} and S_{ij} in such a way that a closed set of equations is obtained.

The problem of the development of turbulence mathematical models then boils down to finding an adequate method of closing the set of equations. The problem in general is called the 'closure problem' and its solutions are called 'turbulence model' or 'closures' (Bradshaw(ed), 1976).

Lower or higher level closures may be employed in closing the set of equations. However in this study, the lower level (second order correlations) closure is employed. They in principle, include one-equation models, two-equation models and stress-equation models. These three models are discussed in details in Bradshaw(ed), 1976, but in the present study, the two-equation models or the (k- ϵ) effective viscosity models is employed, and this forms the subject of next section. The higher level closures are outside the scope of this thesis.

C.5 THE (k-ε)EFFECTIVE VISCOSITY MODEL.

C.51 Basic Concept.

The Transport laws for laminar flows-Newton's law of viscosity and Ficke's law of diffusion are assumed to be valid for turbulent flows as well. These relations are called the 'constitutive relations'.

The turbulent diffusional fluxes are expressed in terms of 'effective' viscosities (or 'exchange' coefficients) multiplied by gradients of mean flow properties. These fluxes may be expressed as,

$$\tau_{ij} = -\rho \overline{u_i u_j} = 2\mu_t S_{ij} \quad (\text{C.46})$$

$$-\rho \overline{\phi' u_j} = \Gamma_{\phi,t} \frac{\partial \phi}{\partial x_j} \quad (\text{C.47})$$

where

$$S_{ij} = \frac{1}{2} \left(\frac{\partial U_i}{\partial x_j} + \frac{\partial U_j}{\partial x_i} \right) \quad (\text{C.48})$$

$$\hat{u} = U_i + u_i ; \overline{u_i} = 0,$$

$$\hat{\phi} = \underline{\phi} + \phi' ; \overline{\phi'} = 0,$$

ϕ = scalar variables,

ϕ' = fluctuating components of $\hat{\phi}$,

u_i = fluctuating components of \hat{u}_i ,

μ_t = turbulent or eddy viscosity,

$\Gamma_{\phi,t}$ = turbulent diffusivity.

Boussinesq in 1877 (Launder, 1972), has suggested that the Reynolds stresses may be represented by the product of the gradient of the mean velocity and turbulent viscosity, μ_t . The value of this viscosity will vary from point to point in the flow domain and hence it is not a property of the fluid itself.

The introduction of μ_t and $\Gamma_{\phi, t}$ provide a framework for constructing a turbulence model. It is necessary to seek a method in determining these quantities in terms of known or calculable quantities.

C.52 An Algebraic Formula for μ_t .

Basically μ_t is obtained from the assumption that near a wall region, the production of turbulence energy k and its dissipation rate, ϵ balance each other. For a two dimensional flow, the cross-stream derivative $\frac{\partial}{\partial y}$ is very much greater than the down-stream derivative $\frac{\partial}{\partial x}$, then equation (C.35) becomes,

$$-\overline{uv} \frac{\partial U}{\partial y} = \epsilon \quad (C.49)$$

where u and v are respectively velocity fluctuations in axial and radial directions.

In a fully turbulent region, the shear stress near a wall τ_w is assumed to be constant and,

$$-\overline{uv} = \frac{\tau_w}{\rho} \quad (\text{C.50})$$

Assuming that the dissipation rate is always maintained by energy extraction from the mean flow, this dissipation rate ϵ is proportional to wall stress, τ_w and the distance normal to the wall, y (Reynolds, 1974), ie

$$\epsilon \propto \frac{\tau_w}{\rho} y \quad (\text{C.51})$$

Hence

$$\epsilon = \frac{A}{y} \left(\frac{\tau_w}{\rho} \right)^{3/2} \quad (\text{C.52})$$

for any constant A.

The choice of relation (C.52) is because when equations (C.50) and (C.52) are placed into equation (C.49), the following relation is obtained,

$$\frac{\partial U}{\partial y} = \frac{A}{y} U_\tau \quad (\text{C.53})$$

where $U_\tau = \sqrt{\frac{\tau_w}{\rho}}$ being the velocity friction. Equation (C.53) may be rewritten as,

$$dU^+ = A \left(\frac{dy^+}{y^+} \right) \quad (\text{C.54})$$

where

$$U^+ = \frac{U}{U_\tau} \quad (\text{C.55})$$

$$y^+ = \frac{y U_\tau}{\nu} \quad (\text{C.56})$$

$\nu = \frac{\mu}{\rho}$ is the kinematic viscosity.

On integration of equation (C.54) will lead to a logarithmic mean velocity variation,

$$U^+ = A \ln(Ey^+) \quad (C.57)$$

where E is some constant. Equation (C.57) is equivalent to those obtained by using Prandtl hypothesis of momentum transport (Hinze, 1959) with mixing length, l_m given by,

$$l_m = \mathcal{K} y \quad (C.58)$$

for any constant \mathcal{K} for wall layer with $\mathcal{K} = \frac{1}{A}$, in this case.

Again, from equation (C.50),

$$-\overline{uv} = \frac{\tau_w}{\rho} \quad (C.50)$$

$$= \nu_t \left(\frac{\partial U}{\partial y} \right) \quad (\text{Boussinesq}) \quad (C.59)$$

$$= l_m^2 \left(\frac{\partial U}{\partial y} \right)^2 \quad (\text{Prandtl}) \quad (C.60)$$

where ν_t and l_m are respectively turbulent kinematic viscosity and mixing length of the turbulence, in such a way that,

$$\mu_t = \rho l_m^2 \left| \frac{\partial U}{\partial y} \right| \quad (C.61)$$

where
$$\nu_t = \frac{\mu_t}{\rho} \quad (C.62)$$

Relation given by (C.61) is known as Prandtl mixing length model (Launder, 1972).

By equating equations (C.59) and (C.60) it can be seen that,

$$\nu_t = l_m \left(l_m \frac{\partial u}{\partial y} \right) \quad (C.63)$$

$$= l_m \left| \frac{\tau_w}{\rho} \right|^{\frac{1}{2}} \quad \text{by (C.50) and (C.60)} \quad (C.64)$$

It is clear that $\left| \frac{\tau_w}{\rho} \right|^{\frac{1}{2}}$ and $\left(l_m \frac{\partial u}{\partial y} \right)$ act as velocity scales for they have same dimension of velocity. Hence equation (C.64) may be rewritten (with the help of equation C.62),

$$\mu_t = \rho l_m u \quad (C.65)$$

where u is the velocity scale. This velocity scale would be the square root of the turbulence energy, k for $k^{\frac{1}{2}}$ has dimension of velocity as well.

Hence μ_t may be expressed as,

$$\mu_t = \rho l k^{\frac{1}{2}} \quad (C.66)$$

where l = length scale (similar to mixing length, l_m),
 k = turbulence energy ($= \frac{1}{2} \overline{u_i u_i}$),
 ρ = fluid density.

In attempting to eliminate the need for specifying the turbulence length scale l as a function of position throughout the flow domain, several workers have explored the use of a second turbulence partial differential equation which in effect gives l . The differential equation is the dissipation rate of energy equation ϵ which coupled with k to give the (k- ϵ) two-equation model of turbulence.

In effective-viscosity models the turbulence quantities employed are the turbulence energy, k and its dissipation rate, ϵ . They have their own transport equations (see appendix D for their derivations) whereas there is no equation for l provided here and deriving a transport equation for l is out of scope in the present study (its derivation may be found in Taylor(ed), 1980).

However, by generalising equation (C.52) to include part of a boundary layer where the 'cascade' process (the process which transfer energy from larger to smaller eddies) may be supposed to depend only on ρ , k and l (Launder, 1972) one take,

$$\epsilon = C_{\mu} \frac{k^2}{l} \quad (C.67)$$

Thus in terms of k and ϵ , μ_t may be rewritten as (ie, by combining equations (C.66) and (C.67)),

$$\mu_t = C_{\mu} \rho \frac{k^2}{\epsilon} \quad (C.68)$$

where C_{μ} = the fundamental coefficient of proportionality between stresses and strain rates.

C.53 Scalar Turbulent Diffusivity $\Gamma_{\phi,t}$ for ϕ .

The turbulence exchange coefficient $\Gamma_{\phi,t}$ is proportional to the local density ρ , mixing length $l_{m,\phi}$ for ϕ and characteristic velocity u of the fluctuation quantity. Mathematically it is written as (Launder, 1972),

$$\Gamma_{\phi,t} = \rho l_{m,\phi} \cdot u \quad (C.69)$$

This mixing length $l_{m,\phi}$ for the scalar variable ϕ has been assumed to be of the same order of magnitude at every point in the flow domain as l_m , the mixing length for momentum transfer. A new quantity $\sigma_{\phi,t}$ has been introduced to represent these ratio (ie. on division of equation (C.65) by equation (C.69)),

$$\sigma_{\phi,t} = \frac{\mu_t}{\Gamma_{\phi,t}} = \frac{l_m}{l_{m,\phi}} \quad (C.70)$$

and is called turbulent Prandtl/Schmidt number. This number has been expected to be of order unity. For free shear flows without buoyant effects, most workers used the values of $\sigma_{\phi,t}$ in the range of .5 to .7. For near wall flows in a round pipe, an average value of .85 has been used successfully in heat transfer calculation (Launder, 1972).

The turbulent viscosity and diffusivity coefficients μ_t and $\Gamma_{\phi,t}$ ($= \frac{\mu_t}{\sigma_{\phi,t}}$) given by the relations (C.68) and (C.70) have been defined using the two-equation model of turbulence. The problem now reduces to obtaining k and ϵ on which they are based for given

Prandtl/Schmidt number $\sigma_{\phi, t}$. The derivations of the (k- ϵ) equations and Prandtl/Schmidt number σ_{ϵ} for ϵ are obtained in appendix D.

APPENDIX D.DERIVATION OF THE 'k-ε' TURBULENT MATHEMATICAL MODEL.D.1: ASSUMPTIONS IN THE TURBULENCE MODEL.

In the modelling of turbulent flows leading to the k-ε models, the following fundamental assumptions have been used.

(i) The local turbulence Reynolds number, Re_t defined by (Launder, 1972), see also equation F.1 (Appendix F),

$$Re_t = \frac{\mu_t}{\mu} = \frac{C_{\mu} \rho k^2}{\mu \epsilon}$$

is assumed to be large enough to neglect viscous actions on the transport of k and ϵ .

(ii) At high Re_t the dissipation of turbulence energy is assumed to be isotropic. This follows from condition (i).

D.2: THE k-EQUATION.

Recall equation (C.34) (see Appendix C) for energy of turbulence,

$$\begin{aligned}
 U_j \frac{\partial}{\partial x_j} \left(\frac{1}{2} \overline{u_i u_i} \right) &= \underbrace{- \frac{\partial}{\partial x_j} \left\{ u_j \left(\frac{p}{\rho} + \frac{1}{2} \overline{u_i u_i} \right) - 2 \nu \overline{u_i s_{ij}} \right\}}_{\text{(Transport)}} \\
 \text{(Convection)} & \\
 & - \underbrace{\overline{u_i u_j} \frac{\partial U_i}{\partial x_j}}_{\text{(Production)}} - \underbrace{\frac{1}{2} \nu \overline{\left(\frac{\partial u_i}{\partial x_j} + \frac{\partial u_j}{\partial x_i} \right)^2}}_{\text{(Dissipation)}}
 \end{aligned} \tag{D.1}$$

Equation (D.1) is for a steady incompressible fluid flow which expresses that the energy supply to the turbulent flow from the

mean flow by the action of the shear stress (i.e. the production term) and by turbulent diffusion due to velocity and pressure fluctuations and viscous action (the transport term) and dissipation of $k = \frac{1}{2} \overline{u_i u_i}$ is equal to the convection of turbulent energy by mean motion.

The production term; $-\overline{u_i u_j} S_{ij}$ has been put in the form of that in equation (D.1) since $\overline{u_i u_j}$ is a symmetric tensor, so the product of $\overline{u_i u_j} S_{ij}$ is equal to the product of $\overline{u_i u_j}$ and the deformation rate $\frac{\partial u_i}{\partial x_j}$ (Tennekes, 1972). This term represents the production of k by turbulent shear stress.

Similarly the dissipation term, which has been obtained by replacing s_{ij} terms by $\frac{1}{2} \left(\frac{\partial u_i}{\partial x_j} + \frac{\partial u_j}{\partial x_i} \right)$ (see also expression C.22 of Appendix C), thus giving the last term of the equation (D.1) as the dissipation of k due to viscous action. The term on the left hand side of the equation (D.1) is the convection of k by the mean flow.

The unmodelled equation for k given by eqn.(D.1) represents the exact equation for k . In modelling this equation to obtain the form of equation the way it is solved in the ($k-\epsilon$) equations, the following assumptions will be made. The transport by viscous stress term will be neglected at high Reynolds number (this will be discussed in the next paragraph) compared with the transport due to pressure and velocity fluctuations. The destruction of turbulence is assumed to be isotropic at high Reynolds number. The constitutive relations (see App.C, section C.5) will be employed to the transport of k as well as ϵ .

The transport of energy by turbulent fluctuating velocities and by viscous stress of equation (D.1) may be estimated respectively as follows,

$$\frac{1}{2} \overline{u_i u_i u_j} \sim u^3 = c u^3 \quad (\text{D.2})$$

and

$$2\nu \overline{u_i s_{ij}} \sim \nu u \frac{u}{\lambda} = D \nu \frac{u^2}{\lambda} \quad (\text{D.3})$$

where λ is the Taylor microscale smaller than ℓ . The ratio of equations (D.2) and (D.3) gives,

$$\frac{\frac{1}{2} \overline{u_i u_i u_j}}{2\nu \overline{u_i s_{ij}}} = E \frac{u \lambda}{\nu} = E R_\lambda \quad (\text{D.4})$$

which states that when the Reynolds number $R_\lambda (= \frac{u \lambda}{\nu})$ is large then from equation (D.4) the viscous terms may be neglected compared to the turbulent velocity fluctuation terms $\frac{1}{2} \overline{u_i u_i u_j}$. Hence equation (D.1) reduces to,

$$U_j \frac{\partial}{\partial x_j} (\frac{1}{2} \rho \overline{u_i u_i}) = - \frac{\partial}{\partial x_j} \left\{ u_j \left(\rho + \frac{1}{2} \rho u_i u_i \right) \right\} - \rho \overline{u_i u_j} \frac{\partial U_i}{\partial x_j} - \rho \epsilon \quad (\text{D.5})$$

where

$$\epsilon = \frac{\nu}{2} \overline{\left(\frac{\partial u_i}{\partial x_j} + \frac{\partial u_j}{\partial x_i} \right)^2} \quad (\text{D.6})$$

The turbulent diffusion of energy is assumed to obey the gradient transport law, as already implied by the eddy viscosity concept for the transport of momentum, (Hinze, 1959)

$$\overline{u_j \left(\rho + \frac{1}{2} \rho u_i u_i \right)} = - \Gamma_k \frac{\partial}{\partial x_j} \left\{ \rho + \frac{1}{2} \rho u_i u_i \right\} = - \Gamma_k \frac{\partial}{\partial x_j} (\frac{1}{2} \overline{u_i u_i}) \quad (\text{D.7})$$

where Γ_k is the turbulent exchange coefficient assumed to be proportional to eddy viscosity, i.e.,

$$\Gamma_k = \frac{\mu_t}{\sigma_k} \quad (\text{see equation C.70, Appendix C}) \quad (\text{D.8})$$

where σ_k is Prandtl/Schmidt number for the turbulent energy, k . This assumption implies that the diffusion length scales for both mean momentum and turbulent energy are proportional to each other and represented by ℓ . Equation (D.5) now becomes,

$$U_j \frac{\partial}{\partial x_j} (\rho k) = \frac{\partial}{\partial x_j} \left(\frac{\mu_t}{\sigma_k} \frac{\partial k}{\partial x_j} \right) - \rho \overline{u_i u_j} \frac{\partial U_i}{\partial x_j} - \rho \epsilon \quad (\text{D.9})$$

where $k = \frac{1}{2} \overline{u_i u_i}$ (D.10)

is the turbulence kinetic energy, and,

$$\epsilon = \frac{1}{2} \nu \overline{\left(\frac{\partial u_i}{\partial x_j} + \frac{\partial u_j}{\partial x_i} \right)^2} \quad (\text{D.6})$$

is the dissipation rates, ν is the (laminar) kinematic viscosity. Equation (D.9) is called the k-equation.

For large Reynolds number, viscous dissipation of the kinetic energy occurs in the smallest eddies. These small-scale structure tend to be isotropic (Tennekes, 1972) so that relation (D.6) becomes,

$$\epsilon = \nu \overline{\frac{\partial u_i}{\partial x_j} \cdot \frac{\partial u_i}{\partial x_j}} \quad (\text{D.11})$$

as local isotropy does not prefer direction from large-scale motions to

smaller ones (Bradshaw(ed), 1976) and there is no correlation between $\frac{\partial u_i}{\partial x_j}$ and $\frac{\partial u_j}{\partial x_i}$ for the smallest eddies (Ideriah, 1977).

D.3: THE ϵ -EQUATION.

This equation may be obtained via the dynamics of mean square vorticity fluctuations $\overline{\omega_i \omega_i} = \overline{\omega^2}$. Below is the derivation of the vorticity equation from which the ϵ -equation may be derived. This approach for obtaining the ϵ -equation is an original one derived by the author.

We have from equation (A.32) (see Appendix A) with body forces neglected, the following equation, after some slight rearrangement,

$$\frac{\partial}{\partial x_i} \left(\frac{\hat{p}}{\rho} + \frac{1}{2} \hat{u}_j \hat{u}_j \right) = \epsilon_{ijk} \left(\hat{u}_j \hat{\omega}_k - \nu \frac{\partial \hat{\omega}_k}{\partial x_j} \right) \quad (\text{D.12})$$

is obtained, where as before $\hat{\omega}_k$ is the instantaneous vorticity associated with the rotation tensor $\hat{\tau}_{kj}$. They are defined by,

$$\hat{\omega}_k = \epsilon_{ijk} \frac{\partial}{\partial x_i} \hat{u}_j \quad (\text{D.13})$$

and
$$\hat{\tau}_{ij} = -\frac{1}{2} \epsilon_{ijk} \hat{\omega}_k \quad (\text{D.14})$$

By applying the operator 'curl' $\epsilon_{ipq} \frac{\partial}{\partial x_p}$ into equation (D.12) we obtain,

$$\epsilon_{ipq} \frac{\partial^2}{\partial x_p \partial x_i} \left(\frac{\hat{p}}{\rho} + \frac{1}{2} \overline{u_j u_j} \right) = (\delta_{pj} \delta_{qk} - \delta_{qj} \delta_{pk}) \frac{\partial}{\partial x_p} \left(\hat{u}_j \hat{\omega}_k - \nu \frac{\partial \hat{\omega}_k}{\partial x_j} \right) \quad (\text{D.15})$$

The term on the left hand side of equation (D.15) involves the product of an antisymmetric tensor ϵ_{ipq} and the symmetric operator tensor $\frac{\partial^2}{\partial x_p \partial x_i}$ and so it should vanish and on the right hand side, the following identity

$$\epsilon_{ipq} \epsilon_{ijk} = (\delta_{pj} \delta_{qk} - \delta_{pk} \delta_{qj}) \quad (D.16)$$

has been used. So equation (D.15) now reduces to

$$0 = \frac{\partial}{\partial x_p} (\hat{u}_p \hat{w}_q) - \frac{\partial}{\partial x_p} (\hat{u}_q \hat{w}_p) - \nu \left(\frac{\partial^2 \hat{w}_q}{\partial x_p \partial x_p} - \frac{\partial^2 \hat{w}_p}{\partial x_p \partial x_p} \right)$$

$$\text{or } 0 = \frac{\partial}{\partial x_p} (\hat{u}_p \hat{w}_q) - \frac{\partial}{\partial x_p} (\hat{u}_q \hat{w}_p) - \nu \frac{\partial^2 \hat{w}_q}{\partial x_p \partial x_p} + \nu \frac{\partial}{\partial x_q} \left(\frac{\partial \hat{w}_p}{\partial x_p} \right) \quad (D.17)$$

By definition, we have,

$$\hat{w}_p = \epsilon_{ijp} \frac{\partial}{\partial x_i} \hat{u}_j \quad (D.18)$$

then on differentiation,

$$\frac{\partial}{\partial x_p} \hat{w}_p = \frac{\partial}{\partial x_p} \left(\epsilon_{ijp} \frac{\partial \hat{u}_i}{\partial x_j} \right) = 0 \quad (D.19)$$

since divergence of a vector product is zero, and equation (D.17) reduces further to,

$$\hat{u}_j \frac{\partial \hat{w}_i}{\partial x_j} = \hat{w}_j \frac{\partial \hat{u}_i}{\partial x_j} + \nu \frac{\partial^2 \hat{w}_i}{\partial x_j \partial x_j} \quad \text{when } p \rightarrow j, q \rightarrow i \quad (D.20)$$

where continuity

$$\frac{\partial \hat{u}_j}{\partial x_j} = 0 \quad (\text{D.21})$$

still applies.

Recall back equation (A.10 of Appendix A),

$$\frac{\partial \hat{u}_i}{\partial x_j} = \hat{s}_{ij} + \hat{r}_{ij} \quad (\text{A.10})$$

On multiplication of (A.10) throughout by $\hat{\omega}_j$ then we have,

$$\hat{\omega}_j \frac{\partial \hat{u}_i}{\partial x_j} = \hat{\omega}_j \hat{s}_{ij} + 0 \quad (\text{D.22})$$

since

$$\begin{aligned} \hat{\omega}_j \hat{r}_{ij} &= \hat{\omega}_j \left(-\frac{1}{2} \epsilon_{ijk} \hat{\omega}_k \right) \\ &= -\frac{1}{2} \epsilon_{ijk} \hat{\omega}_j \hat{\omega}_k \\ &= -\frac{1}{2} \epsilon_{ikj} \hat{\omega}_k \hat{\omega}_j \quad (\text{since } j \text{ and } k \text{ are dummy indices}), \end{aligned} \quad (\text{D.23})$$

or

$$\hat{\omega}_j \hat{r}_{ij} = +\frac{1}{2} \epsilon_{ijk} \hat{\omega}_j \hat{\omega}_k \quad (\text{by interchanging } k \text{ and } j) \quad (\text{D.24})$$

By adding equations (D.24) and (D.23), we get the result that,

$$\hat{\omega}_j \hat{r}_{ij} = 0 \quad (\text{D.25})$$

By replacing equation (D.22) into equation (D.20) we get the vorticity equation,

$$\hat{u}_j \frac{\partial \hat{\omega}_i}{\partial x_j} = \hat{\omega}_j \hat{s}_{ij} + \nu \frac{\partial^2}{\partial x_j \partial x_j} \hat{\omega}_i \quad (\text{D.26})$$

Equation (D.26) may be regarded as a starting point for obtaining the ϵ - equation. The idea is similar to obtaining turbulence energy by first splitting the instantaneous quantities into mean and fluctuating parts, with

$$\hat{u}_i = U_i + u_i \quad (\text{D.27})$$

$$\hat{\omega}_i = \Omega_i + \omega_i \quad (\text{D.28})$$

$$\hat{s}_{ij} = S_{ij} + s_{ij} \quad (\text{D.29})$$

where

$$S_{ij} = \frac{1}{2} \left(\frac{\partial U_i}{\partial x_j} + \frac{\partial U_j}{\partial x_i} \right) \quad (\text{D.30})$$

and

$$s_{ij} = \frac{1}{2} \left(\frac{\partial u_i}{\partial x_j} + \frac{\partial u_j}{\partial x_i} \right) \quad (\text{D.31})$$

By introducing quantities (D.27) through (D.29) into equation (D.26), we get

$$(U_j + u_j) \frac{\partial}{\partial x_j} (\Omega_i + \omega_i) = (\Omega_j + \omega_j) (S_{ij} + s_{ij}) + \nu \frac{\partial^2}{\partial x_j \partial x_j} (\Omega_i + \omega_i) \quad (\text{D.32})$$

and on time averaging shall obtain,

$$U_j \frac{\partial}{\partial x_j} \Omega_i + \overline{u_j \frac{\partial \omega_i}{\partial x_j}} = \Omega_j S_{ij} + \overline{\omega_j s_{ij}} + \nu \frac{\partial^2}{\partial x_j \partial x_j} \Omega_i \quad (\text{D.33})$$

The energy of mean vorticity may be obtained by multiplying Ω_i with equation (D.33),

$$\begin{aligned}
 U_j \frac{\partial}{\partial x_j} \left(\frac{1}{2} \Omega_i \Omega_i \right) + \Omega_i u_j \overline{\frac{\partial \omega_i}{\partial x_j}} &= \Omega_i \Omega_j S_{ij} + \Omega_i \overline{\omega_j s_{ij}} \\
 + \nu \frac{\partial^2}{\partial x_j \partial x_j} \left(\frac{1}{2} \Omega_i \Omega_i \right) - \nu \frac{\partial \Omega_i}{\partial x_j} \cdot \frac{\partial \Omega_i}{\partial x_j} &\quad (D.34)
 \end{aligned}$$

If equation (D.32) is multiplied by $(\Omega_i + \omega_i)$ then we get,

$$\begin{aligned}
 (\Omega_i U_j + \Omega_i u_j + \omega_i U_j + \omega_i u_j) \frac{\partial}{\partial x_j} (\Omega_i + \omega_i) \\
 = (\Omega_i \Omega_j + \Omega_i \omega_j + \omega_i \Omega_j + \omega_i \omega_j) (S_{ij} + s_{ij}) \\
 + \nu (\Omega_i + \omega_i) \frac{\partial^2}{\partial x_j \partial x_j} (\Omega_i + \omega_i)
 \end{aligned}$$

and on time-averaging the following expressions will be obtained,

$$\begin{aligned}
 U_j \frac{\partial}{\partial x_j} \left(\frac{1}{2} \Omega_i \Omega_i \right) + \Omega_i \overline{u_j \frac{\partial \omega_i}{\partial x_j}} + U_j \overline{\omega_i \frac{\partial \omega_i}{\partial x_j}} + \overline{\omega_i u_j \frac{\partial \Omega_i}{\partial x_j}} + \overline{\omega_i u_j \frac{\partial \omega_i}{\partial x_j}} \\
 = \Omega_i \Omega_j S_{ij} + \Omega_i \overline{\omega_j s_{ij}} + \Omega_j \overline{\omega_i s_{ij}} + \overline{\omega_i \omega_j} S_{ij} \\
 + \overline{\omega_i \omega_j s_{ij}} + \nu \frac{\partial^2}{\partial x_j \partial x_j} \left(\frac{1}{2} \Omega_i \Omega_i \right) - \nu \frac{\partial \Omega_i}{\partial x_j} \cdot \frac{\partial \Omega_i}{\partial x_j} \\
 + \nu \frac{\partial^2}{\partial x_j \partial x_j} \left(\frac{1}{2} \overline{\omega_i \omega_i} \right) - \nu \overline{\frac{\partial \omega_i}{\partial x_j} \cdot \frac{\partial \omega_i}{\partial x_j}} \quad (D.35)
 \end{aligned}$$

Subtracting equation (D.34) from (D.35) we get

$$\begin{aligned}
 U_j \frac{\partial}{\partial x_j} \left(\frac{1}{2} \overline{\omega_i \omega_i} \right) &= \left[-\overline{\omega_i u_j} \frac{\partial \Omega_i}{\partial x_j} + \overline{\omega_i \omega_j s_{ij}} + \overline{\omega_i \omega_j S_{ij}} + \Omega_j \overline{\omega_i s_{ij}} \right] \\
 \text{(Convection)} & \qquad \qquad \qquad \text{(Production)} \\
 &+ \left[-\frac{\partial}{\partial x_j} \left(\frac{1}{2} \overline{\omega_i \omega_i u_j} \right) + \nu \frac{\partial^2}{\partial x_j \partial x_j} \left(\frac{1}{2} \overline{\omega_i \omega_i} \right) \right] + \left[-\nu \frac{\partial \omega_i}{\partial x_j} \cdot \frac{\partial \omega_i}{\partial x_j} \right] \quad \text{(D.36)} \\
 & \qquad \qquad \qquad \text{(Transport)} \qquad \qquad \qquad \text{(Dissipation)}
 \end{aligned}$$

and is called the equation for mean square vorticity fluctuations.

Each of the production terms on the right hand side of equation (D.36) are respectively, gradient production of $\overline{\omega_i \omega_i}$, production of $\overline{\omega_i \omega_i}$ by stretching of turbulent vorticity by the action of the fluctuating rate of strain s_{ij} , production of $\overline{\omega_i \omega_i}$ by stretching of turbulent vorticity by the action of the mean strain rate S_{ij} and mixed production term (Tennekes, 1972).

From definition of s_{ij} and r_{ij} , we have

$$\begin{aligned}
 \overline{s_{ij} s_{ij}} - \overline{r_{ij} r_{ij}} &= \overline{\left[\frac{1}{2} \left(\frac{\partial u_i}{\partial x_j} + \frac{\partial u_j}{\partial x_i} \right) \right]^2} - \overline{\left[\frac{1}{2} \left(\frac{\partial u_i}{\partial x_j} - \frac{\partial u_j}{\partial x_i} \right) \right]^2} \\
 &= \overline{\left[\frac{1}{2} \left(\frac{\partial u_i}{\partial x_j} + \frac{\partial u_j}{\partial x_i} \right) + \frac{1}{2} \left(\frac{\partial u_i}{\partial x_j} - \frac{\partial u_j}{\partial x_i} \right) \right] \left[\frac{1}{2} \left(\frac{\partial u_i}{\partial x_j} + \frac{\partial u_j}{\partial x_i} \right) - \frac{1}{2} \left(\frac{\partial u_i}{\partial x_j} - \frac{\partial u_j}{\partial x_i} \right) \right]} \\
 & \qquad \qquad \qquad \left\{ A^2 - B^2 = (A+B)(A-B) \right\} \\
 &= \overline{\left(\frac{\partial u_i}{\partial x_j} \right) \left(\frac{\partial u_j}{\partial x_i} \right)} \\
 &= \overline{\frac{\partial}{\partial x_j} \left(u_i \frac{\partial u_j}{\partial x_i} \right)} - \overline{u_i \frac{\partial}{\partial x_j} \left(\frac{\partial u_j}{\partial x_i} \right)} \\
 &= \overline{\frac{\partial^2 u_i u_j}{\partial x_j \partial x_i}} - \overline{u_i \frac{\partial}{\partial x_i} \left(\frac{\partial u_j}{\partial x_j} \right)} \\
 &= \overline{\frac{\partial^2 u_i u_j}{\partial x_i \partial x_j}} - 0
 \end{aligned}$$

or
$$\overline{S_{ij}S_{ij}} - \overline{r_{ij}r_{ij}} = \frac{\partial^2}{\partial x_i \partial x_j} \overline{u_i u_j} \quad (\text{D.37})$$

since $\frac{\partial u_j}{\partial x_j} = 0$ by continuity.

Now,

$$\overline{g_{ij}S_{ij}} \sim \frac{u^2}{\lambda^2} \quad (\text{D.38})$$

and
$$\frac{\partial^2}{\partial x_i \partial x_j} \overline{u_i u_j} \sim \frac{u^2}{l^2}; \quad l \gg \lambda \quad (\text{D.39})$$

so that their ratio is of the order $\sim \frac{l^2}{\lambda}$ (D.40)

But with estimates of

$$-\overline{u_i u_j} \sim u^2 \quad (\text{D.41})$$

$$S_{ij} \sim \frac{u}{l} \quad (\text{D.42})$$

and
$$\overline{S_{ij}S_{ij}} \sim \frac{u^2}{\lambda^2} \quad (\text{D.38})$$

equation (C.35, see Appendix C) becomes,

$$C_5 \frac{u^3}{l} = 2\nu C_6 \frac{u^2}{\lambda^2} \quad (\text{D.43})$$

or
$$2 \frac{C_6}{C_5} \frac{l^2}{\lambda^2} = \frac{ul}{\lambda} = R_l \quad (\text{D.44})$$

or
$$R_l \sim \frac{l^2}{\lambda^2} \quad (\text{D.45})$$

for some coefficients C_5 and C_6 of order one. Hence for large Reynolds number R (which is of the order $\frac{\ell^2}{\lambda^2}$ (from D.45)), then from relation (D.40) it shows that the term,

$$\frac{\partial^2}{\partial x_i \partial x_j} \overline{u_i u_j} \quad (D.45)$$

may be neglected. Consequently, from equation (D.37), the following is obtained,

$$\overline{s_{ij} s_{ij}} = \overline{r_{ij} r_{ij}} \quad (\text{for high Reynolds number}) \quad (D.47)$$

Also

$$\begin{aligned} \overline{r_{ij} r_{ij}} &= \overline{\left[\frac{1}{2} \left(\frac{\partial u_i}{\partial x_j} - \frac{\partial u_j}{\partial x_i} \right) \right]^2} \\ &= \frac{1}{2} \left[\overline{\left(\frac{\partial u_i}{\partial x_j} \right)^2} - \overline{\frac{\partial u_i}{\partial x_j} \cdot \frac{\partial u_j}{\partial x_i}} \right] \end{aligned} \quad (D.48)$$

for isotropic turbulence, and

$$\begin{aligned} \overline{\omega_k \omega_k} &= \overline{\omega^2} = \overline{\left(\epsilon_{ijk} \frac{\partial u_i}{\partial x_j} \right) \left(\epsilon_{pqk} \frac{\partial u_p}{\partial x_q} \right)} \\ &= \overline{(\delta_{ip} \delta_{jq} - \delta_{iq} \delta_{jp}) \frac{\partial u_i}{\partial x_j} \cdot \frac{\partial u_p}{\partial x_q}} \\ &= \overline{\frac{\partial u_q}{\partial x_p} \cdot \frac{\partial u_p}{\partial x_q} - \frac{\partial u_p}{\partial x_q} \cdot \frac{\partial u_q}{\partial x_p}} \end{aligned}$$

Hence

$$\begin{aligned} \overline{\omega^2} &= \overline{\left(\frac{\partial u_i}{\partial x_j} \right)^2} - \overline{\frac{\partial u_i}{\partial x_j} \cdot \frac{\partial u_j}{\partial x_i}} ; q \rightarrow i, p \rightarrow j \\ &= 2 \overline{r_{ij} r_{ij}} \quad (\text{by D.48}) \end{aligned}$$

or
$$\overline{\omega^2} \stackrel{\Omega}{=} 2\overline{S_{ij}S_{ij}} \text{ (by E.47, see Appendix E)} \quad (\text{D.49})$$

or by multiplying equation (D.49) throughout by ν

$$\nu\overline{\omega^2} = 2\nu\overline{S_{ij}S_{ij}} \equiv \mathcal{E} \quad (\text{by C.38, see Appendix C})$$

where
$$\mathcal{E} = 2\nu\overline{S_{ij}S_{ij}}$$

$$= 2\nu\overline{\left[\frac{1}{2}\left(\frac{\partial u_i}{\partial x_j} + \frac{\partial u_j}{\partial x_i}\right)\right]^2}$$

$$= \frac{1}{2}\nu\overline{\left(\frac{\partial u_i}{\partial x_j} + \frac{\partial u_j}{\partial x_i}\right)^2} \quad (\text{D.50})$$

which is the same as the earlier defined \mathcal{E} (see equation D.6).

Now by multiplying 2μ ($\mu = \rho\nu$) and replacing

$$\nu\overline{\omega^2} = \nu\overline{\omega_i\omega_i} \equiv \mathcal{E} \quad (\text{D.50a})$$

into equation (D.36) we obtain the exact (unmodelled) equation for \mathcal{E} .

$$\begin{aligned} U_j \frac{\partial}{\partial x_j} (\rho\mathcal{E}) &= \left[-\mu \frac{\partial}{\partial x_j} \overline{\omega_i\omega_i u_j} - \mu\nu \frac{\partial^2}{\partial x_j \partial x_j} \overline{\omega_i\omega_i} \right] \\ &+ \left[-2\mu \overline{\omega_i u_j} \frac{\partial \rho_i}{\partial x_j} + 2\mu \overline{\omega_i \omega_j S_{ij}} + 2\mu \overline{\omega_i \omega_j} S_{ij} + 2\mu \Omega_j \overline{\omega_i S_{ij}} \right] \\ &+ \left[-2\mu\nu \frac{\partial \omega_i}{\partial x_j} \cdot \frac{\partial \omega_i}{\partial x_j} \right] \quad (\text{D.51}) \end{aligned}$$

(a) (b) (c) (d) (e) (f) (g) (h)

where the terms (a),..., (h) are respectively given by,

(a)=convection of ϵ by mean motion,

(b)=transport of ϵ due to velocity fluctuation,

(c)=transport of ϵ due to molecular action,

(d)=production of ϵ by mean motion

(e)=production of ϵ by turbulent stretching of turbulent vorticity,

(f)=production of ϵ by stretching of vorticity fluctuations by mean strain rate S_{ij} ,

(g)=mixed production term (Tennekes, 1972), and

(h)=dissipation of ϵ by viscous action.

Modelled ϵ -equation.

For a two-dimensional turbulence flow, there is no vortex-stretching (Tennekes, 1972), so the second, third and fourth of the production terms on the right hand side of equation (D.51) vanish. The estimates of the viscous and transport terms at high Reynolds number will be given as follows.

The transport term due to velocity fluctuation of equation (D.51) is,

$$\begin{aligned} \frac{\partial}{\partial x_j} \overline{\omega_i \omega_i u_j} &= \overline{u_j \frac{\partial}{\partial x_j} \omega_i \omega_i} \\ &\sim \frac{u_l}{l} \cdot \frac{u_l^2}{\lambda^2} \end{aligned}$$

$$\text{or } \frac{\partial}{\partial x_j} \overline{\omega_i \omega_i u_j} = G \frac{v^3}{l \lambda^2} \quad (\text{D.52})$$

and the viscous term is estimated as,

$$\nu \frac{\partial^2}{\partial x_j \partial x_j} \overline{\omega_i \omega_i} \sim \frac{\nu}{l^2} \cdot \frac{v^2}{\lambda^2} = H \nu \frac{v^2}{l^2 \lambda^2} \quad (\text{D.53})$$

for some coefficients G and H of order one. The ratio of those two terms given by (D.52) and (D.53) is of the order $\frac{vl}{\lambda} = Re$. This implies that for high Reynolds number, Re the viscous transport term $\nu \frac{\partial^2}{\partial x_j \partial x_j} \overline{\omega_i \omega_i}$ in equation (D.51) may be neglected; finally, this equation reduces to a simpler form,

$$\begin{aligned} U_j \frac{\partial}{\partial x_j} (\rho \epsilon) &= - \frac{\partial}{\partial x_j} (\mu \overline{\omega_i \omega_i u_j}) - 2 \mu \overline{\omega_i u_j} \frac{\partial}{\partial x_j} \Omega_i \\ &\quad - 2 \mu \nu \frac{\partial \omega_i}{\partial x_j} \cdot \frac{\partial \omega_i}{\partial x_j} \end{aligned} \quad (\text{D.54})$$

As already implied previously, the diffusion term $\frac{\partial}{\partial x_j} (\rho \nu \overline{\omega_i \omega_i u_j})$ (since $\mu = \rho \nu$) for ϵ is assumed to obey the gradient transport law, i.e.

$$\rho \nu \overline{\omega_i \omega_i u_j} = - \Gamma_\epsilon \frac{\partial}{\partial x_j} (\nu \overline{\omega_i \omega_i}) \quad (\text{D.55})$$

in a similar manner as equation (D.7) for turbulence energy k . Here Γ_ϵ is the turbulent exchange coefficient and is assumed to be proportional to eddy viscosity, i.e.,

$$\Gamma_\epsilon = \frac{\mu_t}{\sigma_\epsilon} \quad (\text{D.56})$$

where σ_ϵ is the Prandtl/Schmidt number for the dissipation rate ϵ . Hence equation (D.54) becomes,

$$U_j \frac{\partial}{\partial x_j} (\rho \epsilon) = \frac{\partial}{\partial x_j} \left(\frac{\mu_t}{\sigma_\epsilon} \frac{\partial \epsilon}{\partial x_j} \right) - 2 \rho \nu \overline{\omega_i u_j} \frac{\partial \Omega_i}{\partial x_j} - 2 \rho \nu \nu \overline{\frac{\partial \omega_i}{\partial x_j} \cdot \frac{\partial \omega_i}{\partial x_j}} \quad (\text{D.57})$$

If equation (D.57) for ϵ may be expressed in the form of equation (D.9) for k , i.e. in the form,

$$U_j \frac{\partial}{\partial x_j} (\rho \epsilon) = \frac{\partial}{\partial x_j} \left(\frac{\mu_t}{\sigma_\epsilon} \frac{\partial \epsilon}{\partial x_j} \right) - \rho \left\{ \underbrace{2 \nu \overline{\omega_i u_j} \frac{\partial \Omega_i}{\partial x_j}}_{(a)} \right\} - \rho \left\{ \underbrace{2 \nu \nu \overline{\frac{\partial \omega_i}{\partial x_j} \cdot \frac{\partial \omega_i}{\partial x_j}}}_{(b)} \right\} \quad (\text{D.58})$$

The terms (a) and (b) may be treated as follows. By definition, the term (a) becomes,

$$\begin{aligned} \nu \overline{\omega_i u_j} \frac{\partial \Omega_i}{\partial x_j} &= \nu \cdot \epsilon_{ijk} \overline{\frac{\partial u_k}{\partial x_j} \cdot u_j} \cdot \frac{\partial}{\partial x_j} \left(\epsilon_{ipq} \frac{\partial U_q}{\partial x_p} \right) \\ &= \nu \cdot (\delta_{jp} \delta_{kq} - \delta_{jq} \delta_{kp}) \cdot \overline{u_j \frac{\partial u_k}{\partial x_j}} \cdot \frac{\partial^2 U_q}{\partial x_j \partial x_p} \\ &= \nu \cdot \overline{u_j \frac{\partial u_k}{\partial x_j}} \cdot \frac{\partial^2 U_q}{\partial x_j \partial x_j} - \nu \overline{u_j \frac{\partial u_k}{\partial x_j}} \cdot \frac{\partial^2 U_j}{\partial x_j \partial x_k} \end{aligned}$$

$$\text{or } \overline{\nu \omega_i u_j} \frac{\partial \Omega_i}{\partial x_j} = \overline{\nu u_j} \frac{\partial u_k}{\partial x_j} \cdot \frac{\partial^2 U_k}{\partial x_j \partial x_j} + 0 \quad (\text{D.59})$$

where the second term on the right hand side of equation (D.59) vanishes by continuity. Now the first term of equation (D.59) which represents the generation of ϵ from the mean flow, is simulated in the form proposed by Hanjalic and Launder, 1972, as (See Iieriah, 1977).

$$\overline{\nu u_j} \frac{\partial u_k}{\partial x_j} \cdot \frac{\partial^2 U_k}{\partial x_j \partial x_j} = C_1 \frac{\epsilon}{k} \overline{u_j u_k} \frac{\partial U_k}{\partial x_j} \quad (\text{D.60})$$

Hence

$$\overline{\nu \omega_i u_j} \frac{\partial \Omega_i}{\partial x_j} = C_1 \frac{\epsilon}{k} \overline{u_i u_j} \frac{\partial U_i}{\partial x_j} \quad (k \rightarrow i) \quad (\text{D.61})$$

The term (b) of equation (D.58) may be approximated by,

$$\begin{aligned} \overline{\nu \nu} \frac{\partial \omega_i}{\partial x_j} \cdot \frac{\partial \omega_i}{\partial x_j} &= \overline{\nu \nu} \frac{\partial}{\partial x_j} \left(\epsilon_{ijk} \frac{\partial u_k}{\partial x_j} \right) \cdot \frac{\partial}{\partial x_j} \left(\epsilon_{ipq} \frac{\partial u_q}{\partial x_p} \right) \\ &= \overline{\nu \nu} \cdot (\delta_{jp} \delta_{kq} - \delta_{jq} \delta_{kp}) \frac{\partial}{\partial x_j} \left(\frac{\partial u_k}{\partial x_j} \right) \cdot \frac{\partial}{\partial x_j} \left(\frac{\partial u_q}{\partial x_p} \right) \\ &= \overline{\nu \nu} \cdot \left[\frac{\partial}{\partial x_j} \left(\frac{\partial u_k}{\partial x_j} \right) \cdot \frac{\partial}{\partial x_j} \left(\frac{\partial u_k}{\partial x_j} \right) - \frac{\partial}{\partial x_j} \left(\frac{\partial u_k}{\partial x_j} \right) \cdot \frac{\partial}{\partial x_j} \left(\frac{\partial u_i}{\partial x_k} \right) \right] \\ &= \overline{\left[\nu \frac{\partial}{\partial x_j} \left(\frac{\partial u_k}{\partial x_j} \right) \right]^2} + 0 \\ &= \overline{\left[\nu \frac{\partial^2 u_k}{\partial x_j \partial x_j} \right]^2} \quad (\text{D.62}) \end{aligned}$$

where again continuity equation has been used to remove the second term

on the right hand side of equation (D.62).

The term $\overline{\left[\nu \frac{\partial^2 u_k}{\partial x_j \partial x_j} \right]^2}$ may be treated in the manner proposed by Lumley, 1974, which is also used by Ideriah, 1977, as

$$\overline{\left[\nu \frac{\partial^2 u_k}{\partial x_j \partial x_j} \right]^2} = C_2 \frac{\epsilon^2}{k} \quad (\text{D.63})$$

It is therefore because of the relations (D.59) and (D.63), equation (D.57) may be rewritten as follows,

$$U_j \frac{\partial}{\partial x_j} (\rho \epsilon) = \frac{\partial}{\partial x_j} \left(\frac{\mu_t}{\sigma_\epsilon} \frac{\partial \epsilon}{\partial x_j} \right) - C_1 \frac{\epsilon}{k} \rho \overline{u_i u_j} \frac{\partial U_i}{\partial x_j} - C_2 \frac{\epsilon^2}{k} \quad (\text{D.64})$$

for some constants C_1 and C_2 at high Reynolds number. The values of these constants are given as in table 2.1 (see chapter 2).

Equation (D.64) is called the ϵ -equation.

As can be seen that the transition from Navier-Stokes' equation to Reynolds equation (eqn.C.25) for steady, incompressible flow, creates new terms, $-\overline{\rho u_i u_j}$ called the Reynolds stresses. It is these stresses that one faces difficulties to 'close' those systems of transport equations (see Appendix C for closure problem).

The problem now is to find relationships between these stresses with known mean quantities. However if the Reynolds stresses are expressed in term of 'effective' viscosities multiplied by gradients of mean flow properties, the following relationship is adopted,

for cartesian coordinates,

$$-\rho \overline{u_i u_j} = \mu_t \left(\frac{\partial U_i}{\partial x_j} + \frac{\partial U_j}{\partial x_i} \right), \quad i, j = 1, 2, 3 \quad (D.65)$$

where u_i denote velocity fluctuations, μ_t the turbulent viscosity and U_i the mean velocities independent of time. If equation (D.65) is accepted as basis of calculations, a formula is then needed for the calculation of μ_t (see Appendix C, section C.52 for obtaining formula of μ_t).

When the Reynolds stresses given by equation (D.65) is replaced into equations (D.9) and (D.64) the final (k- ϵ) equations have the following form,

k-equation.

$$\frac{D}{Dt}(\rho k) = \frac{\partial}{\partial x_j} \left(\frac{\mu_t}{\sigma_k} \frac{\partial k}{\partial x_j} \right) + G - C_D \rho \epsilon \quad (D.66)$$

ϵ -equation.

$$\frac{D}{Dt}(\rho \epsilon) = \frac{\partial}{\partial x_j} \left(\frac{\mu_t}{\sigma_\epsilon} \frac{\partial \epsilon}{\partial x_j} \right) + G_\epsilon \frac{\epsilon}{k} - C_2 \rho \frac{\epsilon^2}{k} \quad (D.67)$$

where

$$G = \mu_t \left(\frac{\partial U_i}{\partial x_j} + \frac{\partial U_j}{\partial x_i} \right) \frac{\partial U_i}{\partial x_j} \quad (D.68)$$

$$D \equiv U_j \frac{\partial}{\partial x_j} \quad (D.69)$$

$$k = \frac{1}{2} \overline{u_i u_i} \quad (\text{turbulence kinetic energy}) \quad (D.70)$$

$$\epsilon = \frac{1}{2} \nu \overline{\left(\frac{\partial u_i}{\partial x_j} + \frac{\partial u_j}{\partial x_i} \right)^2}, \text{ (dissipation rate)} \quad (\text{D.71})$$

with

$$\mu_t = C_\mu \rho \frac{k^2}{\epsilon} \quad (\text{D.72})$$

where σ_k and σ_ϵ are turbulent Prandtl/Schmidt number for k and ϵ respectively-usually they are taken to be constants at high Reynolds number; C_1 and C_2 are some constants. The values of these σ 's and C 's are found in table 2.1 (see chapter 2).

The following is shown how Prandtl/Schmidt number σ_ϵ for ϵ in terms of constants \mathcal{K}, C_1, C_2 and C_μ is obtained.

Derivation of Prandtl/Schmidt number σ_ϵ for ϵ .

By neglecting convective transport of ϵ in the inertial sublayer of the modelled ϵ -equation (one-dimensional Couette flow still apply) then equation (D.64) reduces to,

$$C_1 \frac{\epsilon}{k} (-\rho \overline{uv} \frac{\partial U}{\partial y}) = C_2 \rho \frac{\epsilon^2}{k} - \frac{\partial}{\partial y} \left(\frac{\mu_t}{\sigma_\epsilon} \frac{\partial \epsilon}{\partial y} \right) \quad (\text{D.73})$$

By using equations (F.12) and (F.30) (see Appendix F) to eliminate $-\overline{uv} \frac{\partial U}{\partial y}$ and $\frac{\partial}{\partial y} \left(\frac{\partial \epsilon}{\partial y} \right)$ respectively, equation (D.73) reduces to,

$$C_1 \rho \frac{\epsilon^2}{k} = C_2 \rho \frac{\epsilon^2}{k} - \frac{\mathcal{K}^2 \epsilon^3}{k^3 C_\mu^{3/2}} \cdot \frac{\mu_t}{\sigma_\epsilon} \quad (\text{D.74})$$

from where,

$$\sigma_{\epsilon} = \frac{\mathcal{K}^2}{C_{\mu}^{1/2} (C_2 - C_1)} \quad (\text{D.75})$$

will be obtained. In arriving at equation (D.75) equation (C.68) (see Appendix C) for μ_t has been used. Equation (D.75) is called the turbulent Prandtl/Schmidt number for ϵ . The constants of turbulence appearing in equation (D.75) have values given in table 2.1 (see Chapter 2).

APPENDIX E.DERIVATION AND SOLUTION PROCEDURE OF FINITE DIFFERENCE EQUATIONS.E.1 INTRODUCTION.

The following appendix will discuss the derivation of the transport finite difference equations (fdes) for scalar quantities (k and ϵ) and momentum. There are methods of transforming partial differential equations (pdes) into finite difference form. This includes the Taylor series expansion method and micro-integration method. In this study, the latter method of Gosman (1976) is employed.

E.2 TRANSPORT FDES FOR SCALAR VARIABLES.

The procedure of deriving the fdes for scalar properties is to integrate the pdes (see equation 2.24 of Chapter 2) over shaded control volume represented by fig.E.1, i.e.,

$$\int_V \left[\frac{1}{r} \left\{ \frac{\partial}{\partial x} (\rho U r \phi - r \Gamma_\phi \frac{\partial \phi}{\partial x}) + \frac{\partial}{\partial r} (\rho V r \phi - r \Gamma_\phi \frac{\partial \phi}{\partial r}) \right\} - S^\phi \right] dV = 0 \quad (E.1)$$

where dV is the control volume over which the integration is performed,

and
$$dV = r dr dx \quad (E.2)$$

By using Gauss' theorem to replace the volume integrals to surface ones, the convection and diffusion terms give rise to surface

integrals over the faces of the control volume(c.v.)giving,

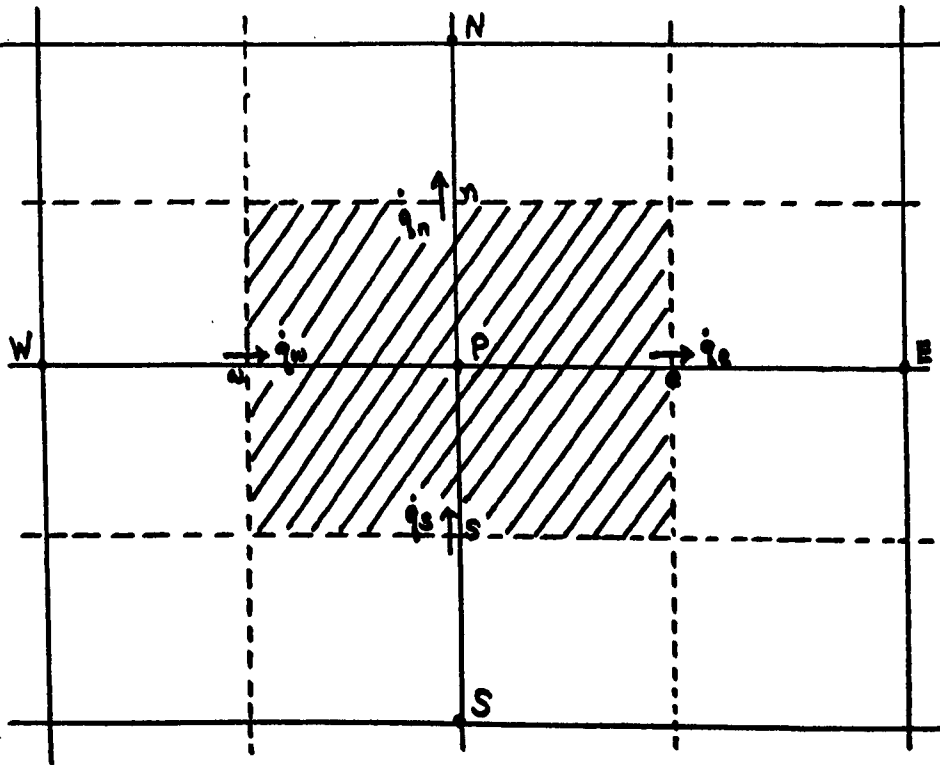


Fig.E.1: A Typical Scalar Cell(Control Volume), ϕ with Fluxes on the Boundaries, \dot{q}_i 's.

$$\int_s^n \left\{ (\rho U r \phi - r \Gamma_\phi \frac{\partial \phi}{\partial r})_e - (\rho U r \phi - r \Gamma_\phi \frac{\partial \phi}{\partial r})_w \right\} dr$$

$$+ \int_w^e \left\{ (\rho V r \phi - r \Gamma_\phi \frac{\partial \phi}{\partial r})_n - (\rho V r \phi - r \Gamma_\phi \frac{\partial \phi}{\partial r})_s \right\} dx - \int_V S^\phi dV = 0 \quad (E.3)$$

or

$$\dot{q}_e - \dot{q}_w + \dot{q}_n - \dot{q}_s = \int_V S^\phi dV \quad (E.4)$$

Each of the terms \dot{q}_i 's ($i=e, w, e, n$ and s where each of these small letters are located mid-way between the point P and its

neighbours, E, W, N and S, see fig. E.1) represent the combined convective and diffusive fluxes located at the boundaries of the c.v denoted by each subscript, S^ϕ is the source term for each individual scalar variable, ϕ .

To express those fluxes in terms of values of ϕ at the node points in the neighbourhood of P, we need to assume the variation of ϕ between those points. In choosing this variation, we should ensure the compatibility of surface integrals between adjacent control volumes for example the expression for the flux across the face between the node points W and P, q_w as in fig. E.1 should be the same irrespective of whether the control volume surrounding W or the one which surrounds P is being considered.

E.21 Convective and Diffusive Flux Expression.

The basic formulation of the convection and diffusion terms may be explained by considering the transport across one face of the control volume.

Fig. E.2 shows a face of area A_w (for the west boundary of the control volume) normal to the X-direction this lies mid-way between the nodes W and P which is at a distance δ_{PW} apart. The variable ϕ is assumed to vary linearly between those nodes. The contribution by this face to the integral represented by equation (E.1) over the control volume is given by,

$$\dot{q}_\omega = \rho_\omega U_\omega \phi_\omega A_\omega - \Gamma_{\phi, \omega} A_\omega \frac{(\phi_P - \phi_W)}{\delta X_{PW}} \quad (\text{E.5})$$

The discrete values of the flow variables ϕ are generally represented by averages over the respective control volumes hence the values ϕ_ω mid-way between W and P may be expressed as,

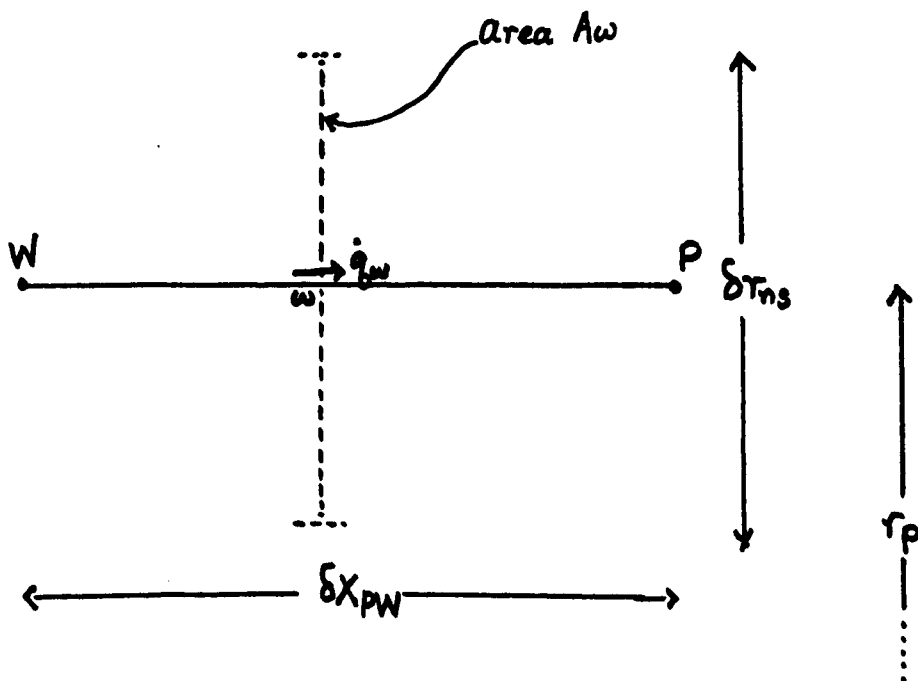


Fig.E.2: A Flux \dot{q}_ω Across a Boundary of the Control Volume.

$$\phi_\omega = \frac{1}{2} (\phi_W + \phi_P) \quad (\text{E.6})$$

By replacing equation (E.6) into (E.5) for ϕ_ω will result, after slight rearrangement,

$$\frac{\dot{q}_\omega}{\rho_\omega U_\omega A_\omega} = \frac{1}{2} \left\{ (1 + 2Pe_\omega^{-1}) \phi_W + (1 - 2Pe_\omega^{-1}) \phi_P \right\} \quad (\text{E.7})$$

where $Pe_\omega = \frac{\rho_\omega U_\omega \delta X_{PW}}{\Gamma_{\phi, \omega}}$ is called a local Peclet number at boundary

w.

Expression (E.7) gives the combined convective and diffusive flux in terms of node values and this has been obtained by employing a central-difference scheme for low $|Pe|$ ie for $-2 < Pe_w < 2$. For large $|Pe_w|$ ie for $Pe_w > 2$ or $Pe_w < -2$, upwind difference scheme is used. The upwind formula may be obtained by setting the local Peclet number, Pe_w to be,

$$Pe_w \rightarrow \begin{matrix} +\infty \\ -\infty \end{matrix} \quad (E.8)$$

from the 'exact' solution formula for \dot{q}_w which is derived with the aid of a 1-D analysis. This 'exact' solution formula is given by (Gosman, 1976),

$$\dot{q}_w = \rho_w U_w A_w \{ f_w \phi_W + (1-f_w) \phi_P \} \quad (E.9)$$

where

$$Pe_w = \frac{\rho_w U_w \delta X_{PW}}{\Gamma_{\phi,w}} \quad (E.10)$$

$$\rho_w = \frac{1}{2} (\rho_W + \rho_P) \quad (E.11)$$

$$\Gamma_{\phi,w} = \frac{1}{2} (\Gamma_{\phi,W} + \Gamma_{\phi,P}) \quad (E.12)$$

$$A_w = \tau_P \cdot \delta \tau_{ns} \quad (E.13)$$

$$f_w = \frac{\exp(Pe_w)}{\exp(Pe_w) - 1} \quad (E.14)$$

Consider equations (E.14) and (E.9),

$$\left. \begin{aligned}
 \text{As } Pe_w \rightarrow \infty, f_w \rightarrow 1, & \Rightarrow \frac{\dot{q}_w}{\rho_w U_w A_w} \rightarrow \phi_w \\
 Pe_w \rightarrow -\infty, f_w \rightarrow 0, & \Rightarrow \frac{\dot{q}_w}{\rho_w U_w A_w} \rightarrow \phi_p.
 \end{aligned} \right\} \quad (\text{E.15})$$

Again from equation (E.7),

$$\left. \begin{aligned}
 \text{When } Pe_w = 2, \frac{\dot{q}_w}{\rho_w U_w A_w} & = \phi_w \\
 Pe_w = -2, \frac{\dot{q}_w}{\rho_w U_w A_w} & = \phi_p
 \end{aligned} \right\} \quad (\text{E.16})$$

Therefore by combining equation (E.7) for low $|Pe_w|$ and equations (E.15) and (E.16) for high $|Pe_w|$, we get the representation of the combined convection and diffusion flux for the whole range of Pe_w . Consequently we use a 'hybrid scheme', i.e. a combination of the so-called the central- and the upwind-difference schemes. This offers good compromise between accuracy and economy and is numerically stable (Gosman, 1976). Its rationale is explained by Spalding (1972). The scheme may therefore be summarised as follows,

$$\frac{\dot{q}_w}{\rho_w U_w A_w} = \begin{cases} \frac{1}{2}[(1+2Pe_w^{-1})\phi_w + (1-2Pe_w^{-1})\phi_p], & -2 < Pe_w < +2 \\ \phi_w & , Pe_w \gg +2 \\ \phi_p & , Pe_w \leq -2 \end{cases} \quad (E.17)$$

From equation (E.9) for the exact solution formula to be identical with the set of equations (E.17), the weighting factor (for example the west boundary) f_w must have the values,

$$f_w = \begin{cases} \frac{1}{2}(1+2Pe_w^{-1}), & -2 < Pe_w < +2 \\ 1 & , Pe_w \gg +2 \\ 0 & , Pe_w \leq -2 \end{cases} \quad (E.18)$$

The remaining total flux expressions \dot{q}_e, \dot{q}_n and \dot{q}_s for the east, north and south boundaries of the control volume may be obtained in exactly the same manner.

E.22 The Source Term, S^ϕ .

The total source over the control volume cannot exactly be integrated without the knowledge of the particular expression of the term S^ϕ of the variable ϕ .

However, whatever the form of the particular expressions may be, it can be anticipated that the result may be forced into a

linearised form, thus

$$\int_V S^\phi dV = S_p^\phi \phi_p + S_U^\phi \quad (\text{E.19})$$

where S_p^ϕ and S_U^ϕ are deduced from the integrated and linearised form of the source and they are in general a function of ϕ .

For variables U, V, k and \mathcal{E} we have respectively,

$$\int_V S^U dV = S_p^U U_p + S_U^U \quad (\text{E.20})$$

$$\int_V S^V dV = S_p^V V_p + S_U^V \quad (\text{E.21})$$

$$\begin{aligned} \int_V S^k dV &= \int_V (G - C_0 \rho \mathcal{E}) dV \\ &= S_p^k k_p + S_U^k \end{aligned} \quad (\text{E.22})$$

$$\begin{aligned} \int_V S^\mathcal{E} dV &= \int_V (C_1 G \frac{\mathcal{E}}{k} - C_2 \rho \frac{\mathcal{E}^2}{k}) dV \\ &= S_p^\mathcal{E} + S_U^\mathcal{E} \end{aligned} \quad (\text{E.23})$$

where the superscripts U, V, k and \mathcal{E} are related to each individual dependent variables; U_p, V_p, k_p and \mathcal{E}_p are values of U, V, k and \mathcal{E} at the point P nearest to a wall. The modifications of the linearised source treatment near a wall will be discussed in Appendix F.

E.23 The Complete Difference Equations.

When the finite-difference representations of all the terms of equation (E.1) have been worked out, then we can assemble the flux

terms (like equation (E.17)) and source terms (equation (E.19)) into equation (E.4). With the aid of continuity, the following finite difference equations for scalar quantities are obtained,

$$(a_p - s_p^\phi) \phi_p = \sum_n a_n \phi_n + S_u^\phi \quad (\text{E.24})$$

where $a_p = \sum_n a_n$ (E.25)

$$\sum_n = \text{summation over neighbours (N, S, E, W),}$$

$$a_w = \rho_w U_w A_w f_w \text{ etc.} \quad (\text{E.26})$$

$$A_w = r_p \cdot \delta r_{ns} \quad (\text{E.27})$$

and f_w etc. are defined by equation (E.18) etc.

Although equation (E.24) has the appearance of a linear equation, it is actually not since the coefficients (a_w etc. which represent combined convection and diffusion coefficients) themselves depend on values of ϕ 's. This non-linearity will be handled by an iteration scheme, in which the coefficients of the finite difference equations are recalculated in every iteration cycle (described later).

Similar equations are derivable for other scalar variables to be solved namely for k and ϵ since transport equations exist for them. No transport equation exists for pressure, p . A later section shall discuss the measure in obtaining the pressure fields.

E.3 FINITE DIFFERENCE MOMENTUM EQUATIONS.

While the foregoing derivation of the finite difference equations is based on general dependent scalar variable, ϕ , the finite difference momentum equations are derived in a similar pattern except that the control volumes are displaced because the velocities themselves are displaced the conventions are otherwise the same.

The finite difference equation for U-momentum (the control volume of which is shown shaded in fig.E.3) is,

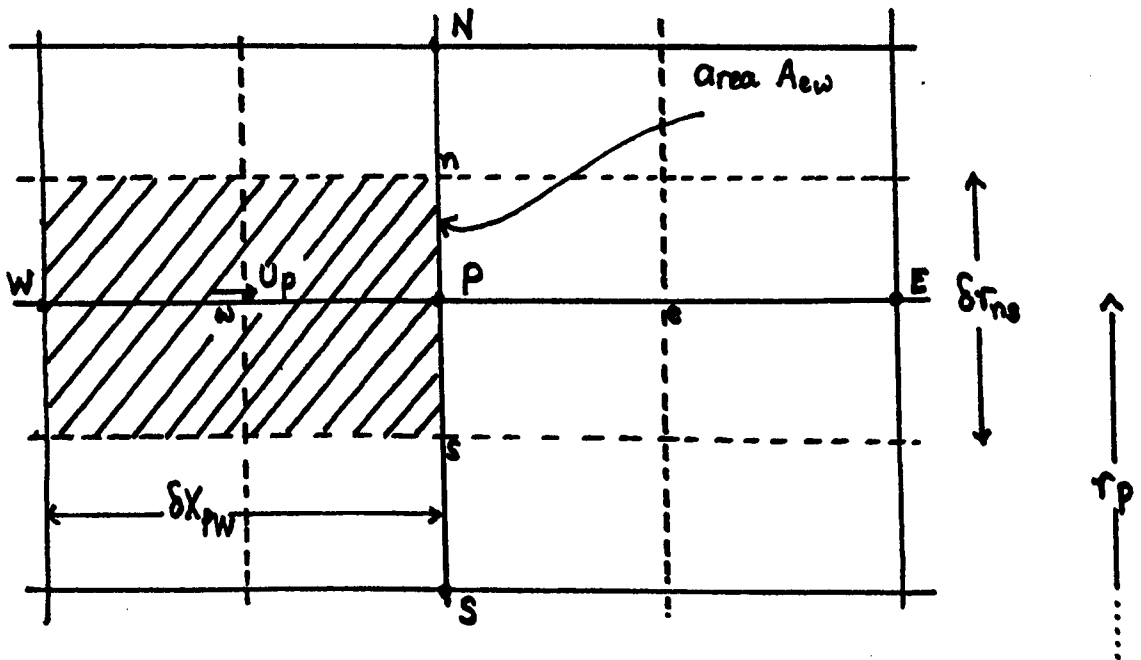


Fig.E.3: A Typical U-Cell (Control Volume).

$$(a_p - s_p^u) U_p = \sum_n a_n U_n + A_{cw} (P_w - P_p) + S_u^u \quad (E.28)$$

where

$$a_p = \sum_n a_n, \quad \sum_n \equiv \text{summing over neighbours}$$

$$a_w = \rho_w U_w A_{cw} f_w \text{ etc.} \quad (E.29)$$

$$A_{ew} = r_p \cdot \delta r_{ns} \quad (E.30)$$

f_w is a hybrid difference of local Reynolds number Re_w defined by,

$$Re_w = \frac{\rho_w U_w \delta x_{pw}}{\mu_w} \quad (E.31)$$

$$\rho_w U_w = \frac{1}{2}(\rho_w U_w + \rho_p U_p) \quad (E.32)$$

and f_w etc are defined by equation (E.18) etc.

E.4 HANDLING OF PRESSURE LINKAGE.

The finite difference equations for non-hydrodynamic variables (in this study only k and ϵ) can be solved directly by the use of TDMA (for Tri-Diagonal Matrix Algorithm). An additional procedure is employed along with the TDMA to solve the hydrodynamic variables (ie U, V and p), called the SIMPLE procedure (described later).

Before discussing the SIMPLE algorithms, it is useful to note briefly the suitability of velocity-pressure equation set for numerical solution.

(i) Requirement.

To solve for a particular variable ϕ , an equation where ϕ appear as dominant of its own differential equation must be needed.

(ii) Assessment.

All the non-hydrodynamic variables satisfy above requirement since they have their own equations (the $k-\epsilon$ equations). Velocity components U and V also satisfy the requirement via momentum equations. However the pressure has no equation of its own. The remaining mass-conservation (continuity) equation does not contain pressure, p .

A special measure is therefore seems to be needed to obtain the pressure fields. The measure employed here is first by estimating the pressure fields at all nodes, then obtaining estimates of U and V by solving the momentum equations. Finally correcting the pressure fields through a pressure-correction equation in such a way that to bring the velocity fields to satisfy continuity equation. The values of U, V and p are now used as new guesses and the process repeated until desired solution is obtained. This procedure is thus known as SIMPLE (for Semi-Implicit Method for Pressure Linked-Equations).

E.41 Pressure Solution

The process in obtaining the pressure fields involve the following steps.

(i) The initial estimated values of pressure (denoted by p^*) is specified at all grid nodes of the computation domain.

(ii) The momentum equations are solved by L-B-L (for Line-By-Line) method (discussed later) to yield corresponding values of U and V . These

values (denoted by U^* and V^*) will probably not satisfy the continuity, but satisfy the following equation for U^* -velocity,

$$(a_p - S_p^U) U_p^* = \sum_n a_n U_n^* + A_{ew} (P_w^* - P_p^*) + S_U^U \quad (E.33)$$

where U^* and V^* are based on the estimated pressure field p^* .

Those 'incorrect' values of U, V and p require the imposition of some correction (denoted by primes) U', V' and p' defined by,

$$\left. \begin{aligned} U' &= U - U^* \\ V' &= V - V^* \\ p' &= p - p^* \end{aligned} \right\} \quad (E.34)$$

From continuity equation, we have

$$\frac{\partial}{\partial x} G_x + \frac{\partial}{\partial y} G_y = \dot{S}_m^m \quad (E.35)$$

where $G_x = \rho U \quad (E.36)$

$$G_y = \rho V \quad (E.37)$$

and \dot{S}_m^m (ideally zero) is mass source (or generation per unit volume).

On integration of equation (E.35) similar to equation (E.1) for a typical control volume as indicated in fig.E.4 to yield,

$$G_e A_e - G_w A_w + G_n A_n - G_s A_s = \dot{S}_m^N \delta V \quad (\text{E.39})$$

where G_e, G_w, G_n and G_s are fluxes across boundaries denoted by e, w, n and s respectively and δV is the control volume enclosing point P as indicated by fig.E.4.

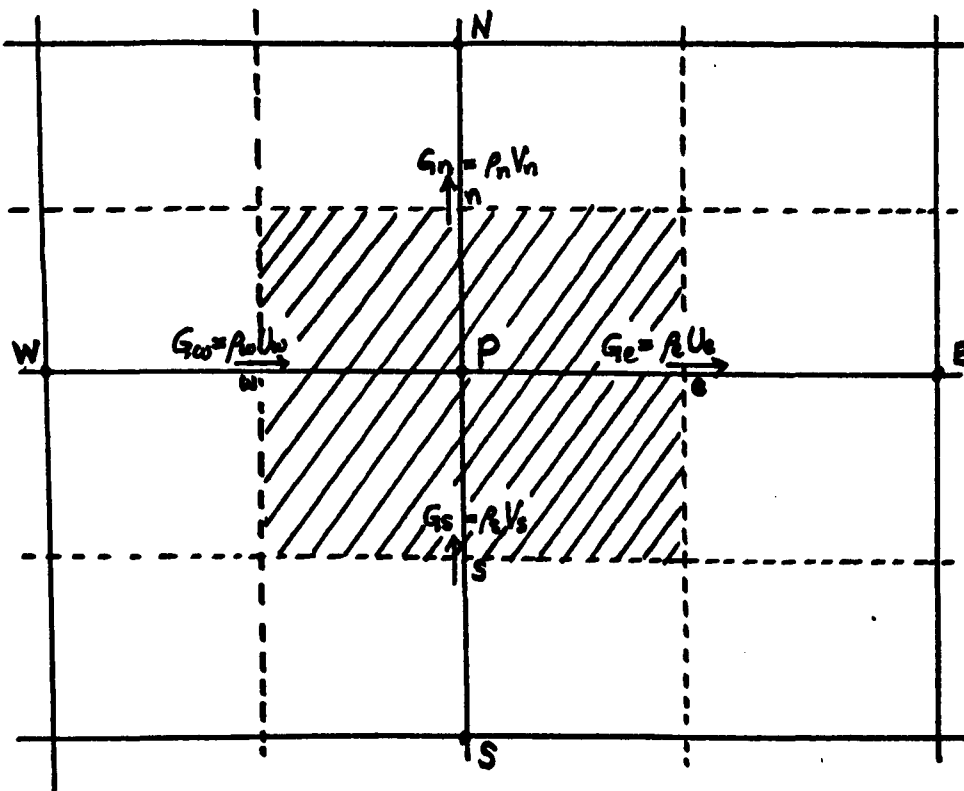


Fig.E.4: Definitions of Fluxes at w,e,n and s Wall Boundaries.

If the velocities are correct, the continuity equation will be satisfied and the mass source \dot{S}_m^N will be zero. However the estimated velocities U^* and V^* and hence G^* (where $G = \text{density} \times \text{velocity}$) will not satisfy continuity but instead produce a net mass source \dot{M}_P defined by,

$$M_p = G_w^* A_w - G_e^* A_e + G_s^* A_s - G_n^* A_n \quad (\text{E.39})$$

E.42 Derivation of Pressure-Correction Equation.

As has been mentioned earlier that when the velocities satisfy the continuity equation, the right hand side of equation (E.38) will be zero and since the true values of the variables are related to their corrections by the following relations,

$$\left. \begin{aligned} U &= U^* + U' \\ V &= V^* + V' \\ P &= P^* + P' \\ G &= G^* + G' \end{aligned} \right\} \quad (\text{E.40})$$

then we have (from equation (E.38) with $\sum_m \dot{S}_m = 0$) the following relation result,

$$\rho_e A_e U_e' - \rho_w A_w U_w' + \rho_n A_n V_n' - \rho_s A_s V_s' = M_p \quad (\text{E.41})$$

where M_p is given by (E.39). For nearly incompressible flow,

$$G' \approx \rho^* U' \quad (\text{E.42})$$

One of the staggered grid system advantageous is used here to derive the corrections for velocities or fluxes G' .

Referring to fig.E.5, G_w' the flux correction on the west wall of the control volume may be expressed as follows,

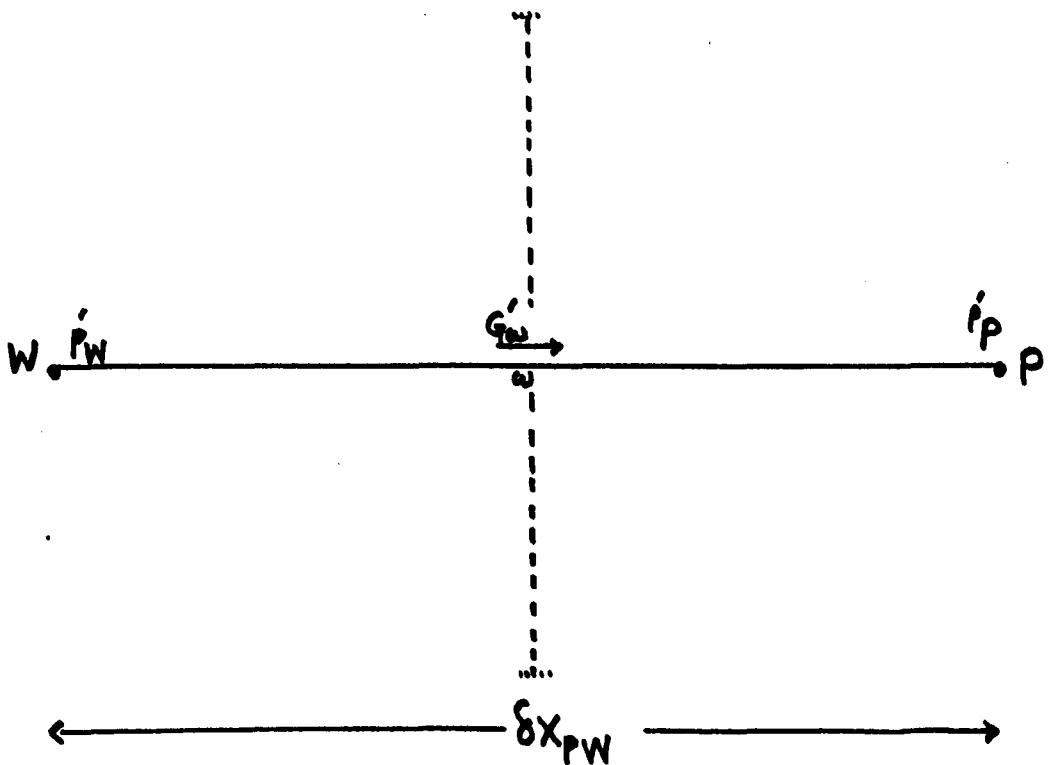


Fig.E.5: Derivation of Flux Corrections.

$$G'_w = - \frac{\Omega'_w (P'_P - P'_W)}{\delta X_{PW}} \quad (\text{E.43})$$

where permeability coefficient Ω'_w may be obtained from the linearisation of resistance law about p_p^* i.e.,

$$\Omega'_w = - \rho^* \delta X_{PW} \frac{\partial U_w^*}{\partial (P'_P - P'_W)} \quad (\text{E.44})$$

By replacing equation (E.44) to (E.43) will result,

$$G'_w = \frac{\rho^* \partial U_w^*}{\partial (P'_P - P'_W)} \cdot (P'_P - P'_W) \quad (\text{E.45})$$

Now the expression,

$$\frac{\partial U_w^*}{\partial (P_w^* - P_p^*)} = \frac{A_{ew}}{(a_p - S_p^U)} \equiv D_w \quad (\text{E.46})$$

may be obtained from equation (E.33) so that equation (E.45) now reduces to a more simpler expression for G'_w ie,

$$G'_w = \rho^* D_w (P'_w - P'_p) \quad (\text{E.47})$$

By combining equations like (E.42) and (E.47) the velocity corrections U'_w has the expression,

$$U'_w = D_w (P'_w - P'_p) \quad (\text{E.48})$$

The remaining velocity corrections U'_e , U'_s and U'_n at boundaries e, s, and n respectively may be obtained by similar analysis as above.

Hence by replacing equation like (E.43) into equation (E.41) will lead to a pressure-correction equation which has the following form,

$$a_p P'_p = \sum_n a_n P'_n + M_p \quad (\text{E.49})$$

where

$$a_p = \sum_n a_n$$

\sum_n = summation over neighbours,

$$a_w = \rho_w U_w D_w \text{ etc.} \quad (\text{E.50})$$

and M_p is given by equation (E.39) is called the residual mass source associated with estimated G^* .

Above finite difference equation is solved for p' (the pressure correction) by L-B-L procedure of TDMA.

E.5 MISCELLANEOUS MATTERS.

E.51 Numerical Stability and Convergence of Solution.

The finite difference equations mentioned earlier, when considered linear, are so constructed as to guarantee convergence of the LBL solution procedure. Often, because of the non-linearities present in the system of differential equations, or because of the large number of algebraic equations resulting from the use of finite difference schemes, divergence may sometimes result.

To suppress any such tendency, it is often necessary to employ underrelaxation. All methods of underrelaxation try to reduce the change in the value of a variable during one iteration. In addition to the dependent variables, auxiliary quantities like viscosity, can be underrelaxed with advantage.

A relaxation factor f is defined by,

$$\phi_p^R = f \phi_p + (1-f) \phi_p^{old} \quad (E.51)$$

where ϕ_p^R = value of ϕ_p at present iteration with underrelaxation.
 ϕ_p = value of ϕ_p at present iteration without underrelaxation.
 ϕ_p^{old} = value of ϕ_p at previous iteration.

and $0 < f < 1$.

When $f > 1$ it implies overrelaxation which is the counterpart of underrelaxation. Since in the problem of interest, the interlinkages between various equations are so strong, it is usually necessary to slow down the changes rather than to encourage them. For $f=1$ the values of ϕ 's are not relaxed.

The underrelaxation factors for each of the variables are presented in the program calculation (see section 3.3, Chapter 3).

Besides underrelaxation, to remedy numerical instability is to increase the number of sweeps of the TDMA this will give more complete solution of the equations during each iterations. The pressure-correction equation is the most sensitive in this respect so that it has highest number of sweeps compared to other dependent variables (see Chapter 3, section 3.3.).

Convergence.

Recall equation (E.24),

$$(a_p - s_p^\phi) \phi_p = \sum_n a_n \phi_n + S_u^\phi \quad (\text{E.24})$$

In general, convergence is guaranteed when following criterion is satisfied, called the Scarborough criterion (Gosman, 1976) ie,

$$|a_p - S_p^\phi| \leq \sum_n |a_n| \quad (\text{E.52})$$

All equations satisfy above condition, since

$$\left. \begin{array}{l} \text{i)} \quad a'_n s > 0 \\ \text{ii)} \quad a_p = \sum_n a_n \\ \text{iii)} \quad S_p^\phi \leq 0 \end{array} \right\} \quad (\text{E.53})$$

In the process of solution procedure, convergence is assessed how nearly the current solution approximates to the exact solution of the finite difference equations for each dependent variables at the end of each iteration.

The main convergence test is based on the "residual sources, R_ϕ 's" of the difference equations defined by,

$$R_\phi = (a_p - S_p^\phi) \phi_p - \sum_n a_n \phi_n - S_u^\phi \quad (\text{E.54})$$

where ϕ is any quantity (velocities or scalar quantities).

A convergence test is made by comparing the accumulation of

the change of R_ϕ over all the grid points to some reference value. Calculation is continued until

$$\max(\sum |R_U|, \sum |R_V|, \sum |R_{p'}|) < \delta \quad (\text{E.55})$$

where R_U, R_V and $R_{p'}$ are residual sources for velocities U, V and pressure correction p' and δ is a preset value which needs to be selected by computer experimental (see Chapter 3, section 3.44).

If the current solution exactly satisfies the difference equation, R_ϕ will eventually be zero.

E.52 Accuracy of Solution.

Of course, once a convergence solution is obtained, we are faced with the problem of accuracy, i.e. how close the finite difference solution so obtained to the true solution of the differential equations. The accuracy of the solution procedure will in general be a function of the number of grid nodes employed. For each flow configuration, a grid independent solution is sought by increasing the number of grid lines until no further changes are observed in the final solution.

The location of inlet and outlet boundaries may be assessed by adjusting the upstream and downstream distances from the orifice plate.

Furthermore, for predictions to reflect reality, it is

necessary to know the adequacy of the use of the turbulence model in the present study. This can be assessed by comparison with experimental data.

E.53. Allowance of Mass-flow Imbalance.

During iteration cycles sometimes may occur that the mass flows do not satisfy continuity. This situation may be represented in fig.E.6.

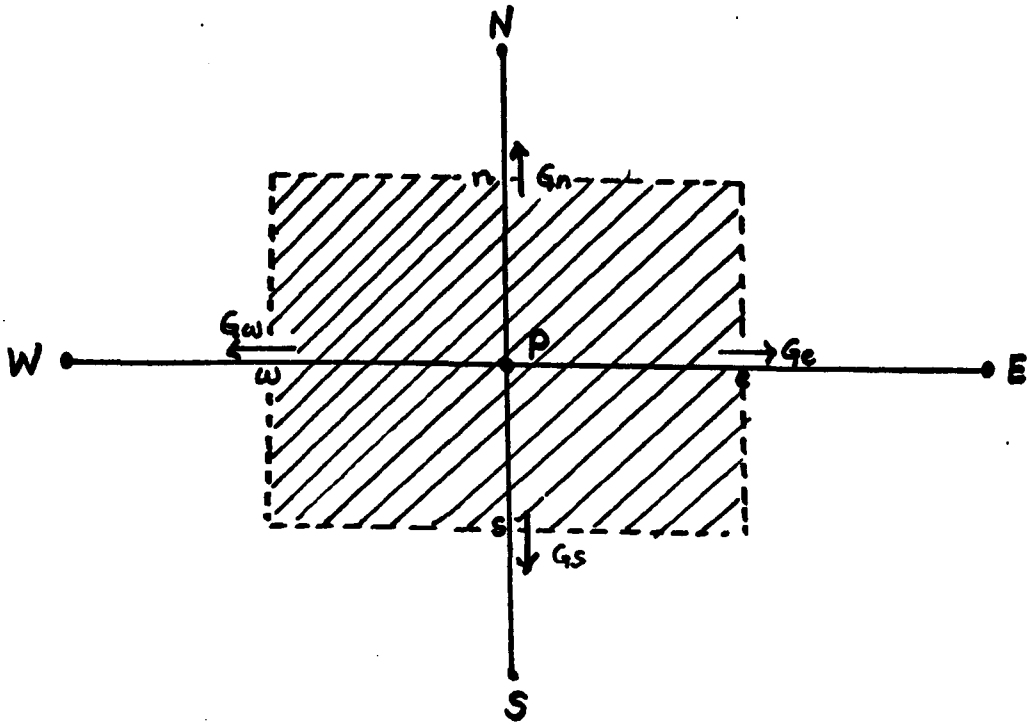


Fig.E.6: Possibility of Mass-Flows do not Satisfy Continuity.

The situation now is that all the a_n 's of equation (E.24) are zero, implying that the finite difference equations then become singular, since

$$a_p = \sum_n a_n \quad (\text{E.56})$$

To overcome that situation, is to add 'false' source S_f through the linearised treatment,

$$S_f \cdot \delta V = |\dot{m}_{net}| (\phi_p^{old} - \phi_p) \quad (\text{E.57})$$

where δV is the control volume of the cell in fig.E.6.

$$\dot{m}_{net} = \sum_n \dot{m}_n \quad (\text{E.58})$$

$$\dot{m}_\omega = G_\omega A_\omega \text{ etc.} \quad (\text{E.59})$$

ϕ_p = value of ϕ at P at present iteration,

ϕ_p^{old} = value of ϕ_p at previous iteration.

By linearising the source term in the manner of equation (E.19),

$$S_f \cdot \delta V = b_f \phi_p + c_f \quad (\text{E.60})$$

and by comparing equations (E.57) and (E.60), following expressions will be obtained,

$$b_f = -|\dot{m}_{net}| \quad (\text{E.61})$$

$$c_f = |\dot{m}_{net}| \cdot \phi_p^{old} \quad (\text{E.62})$$

The final form of finite difference equations solved become,

$$(a_p - S_p^\phi - b_f) \phi_p = \sum_n a_n \phi_n + S_U^\phi + c_f \quad (\text{E.63})$$

where b_f and c_f have values given by equations (E.61) and (E.62). These additional constants has no effect on the final solution, for when

$$\phi_p = \phi_p^{old} \quad (\text{E.64})$$

then $\dot{m}_{net} = 0$ (Gosman, 1976) (E.65)

E.6 SOLUTION PROCEDURE OF THE DIFFERENCE EQUATIONS.

E.61 Introduction.

Having constructed algebraic equations for all nodes in the calculation domain, the next job will be to solve this set of equations simultaneously. Since the equations are non-linear and interlinked, the use of iterative methods become important. The main members of these methods are point iteration and line iteration. The first one includes direct solution by the Gauss elimination method. But this method seems to require too large computer storage and time (Launder(ed), 1975). The Gauss-Seidel method of successive substitution converges rather slowly, especially when the number of equation is large. The latter method is the line iteration, which includes Line-By-Line (L-B-L). At

present, the LBL method seems to be of best choice and therefore in this study we employ the LBL solution procedure which will be described below.

E.62 The LBL Procedure.

Figure E.7 shows the illustration of the procedure. For the solution for points on each line (eg. North-South line) the values of the individual variables ϕ on the neighbouring lines are assumed to be temporarily known. The equation for each point on the N-S line then reduce to one where only three values (ie ϕ_P , ϕ_N and ϕ_S) are unknown. Refer to equation (E.24) we have,

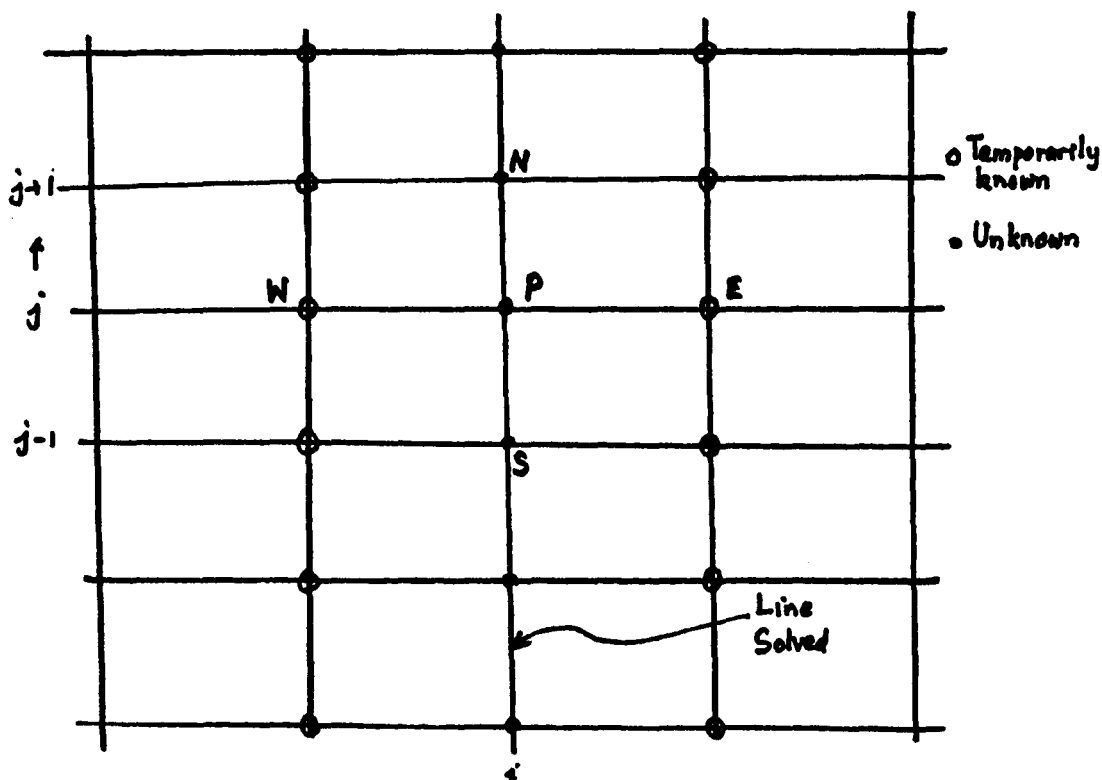


Fig.E.7: The LBL Procedures.

$$a_p' \phi_p = a_N \phi_N + a_S \phi_S + c' \quad (\text{E.66})$$

where
$$c' = a_W \phi_W + a_E \phi_E + S_U^\phi \text{ (known)} \quad (\text{E.67})$$

and
$$a_p' = a_p - S_p^\phi \quad (\text{E.68})$$

With respect to the figure E.7,

$$\left. \begin{aligned} \phi_p &\equiv \phi_j \\ \phi_s &\equiv \phi_{j-1} \\ \phi_N &\equiv \phi_{j+1} \end{aligned} \right\} \quad (\text{E.69})$$

For each grid node on the (N-S) line (the line solved considered) say node j the finite difference equations may be expressed as,

$$\phi_j = Q_j \phi_{j+1} + R_j \phi_{j-1} + Z_j \quad (\text{E.70})$$

where coefficients Q_j , R_j and Z_j take the form,

$$Q_j = \frac{\alpha_j}{D_j}, \quad R_j = \frac{\beta_j}{D_j}, \quad Z_j = \frac{c_j}{D_j} \quad (\text{E.71})$$

$$\alpha \equiv a_N, \quad \beta \equiv a_S, \quad D \equiv a_p' \quad (\text{E.72})$$

where a_p' and c' are given by equations (E.68) and (E.67) respectively. Z_j contains values of ϕ 's of points on the neighbouring

lines which are assumed to be temporarily known and Q_j and R_j are known coefficients.

Equation (E.70) may be written as set of equations, (for $j=2$ to $j=n$),

$$\phi_2 = Q_2 \phi_3 + R_2 \phi_1 + z_2 \quad (i)$$

$$\phi_3 = Q_3 \phi_4 + R_3 \phi_2 + z_3 \quad (ii)$$

$$\phi_4 = Q_4 \phi_5 + R_4 \phi_3 + z_4 \quad (iii)$$

$$\phi_n = Q_n \phi_{n+1} + R_n \phi_{n-1} + z_n$$

ϕ_1 is assumed to be known, then by eliminating ϕ_2 from (ii), ϕ_3 from (iii) etc., a general formula for ϕ_j would be obtained (known as the recurrence relation).

$$\phi_j = A_j \phi_{j+1} + C_j'' \quad , \quad j = 2, \dots, n \quad (E.73)$$

with ϕ_{n+1} a known value too. The coefficients A_j and C_j'' are given by,

$$A_j = \frac{\alpha_j}{(D_j - \beta_j A_{j-1})}$$

$$C_j'' = \frac{(\beta_j C_{j-1}'' + \zeta_j')}{(D_j - \beta_j A_{j-1})} \quad (E.74)$$

Note: $A_1 = 0$ and $C_1'' = \phi_1$ (a known value).

By straight forward algebraic manipulation, the set of equations is converted into one expressible by a general recurrence relation for ϕ_j as indicated above (equation E.73), with the coefficients A_j and C_j'' obtained from the recurrence formulae (equation (E.74)).

It is from this general recurrence relation for ϕ_j that all values for ϕ from $j=2$ to $j=n$ are calculated, and the process is quite easy as one only needs to evaluate the A's and C'' 's in order to obtain ϕ 's.

To apply the TDMA to entire field, the process is started from the extreme left of the (N-S) line and traverse along this line, next it is repeated along successive neighbouring (N-S) lines with most recently calculated ϕ 's and then the entire grid is swept through until the desired solution is obtained.

E.7: CONCLUDING REMARKS.

This appendix completes the derivation of the finite difference equations both for scalar and velocity variables. The main points of the appendix may consist of the following;

The governing partial differential equations are transformed to their algebraic equivalence by finite difference formulations. The partial differential equations are discretised in space to obtain their finite difference counterpart, by the use of 'micro-integration' method, together with the 'hybrid' difference scheme for the convective and diffusive fluxes. These difference equations are solved by LBL iteration method which employs the TDMA.

A consequence of using the 'primitive' variables (U, V and p) is the need to obtain the pressure field by some special measure. The procedure employed here is the SIMPLE algorithms which involves guess and correct method. The pressures are obtained by solving the pressure-correction equation, whose basis are the continuity and momentum equations, together with linearised resistance law.

Other special features of solution procedure (under miscellaneous matters) such as numerical stability and convergence are given. General remedies in overcoming such instabilities has also been indicated together with the method in which accurate solution is obtained.

Finally the solution procedure of solving the finite difference equations (ie the LBL procedure) has been discussed in quite detail in section E.6.

APPENDIX F.NEAR WALL REMEDIES.F.1 INTRODUCTION.

In wall regions there are essentially three major characteristics which distinguish them from central flow region.

(i) Steep non-linear variations in mean-axial velocity U , turbulent viscosity μ_t , temperature and so on. In addition, local Reynolds number changes considerably in that region.

(ii) Laminar and turbulent effects are of the same order of magnitude; levels of local turbulence Reynolds number Re_t defined by (Launder and Spalding, 1972)

$$Re_t = \frac{\mu_t}{\mu} = \frac{C_\mu \rho k^2}{\mu \epsilon} \quad (F.1)$$

is sufficiently low for molecular viscosity to influence the production, diffusional transport and dissipation of turbulence energy. In this region also eddy structure is influenced by the presence of the wall.

(iii) Generally as the wall is approached the flow is essentially 1-D Couette. The layer in this region is assumed to be of constant stress ($\tau = \tau_w$).

The turbulence model has been designed for high Reynolds number, whereas near walls this number becomes very small so the model is inadequate in this region. Both this fact and steep variations of flow properties near walls necessitate special attention for grid nodes close to walls.

F.2 WALL FUNCTIONS.

In order to minimise excessive computer storage and run times near a wall region, the wall function method is employed. As already mentioned, near a wall region, the local Reynolds number, y^+ changes rapidly. This number varies, depending on the normal distance y from the wall, which makes the flow properties are often expressed in terms of y^+ , defined by,

$$y^+ = \frac{y U_\tau}{\nu} \quad (\text{F.2})$$

where y = normal distance from the wall,

$$U_\tau = \sqrt{\tau_w / \rho} \quad (= \text{friction velocity}),$$

τ_w = wall shear stress.

The wall region is made up of three zones (Hinze, 1959) based on y^+ .

- (1) The viscous sublayer ($0 < y^+ < 5$) where the viscous effects dominate.
- (2) The inertial sublayer ($30 < y^+ < 400$) where the flow is assumed to be completely turbulent but sufficiently close to the wall so that the shear stress is approximately constant, $\tau \approx \tau_w$.

(3) Between layers (1) and (2) is the transition (or 'buffer') layer ($5 < y^+ < 30$) of vigorous turbulence dynamics where the flow is neither completely dominated by viscous effect nor turbulent.

In many engineering calculations, the buffer layer is disposed off, so that the result only have two layers- the viscous and inertial sublayers. This is achieved by defining a point $y^+ = 11.63$ where the linear velocity profile in the viscous sublayer meets the logarithmic velocity profile in the inertial sublayer. This approach has extended the viscous sublayer to cover the range $0 < y^+ < 11.63$. The flow within this region is assumed to be purely viscous and above which point ($y^+ > 11.63$) it is purely turbulent.

The characteristic of these regions are well established experimentally and theoretically and a rough sketch of velocity profiles near a wall region is given in fig.F.1.

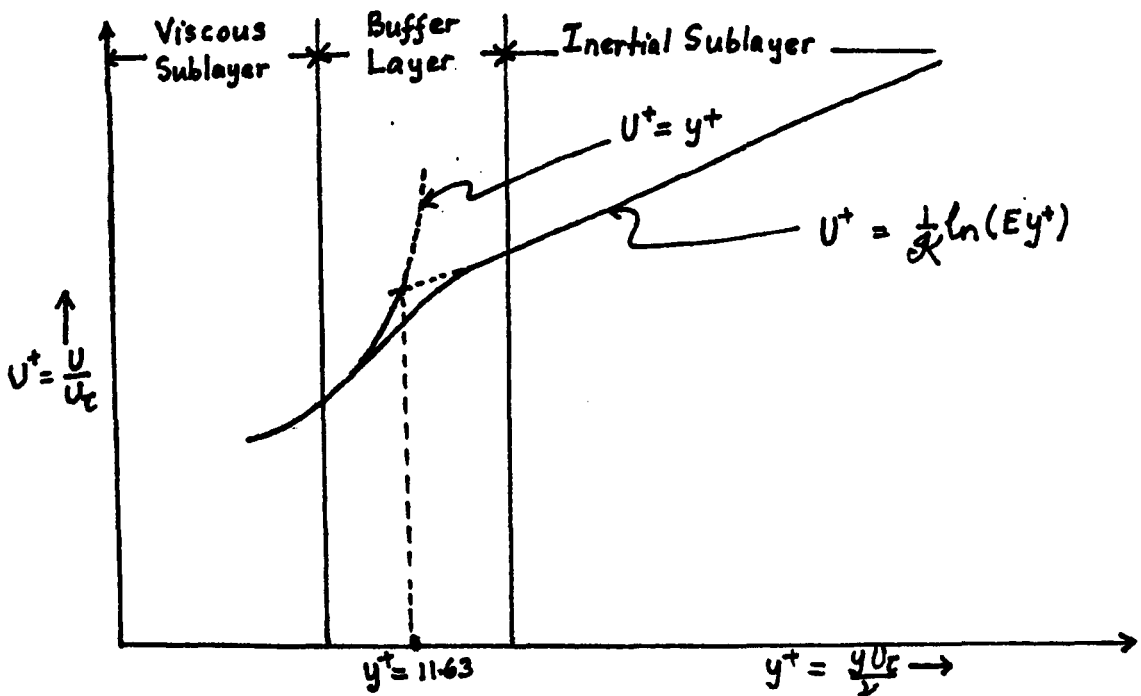


Fig.F.1 The Law of the Wall.

F.21 Equation of Mean Motion.

In this study, the assumption has been made that the thin layer close to the wall is a region of local equilibrium. The shear stress in the layer is approximately uniform and a 1-D Couette flow analysis is made.

The total shear stress may be written as,

$$\tau = \mu \left(1 + \frac{\mu_t}{\mu} \right) \frac{dU}{dy} \quad (\text{F.3})$$

or

$$\frac{\tau}{\tau_w} = \left(1 + \frac{\mu_t}{\mu} \right) \frac{dU^+}{dy^+} \quad (\text{F.4})$$

where

$$\tau_w = \rho U_\tau^2 \quad (\text{wall shear stress}) \quad (\text{F.5})$$

$$U^+ = \frac{U}{U_\tau} \quad (\text{F.6})$$

$$y^+ = \frac{y U_\tau}{\nu} \quad (\text{local Reynolds number}) \quad (\text{F.7})$$

Situation 1

When $y^+ \lesssim 11.63$ (in the viscous sublayer) the turbulent viscosity μ_t is very much smaller than laminar viscosity μ ie,

$$\frac{\mu_t}{\mu} \ll 1$$

and the shear stress is approximately constant, ie,

$$\tau \approx \tau_w$$

then equation (F.4) reduces to a simple relation, given by,

$$U^+ = y^+ \quad (\text{F.8})$$

Situation 2.

When $y^+ > 11.63$ (in the inertial sublayer) μ_t is very much larger than μ and the constancy of shear stress still applies. One dimensional Couette flow analysis has been used for turbulent kinematic viscosity ν_t in the region, and it is assumed to be proportional to the product of the normal distance y from the wall and friction velocity U_τ . Therefore in inertial sublayer region, we have the following,

$$\frac{\mu_t}{\mu} \gg 1$$

$$\tau \approx \tau_w$$

$$\nu_t = \mathcal{K} y U_\tau \quad (\text{Hinze, 1959}) \quad (\text{F.9})$$

and thus reducing equation (F.4) to

$$1 = \frac{\nu_t}{\nu} \frac{dU^+}{dy^+} \quad (\text{F.10})$$

By combining equations (F.9) and (F.10) and on integration, the following equation for $y^+ > 11.63$ is obtained.

$$U^+ = \frac{1}{\kappa} \ln(Ey^+) \quad (F.11)$$

where κ = Von Karman constant = .4187

E = an integration constant = 9.793.

Equations (F.8) and (F.11) are commonly called the law of the wall which may be represented by curves shown in fig.F.1.

F.22 Turbulence Energy, k.

The approach adopted is valid for the inertial sublayer where the flow is assumed completely turbulent, but sufficiently close to the wall so that the shear stress remains approximately constant. In this region the local rate of turbulence energy production, $-\overline{uv} \frac{\partial U}{\partial y}$ is balanced by the viscous dissipation ϵ . Furthermore, in this layer both convection and diffusion of k are negligible, thus giving,

$$-\overline{uv} \frac{\partial U}{\partial y} = \epsilon \quad (F.12)$$

where u and v are velocity fluctuations in axial and radial directions.

By multiplying both sides of equation (F.12) by $\rho \mu_t$ (where ρ is the fluid density and μ_t is the turbulent viscosity and is given by equation C.68 of Appendix C) and using the gradient transport hypothesis (for a 1-D flow) i.e.

$$-\rho \bar{u} \bar{v} = \mu_t \frac{\partial U}{\partial y} \quad (\text{F.13})$$

the following expressions will be obtained,

$$-\rho \mu_t \bar{u} \bar{v} \frac{\partial U}{\partial y} = \rho \cdot c_{\mu} \rho k^2$$

$$\text{or} \quad (-\rho \bar{u} \bar{v}) \cdot \left(\mu_t \frac{\partial U}{\partial y} \right) = \rho^2 k^2 c_{\mu}$$

$$\text{or} \quad \left(\mu_t \frac{\partial U}{\partial y} \right)^2 = \rho^2 k^2 c_{\mu} \quad (\text{by F.13})$$

$$\text{or} \quad \tau_I^2 = \rho^2 k^2 c_{\mu} \quad (\text{F.14})$$

$$\text{where} \quad \tau_I = \mu_t \frac{\partial U}{\partial y} = -\rho \bar{u} \bar{v} \quad (\text{F.15})$$

has been used to obtain equation (F.14).

From equation (F.14) the following expression of shear stress in the inertial sublayer τ_I is obtained,

$$\tau_I = \rho k c_{\mu}^{\frac{1}{2}} \quad (\text{F.16})$$

The wall shear stress τ_w may be derived basically from the definition of U^+ ,

$$U^+ = \frac{U}{u_{\tau}} = U \sqrt{\frac{\rho}{\tau_w}} \quad (\text{F.17})$$

because the friction velocity $U_\tau = \sqrt{\frac{\tau_w}{\rho}}$ (F.18)

As the shear stress near wall region is nearly constant, U^+ may then be approximated as,

$$U^+ \approx \frac{U \sqrt{\rho \bar{v}_I}}{\tau_w}$$

or

$$\begin{aligned} \tau_w &= \left(\frac{U}{U^+}\right) \cdot \rho^{\frac{1}{2}} \cdot \tau_I^{\frac{1}{2}} \\ &= U_\tau \cdot \rho^{\frac{1}{2}} \cdot \rho^{\frac{1}{2}} \cdot k^{\frac{1}{2}} \cdot C_\mu^{\frac{1}{4}} \\ &= U_\tau \cdot \rho \cdot k^{\frac{1}{2}} C_\mu^{\frac{1}{4}} \end{aligned} \quad (\text{F.19})$$

where

$$U_\tau \equiv \frac{U}{U^+} \quad (\text{F.20})$$

and

$$U^+ = \begin{cases} y^+ & \text{for } y^+ \leq 11.63 \text{ for viscous sublayer} \\ \frac{1}{\kappa} \ln(Ey^+) & \text{for } y^+ > 11.63 \text{ for inertial sublayer} \end{cases}$$

By equating equations (F.16) and (F.19) in the inertial sublayer (since $\tau \approx \tau_w$ still applies), k is related to C_μ and U_τ by the following relation,

$$k = C_\mu^{-\frac{1}{2}} U_\tau^2 \quad (\text{F.21})$$

Local Reynolds Number, y^+ .

To obtain the local Reynolds number, it is best to start with the definition of y^+ i.e.

$$y^+ = \frac{y}{\nu} \sqrt{\frac{\tau_w}{\rho}} = \frac{y}{\nu} \sqrt{\frac{\tau_I}{\rho}} \quad (\text{F.22})$$

By using equation (F.16) to replace τ_I in equation (F.22) we get,

$$y^+ = \frac{y}{\nu} \cdot k^{\frac{1}{2}} \cdot c_{\mu}^{\frac{1}{4}} \quad (\text{F.23})$$

where $\nu = \mu \rho^{-1}$ is the (laminar) kinematic viscosity.

F.23 Rate of Energy Dissipation ϵ .

By multiplying equation (F.12) right through by ρ then we have,

$$-\rho \overline{uv} \frac{\partial U}{\partial y} = \rho \epsilon \quad (\text{F.24})$$

Also since the shear stress in the wall region is given by,

$$-\rho \overline{uv} = \tau_I \approx \tau_w \quad (\text{see equation F.15}) \quad (\text{F.25})$$

then we have,

$$\tau_w \frac{\partial U}{\partial y} = \rho \epsilon \quad (\text{F.26})$$

The shear stress at the wall is given by,

$$\tau_w \stackrel{\text{or}}{=} \tau_I = \mu_t \frac{\partial U}{\partial y} \quad (\text{see equation F.15}) \quad (\text{F.27})$$

By eliminating $\frac{\partial U}{\partial y}$ from equations (F.26) and (F.27) the following result for ν_t in terms τ_w , ρ and ϵ will be obtained,

$$\nu_t = \frac{\tau_w^2}{\rho^2 \epsilon} \quad (\text{F.28})$$

By using relation (F.5) for τ_w and equation (F.9) for ν_t into equation (F.28), the dissipation rate ϵ relates to friction velocity U_τ and distance y from the wall as follows,

$$\epsilon = \frac{U_\tau^3}{\kappa y} \quad (\text{F.29})$$

In the inertial sublayer, (when equation (F.21) for U_τ is replaced into equation (F.29)) the dissipation rate may be rewritten as,

$$\epsilon = \frac{k^{3/2} \cdot C_\mu^{3/4}}{\kappa y} \quad (\text{F.30})$$

For extension to 'buffer' and viscous sublayer in the k-balance, ϵ must be modified as follows, -for a region close to a wall equation (F.15) may be approximated by,

$$\tau_I \approx \mu_t \frac{(U_P - U_N)}{y_P} \quad (\text{F.31})$$

where U_P and U_N are respectively velocity at a point P nearest to the wall and at the wall itself. y_P is the normal distance of the point P to the wall. For a non-slip condition, $U_N = 0$.

By equating equations (F.16) and (F.31) the following relation is obtained for μ_t ie,

$$\mu_t = \frac{\rho k_P C_\mu^{\frac{1}{2}} y_P}{U_P} \quad (\text{F.32})$$

where k_P is the value of turbulence energy at the point P.

By solving equations (C.68)(see Appendix C) and (F.32) together, the dissipation rate ϵ_P at the point P is related to y_P and U_P as follows,

$$\epsilon_P = \frac{k_P C_\mu^{\frac{3}{2}} U_P}{y_P} \quad (\text{F.33})$$

where U_P is related to U_τ and U^+ by,

$$U^+ = \frac{U_P}{U_\tau} \quad (\text{F.34})$$

and by eliminating U_p in equations (F.33) and (F.34) and by using relation (F.21) for U_T , the dissipation rate ϵ_p at P in the viscous sublayer may be re written as,

$$\epsilon_p = \frac{k_p^{3/2} c_\mu^{3/4}}{y_p} \cdot U^+ \quad (\text{F.35})$$

$$U^+ = \begin{cases} y^+ & \text{for } y^+ \leq 11.63 \\ \frac{1}{\kappa} \ln(Ey^+) & \text{for } y^+ > 11.63 \end{cases}$$

where

F.3 INCORPORATION OF WALL BOUNDARY CONDITIONS.

F.31 Introduction.

As has been noted in section (3.23, see Chapter 3) that wall boundaries in modelling orifice plate have been divided into five regions, namely the two wall regions (upstream (in region 1) and downstream (region 3) of orifice plate), two boundaries (front face and rear face of orifice plate) and one region at the bottom of orifice plate (region 2). Here the wall boundary conditions will be discussed.

At the wall boundaries of calculation domain, the general finite difference equations (see Appendix E) are not applicable. Hence special measures are then required for the cells (control volumes) next to the wall boundaries. As has also been mentioned, the grid arrangement is such that the boundaries coincide with the control volumes - this is advantageous for ensuring conservation and for flux calculations. The

following lines will show how the wall boundary conditions are incorporated.

It has to be mentioned that in this study, we (Gosman, 1976) adopt the method of 'false' source treatment where flux through boundary of a particular control volume has the form, say for the west boundary of the control volume (see also Appendix E),

$$\dot{q}_w = S_p^\phi \phi_p + S_u^\phi \quad (\text{F.36})$$

where S_p^ϕ and S_u^ϕ are in general function of a variable ϕ and ϕ_p is the value of ϕ at a point P nearest to the wall boundary.

This type of treatment will become clear when dealing with control volumes of velocity components at corners of the orifice plate. This is discussed later under 'corner treatments'.

F.32 Momentum Equations.

(i) Tangential Velocity.

Fig.F.2 shows typical velocity cells with one of their boundaries coincide with walls. The wall in fig.F.2(a) may either be top walls of the pipe (in regions 1 or 3), or bottom face of orifice plate (in region 2) of the flow domain. The walls in fig.F.2(b) and (c) being front face and rear face of orifice plate respectively.

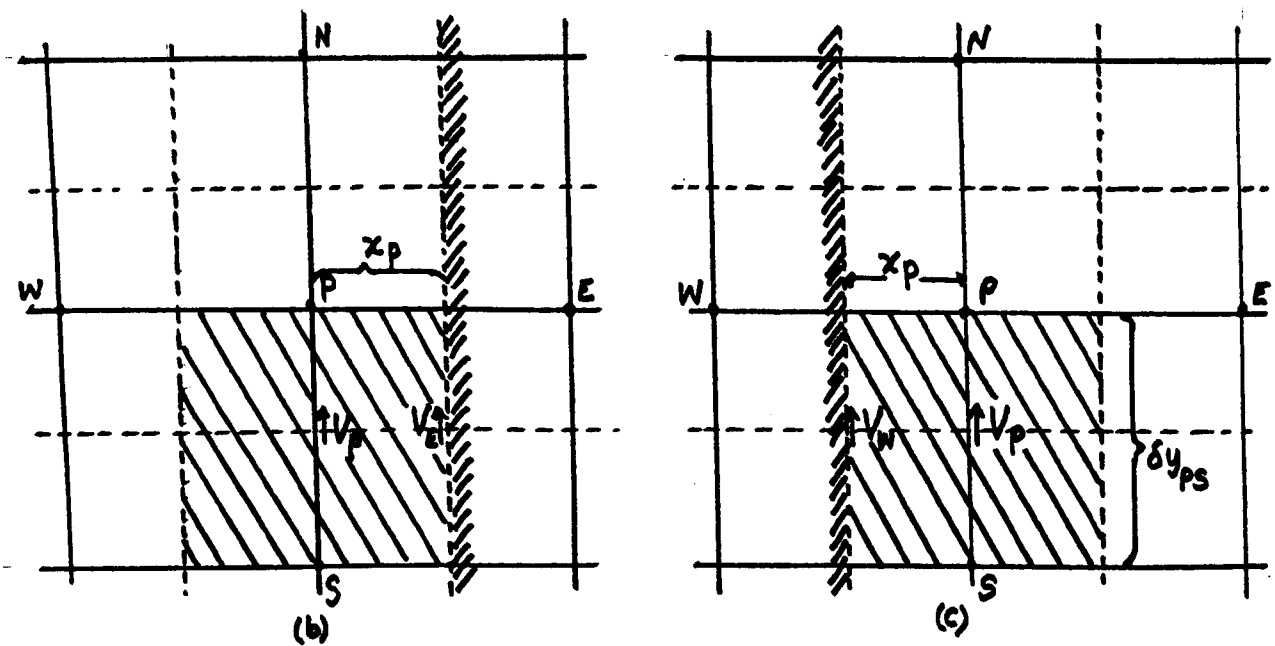
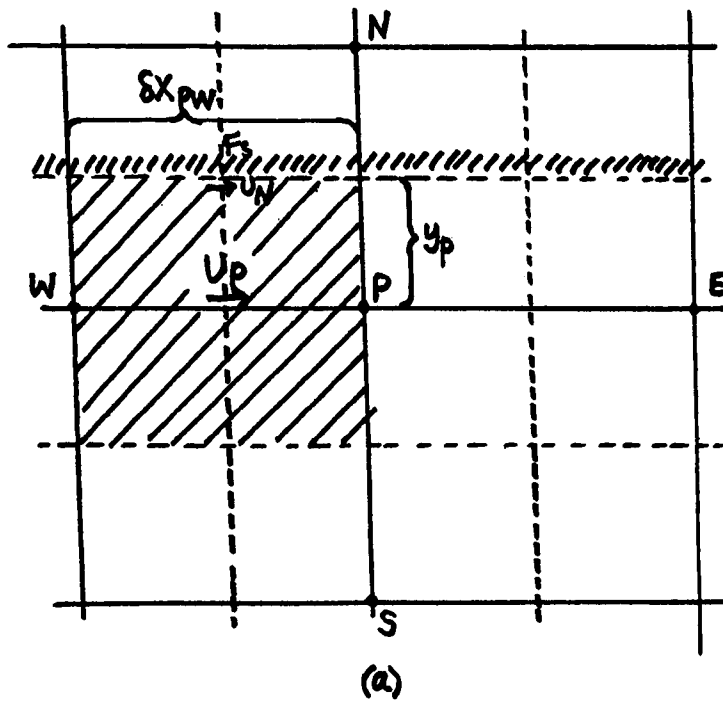


Fig.F.2:(a): A Typical U-Cell with North Wall Coincides with a Wall Boundary.

(b) and (c): A Typical V-Cell with East/West Wall Coincide with Front Face and Rear Face of Orifice Respectively.

A tangential velocity U_P or V_P (depending on which boundaries are referred to, parallel or normal to flow direction) for a point node P nearest to the wall boundary is obtained from usual momentum balance.

Referring to fig.F.2 the general fdes is not applicable-the usual links ($\phi_P \sim \phi_N$ relation in fig.F.2(a), $\phi_P \sim \phi_E$ relation in (b) and $\phi_P \sim \phi_W$ relation in (c)) are suppressed. This can be achieved by setting appropriate coefficients to be zero separately, ie

$$\left. \begin{aligned} a_N &= 0 \\ a_E &= 0 \\ a_W &= 0 \end{aligned} \right\} \quad (F.37)$$

where a_N , a_E , and a_W are defined similar to equation (E.29) (see Appendix E), and N, E and W stand for the North, East and West boundaries of the cells considered.

The shear force F_S (say in fig.F.2(a)) may be expressed as,

$$F_S = -\tau_s \delta x_{PW} \quad (F.38)$$

where τ_s ($\approx \tau_w$) and δx_{PW} are respectively wall shear stress and distance of point P from W.

For the point P nearest to the wall in the turbulence

region (i.e. $y^+ > 11.63$) the wall shear stress τ_w takes the expression given by,

$$\tau_w = \frac{\mathcal{K} \rho C_\mu^{\frac{1}{4}} k_{PW}^{\frac{1}{2}} (U_P - U_N)}{\ln(E y_p^+)} \quad (\text{F.39})$$

where

$$k_{PW} = \frac{1}{2} (k_p + k_w) \quad (\text{F.40})$$

$$y_p^+ = \frac{\rho y_p}{\mu} \cdot k_p^{\frac{1}{2}} C_\mu^{\frac{1}{4}} \quad (\text{F.41})$$

k_p is the value of k at the point P.

Equation (F.39) was obtained by combining equations (F.19) and (F.20) and using equation (F.11) for $y^+ > 11.63$. Again for non-slip condition $U_N = 0$. Equation (F.39) may be rewritten as,

$$\tau_w = t_m \cdot U_p \quad (\text{F.42})$$

where

$$t_m = \frac{\rho C_\mu^{\frac{1}{4}} k_{PW}^{\frac{1}{2}} \mathcal{K}}{\ln(E y_p^+)} \quad (\text{F.43})$$

If P falls within the viscous sublayer (ie $y^+ < 11.63$) the wall shear stress is also expressible as equation (F.42) but now with,

$$t_m = \frac{\mu}{y_p} \quad (\text{F.44})$$

where

- U_p = axial velocity at the point P,
- y_p = normal distance of the point P from the wall,
- ρ = fluid density,

and μ = fluid viscosity.

C_μ , K and E are constants values given by table 2.1 (see Chapter 2) together with other C 's and σ 's constants.

By replacing equation (F.42) into equation (F.38) and by incorporating the result of the shear stress through source treatment in the manner as equation (F.36), we shall get,

$$S_p^U = -t_m \cdot \delta x_{pw} \quad (F.45)$$

$$S_u^U = 0 \quad (F.46)$$

where value of t_m can take either from equations (F.43) or (F.44) depending on y^+ whether it is $>$ or ≤ 11.63 .

Similar treatments may be carried out for V -velocity components having east/ west walls of the control volumes coincide front face (in fig.F.2(b)) or rear face (in fig.F.2(c)) of the orifice plate.

Above treatments of shear stress F_S ($\cong F_w$) was for tangential velocities. However there is no special treatment necessary for normal velocities.

(ii): Corner Treatments.

The following additional treatments are for two corners of

the orifice plate in the flow domain. At the corners of the plate there are positions where half face of the velocity cells (control volumes) are 'exposed' to the calculation domain (flow domain) and half of them coincide with boundaries of the orifice plate (ie front face, bottom face and rear face of orifice plate boundaries). These situations may be shown in fig.F.3.

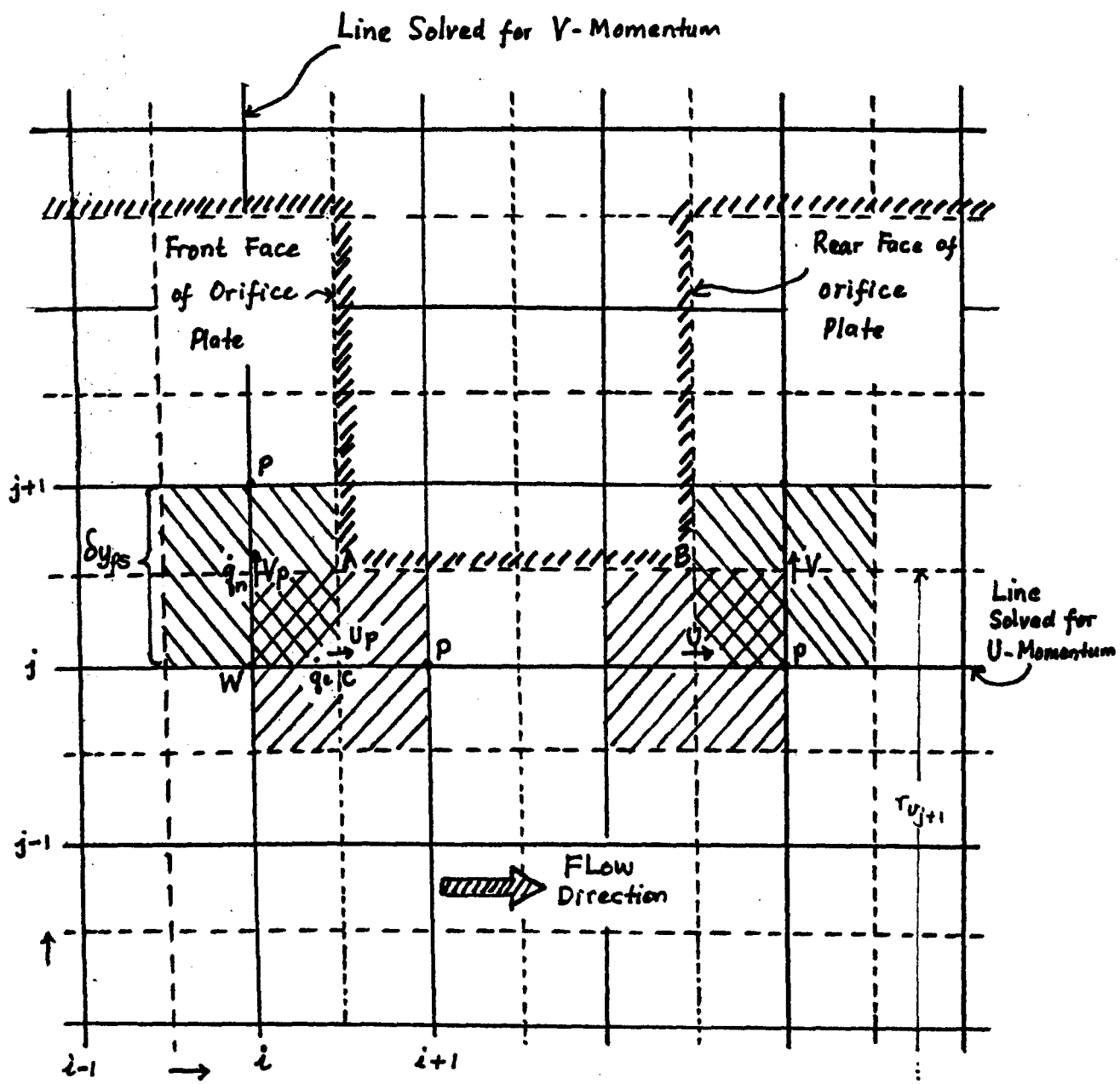


Fig.F.3: Corner Treatments.

U-Momentum.

At corner (A) (see fig F.3) the contribution of flux from east wall of V-cell \dot{q}_e (in the front face of the orifice plate) is given by,

$$\dot{q}_e = \rho_c \cdot U_p \cdot \frac{1}{2} A_{ewr} \quad (\text{F.47})$$

where

$$\rho_c = \frac{1}{2} (\rho_w + \rho_p) \quad (\text{F.48})$$

$$A_{ewr} = \tau_{j+1} \cdot \delta y_{ps} \quad (\text{F.49})$$

and C is a point mid-way between W and P enclosed by the U-cell

The expression of (F.47) is then incorporated through the source treatment similar to equation (F.36) to give,

$$S_p^U = -\frac{1}{4} (\rho_p + \rho_w) \cdot A_{ewr} \quad (\text{F.50})$$

$$S_u^U = 0 \quad (\text{F.51})$$

where negative sign has been introduced to promote stability.

The treatments at corner (B) of fig.F.3 is similar to those at corner (A). Above treatments are applicable only for the bottom face of the orifice plate(in region 2).

V-Momentum.

The treatment for V-momentum at corners (A) and (B) follow the same pattern as for U-momentum except the contribution of flux is from the north wall of U-cell (again consider corner (A)) \dot{q}_n instead of \dot{q}_e in previous calculation. Above treatments are applicable for front face (in region 1) and rear face (in region 3) of the orifice plate.

F.33 Turbulence Quantities.

The boundary values for the turbulent quantities (k and ϵ) at the grid points nearest to the wall are specified in accordance with the law of the wall.

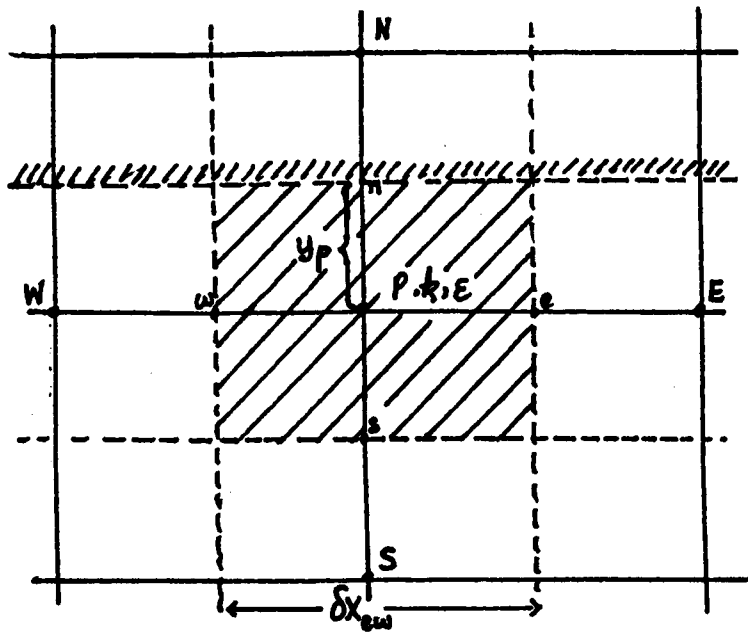
(i) Turbulence Energy k.

Fig.F.4 shows typical k or ϵ scalar-cells with north, east and west walls of cells (control volumes) coincide with the top wall (including bottom face of the orifice plate) front face and rear face of the orifice plate as indicated by small letters (a), (b) and (c) respectively.

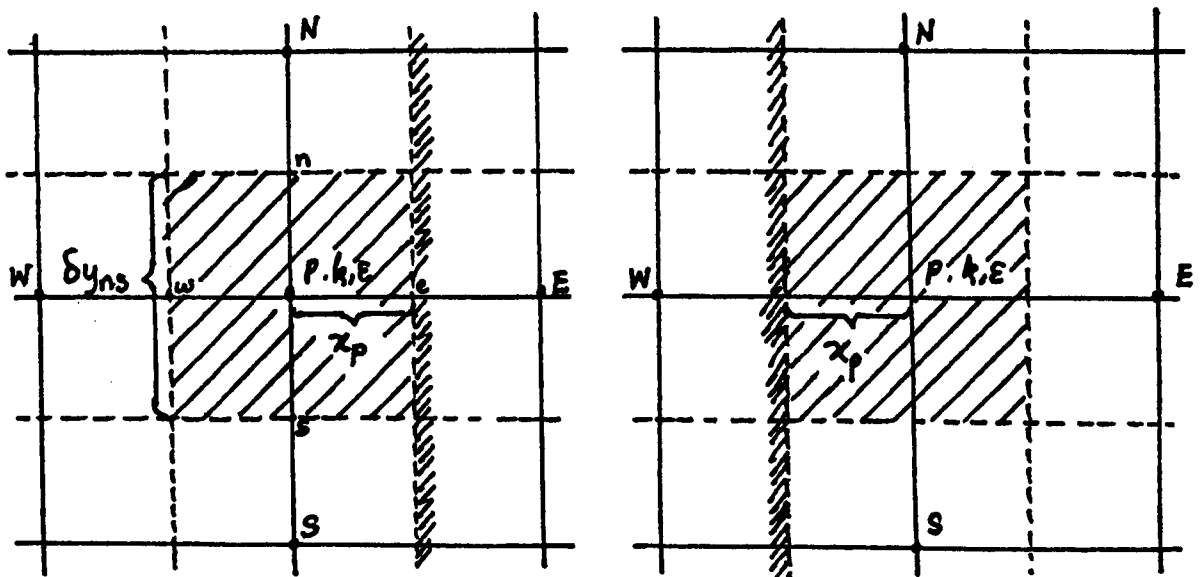
The turbulence energy k at the node point P, k_p is obtained by solving the governing transport equation. Since the energy falls to zero at the wall, the contributions of flux from the wall vanish, i.e.,

$$\left(\frac{\partial k}{\partial n}\right)_{\text{wall}} = 0 \quad (\text{F.52})$$

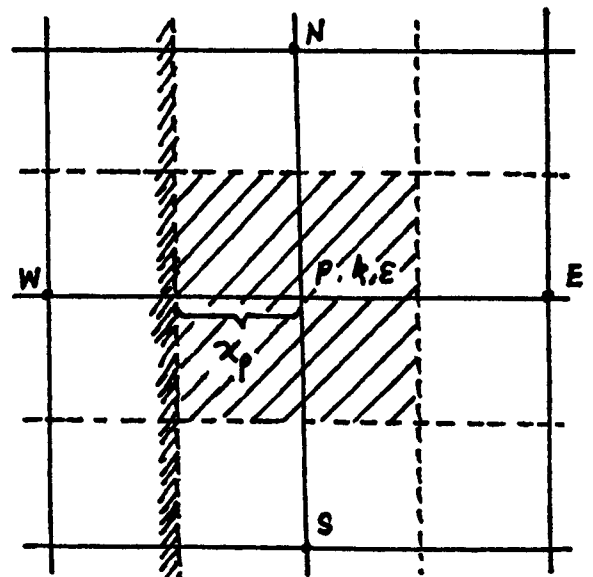
where n being normal to the wall. This can be achieved by setting a_N, a_E and a_W to zero similar to relations (F.37).



(a)



(b)



(c)

Fig.F.4: Typical Scalar Cells (k and E) with North, East and West Walls Coincide with Top Walls(a), Front Face of Orifice Plate(b) and Rear Face of Orifice Plate(c) Respectively.

The generation G (see equation 2.16 of Chapter 2) reduces to a simpler form, as a result of using the assumptions that $\frac{\partial U}{\partial x}$, $\frac{\partial V}{\partial r}$ and V components of velocity near wall region vanish (Bradshaw, 1971), then,

$$G = \mu_t \left(\frac{\partial U}{\partial r} + \frac{\partial V}{\partial x} \right)^2 \quad (\text{F.53})$$

Since at the wall, V -velocity does not change with direction- x , i.e.,

$$\frac{\partial V}{\partial x} = 0 \quad (\text{F.54})$$

and by using equation (F.15) the generation term G is modified to,

$$G = \frac{\tau_s (U_p - U_N)}{y_p} = G_c \quad \text{say} \quad (\text{F.55})$$

where τ_s , U_p and y_p are respectively wall shear stress, mean axial velocity at the point P and the distance of P from the wall. G_c is called part of the generation term modified in terms of wall shear stress (Gosman, 1976). Again in this study U_N is assumed to be zero.

It is also noted that from equations (F.53) and (F.54) the modified generation term may also be written as,

$$G = \mu_t \left(\frac{\partial U}{\partial r} \right)^2 \quad (\text{F.56})$$

If this modified generation of equation (F.56) is subtracted from the unmodified generation of k , then the final expression for the total generation of turbulence energy can be written in the form,

$$G = G_r + G_c \quad (\text{F.57})$$

where G_r is the total unmodified generation of k less $\mu_t \left(\frac{\partial U}{\partial r} \right)^2$ and G_c is given by equation (F.55) (Gosman, 1976).

The dissipation term $C_D \rho \epsilon$ is also modified to reflect equation (F.30) and when it is integrated over the control volume, it takes the value (see eqn. F.35 for ϵ -expression),

$$\begin{aligned} C_D \rho \bar{\epsilon} &= C_D \rho \int_V \epsilon dV \\ &= \frac{C_D \rho C_\mu^{3/4} (k_p^{*1/2} k_p - k_N^{3/2})}{y_p} U^+ \delta V \quad (\text{F.58}) \end{aligned}$$

where δV is the control volume encloses the point P where k is stored. k_p is the value of k at the node point P and the superscript (*) appearing in the equation (F.58) stands for the value of k of the previous iteration, k_N is the turbulence energy at the wall which has zero value, y_p is the normal distance of nearest node P from the wall, ρ is the fluid density C_D and C_μ are constants given in table 2.1 (see Chapter 2).

When the point P falls within the turbulence region (i.e. $y^+ > 11.63$) equation (F.58) may be written as,

$$C_D \rho \bar{E} = d_t \cdot \delta V \cdot k_p \quad (\text{F.59})$$

where

$$d_t = \frac{C_D \rho C_\mu^{3/4} k_p^{*1/2}}{K y_p} \ln(E y_p^+) \quad (\text{F.60})$$

If P lies within the viscous sublayer ($y^+ \leq 11.63$) equation (F.58) has the same equation as equation (F.59) but now with,

$$d_t = \frac{C_D \rho C_\mu^{3/4} k_p^{*1/2}}{y_p} y_p^+ \quad (\text{F.61})$$

where

$$y_p^+ = \frac{\rho y_p}{\mu} k_p^{*1/2} C_\mu^{1/4} \quad (\text{F.62})$$

If equation (2.22) (see Chapter 2) is integrated over the control volume and linearising the result in the manner described by equation (E.19) (see App. E) with $\phi = k$, the following expressions for S_p^k and S_u^k may be deduced

$$S_p^k = -d_t \cdot \delta V \quad (\text{F.63})$$

$$S_u^k = G \cdot \delta V \quad (\text{F.64})$$

where δV is the control volume which encloses P where k is stored. d_t can take values either from equations (F.60) or (F.61) depending on y^+ whether it is $>$ or ≤ 11.63 . The generation term G appearing in equation (F.64) is the same as G in equation (F.57).

(ii) Energy Dissipation Rate ϵ .

Basically the linearisation 'constants' S_P^ϵ and S_U^ϵ are deducible from the integrated source term S^ϵ for ϵ (ie by integrating equation 2.23 of Chapter 2 over the control volume) giving,

$$S_P^\epsilon = \frac{-C_2 \rho \epsilon_P^*}{k_P} \cdot \delta V \quad (\text{F.65})$$

$$S_U^\epsilon = \frac{C_1 \epsilon_P^* G}{k_P^*} \cdot \delta V \quad (\text{F.66})$$

where δV is the control volume for ϵ and k_P and ϵ_P are values of k and ϵ at the point P and superscript (*) indicates the values of individual variables at previous iterations.

However, since in the wall flows, unlike k which falls to zero at the wall, ϵ reaches its maximum value there. This makes ϵ -balance for a cell extending right up to the wall difficult. It is due to this difficulty that we (Gosman, 1976) adopt a fixed value for ϵ_P in the inertial sublayer (irrespective of the local Reynolds number, y^+) based on 'equilibrium' relations (see eqn. F.30). To achieve $\epsilon = \epsilon_P$ (where ϵ_P is the value of ϵ at P) the following changes are made to S_P^ϵ and S_U^ϵ .

$$S_P^\epsilon = -\gamma \quad (\text{F.67})$$

and
$$S_U^\epsilon = \gamma \cdot \epsilon_P \quad (\text{F.68})$$

where γ is a large number of the order 10^{30} and ϵ_P is given by (see equation (F.30) for value of ϵ at P),

$$\epsilon_p = t \cdot k_p^{3/2} \quad (\text{F.69})$$

where

$$t = \frac{c_p^{3/4}}{K_{yp}} \quad (\text{F.70})$$

This will ensure that $\epsilon = \epsilon_p$ in the computer solution.

APPENDIX G.PROGRAM FLOWCHART , SUBROUTINES AND PROGRAM LISTING.

Figure G.1 shows the flow chart of the modified TEACH-T computer program, that will help to increase clarity of the program layout that will be discussed in the following lines. A program listing is provided at the end of this Appendix.

The program was run on both the CDC 7600 machine at the ULCC and also on the departmental PRIME 550. The listing provided is for the ULCC CDC7600 machine. The PRIME version has some minor modifications.

There are six general subroutines relevant to any particular variable solved. They are the CONTRO, INIT, PROPS, PROMOD, LISOLV and PRINT. In addition, there are major set of CALCU, CALCV, CALCP, CALCTE and CALCED subroutines for velocities U and V , pressure correction p' , kinetic energy k and dissipation rate ϵ where the variables of interest are solved for.

Overall control is exerted by the main subroutine CONTRO which performs the initial and final operations and also controls the iteration. The function of this subroutine includes setting the number of sweeps ($NSWP\phi$, for each variable ϕ) throughout domain of calculation. It contains four chapters,

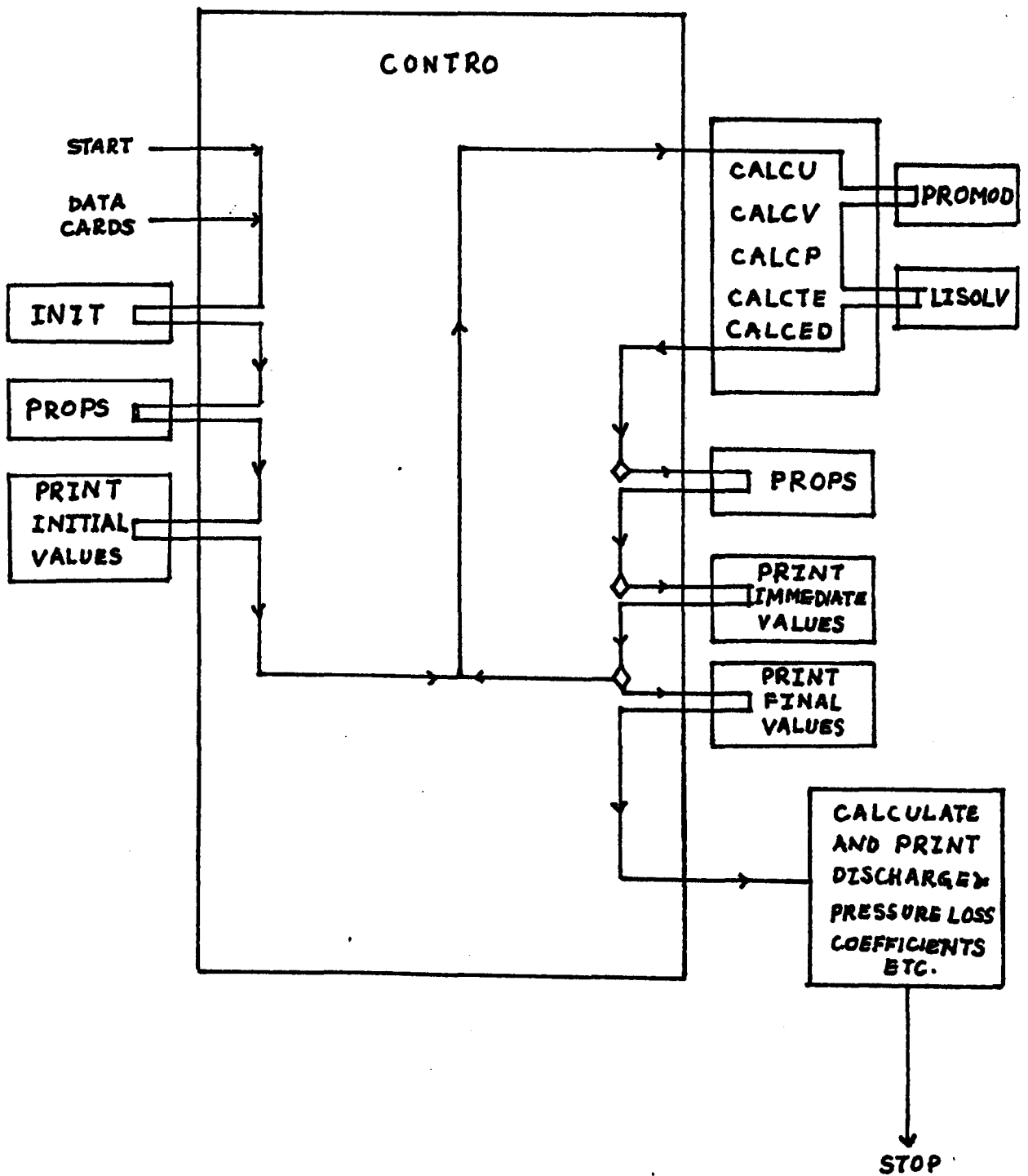


Fig.G.1: The Program Flowchart.

Chapter 1.

In this chapter includes (i) specifying the grid spacing and grid distributions upstream/downstream of orifice plate,(ii) selection of dependent variable to be solved,(iii) reference values for fluid properties,(iv) turbulence constants and boundary values,(v) underrelaxation factors for each variables.

Chapter 2.

This chapter gives the initial variable fields and initial outputs.

Chapter 3.

Chapter 3 gives how the fluid properties are updated and prints out intermediate output for each variables,and

Chapter 4.

The discharge and pressure loss coefficients and also shear stress coefficient along pipe wall when convergence is achieved,were calculated in this final chapter of the routine.

Subroutine INIT performs initialisation jobs,which consists of two chapters,chapter 1 is to establish geometrical configurations and chapter 2 initialises all variables to be solved.

Subroutine PROPS,takes care of calculating fluid properties like μ , ρ etc.

e.g.
$$\mu_{eff} = \mu + \mu_t \quad (G.1)$$

where
$$\mu_t = C_\mu \rho \frac{k^2}{\epsilon} \quad (G.2)$$

is the turbulence viscosity and μ is for the laminar ones.

Subroutines CALC ϕ make the main calculations of the finite difference equations for each ϕ ($\phi \equiv U, V, k, \epsilon$) consisting of,

Chapter 1.

All the convective and diffusive coefficients a_i^ϕ ($i=N, S, E, W$) of the difference equations (of the form E.74 of appendix E) and S_p^ϕ and S_u^ϕ (see equation E.19 appendix E) for each ϕ variables are assembled.

Chapter 2.

Wall modifications are made by calling MOD ϕ for the individual ϕ from subroutine PROMOD.

Chapter 3.

Final coefficients a_p (see equation E.25) are assembled here and residual sources are calculated.

Chapter 4.

Recurrence relation (see equation (E.73) of Appendix E) are solved by TDMA for new values of each variables by first assembling

TDMA coefficients(see Appendix E, equation (E.74)).

CALCP.

In addition to four chapters described above, this CALCP subroutine contains,

Chapter 5.

The correct velocities (see equation E.40) are made here by first correcting pressures according to expression,

$$p = p^* + p' \quad (G.3)$$

Subroutine PROMOD.

All modifications on solid boundaries are made in this subroutine. Corrections due to wall and boundary effects are made here, eg. for a specific cell (control volume) near top wall of pipe, the normal $\phi_p \sim \phi_N$ relation breaks down. This is achieved by setting $AN(I, J) = 0$ (where $AN(I, J)$ is the coefficient of combined convective and diffusive flux through north wall of the control volume and is given by relation E.26, see Appendix E). This routine consists of chapters, each chapter corresponds to a specified variable modifications. It is not necessary to modify fluid properties, pressure and internal energy. These correspond to chapters 1, 4 and 5 respectively, in the program listing provided.

The shear stress on the pipe wall τ_s is calculated and modifications to S_p^ϕ and S_u^ϕ (where S_p^ϕ and S_u^ϕ are defined by equation (E.19)(see Appendix E) at the wall are made in this routine.

Subroutine LISOLV.

This subroutine performs the LBL iteration, which has been discussed in Appendix E. The coefficients correspond to each variables are called in, from individual $CALC\phi$ subroutines. This is used to solve for the flow field variables in the recurrence formulae of the TDMA (see equation E.73 of Appendix E).

Subroutine PRINT.

This routine provides output of variable arrays together with headings for each individual variable, ϕ .

```

C SUBROUTINE CONTRO
C
C*****
C
C.....TEACH-T.....
C * A COMPUTER PROGRAM FOR THE CALCULATION OF **
C * TWO -DIMENSIONAL (PLANE OR AXISYMMETRICAL) **
C * TURBULENT RECIRCULATING FLOWS. **
C *** SIMULATION OF ORIFICE METER MODEL *****
C *** DEVELOPED BY M.HAFIZ *****
C *** SYSTEMS SCIENCE DEPARTMENT *****
C *** THE CITY UNIVERSITY, LONDON EC1V OHB, 1981 *****
C*****
CHAPTER 0 0 0 0 0 0 0 0 PRELIMINARIES 0 0 0 0 0 0 0 0 MAIN
C DIMENSION HEDU(6), HEDV(6), HEDP(6), HEDT(6), HEDK(6), HEDD(6), HEDM(6) MODA
1 , HEDA(6), HEDB(6) MODA
COMMON MAIN
1 /UVEL/RESORU, NSWPU, URFU, DXEPU(40), DXPWU(40), SEWU(40)
1 /VVEL/RESORV, NSWPV, URFV, DYNPV(40), DYPSV(40), SNSV(40), RCV(40)
1 /PCOR/RESORM, NSWPP, URFP, DU(32, 32), DV(32, 32), IPREF, JPREF
1 /TEN/RESORK, NSWPK, URFK MODA
1 /TDIS/RESORE, NSWPD, URFE
1 /VAR/U(32, 32), V(32, 32), P(32, 32), PP(32, 32), TE(32, 32), ED(32, 32)
1 /ALL/IT, JT, NI, NJ, NIM1, NJM1, GREAT
1 /GEOM/INDCOS, X(40), Y(40), DXEP(40), DXPW(40), DYNP(40), DYPS(40),
1 SNS(40), SEW(40), XU(40), YV(40), R(40), RV(40)
1 /FLUPR/URFVIS, VISCOS, DENSIT, PRANDT, DEN(32, 32), VIS(32, 32)
1 /KASE T1/ UIN, TEIN, EDIN, FLOWIN, ALAMDA,
2 RSMALL, RLARGE, AL5, AL6, JSTEP, ISTEP, JSTP1, JSTM1, ISTEP1, ISTM1,
3 ISTEP2, ISTEP3, ISTM2
1 /TURB/GEN(32, 32), CD, CMU, C1, C2, CAPP, ELOG, PRED, PRTE
1 /WALLF/YPLUSN(32), XPLUSE(32), XPLUSW(32), TAUN(32), TAUE(32), TAUW(32)
1 /COEF/AP(32, 32), AN(32, 32), AS(32, 32), AE(32, 32), AW(32, 32), SU(32, 32),
1 SP(32, 32)
LOGICAL INCALU, INCALV, INCALP, INPRO, INCALK, INCALD, INCALM, INCALA,
1 INCALB
C***** DOWNSTREAM OF ORIFICE PLATE(IN REGION3)
GREAT=1.E30 MODA
NITER=0 MAIN
IT=32
JT=32
NSWPU=3
NSWPV=3
NSWPP =5
NSWPK =3
NSWPD =3
READ(5, 010)HEDU, HEDV, HEDP, HEDT, HEDK, HEDD, HEDM, HEDA, HEDB
010 FORMAT(6A6) MAIN
C MAIN
CHAPTER 1 1 1 1 1 PARAMETERS AND CONTROL INDICES 1 1 1 1 1 1 MAIN
C MAIN
C-----GRID MAIN
NI=32
NJ=22
NIM1=NI-1 MODA
NJM1=NJ-1 MODA
INDCOS=2 MODA
ISTEP=16
JSTEP=15
KSTEP=16
IL=KSTEP-1

```

```

IM=IL-1
DXJ=5.
DXD=15.
ISTP1=ISTEP+1
ISTM1=ISTEP-1
ISTP2=ISTEP+2
ISTP3=ISTEP+3
ISTM2=ISTEP-2
JSTP1=JSTEP+1
JSTM1=JSTEP-1
RSDRL=JSTM1/FLOAT(NJ-2)
AR=RSDRL**2
RLARGE=.0508
DIAM=2.0*RLARGE
C***** DOWNSTREAM OF ORIFICE PLATE (IN REGION 3)
ALTOT2=DXD*DIAM
EPSX=1.9
SUMX2=(EPSX**IL-EPSX)/(EPSX-1.)+0.5*EPSX**IM+0.5
DX2=ALTOT2/SUMX2
DX20=DX2
C***** IN REGION2 AND DOWNSTREAM REGION (IN REGION 3)
X(ISTEP)=-0.5*DX2
X(ISTP1)=-X(ISTEP)
DO 100 I=ISTP2,NIM1
X(I)=X(I-1)+EPSX*DX2
100 DX2=EPSX*DX2
X(NI)=X(NIM1)-X(NI-2)+X(NIM1)
C***** UPSTREAM OF ORIFICE PLATE (IN REGION 1)
ALTOT1=DXU*DIAM
SUMX1=(EPSX**ISTM1-EPSX)/(EPSX-1.)+0.5*EPSX**ISTM2
HDX2=0.5*DX20
DX1=(ALTOT1-HDX2)/SUMX1
DX10=DX1
DO 900 I=1,ISTM2
NN=ISTEP-I
NNP1=NN+1
X(NN)=X(NNP1)-EPSX*DX1
900 DX1=EPSX*DX1
X(1)=X(2)-(X(3)-X(2))
ALTOT3=ALTOT1+ALTOT2
AL5=0.5*(X(2)+X(1))
AL6=ALTOT3-AL5
T=0.5*EPSX*(ABS(DX10)+ABS(DX20))+ABS(DX20)
C*****
DY=RLARGE/FLOAT(NJ-2)
Y(1)=-0.5*DY
DO 101 J=2,NJ
101 Y(J)=Y(J-1)+DY
RSMALL=0.5*(Y(JSTEP)+Y(JSTP1))
D1=2.0*RLARGE
D2=2.0*RSMALL
TOD1=T/D1
TOD2=T/D2
D2OT=D2/T
C-----DEPENDENT VARIABLE SELECTION
INCALU=.TRUE.
INCALV=.TRUE.
INCALP=.TRUE.
INCALK=.TRUE.
INCALD=.TRUE.
INPRO=.TRUE.
C-----FLUID PROPERTIES
DENSIT =1000.0
C-----TURBULENCE CONSTANTS
CMU=0.09
CD=1.00

```

MODA
MODA

MODA
MODA

MODA

MODA
MODA
MODA
MODA
MODA

MAIN
MAIN
MAIN
MAIN

MAIN

MAIN
MAIN
MAIN


```

TE(2,J)=TE(1,J)
ED(2,J)=ED(1,J)
202 U(I,J)=UIN2*FACTOR
YPLUSN(1)=0.0
DO 203 I=2,NIM1
203 YPLUSN(I)=11.0
DO 204 J=JSTEP,NJ
XPLUSE(J)=11.0
204 IF(J.EQ.JSTEP)XPLUSE(J)=0.0
DO 902 J=JSTEP,NJ
XPLUSW(J)=11.0
902 IF(J.EQ.JSTEP)XPLUSW(J)=0.0
CALL PROPS

C-----INITIAL OUTPUT
WRITE(6,210)
WRITE(6,211)
WRITE(6,220) UIN
WRITE(6,1034)UIN2
WRITE(6,1035)RE1
WRITE(6,1036)T
WRITE(6,1037)D2
WRITE(6,1038)TOD2
WRITE(6,1060)D200T
WRITE(6,1043)TOD1
WRITE(6,1039)SUMX2
WRITE(6,1040)DX20
WRITE(6,1041)SUMX1
WRITE(6,1042)DX10
WRITE(6,1044)NI
WRITE(6,1045)NJ
WRITE(6,1046)ISTEP
WRITE(6,1047)JSTEP
WRITE(6,1061)KSTEP
WRITE(6,1062)EPSX
WRITE(6,1048)DXJ
WRITE(6,1049)DXD
WRITE(6,1057)SORMAX
WRITE(6,1058)TURBIN
WRITE(6,1059)ALAMDA
WRITE(6,230)RE2
WRITE(6,240) RSDRL
WRITE(6,260) DENSIT
WRITE(6,250) VISCOS
IF(INCALU) CALL PRINT(2,2,NI,NJ,IT,JT,XU,Y,U,HEDU)
IF(INCALV) CALL PRINT(2,2,NI,NJ,IT,JT,X,YV,V,HEDV)
IF(INCALP) CALL PRINT(2,2,NI,NJ,IT,JT,X,Y,P,HEDP)
IF(INCALK) CALL PRINT(2,2,NI,NJ,IT,JT,X,Y,TE,HEDK)
IF(INCALD) CALL PRINT(2,2,NI,NJ,IT,JT,X,Y,ED,HEDD)
C.....CALCULATE RESIDUAL SOURCES NORMALIZATION FACTORS.....
FLOWIN =0.0
XMONIN =0.0
DO 657 J=2,NJM1
ARDEN =0.5*(DEN(1,J)+DEN(2,J))*R(J)*SNS(J)
FLOWIN =FLOWIN+ARDEN*U(2,J)
XMONIN =XMONIN+ARDEN*U(2,J)*U(2,J)
657 CONTINUE
RESORT =0.0

C
CHAPTER 3 3 3 3 3 3 3 ITERATION LOOP 3 3 3 3 3 3 3 3
C
WRITE(6,310) IMON,JMON
300 NITER=NITER+1
IF(INCALU) CALL CALCU
IF(INCALV) CALL CALCV
IF(INCALP) CALL CALCP
IF(INCALK) CALL CALCTE

```

MODA
MODA
MODA

MAIN
MAIN

MODA
MODA
MAIN
MAIN
MAIN
MAIN

MAIN
MAIN
MAIN
MAIN
MAIN
MAIN
MAIN
MAIN


```

I=ISTP2
1 IF(X(I).GE.XFD)GO TO 2
  I=I+1
  GO TO 1
2 IFD=I
  IFDM1=IFD-1
  PIFD=P(IFD,NJM1)
  PIFDM1=P(IFDM1,NJM1)
  XIFD=X(IFD)
  XIFDM1=X(IFDM1)
  PFD=PIFDM1+(PIFD-PIFDM1)*(XFD-XIFDM1)/(XIFD-XIFDM1)
  I=ISTM1
3 IF(X(I).LE.XFU)GO TO 4
  I=I-1
  GO TO 3
4 IFU=I
  IFUP1=IFU+1
  PIFU=P(IFU,NJM1)
  PIFUP1=P(IFUP1,NJM1)
  XIFU=X(IFU)
  XIFUP1=X(IFUP1)
  PFU=PIFUP1+(PIFU-PIFUP1)*(XFU-XIFUP1)/(XIFU-XIFUP1)
  I=ISTP2
5 IF(X(I).GE.XD2D)GO TO 6
  I=I+1
  GO TO 5
6 ID2D=I
  ID2DM1=ID2D-1
  PID2D=P(ID2D,NJM1)
  PID2D1=P(ID2DM1,NJM1)
  XID2D=X(ID2D)
  XID2D1=X(ID2DM1)
  PD2D=PID2D1+(PID2D-PID2D1)*(XD2D-XID2D1)/(XID2D-XID2D1)
  I=ISTM1
7 IF(X(I).LE.XDU)GO TO 8
  I=I-1
  GO TO 7
8 IDU=I
  IDUP1=IDU+1
  PIDU=P(IDU,NJM1)
  PIDUP1=P(IDUP1,NJM1)
  XIDU=X(IDU)
  XIDUP1=X(IDUP1)
  PDU=PIDUP1+(PIDU-PIDUP1)*(XDU-XIDUP1)/(XIDU-XIDUP1)
  DPFT=PFU-PFD
  DPDD2T=PDU-PD2D
  DCFT=UIN*SQRT(DENSIT*(1./RSDRL**4-1.)/2./DPFT)
  DCDD2T=UIN*SQRT(DENSIT*(1./RSDRL**4-1.)/2./DPDD2T)
  WRITE(6,1051)DCFT
  WRITE(6,1052)DCDD2T
  WRITE(6,1053)DCCT
  WRITE(6,1054)XKTHEO
  WRITE(6,1055)XKTCTD
  WRITE(6,1056)XKEXP1
  STOP

```

C-----FORMAT STATEMENTS

MAIN
MAIN

```

210 FORMAT(1H0,47X,*KASE T1 TURBULENT FLOW THROUGH A SUDDEN ENLARGEMEN
1T*////)
211 FORMAT(1H0,50X,29H BACK AND ROSCHKE EXPERIMENTS,////)
220 FORMAT(//1H0,15X,*INLET FLUID VELOCITY UIN*,T60,1H=,3X,1PE11.3)
1034 FORMAT(1H0,15X,*ORIFICE FLUID VELOCITY UIN2*,T60,1H=,3X,1PE11.3)
1035 FORMAT(1H0,15X,*REYNOLDS NUMBER1 RE1*,T60,1H=,3X,1PE11.3)
1036 FORMAT(1H0,15X,*ORIFICE PLATE THICKNESS T*,T60,1H=,3X,1PE11.3)
1037 FORMAT(1H0,15X,*ORIFICE PLATE DIAMETER D2*,T60,1H=,3X,1PE11.3)
1038 FORMAT(1H0,15X,*PLATE THICKNESS OVER ORIFICE DIAMETER T/D2*,T60,
11H=,3X,1PE11.3)

```

1030 FORMAT(1HO,15X,*ORIFICE DIAM.AND PLATE THICKNESS RATIO D2/T*,T60,
 11H=,3X,1PE11.3)
 1039 FORMAT(1HO,15X,*SU4X2*,T60,1H=,3X,1PE11.3)
 1040 FORMAT(1HO,15X,*DX20*,T60,1H=,3X,1PE11.3)
 1041 FORMAT(1HO,15X,*3UMX1*,T60,1H=,3X,1PE11.3)
 1042 FORMAT(1HO,15X,*DX10*,T60,1H=,3X,1PE11.3)
 1043 FORMAT(1HO,15X,*PLATE THICKNESS OVER PIPE DIAMETER T/D1*,T60,
 11H=,3X,1PE11.3)
 1044 FORMAT(1HO,15X,*DIRECTION-X GRID NO.NI*,T60,1H=,3X,1PE11.3)
 1045 FORMAT(1HO,15X,*DIRECTION-Y GRID NO.NJ*,T60,1H=,3X,1PE11.3)
 1046 FORMAT(1HO,15X,*ISTEP*,T60,1H=,3X,1PE11.3)
 1047 FORMAT(1HO,15X,*JSTEP*,T60,1H=,3X,1PE11.3)
 1061 FORMAT(1HO,15X,*KSTEP*,T60,1H=,3X,1PE11.3)
 1062 FORMAT(1HO,15X,*EPSX*,T60,1H=,3X,1PE11.3)
 1048 FORMAT(1HO,15X,*INLET DISTANCE(IN DIAM.)DXU*,T60,1H=,3X,1PE11.3)
 1049 FORMAT(1HO,15X,*OUTLET DIST.(IN DIAM.)DXD*,T60,1H=,3X,1PE11.3)
 1057 FORMAT(1HO,15X,*MAXIMUM SOURCE SORMAX*,T50,1H=,3X,1PE11.3)
 1058 FORMAT(1HO,15X,*TURBULENCE INTENSITY TURBIN*,T60,1H=,3X,1PE11.3)
 1059 FORMAT(1HO,15X,*LENGTH SCALE FACTOR ALAMDA*,T60,1H=,3X,1PE11.3)
 230 FORMAT(1HO,15X,*REYNOLDS NUMBER2 RE2*,T60,1H=,3X,1PE11.3)
 240 FORMAT(1HO,15X,*DIAMETER RATIO D2/D1*,T60,1H=,3X,1PE11.3)
 250 FORMAT(1HO,15X,* LAMINAR VISCOSITY *,T60,1H=,3X,1PE11.3)
 260 FORMAT(1HO,15X,*FLUID DENSITY *,T60,1H=,3X,1PE11.3)

310 FORMAT(1HO,*ITER *,*I-----ABSOLUTE RESIDUAL SOURCE SUM MAIN
 1S-----I I-----FIELD VALUES AT MONITORING LOCATION*,* MODA
 2(*,I2,*,*,I2,*)*,------I* / 2X,*NO.*,3X,*UMOM*,6X,*VMOM*,6X,*MA MAIN
 3SS*,6X,*ENER*,6X,*TKIN*,6X,*DISP*,10X,*U*,9X,*V*,9X,*P*,9X,*T*,9X, MODA
 4*K*,9X,*D*/) MODA
 MODA

311 FORMAT(1H ,I3,4X,1P6E10.3,3X,1P6E10.3)
 402 FORMAT(///5X,1HI,7X,5HXU(I),6X,10HS.S.COEFF.)
 403 FORMAT(/5X,I5,2(1PE11.3))
 1051 FORMAT(//1HO,15X,*DIS.COEF.(FLANGETAP)DCFT*,T60,1H=,3X,1PE11.3)
 1052 FORMAT(1HO,15X,*DIS.COEF.D-D/2TAP DCDD2T*,T60,1H=,3X,1PE11.3)
 1053 FORMAT(1HO,15X,*DIS.COEF.(CORNER TAP)DCCT,T60,1H=,3X,1PE11.3)
 1054 FORMAT(1HO,15X,*THTCAL PRES.LOS.COEF.XKTHEO*,T60,1H=,3X,1PE11.3)
 1055 FORMAT(1HO,15X,*CTDTCALPRES.LOS.COEF.XKTCTD*,T60,1H=,3X,1PE11.3)
 1056 FORMAT(1HO,15X,*EXPTAL PRES.LOS.COEF.XKEXP1*,T60,1H=,3X,1PE11.3)

END
 SUBROUTINE INIT

MAIN
 INIT
 INIT
 INIT
 INIT

C
 CHAPTER 0 0 0 0 0 0 0 0 PRELIMINARIES 0 0 0 0 0 0 0 0
 C

COMMON
 1/UVEL/RESORU,NSWPU,URFU,DXEPU(40),DXPWU(40),SEWU(40)
 1/VVEL/RESORV,NSWPV,URFV,DYNPV(40),DYPSV(40),SNSV(40),RCV(40)
 1/PCOR/RESORM,NSWPP,URFP,DU(32,32),DV(32,32),IPREF,JPREF
 1/VAR/U(32,32),V(32,32),P(32,32),PP(32,32),TE(32,32),ED(32,32)
 1/ALL/IT, JT, NI, NJ, NIM1, NJM1, GREAT
 1/GEOM/INDCOS,X(40),Y(40),DXEP(40),DXPW(40),DYNP(40),DYPS(40),
 1 SNS(40),SEW(40),XU(40),YV(40),R(40),RV(40)
 1/FLUPR/URFVIS,VISCOS,DENSIT,PRANDT,DEN(32,32),VIS(32,32)
 1/KASE T1/UIN,TEIN,EDIN,FLOWIN,ALAMDA,
 2 RSMALL,RLARGE,AL5,AL6,JSTEP,ISTEP,JSTP1,JSTM1,ISTP1,ISTM1,
 3 ISTEP2,ISTP3,ISTM2
 1/TURB/GEN(32,32),CD,CMU,C1,C2,CAPPA,ELOG,PRED,PRTE
 1/COEF/AP(32,32),AN(32,32),AS(32,32),AE(32,32),AW(32,32),SU(32,32),
 1 SP(32,32)

C
 CHAPTER 1 1 1 1 1 CALCULATE GEOMETRICAL QUANTITIES 1 1 1 1 1
 C

DO 100 J=1,NJ
 R(J)=Y(J)
 100 IF(INDCOS.EQ.1)R(J)=1.0
 C***** IN REGION1
 DXPW(1)=0.0
 DO 943 I=1,ISTM1

INIT
 INIT
 INIT
 INIT
 INIT
 INIT


```

DXEPU(1)=0.0
DO 957 I=ISTEP,ISTP1
DXEPU(I)=XU(I+1)-XU(I)
957 DXPWU(I+1)=DXEPU(I)
SEWU(1)=0.0
SEWU(2)=0.0
DO 958 I=ISTEP,ISTP1
958 SEWU(I)=0.5*(DXEPU(I)+DXPWU(I))
YV(1)=0.0
RV(1)=0.0
DO 962 J=2,JSTP1
RV(J)=0.5*(R(J)+R(J-1))
RCV(J)=0.5*(RV(J)+RV(J-1))
962 YV(J)=0.5*(Y(J)+Y(J-1))
DYPSV(1)=0.0
DYPSV(2)=0.0
DYNPV(JSTP1)=0.0
DO 963 J=2,JSTEP
DYNPV(J)=YV(J+1)-YV(J)
963 DYPSV(J+1)=DYNPV(J)
SNSV(1)=0.0
SNSV(2)=0.0
SNSV(JSTP1)=0.0
DO 964 J=3,JSTEP
964 SNSV(J)=0.5*(DYNPV(J)+DYPSV(J))
C***** IN REGION3
DXEP(NI)=0.0
DO 946 I=ISTP2,NIM1
DXEP(I)=X(I+1)-X(I)
946 DXPW(I+1)=DXEP(I)
DYPS(1)=0.0
DYNP(NJ)=0.0
DO 947 J=1,NJM1
DYNP(J)=Y(J+1)-Y(J)
947 DYPS(J+1)=DYNP(J)
SEW(1)=0.0
DO 951 I=ISTP2,NIM1
951 SEW(I)=0.5*(DXEP(I)+DXPW(I))
SNS(1)=0.0
SNS(NJ)=0.0
DO 952 J=2,NJM1
952 SNS(J)=0.5*(DYNP(J)+DYPS(J))
XU(1)=0.0
DO 959 I=ISTP3,NI
959 XU(I)=0.5*(X(I)+X(I-1))
DXPWU(1)=0.0
DXPWU(2)=0.0
DXEPU(1)=0.0
DXEPU(NI)=0.0
DO 960 I=ISTP2,NIM1
DXEPU(I)=XU(I+1)-XU(I)
960 DXPWU(I+1)=DXEPU(I)
SEWU(1)=0.0
SEWU(2)=0.0
DO 961 I=ISTP2,NIM1
961 SEWU(I)=0.5*(DXEPU(I)+DXPWU(I))
YV(1)=0.0
RV(1)=0.0
DO 965 J=2,NJ
RV(J)=0.5*(R(J)+R(J-1))
RCV(J)=0.5*(RV(J)+RV(J-1))
965 YV(J)=0.5*(Y(J)+Y(J-1))
DYPSV(1)=0.0
DYPSV(2)=0.0
DO 966 J=2,NJM1
DYNPV(J)=YV(J+1)-YV(J)

```

```

966 DYP3V(J+1)=DYNPV(J)
    SNSV(1)=0.0
    SNSV(2)=0.0
    SNSV(NJ)=0.0
    DO 967 J=3,NJM1
967 SNSV(J)=0.5*(DYNPV(J)+DYPSV(J))

```

```

C
CHAPTER 2 2 2 2 2 2 SET VARIABLES TO ZERO 2 2 2 2 2 2 INIT
C
DO 200 I=1,NI INIT
DO 200 J=1,NJ INIT
U(I,J)=0.0 INIT
V(I,J)=0.0 INIT
P(I,J)=0.0 INIT
PP(I,J)=0.0 INIT
TE(I,J)=0.0
ED(I,J)=0.0
DEN(I,J)=DENSIT MODA
VIS(I,J)=VISCOS MODA
DU(I,J)=0.0 INIT
DV(I,J)=0.0 INIT
SU(I,J)=0.0 INIT
SP(I,J)=0.0 INIT
200 CONTINUE
RETURN INIT
END INIT
SUBROUTINE PROPS PROPS

```

```

C
CHAPTER 0 0 0 0 0 0 0 0 0 PRELIMINARIES 0 0 0 0 0 0 0 0 PROPS
C
COMMON PROPS

```

```

1/FLUPR/URFVIS,VISCOS,DENSIT,PRANDT,DEN(32,32),VIS(32,32)
1/VAR/U(32,32),V(32,32),P(32,32),PP(32,32),TE(32,32),ED(32,32)
1/ALL/IT, JT, NI, NJ, NIM1, NJM1, GREAT
1/TURB/GEN(32,32), CD, CMU, C1, C2, CAPP, ELOG, PRED, PRTE
1/KASE T1/UIN, TEIN, EDIN, FLOWIN, ALAMDA,
2 RSMALL, RLARGE, AL5, AL6, JSTEP, ISTEP, JSTP1, JSTM1, ISTEP1, ISTM1,
3 ISTEP2, ISTEP3, ISTM2

```

```

C
CHAPTER 1 1 1 VISCOSITY 1 1 1 PROPS
C

```

```

DO 100 I=2,NIM1
VIS(I,1)=VIS(I,2)
DO 100 J=2,NJM1
VISOLD=VIS(I,J)
IF(ED(I,J).EQ.0.) GO TO 102
VIS(I,J)=DEN(I,J)*TE(I,J)**2*CMU/ED(I,J)+VISCOS
GO TO 101
102 VIS(I,J)=VISCOS
IF(I.EQ.ISTEP.AND.J.GE.JSTP1)VIS(I,J)=0.0
IF(I.EQ.ISTEP1.AND.J.GE.JSTP1)VIS(I,J)=0.0
101 VIS(I,J)=URFVIS*VIS(I,J)+(1.-URFVIS)*VISOLD
C-----UNDER-RELAX VISCOSITY
100 CONTINUE
RETURN
END
SUBROUTINE CALCU

```

```

C
CHAPTER 0 0 0 0 0 0 0 0 0 PRELIMINARIES 0 0 0 0 0 0 0 0 CALCU
C
COMMON CALCU

```

```

1/VEL/RESORU, NSWPU, URFU, DXEPU(40),DXPWU(40),SEWU(40)
1/PCOR/RESORM, NSWPP, URFU, DU(32,32),DV(32,32),IPREF,JPREF
1/VAR/U(32,32),V(32,32),P(32,32),PP(32,32),TE(32,32),ED(32,32)
1/ALL/IT, JT, NI, NJ, NIM1, NJM1, GREAT
1/GEOM/INDCOS, X(40),Y(40),DXEP(40),DXPW(40),DYNP(40),DYPS(40),

```

1 SNS(40),SEW(40),XJ(40),YV(40),R(40),RV(40)
 1/FLUPR/URFVIS,VISCOS,DENSIT,PRANDT,DEN(32,32),VIS(32,32)
 1/COEF/AP(32,32),AN(32,32),AS(32,32),AE(32,32),AW(32,32),SU(32,32),
 1 SP(32,32)
 1/KASE T1/UIN,TEIN,EDIN,FLOWIN,ALAMDA,
 2 RSMALL,RLARGE,AL5,AL6,JSTEP,ISTEP,JSTP1,JSTM1,ISTP1,ISTM1,
 3 ISTEP2,ISTP3,ISTM2

C
 CHAPTER 1 1 1 1 1 1 ASSEMBLY OF COEFFICIENTS 1 1 1 1 1 1 1 CALCU
 C

DO 100 I=3,NIM1 CALCU
 DO 101 J=2,NJM1 CALCU

C-----COMPUTE AREAS AND VOLUME CALCU
 AREAN=RV(J+1)*SEWU(I) CALCU
 AREAS=RV(J)*SEWU(I) CALCU
 AREAEW=R(J)*SNS(J) CALCU
 VOL=R(J)*SEWU(I)*SNS(J) CALCU

C-----CALCULATE CONVECTION COEFFICIENTS CALCU
 GN=0.5*(DEN(I,J+1)+DEN(I,J))*V(I,J+1) CALCU
 GNW=0.5*(DEN(I-1,J)+DEN(I-1,J+1))*V(I-1,J+1) CALCU
 GS=0.5*(DEN(I,J-1)+DEN(I,J))*V(I,J) CALCU
 GSW=0.5*(DEN(I-1,J)+DEN(I-1,J-1))*V(I-1,J) CALCU
 GE=0.5*(DEN(I+1,J)+DEN(I,J))*U(I+1,J) CALCU
 GP=0.5*(DEN(I,J)+DEN(I-1,J))*U(I,J) CALCU
 GW=0.5*(DEN(I-1,J)+DEN(I-2,J))*U(I-1,J) CALCU
 CN=0.5*(GN+GNW)*AREAN CALCU
 CS=0.5*(GS+GSW)*AREAS CALCU
 CE=0.5*(GE+GP)*AREAEW CALCU
 CW=0.5*(GP+GW)*AREAEW CALCU

C-----CALCULATE DIFFUSION COEFFICIENTS CALCU
 VISN=0.25*(VIS(I,J)+VIS(I,J+1)+VIS(I-1,J)+VIS(I-1,J+1)) CALCU
 VISS=0.25*(VIS(I,J)+VIS(I,J-1)+VIS(I-1,J)+VIS(I-1,J-1)) CALCU
 DN=VISN*AREAN/DYNP(J) CALCU
 DS=VISS*AREAS/DYPS(J) CALCU
 DE=VIS(I,J)*AREAEW/DXEP(I) CALCU
 DW=VIS(I-1,J)*AREAEW/DXPWU(I) CALCU

C-----CALCULATE COEFFICIENTS OF SOURCE TERMS CALCU
 SMP=CN-CS+CE-CW CALCU
 CP=AMAX1(0.0,SMP) CALCU
 CPO=CP CALCU

C-----ASSEMBLE MAIN COEFFICIENTS CALCU
 AN(I,J)=AMAX1(ABS(0.5*CN),DN)-0.5*CN CALCU
 AS(I,J)=AMAX1(ABS(0.5*CS),DS)+0.5*CS CALCU
 AE(I,J)=AMAX1(ABS(0.5*CE),DE)-0.5*CE CALCU
 AW(I,J)=AMAX1(ABS(0.5*CW),DW)+0.5*CW CALCU
 DU(I,J)=AREAEW CALCU
 SU(I,J)=CPO*U(I,J)+DU(I,J)*(P(I-1,J)-P(I,J)) CALCU
 SP(I,J)=-CP CALCU
 DUDXP=(U(I+1,J)-U(I,J))/SEW(I) CALCU
 DUDXM=(U(I,J)-U(I-1,J))/SEW(I-1) CALCU
 SU(I,J)=(VIS(I,J)*DUDXP-VIS(I-1,J)*DUDXM)/SEWU(I)*VOL+SU(I,J) CALCU
 GAMP=0.25*(VIS(I,J)+VIS(I-1,J)+VIS(I,J+1)+VIS(I-1,J+1)) CALCU
 DVDXP=RV(J+1)*(V(I,J+1)-V(I-1,J+1))/DXEP(I) CALCU
 GAMM=0.25*(VIS(I,J)+VIS(I-1,J)+VIS(I,J-1)+VIS(I-1,J-1)) CALCU
 DVDXM=RV(J)*(V(I,J)-V(I-1,J))/DXEP(I) CALCU
 SU(I,J)=SU(I,J)+(GAMP*DUDXP-GAMM*DVDXM)/SNS(J)/R(J)*VOL CALCU

101 CONTINUE CALCU
 100 CONTINUE CALCU

C
 CHAPTER 2 2 2 2 2 2 2 PROBLEM MODIFICATIONS 2 2 2 2 2 2 2 CALCU
 C

CALL MODU CALCU

C
 CHAPTER 3 FINAL COEFF. ASSEMBLY AND RESIDUAL SOURCE CALCULATION 3 3 CALCU
 C

RESORU=0.0 CALCU


```

DS=VIS(I, J-1)*AREAS/DYPSV(J)
DE=VISE*AREAEN/DXEP(I)
DW=VISEW*AREAEN/DXPW(I)
C-----CALCULATE COEFFICIENTS OF SOURCE TERMS
SMP=CN-CS+CE-CW
CP=AMAX1(O.O, SMP)
CPO=CP
C-----ASSEMBLE MAIN COEFFICIENTS
AN(I, J)=AMAX1(ABS(O.5*CN), DN)-O.5*CN
AS(I, J)=AMAX1(ABS(O.5*CS), DS)+O.5*CS
AE(I, J)=AMAX1(ABS(O.5*CE), DE)-O.5*CE
AW(I, J)=AMAX1(ABS(O.5*CW), DW)+O.5*CW
DV(I, J)=O.5*(AREAN+AREAS)
SU(I, J)=CPO*V(I, J)+DV(I, J)*(P(I, J-1)-P(I, J))
SP(I, J)=-CP
IF(INDCOS.EQ.2) SP(I, J)=SP(I, J)-VIS(I, J)*VOL/RV(J)**2
IF(INDCOS.EQ.2) SP(I, J)=SP(I, J)-VIS(I, J)*VOL/RV(J)**2
DUDYP =(U(I+1, J)-U(I+1, J-1))/DYPS(J)
GAMP =O.25*(VIS(I, J)+VIS(I+1, J)+VIS(I, J-1)+VIS(I+1, J-1))
GAMM =O.25*(VIS(I, J)+VIS(I-1, J)+VIS(I, J-1)+VIS(I-1, J-1))
DUDYM =(U(I, J)-U(I, J-1))/DYPS(J)
SU(I, J) =SU(I, J)+(GAMP*DUDYP-GAMM*DUDYM)/SEW(I)*VOL
DVDYP =(V(I, J+1)-V(I, J))/SNS(J)
RGAMP =VIS(I, J)*R(J)
DVDYM =(V(I, J)-V(I, J-1))/SNS(J-1)
RGAMM =VIS(I, J-1)*R(J-1)
SU(I, J) =SU(I, J)+(RGAMP*DVDYP-RGAMM*DVDYM)/(R(J)*SNS(J))*VOL
101 CONTINUE
100 CONTINUE
C
CHAPTER 2 2 2 2 2 2 2 PROBLEM MODIFICATIONS 2 2 2 2 2 2 2
C
CALL MODV
C
CHAPTER 3 FINAL COEFF. ASSEMBLY AND RESIDUAL SOURCE CALCULATION 3 3
C
RESORV=O.O
DO 300 I=2, NIM1
DO 301 J=3, NJM1
AP(I, J)=AN(I, J)+AS(I, J)+AE(I, J)+AW(I, J)-SP(I, J)
DV(I, J)=DV(I, J)/AP(I, J)
RESOR=AN(I, J)*V(I, J+1)+AS(I, J)*V(I, J-1)+AE(I, J)*V(I+1, J)
1 +AW(I, J)*V(I-1, J)-AP(I, J)*V(I, J)+SU(I, J)
VOL=R(J)*SEW(I)*SNS(J)
SORVOL=GREAT*VOL
IF(-SP(I, J).GT.O.5*SORVOL) RESOR=RESOR/SORVOL
RESORV=RESORV+ABS(RESOR)
C-----UNDER-RELAXATION
AP(I, J)=AP(I, J)/URFV
SU(I, J)=SU(I, J)+(1.-URFV)*AP(I, J)*V(I, J)
DV(I, J)=DV(I, J)*URFV
301 CONTINUE
300 CONTINUE
C
CHAPTER 4 4 4 SOLUTION OF DIFFERENCE EQUATION 4 4 4 4 4 4 4
C
DO 400 N=1, NSWPV
400 CALL LISOLV(2, 3, NI, NJ, IT, JT, V)
RETURN
END
SUBROUTINE CALCP
C
CHAPTER 0 0 0 0 0 0 0 PRELIMINARIES 0 0 0 0 0 0 0
C
COMMON
1/PCOR/RESORM, NSWPP, URFV, DU(32, 32), DV(32, 32), IPREF, JPREF

```



```

1 /VAR/J(32,32),V(32,32),P(32,32),PP(32,32),TE(32,32),ED(32,32)
1 /ALL/IT, JT, NI, NJ, NIM1, NJM1, GREAT
1 /GEOM/INDCOS, X(40), Y(40), DXEP(40), DXPW(40), DYNP(40), DYP3(40),
1     SNS(40), SEW(40), XU(40), YV(40), R(40), RV(40)
1 /FLUPR/JRFVIS, VISCOS, DENSIT, PRANDT, DEN(32,32), VIS(32,32)
1 /COEF/AP(32,32), AN(32,32), AS(32,32), AE(32,32), AW(32,32), SU(32,32),
1     SP(32,32)
1 /KASE T1/UIN, TEIN, EDIN, FLOWIN, ALAMDA,
2     RSMALL, RLARGE, AL5, AL6, JSTEP, ISTEP, JSTP1, JSTM1, ISTEP1, ISTM1,
3     ISTEP2, ISTEP3, ISTM2
RESORM=0.0

```

```

C                                     CALCP
CHAPTER 1 1 1 1 1 1 ASSEMBLY OF COEFFICIENTS 1 1 1 1 1 1 1 CALCP
C                                     CALCP
DO 100 I=2, NIM1                       CALCP
DO 101 J=2, NJM1                       CALCP
C-----COMPUTE AREAS AND VOLUME      CALCP
AREAN=RV(J+1)*SEW(I)                   CALCP
AREAS=RV(J)*SEW(I)                    CALCP
AREAEN=R(J)*SNS(J)                    CALCP
VOL=R(J)*SNS(J)*SEW(I)                CALCP
C-----CALCULATE COEFFICIENTS        CALCP
DENN=0.5*(DEN(I, J)+DEN(I, J+1))      CALCP
DENS=0.5*(DEN(I, J)+DEN(I, J-1))      CALCP
DENE=0.5*(DEN(I, J)+DEN(I+1, J))      CALCP
DENW=0.5*(DEN(I, J)+DEN(I-1, J))      CALCP
AN(I, J)=DENN*AREAN*DV(I, J+1)        CALCP
AS(I, J)=DENS*AREAS*DV(I, J)          CALCP
AE(I, J)=DENE*AREAEN*DU(I+1, J)       CALCP
AW(I, J)=DENW*AREAEN*DU(I, J)         CALCP
C-----CALCULATE SOURCE TERMS        CALCP
CN=DENN*V(I, J+1)*AREAN                CALCP
CS=DENS*V(I, J)*AREAS                  CALCP
CE=DENE*J(I+1, J)*AREAEN              CALCP
CW=DENW*U(I, J)*AREAEN                CALCP
SMP=CN-CS+CE-CW                       CALCP
SP(I, J)=0.0                           CALCP
SU(I, J)=-SMP                          CALCP
C-----COMPUTE SUM OF ABSOLUTE MASS SOURCES
RESORM=RESORM+ABS(SMP)                 CALCP
101 CONTINUE                            CALCP
100 CONTINUE                            CALCP
C                                     CALCP
CHAPTER 2 2 2 2 2 2 PROBLEM MODIFICATIONS 2 2 2 2 2 2 2 CALCP
C                                     CALCP
CALL MODP                               CALCP
C                                     CALCP
CHAPTER 3 3 3 3 3 FINAL COEFFICIENT ASSEMBLY 3 3 3 3 3 3 3 CALCP
C                                     CALCP
DO 300 I=2, NIM1                       CALCP
DO 301 J=2, NJM1                       CALCP
301 AP(I, J)=AN(I, J)+AS(I, J)+AE(I, J)+AW(I, J)-SP(I, J) CALCP
300 CONTINUE                            CALCP
C                                     CALCP
CHAPTER 4 4 4 4 4 SOLUTION OF DIFFERENCE EQUATIONS 4 4 4 4 4 CALCP
C                                     CALCP
CHAPTER 5 5 5 5 CORRECT VELOCITIES AND PRESSURE 5 5 5 5 5 5 5 CALCP
DO 400 N=1, NSWPP                      CALCP
400 CALL LISOLV(2, 2, NI, NJ, IT, JT, PP) CALCP
C                                     CALCP
C-----VELOCITIES                    CALCP
DO 500 I=2, NIM1                       CALCP
DO 501 J=2, NJM1                       CALCP
IF(I.NE.2) U(I, J)=U(I, J)+DU(I, J)*(PP(I-1, J)-PP(I, J)) CALCP
IF(J.NE.2) V(I, J)=V(I, J)+DV(I, J)*(PP(I, J-1)-PP(I, J)) CALCP

```

501 CONTINUE	CALCP
500 CONTINUE	CALCP
C-----PRESSURES (WITH PROVISION FOR UNDER-RELAXATION)	CALCP
PPREF=PP(I PREF, JPREF)	CALCP
DO 502 I=2, NIM1	CALCP
DO 503 J=2, NJM1	CALCP
IF(I.EQ.ISTEP.AND.J.GE.JSTP1)PP(I, J)=0.0	CALCP
IF(I.EQ.ISTEP.AND.J.GE.JSTP1)P(I, J)=0.0	CALCP
IF(I.EQ.ISTEP.AND.J.GE.JSTP1)PP(I, J)=0.0	CALCP
IF(I.EQ.ISTEP.AND.J.GE.JSTP1)P(I, J)=0.0	CALCP
P(I, J)=P(I, J)+URFP*(PP(I, J)-PPREF)	CALCP
PP(I, J)=0.0	CALCP
503 CONTINUE	CALCP
502 CONTINUE	CALCP
RETURN	CALCP
END	CALCP
SUBROUTINE CALCTE	CALCP
C	KINE
CHAPTER 0 0 0 0 0 0 0 PRELIMINARIES 0 0 0 0 0 0 0	KINE
C	KINE
COMMON	KINE
1/TEN/RESORK, NSWPK, URFK	KINE
1/VAR/U(32, 32), V(32, 32), P(32, 32), PP(32, 32), TE(32, 32), ED(32, 32)	
1/ALL/IT, JT, NI, NJ, NIM1, NJM1, GREAT	
1/GEOM/INDCOS, X(40), Y(40), DXEP(40), DXPW(40), DYNP(40), DYPS(40),	
1 SNS(40), SEW(40), XU(40), YV(40), R(40), RV(40)	
1/FLUPR/URFVIS, VISCOS, DENSIT, PRANDT, DEN(32, 32), VIS(32, 32)	
1/COEF/AP(32, 32), AN(32, 32), AS(32, 32), AE(32, 32), AW(32, 32), SU(32, 32),	
1 SP(32, 32)	
1/TURB/GEN(32, 32), CD, CMU, C1, C2, CAPP, ELOG, PRED, PRTE	
1/WALL/YPLUSN(32), XPLUSW(32), TAUN(32), TAUW(32)	
1/KASE T1/JIN, TEIN, EDIN, FLOWIN, ALAMDA,	
2 RSMALL, RLARGE, AL5, AL6, JSTEP, ISTEP, JSTP1, JSTM1, ISTEP1, ISTM1,	
3 ISTEP2, ISTEP3, ISTM2	
1/SUSP/SUKD(32, 32), SPKD(32, 32)	
C	KINE
CHAPTER 1 1 1 1 1 1 ASSEMBLY OF COEFFICIENTS 1 1 1 1 1 1	KINE
C	KINE
PRTE=1.0	
DO 100 I=2, NIM1	KINE
DO 101 J=2, NJM1	KINE
C-----COMPUTE AREAS AND VOLUME	KINE
AREAN=RV(J+1)*SEW(I)	KINE
AREAS=RV(J)*SEW(I)	KINE
AREAEW=R(J)*SNS(J)	KINE
VOL=R(J)*SNS(J)*SEW(I)	KINE
C-----CALCULATE CONVECTION COEFFICIENTS	KINE
GN=0.5*(DEN(I, J)+DEN(I, J+1))*V(I, J+1)	KINE
GS=0.5*(DEN(I, J)+DEN(I, J-1))*V(I, J)	KINE
GE=0.5*(DEN(I, J)+DEN(I+1, J))*U(I+1, J)	KINE
GW=0.5*(DEN(I, J)+DEN(I-1, J))*U(I, J)	KINE
CN=GN*AREAN	KINE
CS=GS*AREAS	KINE
CE=GE*AREAEW	KINE
CW=GW*AREAEW	KINE
C-----CALCULATE DIFFUSION COEFFICIENTS	KINE
GAMN=0.5*(VIS(I, J)+VIS(I, J+1))/PRTE	KINE
GAMS=0.5*(VIS(I, J)+VIS(I, J-1))/PRTE	KINE
GAME=0.5*(VIS(I, J)+VIS(I+1, J))/PRTE	KINE
GAMW=0.5*(VIS(I, J)+VIS(I-1, J))/PRTE	KINE
DN=GAMN*AREAN/DYNP(J)	KINE
DS=GAMS*AREAS/DYPS(J)	KINE
DE=GAME*AREAEW/DXEP(I)	KINE
DW=GAMW*AREAEW/DXPW(I)	KINE
C-----SOURCE TERMS	KINE
SMP=CN-CS+CE-CW	KINE


```

1 SP(32, 32)
1/TURB/GEN(32, 32), CD, CMU, C1, C2, CAPPA, ELOG, PRED, PRTE
1/WALLF/YPLUSN(32), XPLUSW(32), TAUN(32), TAUW(32)
1/SUSP/SUKD(32, 32), SPKD(32, 32)
1/VAR/U(32, 32), V(32, 32), P(32, 32), PP(32, 32), TE(32, 32), ED(32, 32)
1/KASE T1/JIN, TEIN, EDIN, FLOWIN, ALA:IDA,
2 RSMALL, RLARGE, AL5, AL6, JSTEP, ISTEP, JSTP1, JSTM1, ISTP1, IST11,
3 ISTP2, ISTP3, ISTA2

```

```

C
CHAPTER 1 1 1 1 1 1 ASSEMBLY OF COEFFICIENTS 1 1 1 1 1 1 DISP
C
DO 100 I=2, NIM1 DISP
DO 101 J=2, NJM1 DISP
C-----COMPUTE AREAS AND VOLUME DISP
AREAN=RV(J+1)*SEW(I) DISP
AREAS=RV(J)*SEW(I) DISP
AREAEW=R(J)*SNS(J) DISP
VOL=R(J)*SNS(J)*SEW(I) DISP
C-----CALCULATE CONVECTION COEFFICIENTS DISP
GN=0.5*(DEN(I, J)+DEN(I, J+1))*V(I, J+1) DISP
GS=0.5*(DEN(I, J)+DEN(I, J-1))*V(I, J) DISP
GE=0.5*(DEN(I, J)+DEN(I+1, J))*J(I+1, J) DISP
GW=0.5*(DEN(I, J)+DEN(I-1, J))*U(I, J) DISP
CN=GN*AREAN DISP
CS=GS*AREAS DISP
CE=GE*AREAEW DISP
CW=GW*AREAEW DISP
C-----CALCULATE DIFFUSION COEFFICIENTS DISP
GAMN=0.5*(VIS(I, J)+VIS(I, J+1))/PRED DISP
GAMS=0.5*(VIS(I, J)+VIS(I, J-1))/PRED DISP
GAME=0.5*(VIS(I, J)+VIS(I+1, J))/PRED DISP
GAMW=0.5*(VIS(I, J)+VIS(I-1, J))/PRED DISP
DN=GAMN*AREAN/DYNP(J) DISP
DS=GAMS*AREAS/DYPS(J) DISP
DE=GAME*AREAEW/DXEP(I) DISP
DW=GAMW*AREAEW/DXPW(I) DISP
C-----SOURCE TERMS DISP
SMP=CN-CS+CE-CW DISP
CP=AMAX1(0.0, SMP) DISP
CPO=CP DISP
C-----ASSEMBLE MAIN COEFFICIENTS DISP
AN(I, J)=AMAX1(ABS(0.5*CN), DN)-0.5*CN DISP
AS(I, J)=AMAX1(ABS(0.5*CS), DS)+0.5*CS DISP
AE(I, J)=AMAX1(ABS(0.5*CE), DE)-0.5*CE DISP
AW(I, J)=AMAX1(ABS(0.5*CW), DW)+0.5*CW DISP
SU(I, J)=CPO*ED(I, J) DISP
SUKD(I, J)=SU(I, J) MODA
SU(I, J)=SU(I, J)+C1*CMU*GEN(I, J)*VOL*DEN(I, J)*TE(I, J)/VIS(I, J)
SP(I, J)=-CP DISP
SPKD(I, J)=SP(I, J) MODA
SP(I, J)=SP(I, J)-C2*DEN(I, J)*ED(I, J)*VOL/TE(I, J) DISP
101 CONTINUE DISP
100 CONTINUE DISP

```

```

C
CHAPTER 2 2 2 2 2 2 PROBLEM MODIFICATIONS 2 2 2 2 2 2 DISP
C
CALL MODED DISP

```

```

C
CHAPTER 3 FINAL COEFFICIENT ASSEMBLY AND RESIDUAL SOURCE CALCULATION 3 DISP
C

```

```

RESORE=0.0 DISP
DO 300 I=2, NIM1 DISP
DO 301 J=2, NJM1 DISP
AP(I, J)=AN(I, J)+AS(I, J)+AE(I, J)+AW(I, J)-SP(I, J) DISP
RESOR=AN(I, J)*ED(I, J+1)+AS(I, J)*ED(I, J-1)+AE(I, J)*ED(I+1, J) DISP
1 +AW(I, J)*ED(I-1, J)-AP(I, J)*ED(I, J)+SU(I, J) DISP

```

VOL=R(J)*SN3(J)*SEW(I)	MODA
SORVOL=7REAT*VOL	
IF(-SP(I,J).GT.0.5*SORVOL) RESOR=RESOR/SORVOL	
RESORE=RESORE+ABS(RESOR)	MODA 250.
C-----UNDER-RELAXATION	DISP
AP(I,J)=AP(I,J)/URFE	DISP
SU(I,J)=3U(I,J)+(1.-URFE)*AP(I,J)*ED(I,J)	MODA
301 CONTINUE	DISP
300 CONTINUE	DISP
C	DISP
CHAPTER 4 4 4 4 4 SOLUTION OF DIFFERENCE EQUATIONS 4 4 4 4 4	DISP
C	DISP
DO 400 N=1,NSWPD	
400 CALL LISOLV(2,2,NI,NJ,IT,JT,ED)	DISP
RETURN	DISP
END	DISP
SUBROUTINE LISOLV(ISTART,JSTART,NI,NJ,IT,JT,PHI)	LISOLV
C	LISOLV
CHAPTER 0 0 0 0 0 0 0 0 0 PRELIMINARIES 0 0 0 0 0 0 0 0	LISOLV
C	LISOLV
DIMENSION PHI(IT,JT),A(40),B(40),C(40),D(40)	
COMMON	LISOLV
1/COEF/AP(32,32),AN(32,32),AS(32,32),AE(32,32),AW(32,32),SU(32,32),	
1 SP(32,32)	
NIM1=NI-1	LISOLV
NJM1=NJ-1	LISOLV
JSTM1=JSTART-1	LISOLV
A(JSTM1)=0.0	LISOLV
C-----COMMENCE W-E SWEEP	LISOLV
DO 100 I=ISTART,NIM1	LISOLV
C(JSTM1)=PHI(I,JSTM1)	LISOLV
C-----COMMENCE S-N TRAVERSE	LISOLV
DO 101 J=JSTART,NJM1	LISOLV
C-----ASSEMBLE TDMA COEFFICIENTS	LISOLV
A(J)=AN(I,J)	LISOLV
B(J)=AS(I,J)	LISOLV
C(J)=AE(I,J)*PHI(I+1,J)+AW(I,J)*PHI(I-1,J)+SU(I,J)	LISOLV
D(J)=AP(I,J)	LISOLV
C-----CALCULATE COEFFICIENTS OF RECURRENCE FORMULA	LISOLV
TERM=1./(D(J)-B(J)*A(J-1))	LISOLV
A(J)=A(J)*TERM	LISOLV
101 C(J)=(C(J)+B(J)*C(J-1))*TERM	LISOLV
C-----OBTAIN NEW PHI"S	LISOLV
DO 102 JJ=JSTART,NJM1	LISOLV
J=NJ+JSTM1-JJ	MODA
102 PHI(I,J)=A(J)*PHI(I,J+1)+C(J)	LISOLV
100 CONTINUE	LISOLV
RETURN	LISOLV
END	LISOLV
SUBROUTINE PROMOD	PROMOD
C	PROMOD
CHAPTER 0 0 0 0 0 0 0 0 0 PRELIMINARIES 0 0 0 0 0 0 0 0	PROMOD
C	PROMOD
COMMON	PROMOD
1/UVEL/RESORU,NSWPU,URFU,DXEPU(40),DXPWU(40),SEWU(40)	
1/VVEL/RESORV,NSWPV,URFV,DYNPV(40),DYPSV(40),SNSV(40),RCV(40)	
1/PCOR/RESORM,NSWPP,URFP,DU(32,32),DV(32,32),IPREF,JPREF	
1/VAR/U(32,32),V(32,32),P(32,32),PP(32,32),TE(32,32),ED(32,32)	
1/ALL/IT,JT,NI,NJ,NIM1,NJM1,GREAT	
1/GEOM/INDCOS,X(40),Y(40),DXEP(40),DXPW(40),DYNP(40),DYPS(40),	
1 SNS(40),SEW(40),XU(40),YV(40),R(40),RV(40)	
1/FLUPR/URFVIS,VISCOS,DENSIT,PRANDT,DEN(32,32),VIS(32,32)	
1/KASE T1/UIN,TEIN,EDIN,FLOWIN,ALAMDA,	
2 RSMALL,RLARGE,AL5,AL6,JSTEP,ISTEP,JSTP1,JSTM1,ISTP1,ISTM1,	
3 ISTEP2,ISTP3,ISTM2	
1/SUSP/SUKD(32,32),SPKD(32,32)	


```

TMULT=DENU*CDTERM*SQRK*CAPPA/ALOG(ELOG*YPLUSA)
GO TO 912
911 TMULT=VISCOS/YP
912 TAUN(I)=-TMULT*J(I, J)
SP(I, J)=SP(I, J)-TMULT*SEWU(I)*RV(NJ)
910 AN(I, J)=0.0
TAUN(NI)=TAUN(NIM1)
C-----SIDE WALL
C***** FRONT FACE OF ORIFICE PLATE(SIDE WALL1)
DO 913 J=JSTP1, NJM1
913 AE(ISTEP, J)=0.0
C***** REAR FACE OF ORIFICE PLATE(SIDE WALL3)
ISTP2=ISTEP+2
DO 914 J=JSTP1, NJM1
914 AW(ISTP2, J)=0.0
C-----SYMMETRY AXIS
DO 203 I=1, NI
U(I, 1)=U(I, 2)
203 AS(I, 2)=0.0
C-----OUTLET
ARDENT=0.0
FLOW=0.0
DO 204 J=2, NJM1
ARDEN= 0.5*(DEN(NIM1, J)+DEN(NIM1-1, J))*R(J)*SNS(J)
ARDENT=ARDENT+ARDEN
204 FLOW=FLOW+ARDEN*U(NIM1, J)
UINC=(FLOWIN-FLOW)/ARDENT
DO 205 J=2, NJM1
205 U(NI, J)=U(NIM1, J)+UINC
RETURN
C
CHAPTER 3 3 3 3 3 3 3 3 V MOMENTUM 3 3 3 3 3 3 3 3 3
C
ENTRY MODV
C***** INSIDE ORIFICE PLATE
DO 1031 I=ISTEP, ISTP1
DO 1031 J=JSTP1, NJM1
1031 SP(I, J)=-GREAT
C-----SIDE WALL
C***** FRONT FACE OF ORIFICE PLATE(SIDE WALL1)
CDTERM=CMU**0.25
XP=XU(ISTEP)-X(ISTM1)
I=ISTM1
DO 915 J=JSTP1, NJM1
SQRK=SQRT(0.5*(TE(I, J)+TE(I, J-1)))
DENV=0.5*(DEN(I, J)+DEN(I, J-1))
AREANU=RV(J)*SEWU(I+1)
DENAR3=0.25*(DEN(I, J)+DEN(I, J-1))*AREANU
DENAR4=DENAR3
XPLUSA=0.5*(XPLUSE(J)+XPLUSE(J-1))
IF(XPLUSA.LE.11.63)TMULT=VISCOS/XP
TMULT=DENV*CDTERM*SQRK*CAPPA/ALOG(ELOG*XPLUSA)
TAUE(J)=-TMULT*V(I, J)
IF(J.EQ.JSTP1)SP(I, J)=SP(I, J)-DENAR3
SP(I, J)=SP(I, J)-TMULT*SNSV(J)*RV(J)
IF(J.EQ.JSTP1)TAUE(J)=.5*TAUE(J)
TAUE(J)=TAUE(J)
915 AE(I, J)=0.0
TAUE(JSTEP)=TAUE(JSTP1)
TAUE(NJ)=TAUE(NJM1)
C***** REAR FACE OF ORIFICE PLATE(SIDE WALL3)
CDTERM=CMU**0.25
XP=X(ISTEP)-XU(ISTEP)
ISTP2=ISTEP+2
I=ISTP2
DO 918 J=JSTP1, NJM1

```

MODA

MODA

MODA

MODA

MODA

MODA

MODA

MODA

MODA

MODA

MODA

MODA

MODA

PROMOD

PROMOD

PROMOD

PROMOD

PROMOD

MODA

MODA

MODA

MODA

MODA

MODA

```

SQRTK=SQRT(0.5*(TE(I,J)+TE(I,J-1)))
DENV=0.5*(DEN(I,J)+DEN(I,J-1))
XPLUSA=0.5*(XPLUSW(J)+XPLUSW(J-1))
IF(XPLUSA.LE.11.63)TMULT=VISCOS/XP
TMULT=DENV*CDTERM*SQRTK*CAPPA/ALOG(3LOG*XPLUSA)
TAUN(J)=-TMULT*V(I,J)
IF(J.EQ.JSTP1)SP(I,J)=SP(I,J)-DENAR4
SP(I,J)=SP(I,J)-TMULT*SNSV(J)*RV(J)
IF(J.EQ.JSTP1)TAUN(J)=.5*TAUN(J)
TAUN(J)=TAUN(J)
918 AW(I,J)=0.0
TAUN(JSTEP)=TAUN(JSTP1)
TAUN(NJ)=TAUN(NJM1)
C-----TOP WALL
C***** TOP WALL1(IN REGION1)
DO 313 I=2,ISTM1
313 AN(I,NJM1)=0.0
C***** BOTTOM FACE OF ORIFICE PLATE(TOP WALL2(IN REGION2))
DO 1006 I=ISTEP,ISTP1
1006 AN(I,JSTP1)=0.0
C***** TOP WALL3(IN REGION3)
DO 1007 I=ISTP2,NIM1
1007 AN(I,NJM1)=0.0
C-----SYMMETRY AXIS
DO 302 I=2,NIM1
302 AS(I,3)=0.0
RETURN
C
CHAPTER 4 4 4 4 4 4 PRESSURE CORRECTION 4 4 4 4 4 4 4 4
C
ENTRY MODP
RETURN
C
CHAPTER 5 5 5 5 5 5 5 THERMAL ENERGY 5 5 5 5 5 5 5 5 5
C
ENTRY MODT
C-----NO MODIFICATIONS FOR THIS PROBLEM
RETURN
C
CHAPTER 6 6 6 6 6 6 6 TURBULENT KINETIC ENERGY
C
ENTRY MODTE
C***** INSIDE ORIFICE PLATE
DO 1032 I=ISTEP,ISTP1
DO 1032 J=JSTP1,NJM1
1032 SP(I,J)--GREAT
C-----TOP WALL
C***** TOP WALL1(IN REGION1)
CDTERM=CMU**0.25
YP=YV(NJ)-Y(NJM1)
J=NJM1
DO 924 I=2,ISTM1
DENU=DEN(I,J)
SQRTK=SQRT(TE(I,J))
VOL=R(J)*SNS(J)*SEW(I)
GENCOU=0.5*(ABS(TAUN(I+1)*U(I+1,J))+ABS(TAUN(I)*U(I,J)))/YP
YPLUSN(I)=DENU*SQRTK*CDTERM*YP/VISCOS
DUDY=((U(I,J)+U(I+1,J)+U(I,J+1)+U(I+1,J+1))/4.-(J(I,J)+U(I+1,J)+
1U(I,J-1)+U(I+1,J-1))/4.)/SNS(J)
GENRES=GEN(I,J)-VIS(I,J)*DUDY**2
GEN(I,J)=GENRES+GENCOU
IF(YPLUSN(I).LE.11.63)GO TO 925
DITERM=DEN(I,J)*(CMU**.75)*SQRTK*ALOG(ELOG*YPLUSN(I))/(CAPPA*YP)
GO TO 926
925 CONTINUE
DITERM=DEN(I,J)*(CMU**.75)*SQRTK*YPLUSN(I)/YP

```

MODA

MODA

MODA

MODA

PROMOD

PROMOD

PROMOD

PROMOD

PROMOD

PROMOD

PROMOD

PROMOD

PROMOD

PROMOD

PROMOD

PROMOD

PROMOD

PROMOD

PROMOD

PROMOD

MODA

MODA

MODA

MODA

MODA

MODA

MODA

MODA

MODA

MODA

MODA

MODA

MODA

MODA

MODA

MODA

MODA

MODA

926 CONTINUE

SU(I, J)=GEN(I, J)*VOL+SUKD(I, J)

SP(I, J)=-DITERM*VOL+SPKD(I, J)

MODA

MODA

254.

924 AN(I, J)=0.0

C***** BOTTOM FACE OF ORIFICE PLATE(TOP WALL2(IN REGION2))

CDTERM=CMU**0.25

YP=YV(JSTP1)-Y(JSTEP)

J=JSTEP

DO 927 I=ISTEP, ISTEP1

DENU=DEN(I, J)

SQRTK=SQRT(TE(I, J))

VOL=R(J)*SNS(J)*SEW(I)

GENCOU=0.5*(ABS(TAUN(I+1)*J(I+1, J))+ABS(TAUN(I)*J(I, J)))/YP

YPLUSN(I)=DENU*SQRTK*CDTERM*YP/VISCOS

DUDY=((U(I, J)+U(I+1, J)+U(I, J+1)+U(I+1, J+1))/4.-(U(I, J)+U(I+1, J)+

1U(I, J-1)+U(I+1, J-1))/4.)/SNS(J)

GENRES=GEN(I, J)-VIS(I, J)*DUDY**2

GEN(I, J)=GENRES+GENCOU

IF(YPLUSN(I).LE.11.63)GO TO 928

DITERM=DEN(I, J)*(CMU**.75)*SQRTK*ALOG(ELOG*YPLUSN(I))/(CAPPA*YP)

GO TO 929

928 CONTINUE

DITERM=DEN(I, J)*(CMU**.75)*SQRTK*YPLUSN(I)/YP

929 CONTINUE

SU(I, J)=GEN(I, J)*VOL+SUKD(I, J)

SP(I, J)=-DITERM*VOL+SPKD(I, J)

927 AN(I, J)=0.0

C***** TOP WALL3(IN REGION3)

CDTERM=CMU**0.25

YP=YV(NJ)-Y(NJM1)

J=NJM1

DO 930 I=ISTP2, NIM1

DENU=DEN(I, J)

SQRTK=SQRT(TE(I, J))

VOL=R(J)*SNS(J)*SEW(I)

GENCOU=0.5*(ABS(TAUN(I+1)*U(I+1, J))+ABS(TAUN(I)*U(I, J)))/YP

YPLUSN(I)=DENU*SQRTK*CDTERM*YP/VISCOS

DUDY=((U(I, J)+U(I+1, J)+U(I, J+1)+U(I+1, J+1))/4.-(U(I, J)+U(I+1, J)+

1U(I, J-1)+U(I+1, J-1))/4.)/SNS(J)

GENRES=GEN(I, J)-VIS(I, J)*DUDY**2

GEN(I, J)=GENRES+GENCOU

IF(YPLUSN(I).LE.11.63)GO TO 931

DITERM=DEN(I, J)*(CMU**.75)*SQRTK*ALOG(ELOG*YPLUSN(I))/(CAPPA*YP)

931 CONTINUE

DITERM=DEN(I, J)*(CMU**.75)*SQRTK*YPLUSN(I)/YP

GO TO 932

932 CONTINUE

SU(I, J)=GEN(I, J)*VOL+SUKD(I, J)

SP(I, J)=-DITERM*VOL+SPKD(I, J)

930 AN(I, J)=0.0

C-----SIDE WALL

MODA

C***** FRONT FACE OF ORIFICE PLATE(SIDE WALL1)

CDTERM=CMU**0.25

XP=XU(ISTEP)-X(ISTM1)

I=ISTM1

DO 933 J=JSTP1, NJM1

DENV=DEN(I, J)

SQRTK=SQRT(TE(I, J))

VOL=R(J)*SNS(J)*SEW(I)

XPLUSE(J)=DENV*SQRTK*CDTERM*XP/VISCOS

GENCOU=0.5*(ABS(TAUE(J+1)*V(I, J+1))+ABS(TAUE(J)*V(I, J)))/XP

DVDX=((V(I, J)+V(I, J+1)+V(I+1, J)+V(I+1, J+1))/4.-(V(I, J)+V(I, J+1)+V(I

1I-1, J)+V(I-1, J+1))/4.)/SEW(I)

GENRES=GEN(I, J)-VIS(I, J)*DVDX**2

GEN(I, J)=GENRES+GENCOU

IF(XPLUSE(J).LE.11.63)GO TO 934

MODA

MODA

MODA

MODA

MODA

MODA

959 SP(I, J)=-GREAT

C***** TOP WALL3(IN REGION3)

YP=YV(NJ)-Y(NJM1)

J=NJM1

TERM=(CMU**.75)/(CAPPA*YP)

DO 940 I=ISTP2, NIM1

SU(I, J)=GREAT*TERM*TE(I, J)**1.5

940 SP(I, J)=-GREAT

C-----SIDE WALL

C***** FRONT FACE OF ORIFICE PLATE(SIDE WALL1)

XP=XU(ISTEP)-X(ISTM1)

I=ISTM1

TERM=(CMU**.75)/(CAPPA*XP)

NJM2=NJ-2

DO 941 J=JSTP1, NJM2

SU(I, J)=GREAT*TERM*TE(I, J)**1.5

941 SP(I, J)=-GREAT

C***** REAR FACE OF ORIFICE PLATE(SIDE WALL3)

XP=X(ISTEP)-XU(ISTEP)

ISTP2=ISTEP+2

I=ISTP2

TERM=(CMU**.75)/(CAPPA*XP)

NJM2=NJ-2

DO 942 J=JSTP1, NJM2

SU(I, J)=GREAT*TERM*TE(I, J)**1.5

942 SP(I, J)=-GREAT

C-----SYMMETRY AXIS

DO 730 I=2, NIM1

730 AS(I, 2)=0.0

RETURN

END

SUBROUTINE PRINT(ISTART, JSTART, NI, NJ, IT, JT, X, Y, PHI, HEAD)

DIMENSION PHI(IT, JT), X(IT), Y(JT), HEAD(6), STORE(50)

DIMENSION F(7), F4(11)

DATA F/4H(1H ,4H, A6, ,4HI3, ,4H11I ,4H10, ,4H7X, ,
14HA6) /

DATA F4/4H 1I ,4H 2I ,4H 3I ,4H 4I ,4H 5I ,4H 6I ,
1 4H 7I ,4H 8I ,4H 9I ,4H10I ,4H11I /

DATA HI, HY/6H I = , 6H Y = /

ISKIP=1

JSKIP=1

WRITE(6, 110)HEAD

ISTA=ISTART-12

100 CONTINUE

ISTA=ISTA+12

IEND=ISTA+11

IEND=MINO(NI, IEND)

F(4)=F4(IEND-ISTA)

WRITE(6, 112)

DO 101 JJ=JSTART, NJ, JSKIP

J=JSTART+NJ-JJ

DO 120 I=ISTA, IEND

A=PHI(I, J)

IF(ABS(A).LT.1.E-20) A=0.0

120 STORE(I)=A

101 WRITE(6, 113) J, (STORE(I), I=ISTA, IEND, ISKIP), Y(J)

WRITE(6, 114) (X(I), I=ISTA, IEND, ISKIP)

C-----

IF(IEND.LT.NI)GO TO 100

RETURN

110 FORMAT(1HO, 2O(2H*-), 7X, 6A6, 7X, 2O(2H*-))

111 FORMAT(1HO, 6H I = , I3, 11I10, 7X, * Y = *)

112 FORMAT(3H J)

113 FORMAT(1H , I3, 1P12E10.2, OPF7.3)

114 FORMAT(6HOX= , F7.3, 11F10.3)

END

MODA

MODA

MODA

MODA

MODA

MODA

PROMOD

PROMOD